UNIVERSITY OF OKLAHOMA

GRADUATE COLLEGE

ANALYSIS OF BACKBONE TECHNIQUE: A HILBERT TRANSFORM AND DISCRETE HILBERT TRANSFORM-BASED TECHNIQUE

A DISSERTATION

SUBMITTED TO THE GRADUATE FACULTY

in partial fulfillment of the requirements for the

Degree of

DOCTOR OF PHILOSOPHY

By

PENG F. TANG
Norman, Oklahoma
2015

ANALYSIS OF BACKBONE TECHNIQUE: A HILBERT TRANSFORM AND DISCRETE HILBERT TRANSFORM-BASED TECHNIQUE

A DISSERTATION APPROVED FOR THE
SCHOOL OF ELECTRICAL AND COMPUTER ENGINEERING

BY

Dr. Jin-Song Pei, Chair

Dr. Joseph P. Havlicek

Dr. S. Lakshmivarahan

Dr. Choon-Yik Tang

Dr. Peter Attar

DEDICATION

to

My parents

Xian-Yin Tang, and

De-Ying He

For

Encouraging me to follow my dreams

Acknowledgements

First, I wish to express my gratitude to my research advisor, Professor Jin-Song Pei, for her guidance and unconditional support during all these years of graduate school, and for being a excellent mentor. I am grateful for having had the opportunity to work with her.

I also wish to thank Dr. Joseph P. Havlicek and Professor Joseph Wright, for spending their precious time to teach me concepts related to Hilbert transform and discrete Hilbert transform and also to suggest several important references relevant to my research topic, which greatly accelerated my understanding of the research topic.

I would like to acknowledge the support of the ODOT grant, SP&R 2256 as well.

Last but not least, I wish to thank all my committee members for their time in going through my Ph.D. research, and their suggestions and approval of my work.

Contents

List of Tables

List of Figures

Abstract

This dissertation focuses on understanding and improving the "backbone" technique, a Hilbert-transform based vibration signal processing technique developed by Dr. Michael Feldman started in 1994. The concept of backbone seems straightforward being a mapping between the instantaneous amplitude and instantaneous frequency of vibration signals – mostly, free vibration signals of single-degree-of-freedom (SDOF) systems. Dr. Feldman shows a correlation between backbone pattern and the type of the underlying system nonlinearity. This motivated the utilization of the backbone as a pattern classifier for rapid system identification and damage detection. Nonetheless, unexpected "noisy" backbones – with oscillatory bodies and end(s) of these backbones – were obtained previously instead without an understanding of what caused and how to fix the problem that made the realization of the pattern classifier challenging. The author therefore was set to find out the reason and fix the problem; a theoretical approach would be taken whenever possible for a thorough understanding and remedy in a fundamental manner.

First, we pay attention to the discrete Hilbert transform (DHT) as we deal with real-world vibration signals that are, in general, finite and discrete. The end effect of DHT is investigated, after which a two-step preprocessing procedure is introduced. On one hand, theoretical justifications are provided for the preprocessing procedure. On the other hand, numerical simulation examples are provided to demonstrate the effectiveness in reducing end effect resulted from the procedure.

Unfortunately, even with the improved DHT procedure, we would still obtain

"noisy" backbones. We thus contemplate with a couple of carefully designed double-component signals. We show both theoretically and numerically that "noisy" backbones with oscillatory bodies and heads are supposed to occur in this and other multi-component signal. In the exploration of this phenomenon, we propose a concept named after "time index" to capture the interaction of the two mono-components that follow prescribed relations in their instantaneous quantities. By using this concept, we arrive at a signal decomposition method and correct a major integral formula in Dr. Feldman's work.

The two-step preprocessing procedure for DHT and the time index-based signal decomposition method are then used to extract backbones of a series of Duffing oscillators, whose parameter values are designed so that these models mimic typical nonlinear SDOF systems in structural engineering, the focused application domain in this study. We perform a parametric study on the key parameters in these Duffing oscillators, which confirms the validity of the backbone technique. More importantly, we introduce the concept of instantaneous bandwidth to the backbone technique. By using instantaneous bandwidth, we quantify the relations among displacement, velocity and acceleration backbones in addition to other practical implementation issues.

Last but not least, the improved backbone technique is applied to a couple of real world data sets as the final tough test. Both promising results and technical challenges are reported in the thesis. With the accomplished theoretical and numerical investigation, this study lays a solid foundation for further advancing both digital signal processing and practical application aspects of this relatively new pattern classifier for many possible engineering applications.

Chapter 1

INTRODUCTION

1.1 Overview

Vibration signals have been heavily studied for the purpose of many engineering disciplines including aerospace engineering, bio-medical engineering, civil engineering, electrical engineering, mechanical engineering, and more. Figure 1.1(a) illustrates a vibration signal as the free response of a single-degree-of-freedom (SDOF) system which can be used to represent an object in the aforementioned disciplines.

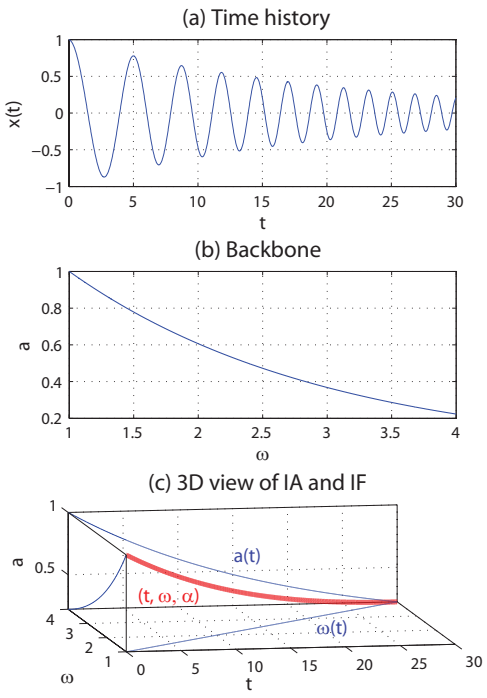

Figure 1.1: An idealized illustration of the backbone as a projection of a three-dimensional (3D) view of time, instantaneous frequency (IF) and instantaneous amplitude (IA) of a vibration signal. (a) is signal in time domain; (b) is the backbone curve, i.e., a projection of $(t,\ \omega,\ \mathfrak{a})$ onto the $(\omega,\ \mathfrak{a})$ plane; (c) is the 3D view of IF (ω) and IA ($\mathfrak{a}$) time histories (in red) and three two-dimensional (2D) projections (in blue).

This signal is normally a transient signal with a decaying profile in amplitude – among many other subtle details. Such a signal is the focus of this entire dissertation. Many vibration signal analysis research topics are dedicated to identifying the properties of the system underlying the signal, such as modal frequencies and damping ratio. Here, the goal would be to extract system properties concerning the *existence and types* of nonlinearities. This is the big picture concerning nonlinear system identification and damage detection, where signal processing and data analysis play a critical role.

The heart of this research is to represent a transient signal as illustrated above using a two-dimensional curve with a distinct feature called "backbone" – see Fig. 1.1(b) – defined by the signal's instantaneous characteristics. The concept of the "backbone"

originates from Feldman's work, e.g., [23, 29, 30]. It is said to be "a very helpful and traditional instrument in vibration analysis" [30]. Fig. 1.2 showcases the capability of the backbone technique for identifying many types of nonlinearity of SDOF models including but not limited to – according to [23] – nonlinear spring models (such as hardening, softening, backlash, pre-compressed strings, bilinear, or impact), and nonlinear damping models (frequency-dependent or frequency-independent).

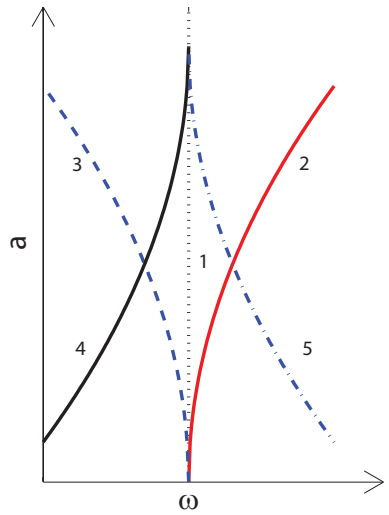

Figure 1.2: Backbones of typical nonlinear models: (1) linear; (2) hardening; (3) softening; (4) backlash; (5) preload. This figure is reproduced by following [30].

We consider the backbone technique a nonlinear system identification technique based upon instantaneous amplitude and frequency. The correspondence between the backbone feature and type of nonlinearity given in Fig. 1.2 could be used as a pattern classifier because different types of nonlinearities in the system would cause the backbone to bend in different directions (with more details), whilst the backbone will not bend at all for a pure linear system.

It needs to be emphasized that a meaningful backbone is not as easy to obtain as it appears. We are usually left to deal with much more noisy backbones than the one shown in Fig. 1.1(b). This is exactly the challenge our previous research team encountered [46]. Understanding the reason underneath the noisy backbones and also

overcoming them was the first motivation for this research so that feature extraction and pattern classification could be achieved more confidently and conveniently as an outcome.

Since no rigorous definition of backbone was given in any of Feldman's series of publications, one is proposed herein based on the understanding of his work:

Definition 1. The backbone for a real signal $x(t)$ is the curve $\{(\omega(t),\ \mathfrak{a}(t)) \mid t \geq 0\}$ in the amplitude-frequency plane, where $\mathfrak{a}(t)$ is the instantaneous amplitude and $\omega(t)$ is the instantaneous frequency of the signal $x(t)$, respectively.

The mapping from instantaneous amplitude to instantaneous frequency as shown in Fig. 1.1(b) (or vice versa) is not necessarily one-to-one, even though a one-to-one mapping would be preferred for the intended application specified above. Alternatively, the backbone could be viewed as a projection of a three-dimensional curve (t, $\omega(t)$, $\mathfrak{a}(t)$) onto the plane of ω and $\mathfrak{a}$ - with t playing an important role in understanding the backbone, as illustrated in Fig. 1.1(c).

The existence and types of nonlinearities are considered an indicator in system identification and damage detection [22, 76]. Motivated by identifying the existence and types of nonlinearities, three-dimensional features, or, two-dimensional contours, such as those from time-frequency analysis may or may not be a good option given another equally important practical concern of compressing rather than expanding data. Fortunately, the backbone representation offers a means for compressing data leading to simplified patterns. This facilitate real-world applications in classification of problems, which will enable, say, embedded systems, wireless communication, and quick decision making. This is the intended application of this Ph.D. research.

The reason for choosing backbone technique over other well known techniques is further explained herein. Traditionally, processing a signal like that in Fig. 1.1(a) could be carried out by using Fourier analysis. However, Fourier transform (FT) suffers to a great deal when signals are non-stationary, which is exactly the case here.

Short-time-Fourier-transform (STFT) could be useful for time-frequency analysis, however it is not surprising to know that STFT suffers from the same limitation due to its origin from FT. Other widely used signal processing techniques such as Wavelets or Wigner-Ville distribution (WVD) have been well studied, however they are not suitable for the purpose of this study as the outcome of neither method could be easily transferred into a pattern classifier.

Technical challenges in this dissertation are summarized as follows:

The first aspect that we paid attention to is the instantaneous characteristics of the signal, even though it is well-known that Hilbert transform can be used to perform this task. For example, the instantaneous frequency can become "messy" or even lack physical meaning if not handled with care, even though it is still mathematically sound. This is commonly seen for signals that is a mixture of several different frequencies, which unfortunately is the case in most scenarios. Because of this fact, it is generally required to decompose the signals and analyze each decomposed components separately so that their instantaneous frequencies would make physical sense. In general, this can be referred to as the challenge in instantaneous frequency estimation.

When it comes to simulated or real-world signals, we often face the discrete form of an algorithm. Unfortunately, discrete Hilbert transform tends to suffer from the end effect as it originates from discrete Fourier transform. An efficient two-step preprocessing treatment that significantly reduces this end effect is utilized in this dissertation and made a new routine into the backbone procedure. For illustration purpose, Fig. 1.3 shows a comparison of the instantaneous amplitude and frequency between with and without such a treatment. The selected signal is highly simple, yet the significance of this technical problem is nontrivial and the improvement is drastic.

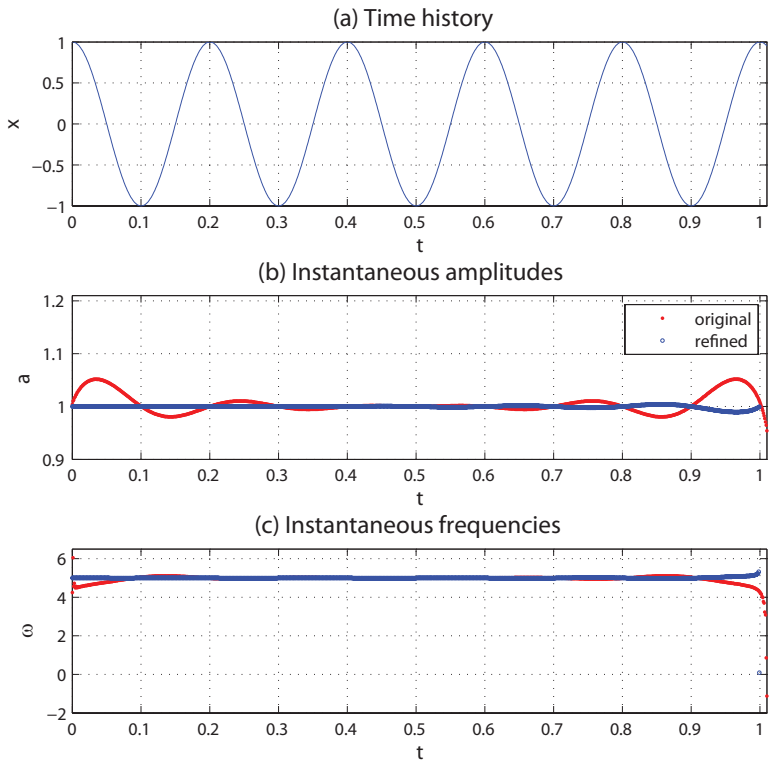

Figure 1.3: Comparison of the instantaneous amplitude and frequency of the original DHT method with the refined method on a pure sinusoidal wave. The signal tested here is $x[n] = \cos(2\pi f n/F_s)$, $n = 0, 1, \cdots, N-1$, where $f = 5,\ F_s = 1000,\ N = 1010$. The original result refers to the one obtained by using discrete Hilbert transform method stated in reference [13, 58], and the refined one refers to the method in Chapter 3.

More importantly, the author conducted a thorough literature review to establish the equivalency between two existing DHT algorithms through mathematical manipulations offering new insights to DHT because one of the two algorithms has not been utilized much. In addition, the author provided mathematical evidence to justify the two add-on procedures, which are in essence preprocessing for DHT.

As the third aspect directly related to the backbone technique, we studied in-depth a concept that is closely related to instantaneous amplitude and instantaneous frequency but has not been used by Dr. Feldman, i.e., instantaneous bandwidth. Instantaneous bandwidth is not only an indicator of the integrity of estimated instantaneous frequency [15], but also directly related to damping estimation, and the

relationship between the backbones of displacement, velocity and acceleration.

All of the aspects help fulfill the sole goal of understanding the reason for noisy backbones suffered by our research team previously and improving the backbone technique such that the backbone technique is more readily applicable to real-world signals. Therefore, as the last step of this dissertation, the backbone technique is tested on a couple of real-world data sets.

This research is focused on Dr. Feldman's series of publications on the backbone technique. However, the author is not simply implementing his methods or advertising his achievements. In concrete, first, the author makes the technique more theoretically grounded and closer to the intended (new) real-world applications. Secondly, we have reexamined his work using electrical engineering concepts. Lastly, we have achieved the goal of improving several aspects of the backbone technique as desired. In addition, new techniques such as the proposed new signal decomposition method and piecewise DHT are developed, which are not empirical methods and could benefit beyond the backbone technique.

1.2 Background

1.2.1 Objectives and nature of research

The author is aimed at making the backbone technique more understandable, justifiable, and applicable in terms of its capability of being a nonlinear classifier. To achieve this goal, the author is grounded in Digital Signal Processing (DSP) technique as the fundamental approach for this work. Specifically, a well-known signal processing algorithm - the Hilbert transform (HT) - serves as the key algorithm. A relatively new nonlinear system identification method named the "backbone" is the dominant technique studied.

The nature of this study is not only quantitative but also theoretical whenever

proper. On one hand, the author has re-derived and reconstructed or refined several key formulas that are important for the studies. On the other hand, practical methods for backbone technique implementation has been proposed.

1.2.2 Motivations

The reason for choosing this research topic is multifold. First of all, Structural Health Monitoring (SHM) and damage detection has been a popular and important research area for decades [18, 42, 70, 11, 55, 48, 21, 36]. As an important component of SHM, advancement in system identification especially nonlinear system identification is in demand.

The author focuses on SDOF systems in this study for two reasons: First, studying SDOF systems is a prerequisite for looking into MDOF systems. Next, SDOF system itself has strong utility for modeling in practice. For example, in earthquake engineering, the design spectrum is based on SDOF models [12].

Hilbert transform is the focus of the studies due to its well-known aspect of being suitable for nonlinear and non-stationary signal processing [14, 37, 49, 50, 29], just to name a few key classical references studied by the author and used as the main tool. Backbone – as a system identification method introduced by Dr. Feldman based on Hilbert transform – has also been around for 20 years. While all relevant aspects in Dr. Feldman's work will be reviewed in detail from Chapter 2 to 4, his series of publications related to Hilbert transform and backbone technique starting from 1990's is summarized in Table 1.1. These are the major references for the author to start with this research.

Table 1.1: Overview of selected publications by Dr. Feldman starting from 1990's.

Year	Reference	Topic	Summary
1994	[23, 24]	system vibration analysis	introduced backbone technique for detecting nonlinearity and viscous damping ratio of a SDOF model based on its free or forced response, i.e., FREEVIB and FORCEVIB
1995	[32]	nonlinear system parameter identification	introduced the idea of estimating system parameters by using a lowpass filter on the system backbone
1997	[8]	time-frequency characteristics	introduced the idea of possibly characterizing nonlinear systems by the time-frequency variations of the system response signals
1997	[25]	nonlinear free vibration identification	introduced the idea of approximating the backbone of the free response of a nonlinear model by using the average instantaneous amplitude and instantaneous frequency
2005	[26]	nonlinear dynamical system identification	introduced a method for estimating instantaneous system dynamic parameters, such as natural frequencies, damping characteristics, etc, under different kinds of system excitation based on Hilbert transform
2006	[27]	signal decomposition technique	proposed a nonlinear signal decomposition method named Hilbert Vibration Decomposition (HVD)
2011	[30, 29]	review of Hilbert transform applications	presented a thorough review of topics related to Hilbert transform applications

1.2.3 Identified research needs

Despite the pioneering contributions brought forward by Dr. Feldman, severe technical challenges were encountered in [46] when making an attempt to directly employ his earlier work in reference [23]. We thus regard it critical to clearly point out the flaws, ambiguities and unaddressed critical details in his publications so that researchers in the future can better implement his work. Although such facts will be given in detail in later sections, the author feel it necessary to present some quick examples here such that the readers can have a more concrete understanding of the relevant work done by Dr. Feldman.

In terms of the flaw, the "zero integral" claimed in reference [27] is regarded inaccurate according to this study; details with respect to this can be found under Chapter 3. For the ambiguities, an important term called "congruent envelope" or

"envelope of envelope" (EOE) given in reference [30] is not well explained, especially the formula for EOE, i.e., Eq. (37) on page 774 is not explained clearly. With respect to the unaddressed critical details, Dr. Feldman does not seem to have emphasized (enough) the noisy backbones obtained from real-world data, which is exactly what our previous research team suffered from as can be seen in reference [46] (Figs. 7 and 8). In other words, a clean backbone curve as seen in Fig. 1.1 does not come across often. Rather, a "noisy" backbone is often obtained. The reason behind the so-called "noisy" backbones deserves a thorough study. Moreover, driven by the intended application of backbone as a nonlinear classifier, clean backbone curves are much more preferred.

1.2.4 Duffing oscillator

Duffing oscillator has been selected as a major validation platform for us to explore and further develop the backbone technique. As a popular topic in engineering research family, Duffing oscillator or Duffing equation represents a typical normalized nonlinear system which expresses as [51]:

$$\ddot{x}(t) + 2\zeta\omega_n\dot{x}(t) + \omega_n^2 x(t) + \alpha x^3(t) \;=\; F(t) \tag{1.1}$$

where $x(t)$ is the response to be solved. $\zeta,\ \omega_n,\ \alpha$ stand for three system properties, damping ratio, natural frequency in rad/sec, and nonlinear stiffness coefficient, respectively. We have $\omega_n = 2\pi f_n$ with f_n being the natural frequency in Hz. $F(t)$ denotes the excitation force. Depending on the value or sign of the parameters in Eq. (1.1), various situations exist as summarized in Table 1.2. The author focuses on free Duffing only, where both damped and undamped, hardening and softening cases are considered in this dissertation.

Table 1.2: Different types of dynamics problems involving Duffing oscillator. † Not considered in this study.

Parameter	Value / Sign	Type of problem
ζ	zero	undamped Duffing
	$(0, 1)$	lightly damped Duffing
	others †	critically damped, over-damped, and self-excited Duffing
α	positive	hardening Duffing
	negative	softening Duffing
$F(t)$	zero	free (unforced) Duffing
	nonzero †	forced Duffing

Numerical simulation is essential to this investigation using Duffing oscillator. For undamped free Duffing, harmonic-balance method [62] provides an approximate solution. However, it demands solving highly coupled algebraic equations as will be seen in Chapter H. For damped free Duffing, closed-form approximate solution can be obtained by using Jacobi elliptic functions as provided in reference [51] (Eq. 4.3.18 on pp. 92). However, such a theoretical solution is not very helpful as it does not provide a straightforward formula for the response in most cases. Therefore, numerical solutions are used in this study. Runge-Kutta method is the key algorithm used to obtain the response. MATLAB solver ode45, which implements RK45 method ([19]), is the algorithm used herein.

For free softening Duffing oscillators, the stability issue needs to be taken into consideration, as the response may blow up due to the existence of saddle points. For under-damped Duffing with negative nonlinearity, Eq. (1.1) has a trivial fixed point at $(0, 0)$ and two saddle points at $(y_{1st+}, 0)$ and $(y_{1st-}, 0)$, where

$$y_{1st\pm} = \pm\sqrt{-\omega_n^2/\alpha}$$

where ω_n and α are specified previously. Therefore, the initial condition of the softening Duffing oscillators need to be chosen with care to avoid this instability issue.

1.3 Contributions of this Dissertation

By thoroughly reviewing Feldman's series of publications in the last 20 years, the author has achieved a couple of goals. First of all, a simple yet effective modification is applied to the current DHT algorithm given in references [13, 58] aiming at a reduced end effect. Although the newness of the method itself is debatable due to existing literature, i.e., [43], we have not only provided the method, but also presented the reasoning that validates the proposed modification. The transformed signals under such a modification suffer significantly less from the end effect. Moreover, the instantaneous amplitude and instantaneous frequency behave much better than without such a modification especially at the two ends - again see Fig. 1.3 for a quick example.

Secondly, driven by overcoming the noisy backbones encountered by our research team previously, the analysis in this chapter indicates why backbones could become noisy by using noise-free double-component signals. In the investigation, the author has also put forth a novel signal decomposition technique that is most suitable for double-component signal decomposition and, more importantly, theoretically sound.

Thirdly, we have applied another instantaneous characteristic to the backbone technique, i.e., instantaneous bandwidth. As a result, we have revealed why obtaining a backbone using displacement time history is preferable over acceleration time history, even though the latter is what is in generally readily available from dynamic tests. In addition, instantaneous bandwidth has been proposed as a practical measure for the integrity of instantaneous frequency estimation.

Last but not least, we have applied the improved backbone technique on several different sets of real-world data all of which being the free vibration of either a model or structure. Although the obtained backbones still suffer from heavy noise, we can still extract clear feature from not only the acceleration data but also correctly estimated displacement, indicating the usefulness of this technique in the real world.

1.4 Structure of this Dissertation

The structure of this dissertation is as follows:

Chapter 2 focuses on first revealing the reason for the end effect of discrete Hilbert transform and afterwards, a procedure to address such an issue. In Chapter 3, double-component signals are designed to reveal the reason of the "noisy" backbones. Time indices are proposed to characterize the interaction of two mono-components. An important integral formula in reference [27] is corrected. A signal decomposition technique is proposed as a by-product. In Chapter 4, instantaneous bandwidth is studied in-depth. The mathematical relationship between the backbones of displacement, velocity and acceleration is given as a function of both instantaneous frequency and instantaneous bandwidth – among other technical discoveries, such as piecewise DHT procedure. Both hardening and softening Duffing oscillators with parameter values that are meaningful for structural engineering applications are studied. Much smoother backbones are obtained in numerical exercises with the proposed decomposition method. The improved backbone technique is applied to real-world data in Chapter 5, where backbones with less "noise" are obtained in general. The future work and conclusions are given in Chapters 7 and 6, respectively.

Chapters 2 to 5 are prepared as individual manuscripts for review for publication, where relevant literature review will be provided independently within each section. To illuminate the understanding of the most challenging technique aspect related to this research, all leading concepts in HT and DHT are reviewed *critically* with examples developed by the author in Chapter 1.5. Since each of Chapters 2 to 5 contains a discussion, an additional discussion section in this dissertation is thus omitted. All derivations generated from this study, derivations for reviewing major literature, and some relevant m-files are included as appendices.

1.5 Additional Literature Review of Hilbert Transform and Discrete Hilbert Transform

There is a vast body of well-established literature on HT and DHT; it is worth a careful thought as to how to present a helpful big picture-like literature review herein to assist future researchers working on the backbone technique and more. With this said, instead of giving a laundry-list style of summary review, the author develops the following critical review especially by targeting those challenging (and even confusing) concepts, and by commenting on commonly-made mistakes in understanding these concepts following [13, 15, 73, 58, 49, 50]:

1. Hilbert Transform (HT) and analytic signal (AS)
2. Instantaneous amplitude (IA), instantaneous phase (IP), instantaneous frequency (IF) and instantaneous bandwidth (IB)
3. Discrete Hilbert transform (DHT)

While the succeeding subsections will continue with this critical review, as an overview, Table 1.3 summarizes a couple of important concepts related to the backbone technique:

Table 1.3: Overview of important concepts from digital signal processing (DSP) that are applied to backbone technique. Some key concepts will be formally introduced later on in this section. † For future work.

Concept	Formula	Remark
original signal	$x(t) = \mathfrak{a}(t)\cos\phi(t)$	$x(t)$ is a real signal with instantaneous amplitude $\mathfrak{a}(t)$ and instantaneous phase $\phi(t)$.
Fourier transform (FT) [60]	$X(\omega) = A(\omega)e^{j\Phi(\omega)}$	$X(\omega)$ is the Fourier transform of $x(t)$.
Hilbert transform (HT) [49]	$\tilde{x}(t) = \frac{1}{\pi t} * x(t) = \mathfrak{a}(t)e^{j\left(\phi(t)+\frac{\pi}{2}\right)}$	$\tilde{x}(t)$ is half-π phase shift of $x(t)$.
instantaneous amplitude (IA) [49]	$\mathfrak{a}(t) = \sqrt{x^2(t)+\tilde{x}^2(t)}$	$\mathfrak{a}(t)$ stands for the envelope of $x(t)$.
instantaneous phase (IP) [49]	$\phi(t) = \arctan\frac{\tilde{x}(t)}{x(t)} \mod \pi$	$\phi(t)$ is taken as the unwrapped phase in this dissertation.
instantaneous frequency (IF) [49]	$\omega(t) = \frac{d\phi(t)}{dt}$	This seemingly straightforward definition can be misleading; details will be given shortly.
instantaneous bandwidth (IB) [15]	$\mathfrak{b}(t) = \left\lvert\frac{\dot{\mathfrak{a}}(t)}{\mathfrak{a}(t)}\right\rvert$	$\mathfrak{b}^2(t)$ is regarded the standard deviation of the instantaneous frequency, i.e., an indicator of the spread out of the instantaneous frequency.
group delay (GD) † [60]	$\tau_g(\omega) = -\frac{d\Phi(\omega)}{d\omega}$	$\tau_g(\omega)$ is defined as the rate of change of the total phase shift with respect to angular frequency.

1.5.1 Hilbert transform (HT) and analytic signals (AS)

mathematical definition

Mathematically, the Hilbert transform of $x(t)$ is the time convolution of $x(t)$ with $\frac{1}{\pi t}$ (e.g., Eq. (1.9) on pp. 4 in reference [37]):

$$\tilde{x}(t) = \mathcal{H}[x(t)] = x(t) * \frac{1}{\pi t} = \frac{1}{\pi} P\int_{-\infty}^{\infty} \frac{x(\tau)}{t-\tau} d\tau \tag{1.2}$$

where $\tilde{x}(t)$ is denoted as the transformed signal and P denotes an improper integral in the sense of the Cauchy principal value. With $x(t)$ and $\tilde{x}(t)$, we can then construct

a special complex signal $z(t)$, i.e., an analytic signal (AS) as follows [35]:

$$z(t) \;=\; x(t) + j\tilde{x}(t) \tag{1.3}$$

analytic signal and analytic function

The concept of "analytic signal" comes from the concept of "analytic function," the latter of which refers to a class of complex functions that satisfies Cauchy-Riemann conditions for differentiability [14, 37], i.e., a complex function as follows

$$w(t,\tau) \;=\; u(t,\tau) + jv(t,\tau) \tag{1.4}$$

is an analytic function if

$$\frac{\partial u}{\partial t} \;=\; \frac{\partial v}{\partial \tau}\;; \quad \frac{\partial u}{\partial \tau} \;=\; -\frac{\partial v}{\partial t} \tag{1.5}$$

where $w,\ u$, and v are all two-dimensional functions of t and τ.

implication in frequency domain

The goal of performing the Hilbert transform is that the constructed complex signal $z(t)$ has a zero frequency response in the negative half frequency plane. In other words, $\tilde{x}(t)$ is special in a way that its frequency response is exactly the complex conjugate of the original signal $x(t)$. Reference [14] (Section 2.3, pp. 30) proved why Hilbert transform could achieve this goal. With equal importance, this is the foundation for the famous algorithm proposed in reference [58] for DHT.

mathematical and physical viewpoints

It is reasonable to state that for an arbitrary signal, the Hilbert transform can be obtained where the instantaneous amplitude, phase and frequency (APF) makes *math-*

ematical sense. However, whether the corresponding APF makes *physical* sense is a totally different question that demands full attention. Unfortunately, a completely unified understanding does *not* seem to exist in the current literature.

As early as 1996, [73] shows that Hilbert transform is special as it is the only transform that satisfies the three necessary conditions such that APF makes physical sense. The three necessary conditions are as follows:

A. The instantaneous amplitude needs to be continuous and *differentiable*. This results in a requirement of continuity of the transform operator.

B. The instantaneous phase must be independent of scaling and homogeneity, i.e., if $x(t)$ is replaced with $cx(t)$ for a real constant $c > 0$, then the instantaneous phase must remain the same. This requires the transform operator being homogeneous.

C. The constant amplitude and frequency of a simple sinusoid wave should remain their values, i.e., harmonic correspondent. This means the operator must transform $a\cos(\omega t + \phi)$ into $a\sin(\omega t + \phi)$ for any constant $a > 0,\ \omega > 0$, and constant ϕ.

Nonetheless, the differentiability requirement on instantaneous amplitude is no longer mentioned at all in reference [17] dated 1999 where Dr. Vakman, the author for [73], is a co-author. It is unclear why this change happened. One such consequence can be referred to in the following example:

Example 1 (IA and IP of the product of two cosine waves)**.**

Take a product of two cosine waves as an example,

$$x(t) \ = \ \cos(\omega_l t)\cos(\omega_h t), \ \text{with } \omega_h > \omega_l \geq 0 \tag{1.6}$$

The IA and IP under two different choices are given in Eqs. (1.7) and (1.8), respec-

tively following [17]:

$$\mathfrak{a}_{c1}(t) \;=\; |\cos(\omega_l t)| \quad \phi_{c1}(t) \;=\; \omega_h t + \frac{1}{2}\pi\left(1 - \operatorname{sgn}(\cos(\omega_l t))\right) \tag{1.7}$$

$$\mathfrak{a}_{c2}(t) \;=\; \cos(\omega_l t) \quad \phi_{c2}(t) \;=\; \omega_h t \tag{1.8}$$

According to [73] in 1996, the first choice in Eq. (1.7) would not be valid due to the violation of the differentiability of IA, while the second choice in Eq. (1.8) makes sure the satisfaction of the continuity of IP. However, following [17], both choices are legitimate, and it is only "a matter of taste and convenience" to decide which one to choose [17]. It can be seen later in Eq. (1.17), the author sticks to the first choice, i.e., assuming nonnegative amplitude.

1.5.2 Instantaneous amplitude (IA), instantaneous phase (IP) and instantaneous frequency (IF)

The concepts of instantaneous amplitude (IA), instantaneous phase (IP) and instantaneous frequency (IF) are a direct result of the analytic signal. First of all, an analytic signal in Eq. (1.3) can also be expressed in a unique polar form as follows (e.g., Eq. (15b) on pp. 522 in reference [5]):

$$z(t) \;=\; \mathfrak{a}(t)e^{j\phi(t)} \tag{1.9}$$

where $\mathfrak{a}(t)$ and $\phi(t)$ are called, respectively, the instantaneous amplitude (IA) and instantaneous phase (IP) of $z(t)$. A commonly made mistake is given as follows:

<u>Mistake</u> **1.** For any signal written in the form of Eq. (1.9), take a and ϕ as the IA and IP, respectively. This is elucidated in the following example:

Example 2 (Instantaneous characteristics of a chirp signal.)**.**

Take a simple linear chirp as an example,

$$x(t) \;=\; a(t)e^{j\phi(t)} \;=\; a(t)e^{j(\omega t+\frac{\rho}{2}t^2)} \tag{1.10}$$

one potential mistake here is that the IA and IF are taken intuitively as

$$\text{IA} \;= a(t) \tag{1.11}$$

$$\text{IF} \;= \frac{d\phi(t)}{dt} \;=\; \omega+\rho t \tag{1.12}$$

Such a mistake can be found even in relatively recent literatures such as [14] (Example 1.8 on pp. 18). [65] points out this potential mistake and proves that the true HT of a chirp signal with zero initial frequency

$$x(t)=\cos\left(\frac{\rho}{2}t^2\right) \tag{1.13}$$

be the following

$$\tilde{x}(t) \;=\; \sqrt{\frac{1}{\pi}}\left(\left(C(\sqrt{\rho t})+S(\sqrt{\rho t})\right)\right)\sin\left(\frac{\rho}{2}t^2\right)+\sqrt{\frac{1}{\pi}}\left(C(\sqrt{\rho t})-S(\sqrt{\rho t})\right)\cos\left(\frac{\rho}{2}t^2\right) \tag{1.14}$$

where

$$C(t) \;=\; \int_0^t \cos^2\tau d\tau;\; S(t) \;=\; \int_0^t \sin^2\tau d\tau \tag{1.15}$$

As stated in reference [65], the HT of Eq. (1.13) is simplified to

$$\tilde{x}(t) \;=\; \sin\left(\frac{\rho}{2}t^2\right) \tag{1.16}$$

only when the signal length is infinite. However, we focus on finite signals in this study as in many practical situations.

Along the same line and as a continuation of the discussion given previously

concerning physical meaning, we would like to highlight this fact: Although we have written down the instantaneous amplitude as

$$\mathfrak{a}(t) \;=\; \sqrt{x^2(t) + \tilde{x}^2(t)} \tag{1.17}$$

as shown in Table 1.3, the definitions for instantaneous amplitude and phase may not be unique as pointed out in reference [17]. To be concrete, there was actually a debate on the uniqueness of these two instantaneous quantities between Cohen and Hahn [17, 38, 16]. [17] introduced two choices for instantaneous amplitude and phase. One choice ends up with a nonnegative amplitude but an instantaneous frequency with infinite spikes, while the other yields a bounded instantaneous frequency but an instantaneous amplitude that might become negative. This is already illustrated in Example 1.

Continuing on, the instantaneous amplitude and instantaneous phase pair - [$\mathfrak{a}(t)$, $\phi(t)$] - is often referred to as a canonical pair (e.g., [65], [7]). A canonical pair always form a Hilbert pair, i.e.,

$$\mathcal{H}[\mathfrak{a}(t)\cos\phi(t)] \;=\; \mathfrak{a}(t)\sin\phi(t) \tag{1.18}$$

Mistake 2. Use Bedrosian's identity [4] to explain Eq. (1.18).

This statement is incorrect: Bedrosian's identity requires the frequency modulation part having a higher frequency than that of the amplitude modulation part. However, this does not need to be satisfied by the canonical pair – by definition.

Mistake 3. Not be careful with IF not being physically meaningful.

With instantaneous amplitude and phase elucidated as above, the concept of the instantaneous frequency (IF) would seem natural. The IF is commonly defined as the time derivative of the instantaneous phase $\phi(t)$, as shown below (e.g., Eq. (18) on

pp. 522 in reference [5]):

$$\omega(t) \;=\; \frac{d\phi(t)}{dt} \tag{1.19}$$

Unfortunately, this seemingly straightforward definition can lead to paradoxes. For example, if $\phi(t)$ is not monotonically increasing, we may end up with negative instantaneous frequency, which makes no physical sense "intuitively". This could happen even when the original signal makes perfect sense.

Example 3 (Negative IF)**.**

This example consists of several sub-examples.

First, a sum of two sinusoidal waves $x(t) = -2\cos(2\pi 0.1t) + \cos(2\pi 0.4t)$ has a time varying instantaneous frequency that goes to negative occasionally.

To have a more concrete understanding of the paradox, Fig. 1.4 exercises two seemingly simple signals, where Panel (a1) is a chirp signal while Panel (a2) is a sum of two chirps. The IF in Panel (a2) is an intentionally presented wrong result, which one would intuitively conceive. The correct IF results for Panels (a1) and (a2) are presented in Panels (b1) and (b2), respectively. In particular, Panel (b2) consists of discrete results of IF that switching between two values – with one physically meaningful and the other, not.

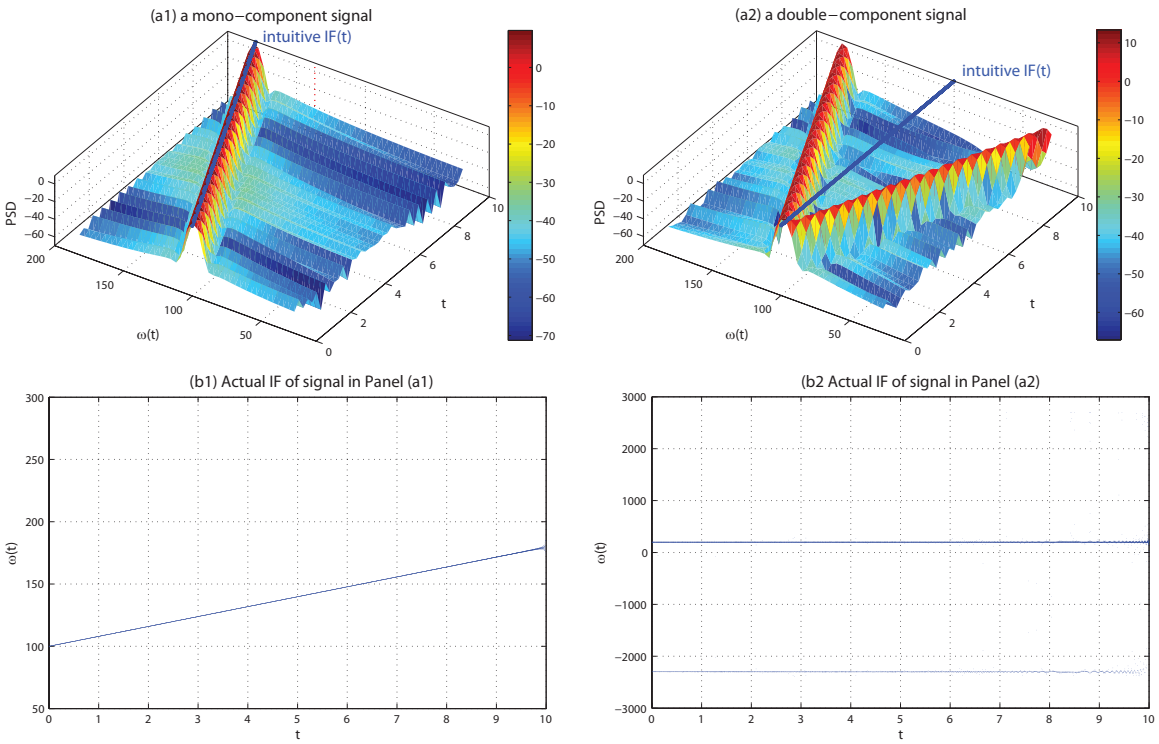

Figure 1.4: Illustration of the "IF" of two signals. (a1) refers to a chirp signal and (a2) is a sum of two chirp signals. The blue line segments in (a1) and (a2) refer to the intuitive IF of the two signals, while the actual IF of the two signals are presented in (b1) and (b2).

This paradox naturally introduces the topic of mono- and multi-component signals [5]. Taken directly from [5], the definition of mono- and multi-component signals are as follows:

mono-component "An asymptotic signal, $x(t)$, is referred to as a mono-component (or invertible) signal if for that signal, the instantaneous frequency, $f_i(t)$, accurately represents the frequency modulation law of the signal and is single-valued and invertible, so that the function $f_i^{-1}(f)$ exists," where f is the frequency axis.

multi-component "An asymptotic signal, $x(t)$, is referred to as a multi-component signal if there exists a finite number, N, of mono-component signals, $x_i(t)$, $i = 1, \cdots, N$, such that the relation $x(t) = \sum_{i=1}^{N} x_i(t)$ holds for all values of t for which $x(t)$ is defined, i.e., if $x(t)$ can be characterized as the sum of several

mono-component signals, and such that the decomposition is meaningful."

It is emphasized in reference [5] that the decomposition of a multi-component signal into mono-components is not unique and is application-dependent as illustrated in Fig. 1.5.

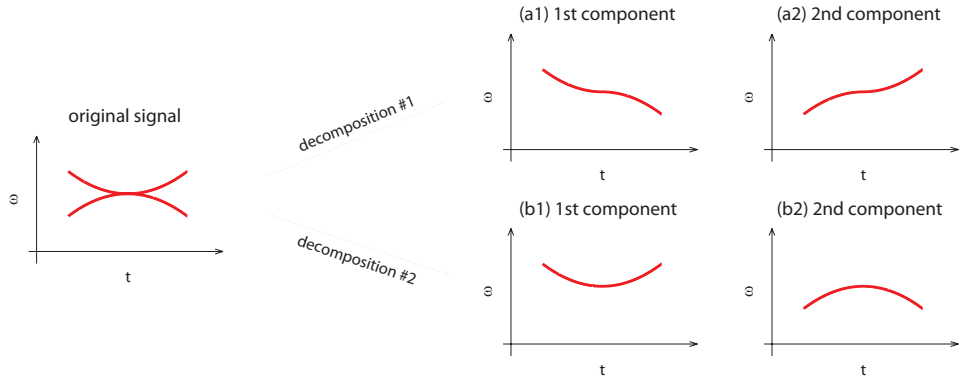

Figure 1.5: Two decomposition methods of a multi-component signal. This figure directly follows reference [5] with minor modifications.

Beyond the non-unique decomposition methods, the author would like to point out the mistakes people could make related to the definition of mono-component signals. For example, the following presents a mistake in a recent paper.

Mistake 4. Misunderstand the definition of a mono-component signal.

Reference [66] gives a mathematical definition for mono-component signal as follows:

> $z(t) = a(t)e^{j\phi(t)}$ is a mono-component if $\tilde{z}(t) = -jz(t)$, $\mathfrak{a}(t) \geq 0$ and $\dot{\phi}(t) \geq 0$.

The author has to emphasize that the above definition is quite different from the original one in [5] even though [66] claims that it follows the original mono-component definition in reference [5]. Before providing a counter example, let us first interpret the definition above. When $\tilde{z} = -jz(t)$, $a(t)$ and $\phi(t)$ are the IA and IP of $z(t)$, respectively. Thus, we can interpret the definition as "$z(t)$ is a mono-component

signal if its IA and IF are both non-negative," which, unfortunately, is not correct. A contradictory example is given below.

Example 4 (IA and IF of a double-component signal)**.**

Take a double-component signal $z(t) = -2e^{j2\pi 0.1t} + 2e^{j2\pi 0.4t}$ as an example. The IA and IF are as follows as derived formulas in Chapter 3 indicate:

$$\begin{aligned} \mathfrak{a}(t) &= (8 - 8\cos(2\pi 0.3t))^{1/2} \\ \omega(t) &= 0.5\pi \end{aligned}$$

both of which are indeed non-negative. However $z(t)$ is not a mono-component signal as it has two clearly separated stripes, one at 0.2π and the other at 0.8π.

This counter example might leave the readers with a wrong impression stated below as 0.5π is right in the middle of 0.2π and 0.8π.

<u>Mistake</u> **5.** Take IF as an average of the IFs of its mono-components.

While a detailed explanation is given in reference [54], the author would like to provide a quick example here to justify why interpreting the IF as an average of the frequencies of a multi-component signal is incorrect. This is illustrated in the following example.

Example 5 (Negative IF of a double-component whose two mono-components have positive IFs)**.**

The IF of a double-component signal $x(t) = -2\cos(2\pi 0.1t) + \cos(2\pi 0.4t)$ is as follows by again following the derived formula in Chapter 3:

$$\omega(t) = 2\pi 0.25 + 2\pi 0.15 \frac{-3}{5 - 4\cos(2\pi 0.3t)}$$

and it is occasionally negative.

1.5.3 Instantaneous bandwidth (IB)

We will firstly give the definition formula of IB following [15] and later explain the physical meaning of this concept:

$$\mathfrak{b}(t) \;=\; \left|\frac{\dot{\mathfrak{a}}(t)}{\mathfrak{a}(t)}\right| \tag{1.20}$$

Although this definition is not at all intuitive and the physical meaning is not that obvious, [15] gives a very vivid analogy between the IF v.s. IB relationship and the mean v.s. standard deviation relationship. In concrete, the IB is taken as the standard deviation of the IF estimation, which is an effective indicator of the integrity of the estimated IF. Refer to Chapter 4 for examples.

Instantaneous bandwidth is not only directly related to the IF estimation, but also closely related to damping in the system. Moreover, IB (joining IF) makes the connection amongst the backbones of displacement, velocity and acceleration. All of these subjects will be elaborated in detail later in Chapter 4.

1.5.4 Discrete Hilbert transform (DHT)

Hilbert transform becomes Discrete Hilbert transform (DHT) in the intended real-world applications since these real-world signals are not only finite but also discrete. Going from continuous signals to discrete signals can introduce frequency leakage. This is exactly why this dissertation studies this topic of DHT in great detail.

Although it is not stated in any other publication, the very concept of DHT was first introduced by Cizek in reference [13] according to the author's literature search, where the DHT of a signal $x[n]$ is defined as follows:

$$\tilde{x}[n] \;=\; x[n] \otimes h_c[n] \;=\; \sum_{k=0}^{N-1} x[k] h_c[n-k] \tag{1.21}$$

where $h_c[n]$ is the impulse response in time domain, whose DFT is

$$
\begin{aligned}
H_c[n] &= -j\mathrm{sgn}\left(\frac{N}{2}-n\right)\mathrm{sgn}(n) \\
&= \begin{cases}
\begin{cases}
-j & n = 1, 2, \cdots, N/2-1 \\
0 & n = 0, N/2 \\
j & n = N/2+1, N/2+2, \cdots, N-1
\end{cases} & \text{for } N \in \mathbb{E} \\
\begin{cases}
-j & n = 1, 2, \cdots, (N-1)/2 \\
0 & n = 0 \\
j & n = (N+1)/2, (N+3)/2, \cdots, N-1
\end{cases} & \text{for } N \in \mathbb{O}
\end{cases}
\end{aligned}
\tag{1.22}
$$

The reason why $H_c[n]$ is defined as above is to mimic the case for continuous time, i.e., to ensure that the right half of the samples result in a complex conjugate frequency response as of the left half.

The concept of analytic signal might become controversial in the case of DHT as pointed out in reference [58]. This is because analytic function is a type of function that requires continuously differentiability as a minimum. This can never be satisfied for discrete signals. [58] mimics the concept of continuous analytic signal by defining the complex signal $z[n] = x[n] + j\tilde{x}[n]$ as an "analytic-like" signal [58], which will be followed in the studies.

DHT demands discrete Fourier transform (DFT), a crucial step in the DHT procedure in reference [58]. However, DFT suffers from the end effect resulted from spectral leakage. This is reviewed and resolved in Chapter 2.

Last but not least and as discovered in this study, DHT – as a circular convolution algorithm – may introduce amplification error toward the end of instantaneous amplitude time history. This happens when a transient signal's amplitude drops significantly. This is investigated in Chapter 4, where a piecewise treatment is introduced to correct such an error.

1.6 Additional Literature Review of Methods Relevant to Backbone Technique

In this section, additional literature relevant to the intended applications of the backbone technique is reviewed so as to address why the focus of this dissertation is given to the backbone technique (other than other techniques to fulfill the same/similar purposes).

As a well-established tool for analyzing dynamics and performing system identification of dynamical systems, frequency response function (FRF) for vibration analysis and modal analysis has shown its usefulness. The FRF of a system is a function between the driving frequency of the external force and the response of the system [51]. Interestingly enough, there is also a feature called "backbone curve" in the context of the FRF. That is, if we connect all of the peaks of the amplitudes of the FRFs under different damping ratios, a curve is then formed and often referred to as a backbone curve. An illustrative figure is given in reference [51], e.g., Figure 5.4. However, this backbone curve is not the same as the backbone curve studied in this dissertation.

[48] presents a comprehensive review of the past and recent work in system identification of nonlinear dynamical systems. Techniques are examined based on different aspects including linearization method, time-domain method, frequency-domain method, modal analysis method, time-frequency analysis, black-box modeling, structural model updating, etc. Although the author will not present a comprehensive recap of all relevant system identification techniques, one of them is worth a highlight given its close relevance to the backbone technique and Dr. Feldman's study of this technique in his publications on the backbone technique (e.g., [30, 29]. This well-known nonlinear system identification technique is commonly referred to as the Hilbert-Huang transform (HHT).

The HHT was first proposed in reference [44] and later improved in reference [77]

among others. A key component in HHT is a signal decomposition procedure called empirical mode decomposition (EMD). The EMD decomposes a multi-component signal into a finite number of intrinsic mode functions (IMFs). An IMF is an function that satisfies two properties: it has the same number (or, at most, one in difference) of local extrema and zero crossings, and its positive and negative envelopes are symmetric.

A typical procedure for obtaining an IMF of a data set $x[n]$ is called sifting, which is explained as follows:

1. Identify all local extrema in the data set $x[n]$.

2. Apply cubic spline fitting to all local maxima (minima) to form the upper (lower) envelope.

3. Compute the mean of the upper and lower envelopes, and denote it as $m_1[n]$. Subtract the mean from the data; denote the difference as $h_1[n]$, i.e.,

$$h_1[n] \;=\; x[n] \;-\; m_1[n] \tag{1.23}$$

4. If h_1 is not an IMF, denote it as h_{10}. Take h_{10} through the aforementioned three steps until the stopping criterion by following [44] is met. The stopping criterion is to limit the standard deviation (SD):

$$\text{SD} \;=\; \sum_{i=0}^{N-1} \frac{|h_{1(k-1)}[i] - h_{1k}[i]|^2}{h_{1(k-1)}^2[i]}, \quad \text{with} k = 1, 2, \ldots \tag{1.24}$$

   to be between 0.2 and 0.3, where h_{1k} is the outcome of the $k+1$th sifting process and is also the first IMF c_1.

After the first IMF is obtained, it is subtracted from the original data $x[n]$. The residue is sent through the same procedure so that the second IMF can be obtained.

The IMF extraction procedure stops when the final residue r_l is negligible or is a monotonic function. The original signal $x[n]$ can thus be written as a sum of its l numbers of IMFs and the final residue as follows:

$$x[n] \;=\; \sum_{i=1}^{l} c_i + r_l \tag{1.25}$$

After the sifting process is completed, Hilbert transform is applied to every IMF to obtain the Hilbert spectrum of $x[n]$.

The HHT technique is popular for its ease for implementation and its adaptivity to data. Nonetheless, as a major limitation, it lacks theoretical support in a couple of aspects thus it depends heavily on empirical procedures. For this reason, the author chooses not to adopt this technique in this dissertation.

Chapter 2

DISCRETE HILBERT TRANSFORM (DHT): TWO ADD-ON PROCEDURES

2.1 Introduction

2.1.1 Motivations

The Hilbert transform (HT) has been playing an important role in digital signal processing for decades. In this chapter, we focus on discrete signals, where the discrete Hilbert transform (DHT) is necessary. One popular DHT algorithm is Marple's DHT algorithm, documented in reference [58] and programmed into MATLAB [59]. However, applying this algorithm can cause issues due to the fact that Marple's DHT algorithm is based on discrete Fourier transform (DFT), which introduces spectral leakage and further leads to the so-called "end effect". The end effect could become so severe that the good properties of Marple's DHT algorithm is being challenged.

As a motivating example, Fig. 2.1 uses a toy problem of one cycle of a cosine wave to compare known theoretical HT results versus those obtained through Marple's

DHT algorithm implemented to MATLAB under hilbert.m. Three slightly different cases are considered in Fig. 2.1: After a periodic extension, Case (a) yields a perfect sinusoidal wave while Cases (b) and (c) do not. Looking closely, Case (b) includes just one more point at the end of the signal, while Case (c) omits just one point, the last point. After a periodic extension, Cases (b) and (c) introduce erroneous low and high frequencies, respectively. The frequency leakage is the roots of the poor performance of Marple's DHT algorithm in Cases (b) and (c), which is not hard to tell from this toy problem. In practice, however, the cause and remedy would not be as trivial when signals to be transformed are not always harmonics but could be with time-varying amplitude and frequency, and are not of a not-so-perfect sampling rate.

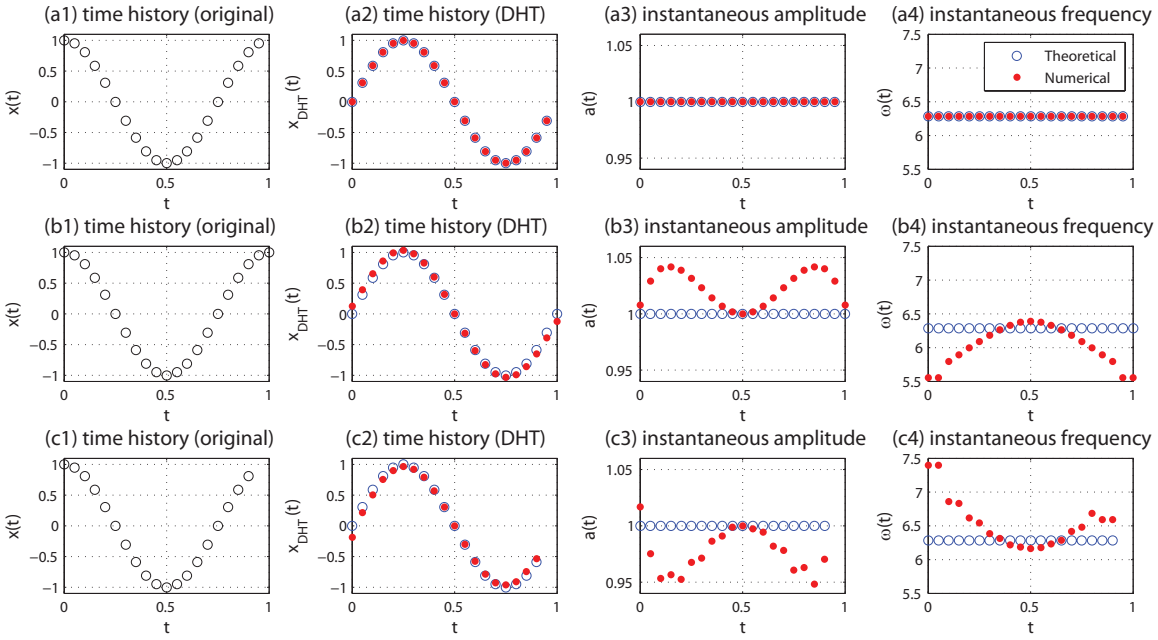

Figure 2.1: An illustration of spectral leakage by comparing the exact versus Marple's DHT results for signal $x[n] = \cos(2\pi n/Fs)$ where $Fs = 20$ and $n = 0, 1, \cdots, N-1$. Cases (a), (b), and (c) refer to the cases when $N = 20$, 21 and 19, respectively. In each case, the blue circles denote the exact result, which in time domain is simply $\tilde{x}[n] = \sin(2\pi n/Fs)$, while the red dots represent the DHT results.

While Fourier transform-based signal processing algorithms are highly well-known and widely applied to practice, DHT-based algorithms are not as well-known and popular in real-world applications. In contrast to this reality, it is the Hilbert transform

not Fourier transform that is expected to be more powerful in handling non-stationary and nonlinear signals. Given this belief, numerous researchers have been motivated to look into various aspects of the Hilbert transform aiming for its wider acceptance and better practice including but not limited to [23, 30, 29, 44]. This study contributes to this line of research with a clear focus on the numerical procedure of performing DHT algorithms.

2.1.2 Technical challenge and proposed approach

The seemingly signal-dependent performance of Marple's DHT algorithm (as illustrated in Fig. 2.1) is a major technical challenge for a couple of reasons. Theoretically, Marple's DHT algorithm is known to satisfy the two important magnitude and phase preserving properties in contrast to satisfying one but not both by almost all other DHT algorithms [58]. For example, a time-domain complex filtering technique that produces the real and imaginary responses $z_r[n]$ and z_i [68, 63] does not satisfy the first property; single finite impulse response (FIR) filter technique that approximates the Hilbert transform [63] does not satisfy the second property. A modification to the Marple's DHT algorithm may come at the price of dissatisfying one or both properties (as a side effect). Nonetheless, the need of correcting the end effect may outweigh this undesired side effect. To address the issue theoretically (thus fundamentally), the controversy is not less. On one hand, it is useful to look into some carefully defined toy problems. Fig. 2.1 is such an example. On the other hand, one has to face the music by dealing with real-world signals/situations but not surrender to some anecdotal cases.

In light of these difficulties, we seek inspirations first from the history of DHT algorithm development. In particular, we learn from [13], an earlier but lesser cited work than [58], which focuses on using a non-causal circular convolution formula and deriving the required impulse response function for Hilbert transform. This is the

technique to be exercised throughout this chapter for quantitative analysis. The main bulk of the work concentrates on devising the two proposed add-on procedures, providing quantitative analysis whenever possible including those to the well-defined toy problem, and eventually presenting numerical examples for validation. Nonetheless, the author specifies carefully the applicable range of the work: We aim to vibration signals - a fairly large subset of real-world signals, but not arbitrary signals.

2.1.3 Intended contributions

For a general vibration signal, there would be multiple cycles of oscillations. One such example is given in Fig. 2.2. We propose two add-on procedures that could complement Marple's DHT algorithm to significantly reduce the end effect. In addition, we examine in-depth three major DHT algorithms, i.e., Cizek in reference [13], Kak in reference [47], and Marple in reference [58] and conclude their mathematical equivalence. This fact about their mathematical equivalence alone could help better understand and expedite the development of DHT theories and practice as will be elaborated later in Chapter 2.3. Proofs concerning the two properties in reference [58] are provided as well.

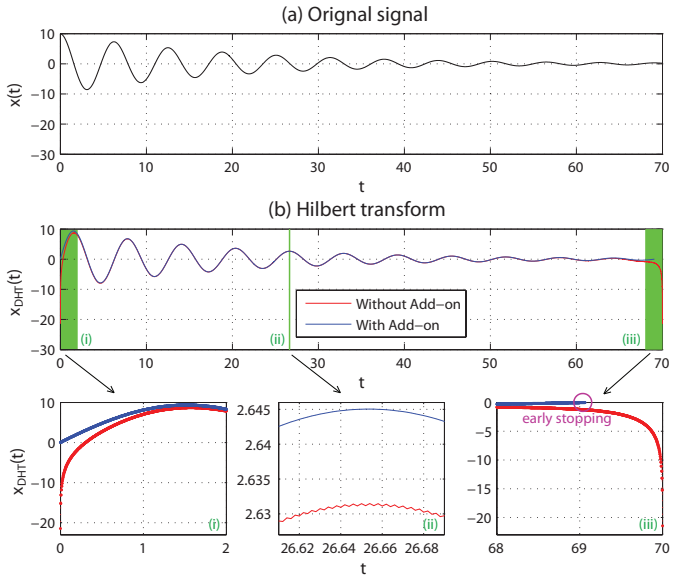

Figure 2.2: Comparison of the results obtained with and without the proposed add-on procedures when Marple's DHT algorithm is used. The signal is the simplest free vibration signal and has a form of $x[n] = e^{-0.05n/Fs}\cos(n/Fs)$ with $Fs = 500$ and $n = 0, 1, \cdots, 35000$. The comparison clearly indicates that the add-on procedures not only reduce the end effect to a large extent (see Panels (i) and (ii)) but also eliminate erroneous ripples towards the mid-section (see Panel (ii)).

2.1.4 Structure of this chapter

In Chapter 2.2, key concepts are reviewed. Three major DHT algorithms are presented. Spectral leakage, the heart of the problem, is reviewed. Chapter 2.3 compares the three DHT algorithms for their mathematical equivalence, a fact that has been overlooked in the literature. In Chapter 2.4, two add-on procedures that will be used in conjunction with Marple's DHT algorithm are presented, analyzed, and illustrated. The aim is at a more desirable DHT result in practice. Eventually, two sets of carefully designed or selected numerical examples are given in Chapter 2.5, where the efficiency of the two proposed add-on procedures is validated. Finally, conclusions are given in Chapter 2.6. Appendices A to D contain all relevant derivations in this work that are not given in the main body.

2.2 Literature Review

2.2.1 Discrete-time "analytic" signal

For real-world applications, signals are mostly not only finite but also discrete, in which case Hilbert transform is often realized through discrete Hilbert transform (DHT). Analytic signal, however, was initially defined for continuous time signals as in reference [35]. [58] emphasizes this fact and names a discrete complex signal obtained through DHT an "analytic-like" signal. We follow this terminology in this dissertation.

One major difference between DHT and HT is that the former suffers from the end effect resulted from spectral leakage introduced by DFT, a crucial step in the DHT procedure in reference [58]. This will be discussed in more detail in Chapter 2.2.4. We will go through two well-known DHT algorithms next.

2.2.2 Cizek (1970) and Kak's (1977) discrete Hilbert transform algorithm in references [13] and [47]

The concept of DHT was first proposed in reference [13], where a DSP formula for computing DHT is given. Basically, the goal is to find an impulse response function $h_c[n]$ so that the Hilbert transform can be readily computed by the circular convolution of $h_c[n]$ with the input $x[n]$. [13] limited its scope of interest to the case when the length of signal N is even, while Kak discussed the case when N is odd. We summarize Cizek and Kak's algorithms as follows:

Step 1 Define a transfer function in frequency domain as follows:

$$
\begin{aligned}
H_c[n] &= -j\mathrm{sgn}\left(\frac{N}{2}-n\right)\mathrm{sgn}(n) \\
&= \begin{cases}
\begin{cases} -j & n = 1, 2, \cdots, N/2-1 \\ 0 & n = 0, N/2 \\ j & n = N/2+1, N/2+2, \cdots, N-1 \end{cases} & N \in \mathbb{E} \\
\begin{cases} -j & n = 1, 2, \cdots, (N-1)/2 \\ 0 & n = 0 \\ j & n = (N+1)/2, (N+3)/2, \cdots, N-1 \end{cases} & N \in \mathbb{O}
\end{cases}
\end{aligned} \tag{2.1}
$$

This can be considered removing negative frequency components while doubling positive frequency components as done in Hilbert transform.

Step 2 Obtain the impulse response in time domain by using inverse DFT as follows:

$$
\begin{aligned}
h_c[n] &= \frac{1}{N}\sum_{l=0}^{N-1} H_c[l]e^{j\frac{2\pi ln}{N}} = \frac{1}{N}\left[1-(-1)^n\right]\cot\frac{\pi n}{N} \\
&= \begin{cases}
\begin{cases} 0 & n \in \mathbb{E} \\ \frac{2}{N}\cot\frac{\pi n}{N} & n \in \mathbb{O} \end{cases} & N \in \mathbb{E} \\
\begin{cases} -\frac{1}{N}\tan\frac{\pi n}{2N} & n \in \mathbb{E} \\ \frac{1}{N}\cot\frac{\pi n}{2N} & n \in \mathbb{O} \end{cases} & N \in \mathbb{O}
\end{cases}
\end{aligned} \tag{2.2}
$$

Step 3 Obtain the DHT of $x[n]$ by performing the circular convolution of $x[n]$ and $h_c[n]$:

$$
\tilde{x}[n] = x[n] \otimes h_c[n] = \sum_{k=0}^{N-1} x[k]h_c[n-k] \tag{2.3}
$$

2.2.3 Marple's discrete Hilbert transform algorithm in reference [58] (1999)

Marple put forward an implementation algorithm for the DHT in reference [58], where he also discussed the case for $N \in \mathbb{E}$ only. According to [58], the three steps for obtaining a discrete-time "analytic-like" signal are as follows:

Step 1 Compute the N-point discrete Fourier transform (DFT) of the original N real data samples:

$$X[n] \;=\; \sum_{k=0}^{N-1} x[k] e^{-j2\pi kn/N} \tag{2.4}$$

Step 2 Form the N-point one-sided discrete-time "analytic-like" signal in frequency domain:

$$Z[n] \;=\; \begin{cases} X[0] & \text{for } n = 0 \\ 2X[n] & \text{for } n = 1, 2, \cdots, N/2 - 1 \\ X[N/2] & \text{for } n = N/2 \\ 0 & \text{for } n = N/2 + 1, N/2 + 2, \cdots, N - 1 \end{cases} \tag{2.5}$$

This step can be considered performing a length-N windowing $W_m[n]$ on $X[n]$, where W_m is as follows:

$$W_m \;=\; [\;\; 1 \;\; \underbrace{2 \;\; 2 \;\; \cdots \;\; 2}_{N/2-1} \;\; 1 \;\; \underbrace{0 \;\; 0 \;\; \cdots \;\; 0}_{N/2-1} \;\;] \tag{2.6}$$

Step 3 Compute the N-point inverse DFT to yield the discrete-time "analytic-like" signal $z[n]$:

$$z[n] \;=\; \frac{1}{N} \sum_{l=0}^{N-1} Z[l] e^{-j2\pi ln/N} \tag{2.7}$$

Reference [58] states that this algorithm satisfies two important magnitude and phase preserving properties as follows (with support of simulation results but not

proofs):

Property 1 The real part of the complex signal $z[n]$ yields the original signal $x[n]$

Property 2 The real and imaginary components are orthogonal:

$$\sum_{n=0}^{N-1} \Re\{z[n]\}\Im\{z[n]\} \;=\; 0 \tag{2.8}$$

Note that the signal length N is assumed to be even for this implementation algorithm. This algorithm is adopted by MATLAB in its built-in function hilbert.m, where the case when $n \in \mathbb{O}$ is included. The windowing function in Step 2 is as follows:

$$W_m \;=\; [\;\; 1 \;\; \underbrace{2 \;\; 2 \;\; \cdots \;\; 2}_{(N-1)/2} \;\; \underbrace{0 \;\; 0 \;\; \cdots \;\; 0}_{(N-1)/2} \;\;] \tag{2.9}$$

This windowing function will be used for the derivation of the DHT formula for the case of $N \in \mathbb{O}$ in Chapter 2.3.

With the DHT algorithm, Fig. 2.1 can be explained theoretically. Details are given in A.

2.2.4 Spectral leakage

Spectral leakage refers to the the spreading of frequency components of a given signal mainly due to the fact of finite duration of the signal [41]. As a well-known concept, spectral leakage occurs when we perform Fourier transform on a finite-length signal that requires periodic extension of the signal. [58] elucidates the periodic extension involved in DHT. This periodic extension would possibly cause discrepancy to the two ends of the original signal in time domain; such discrepancy happens to be a spread out in frequency domain, i.e., leakage.

Since Marple's DHT algorithm is performed by first taking the DFT of a given signal, leakage is almost unavoidable. The toy problem in Fig. 2.1 is revisited here

first. A periodic extension of Cases (b) and (c) in Fig. 2.1 would cause a high- and low-frequency leakage, respectively. A more general case of sinusoidal wave form with more than one cycle is shown in Fig. 2.3. Fig. 2.3(a) shows the original signal with its DHT, where the end effect is obvious at both ends. Subsequently, the instantaneous characteristics are highly corrupted in Fig. 2.3(b) and (c) - both with erroneous high frequency. Consequently, the backbone (to be introduced in Chapter 2.2.5) in (d) is far from being a dot as it should be theoretically.

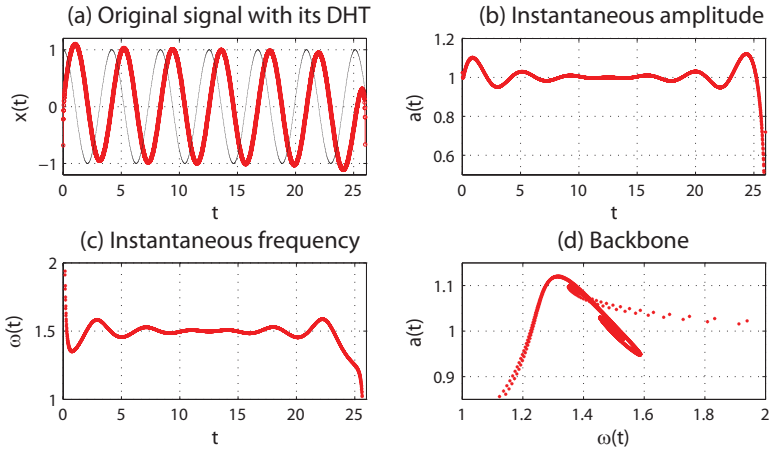

Figure 2.3: Another illustration of spectral leakage. In Panel (a), black and red lines are used for the original signal, and its DHT based on Marple's algorithm, respectively. Panels (b) to (d) present the instantaneous amplitude, instantaneous frequency and backbone based on the DHT result, respectively. Disclaimer: Panels (b) to (d) are zoomed-in views such that not all points are shown.

2.2.5 Others

Instantaneous characteristics of a signal go hand-in-hand with the HT of the signal as commonly seen. For finite discrete-time signals, we will simply generalize the definitions for instantaneous amplitude and frequency for continuous-time signals to discrete time. Spectral leakage would cause corrupted instantaneous characteristics of the signal. In applications, instantaneous characteristics are useful for system identification. One such technique is the backbone technique given in references [23, 30, 29], which are being studied by us. The term of "backbone" here refers to "a

mapping from instantaneous amplitude to instantaneous frequency (or vice versa)". A robust implementation of the Marple's DHT algorithm is critical to produce a meaningful backbone; contrasting numerical examples using the backbone are thus given throughout this chapter.

2.3 Two Discrete Hilbert Transform Algorithms

Interestingly enough, the algorithms in reference [13] and [47] yield exactly the same DHT result as Marple's DHT algorithm in reference [58]. To start, the final outcome of Cizek's and Kak's algorithms can be utilized first:

$$\tilde{x}[n] \;=\; x[n] \otimes h_c[n] \tag{2.10}$$

The "analytic-like" signal $z[n]$ will then be as follows:

$$z[n] \;=\; x[n] + j\tilde{x}[n] \;=\; x[n] + jx[n] \otimes h_c[n] \tag{2.11}$$

Taking the DFT on both sides of Eq. (2.11) yields the following equation:

$$Z[n] \;=\; X[n] + jX[n]H_c[n] \;=\; X[n]\left(1 + jH_c[n]\right) \;=\; X[n]W_c[n] \tag{2.12}$$

where the convolution theory is utilized [3], i.e., convolution of $x[n]$ and $h_c[n]$ in time domain is multiplication of $X[n]$ and $H_c[n]$ in frequency domain. The windowing

function $W_c[n]$ is obtained as follows:

$$W_c[n] \;=\; 1 + jH_c[n] \;=\; \begin{cases} \begin{cases} 2 & n = 1, 2, \cdots, N/2 - 1 \\ 1 & n = 0, N/2 \\ 0 & n = N/2 + 1, N/2 + 2, \cdots, N - 1 \end{cases} & N \in \mathbb{E} \\ \begin{cases} 1 & n = 0 \\ 2 & n = 1, 2, \cdots, (N-1)/2 \\ 0 & n = (N+1)/2, (N+3)/2, \cdots, N - 1 \end{cases} & N \in \mathbb{O} \end{cases} \tag{2.13}$$

It can be seen that $W_c[n]$ is the same as $W_m[n]$ in Eq. (2.6) from [58] for $N \in \mathbb{E}$ and Eq. (2.9) from MATLAB for $N \in \mathbb{O}$.

To this point, the three major DHT algorithms, i.e., [13] together with [47] and [58], are shown to be mathematically equivalent. Even though this derivation may seem trivial, historically it seems necessary to acknowledge that [13] introduced the concept of DHT nearly 30 years ahead of [58] while the latter seems to have received more recognition. Technically, it appears to us that [13] and [58] somehow complement each other: While [58] presents an implementation algorithm but not a mathematical formula, [13] offers a DSP formulas but not an implementing algorithm. Last but not least, realizing the mathematical equivalence of the two algorithms may help future researchers avoid tedious manipulations when they start with the algorithm in reference [58]. For example, almost one and half pages are used to derive two formulas in Proposition I of [20]. In fact, the formulas are readily available in reference [13].

By directly using this mathematical equivalence, it becomes apparent that the first property in Chapter 2.2.3 is true as explained in B.

2.4 Proposed Preprocessing Procedures

2.4.1 Overview

The proposed two add-on procedures are named after **local extrema trimming** and **even extension**. With these, the entire process of DHT can be described as follows:

Step A Identify and select local extrema each close to the two end of a specified real signal for the proposed **local extrema trimming**, and obtain a truncated real signal.

Step B Perform the proposed **even extension** to the truncated signal to obtain an extended real signal.

Step C Apply Marple's DHT algorithm to the extended signal to obtain a transformed signal.

Step D Extract the portion corresponding to the truncated real signal from the transformed signal, and take this signal as the final DHT result.

An inherent limitation with the proposed add-on procedures is that they lead to a DHT of a truncated version of a specified real signal - rather than the entire length of the real signal itself. The shortening of the signal may or may not be a practical issue depending on the situation. For the specified applications where vibration signals can have many cycles in a data set, we believe that this sacrifice could be affordable in the first place. Additionally and more importantly, this sacrifice can be a wise tradeoff since it eases the adverse end effect that could impact a large portion of the entire signal length.

In fact, the add-on procedure of even extension was developed first as an inspiration from an even extension in Fourier series, or discrete cosine transform (DCT). When combining this add-on procedure alone with Marple's DHT algorithm, a significant reduction of end effect was achieved sometimes but not at other time indicating

a strong signal-dependent performance. After a careful examination of all signals, and more importantly, after a mathematical analysis conducted on the DHT result from using even extension (that will be presented in Chapter 2.4.3, we realized that this add-on procedure would be responsible for both ends of the DHT being zero. We thus further proposed the add-on procedure of local extrema trimming to take full advantage of the limitation caused by even extension. In other words, local extrema trimming makes even extension far more robust in the specified applications but at a cost of truncating the original signal, or "an early stopping" of the original signal. The obtained DHT of the truncated signal is subject to the least end effect comparing with those obtained from using even extension alone, and from using no add-on procedures at all.

2.4.2 Even extension

To minimize frequency leakage, it is essential to reduce the discrepancy caused by periodic extension (referring back to Chapter 2.2.4 for the discrepancy). One way to achieve this goal is to reverse the original signal and concatenate this with the original signal. Fig. 2.4 illustrates this idea when the reversal and concatenation take place at the right end of the original signal. The reversal and concatenation can take place at the left end of the original signal as well, however we will not illustrate and discuss this situation hereafter. This is referred to as "even extension" by following the same terminology for Fourier series and in DCT.

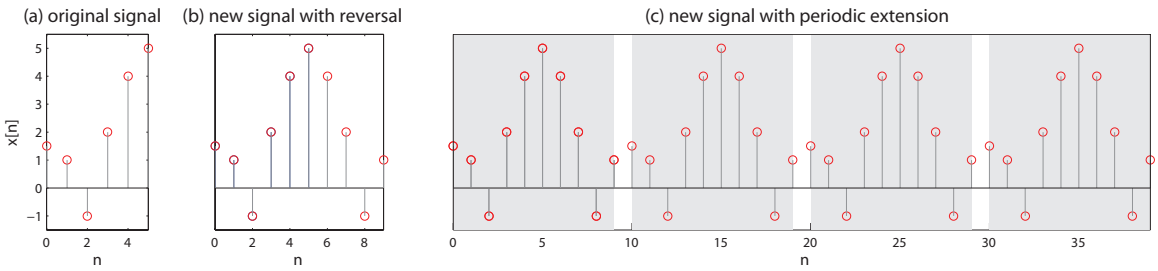

Figure 2.4: Illustration of mirroring (b) and periodic extension (c). The original signal in (a) has a length of $N = 6$ and is defined for $n = 0, 1, 2, 3, 4, 5$. The new signal in (b) has a length of $2N - 2 = 10$ and is defined for $n = 0, 1, \cdots, 8, 9$.

It is important to emphasize that the proposed even extension must be taken with care: The first and last points of the original signal need to be omitted for reversal thus leading to a total length of $2N - 2$ after concatenation with the original signal - as illustrated in Fig. 2.4 (a) and (b). Not removing these two points would lead to a situation similar to that in Fig. 2.1 (b) where low-frequency leakage would be introduced.

Intuitively, this add-on procedure eliminates a sudden "jump", i.e., a high-frequency leakage that could otherwise happen during a periodic extension. For DFT, this would help cure Gibb's phenomenon. Nonetheless, this add-on procedure may still cause another unwanted side effect. Referring to Fig. 2.4(c), the two ends of the original signal become local extrama (i.e., minima or maxima) after the proposed even extension, which may or may not be consistent with the original signal as illustrated in Fig. 2.5. This intuition can be quantified in the analysis given in Chapter 2.4.3.

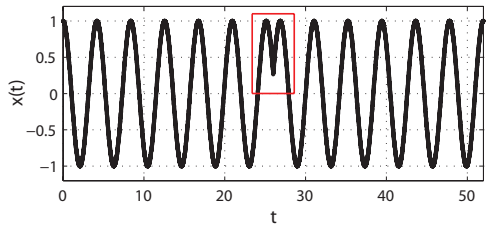

Figure 2.5: An illustration of the limitation with the proposed even extension by using the signal in Fig. 2.3. The red box highlights the undesired local extrema introduced by even extension.

2.4.3 Quantitative analysis of proposed even extension

Following [13], here we intend to derive a circular convolution formula for the DHT of the signal after the proposed even extension. Denote the extended signal as $y[n]$, where $n = 0, 1, \cdots, 2N-2$, and

$$y[n] = \begin{cases} x[n] & n = 0, 1, ..., N-1 \\ x[2N-2-n] & n = N, N+1, ..., 2N-3 \end{cases} \tag{2.14}$$

where $x[n]$ is the original real signal.

Following the general DHT formula in Eq. (2.3), the DHT of $y[n]$ can be obtained as follows with derivations given in C:

$$\begin{aligned} \tilde{y}[n] &= \sum_{k=0}^{N-1} x[k]\left(h_y[n-k] + h_y[n+k]\right) - \left(x[0]h_y[n] + x[N-1]h_y[n+N-1]\right), \\ &\text{for } n = 0, 1, \cdots, 2N-3 \end{aligned} \tag{2.15}$$

where

$$h_y[n] = \begin{cases} 0 & n \in \mathbb{E} \\ \frac{1}{N-1}\cot\frac{n\pi}{2N-2} & n \in \mathbb{O} \end{cases} \tag{2.16}$$

The computation error measured by the difference between $\tilde{y}[n]$ and $\tilde{x}[n]$ for the range of $n = 0, 1, \cdots, N-1$ would thus be as follows:

$$\begin{aligned} \tilde{y}[n] - \tilde{x}[n] = &\sum_{k=0}^{N-1} x[k] \underbrace{\left(h_y[n-k] + h_y[n+k] - h_x[n-k]\right)}_{\Delta h(n,k)} \\ &- \left(x[0]h_y[n] + x[N-1]h_y[n+N-1]\right) \end{aligned} \tag{2.17}$$

To further evaluate this error formula, Fig. 2.6 presents a 3D plot and 2D contour plot of $\Delta h(n,k)$, respectively. It can be seen that this value is small in general, indicating that $\tilde{y}[n]$ is close to $\tilde{x}[n]$ in general.

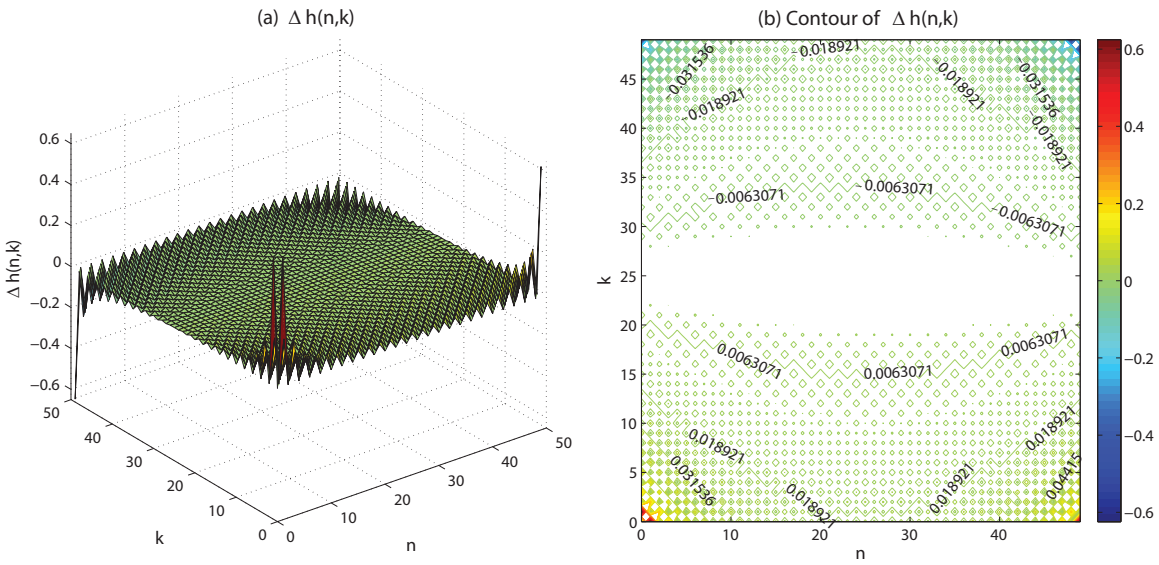

Figure 2.6: The function of $\Delta h(n,k)$ that shows a magnitude close to zero at most points.

Concerning the two important properties, it is clear that the proposed even extension does not change the first property because it applies Marple's DHT algorithm to $y[n]$ with $y[n]$ containing all of $x[n]$. Unfortunately, the proposed even extension destroys the orthogonality property between the original signal and its DHT, i.e., $\sum_{n=0}^{N-1} y[n]\tilde{y}[n] \neq 0$. Take $x[n] = [1, 3, 2, -5]$ as an example. After even extension, we have $y[n] = [1, 3, 2, -5, 2, 3]$. $\tilde{y}[n]$ is calculated to be $\tilde{y}[n] = [0,\ -0.5774,\ 4.6188,\ 0,\ 4.6188,\ 0.5774]$. Thus, $\sum_{n=0}^{N-1} y[n]\tilde{y}[n] = \sum_{n=0}^{3} y[n]\tilde{y}[n] = 1 \times 0 + 3 \times (-0.5774) + 2 \times 4.6188 + (-5) \times 0 = 7.5054 \neq 0$.

Another important consequence of the proposed even extension given in Eq. (2.15) is that the two ends of $\tilde{y}[n]$ is always zero, i.e.,

$$\tilde{y}[0] \ = \ \tilde{y}[N-1] \ = \ 0 \tag{2.18}$$

While the detail of this is shown in D, the implication of this is given hereafter to achieve, at a price of truncating part of the original signal, a more robust execution of Marple's DHT algorithm than otherwise.

2.4.4 Local extrema trimming

An inherent limitation with the proposed even extension seems to lie in two consistent facts: Both ends of the original signal being treated as local extrema regardless of the truth with the original signal, and the DHT results of the both ends always being zero. One quick fix but at the cost of shortening the original signal is to intentionally select some local extrema in the original signal being the ends of the signal for even extension and so on. In other words, this refers to trimming the original signal at a user-defined leftmost and rightmost local extrema before starting the proposed even extension procedure. This indeed is a trivial detail, however it is originated from Eq. (2.18) with a rigorous mathematical proof, and will be validated in numerical examples hereafter.

It is of great importance to highlight that when a signal is discrete, sampling would very likely cause us to miss true local extrema. Having said this, the proposed local extrema trimming would not be perfect most of time, a fundamental limitation that cannot be overcome easily. In other words, errors caused by the proposed local extrema trimming lies in the sampling process of the signal.

2.5 Numerical Examples

Two sets of case studies are designed to compare the performance under three options:

- Marple's DSP algorithm alone (shorthanded as "M" in the figures)
- Marple's DSP algorithm with proposed even extension procedure only (shorthanded as "E + M" in the figures)
- Marple's DSP algorithm with the proposed two add-on procedures (shorthanded as "T + E + M" in the figures)

The second option is taken as a reference to compare the improvement by the proposed local extrema trimming procedure. For illustration purpose, all signals are designed so that we do not need to discard any point in the beginning of these signals. In other words, the starting point in a signal is indeed a local minimum/maximum.

A total of six different types of signals are used as the first set of case studies. See details in Table 2.1. While more information on how these signals designed will be given in Chapter 3, we include three basic types of signals in Cases (a) to (c) and some other signals that can be used to mimic the free vibration of a single-degree-of-freedom (SDOF) system. Last but not least, it is very important to highlight the concepts of mono- and multi-component signals. Hilbert transform should only be directly applied to mono-component signals - not multi-component signals. All six signals in this set of case studies are qualified as mono-component signals.

Table 2.1: Overview of the six case studies.

ID	Description	Signal
1	pure sinusoid	$\cos(t)$
2	FM signal	$10\cos(t + 0.05t^2/2)$
3	AM signal	$(10\cos(0.3t) + 20)\cos(2t)$
4	exponentially decaying sinusoid	$10e^{-0.05t}\cos t$
5	AM-FM signal	$10e^{-0.05t}\cos(t + 0.05t^2/2)$
6	AM-FM signal 2	$10e^{-0.05t}\cos\left(1t - 1.5e^{-0.3t}\right)$

Other details concerning all numerical exercises in this study are as follows: The MATLAB built-in function hilbert.m is used to implement the Marple's DHT algorithm. Peak picking required in the proposed local extrema trimming is done by using MATLAB built-in function findpeaks.m. The instantaneous frequency is obtained by using a commonly seen central difference method, with a modification to the algorithm given in reference [30]:

$$\omega[n] \;=\; \frac{\phi[n+1] - \phi[n-1]}{2} \;=\; \frac{1}{2}\arctan\left(z[n-1]z^*[n+1]\right) \qquad (2.19)$$

where $z[n]$ is the "analytic-like" signal of the original signal $x[n]$, i.e., $z[n] = x[n] + j\tilde{x}[n]$, and z^* is the complex conjugate of $z[n]$, i.e., $z^*[n] = x[n] - j\tilde{x}[n]$. To make $\omega[n]$ of the same length as $x[n]$, we let $\omega[0] = \omega[1]$ and $\omega[N-1] = \omega[N-2]$.

For the first set of case studies, comparisons in terms of the obtained DHT, its instantaneous characteristics and backbones are shown in Fig. 2.7. It can be seen that the proposed two add-on procedures greatly complement Marple's DHT algorithm. Using the proposed even extension alone would not be as robust as using both of the proposed two procedures especially when the specified signal does not end with a local maximum or minimum.

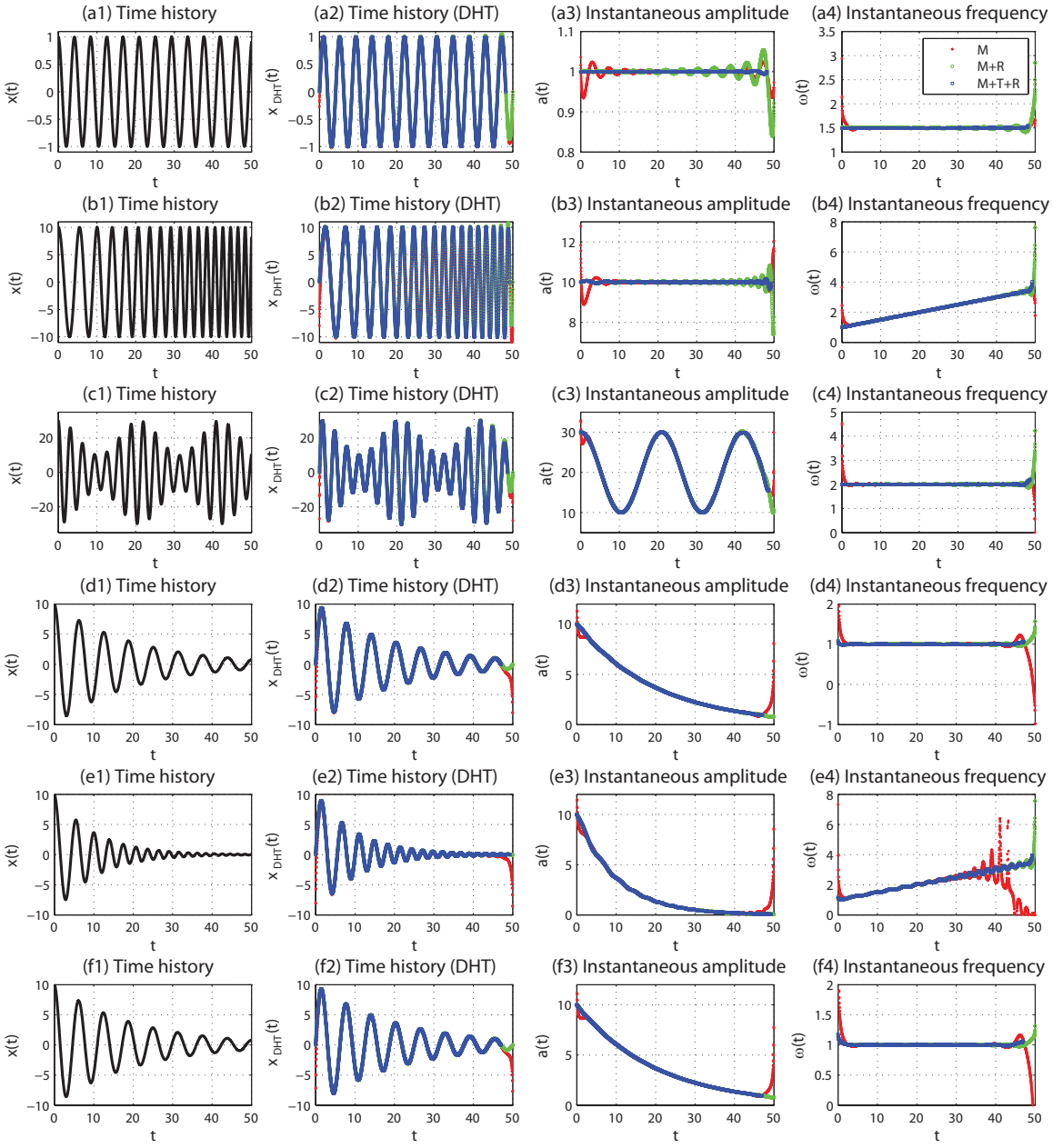

Figure 2.7: Comparisons for case studies by using the three different options in executing DHT, where "M", "E+M", and "T+E+M" stand for using the Marple's DHT algorithm only, using the Marple's DHT algorithm with the proposed even extension, and using the Marple's DHT algorithm with the proposed local extrema trimming and even extension, respectively. Case (a): $\cos(t)$; Case (b): $10\cos(t+0.05t^2/2)$; Case (c): $(10\cos(0.3t)+20)\cos(2t)$; Case (d): $10e^{-0.05t}\cos t$; Case (e): $10e^{-0.05t}\cos(t+0.05t^2/2)$; Case (f): $10e^{-0.05t}\cos(1t-1.5e^{-0.3t})$.

Even though the focus of this work is vibration signals, the proposed two add-on procedures may not be limited to vibration signals. To illustrate other potential

applications, the second set of case studies is presented in Fig. 2.8. We carefully selected three typical signals from [67], [44] and [45]. The signal in Fig. 2.8(a) is a phase signal, commonly seen in HT analysis, while those in Fig. 2.8 (b) and (c) are important test signals for Nordan Huang's empirical mode decomposition (EMD) method proposed to enable general Hilbert spectrum analysis ([44]). Once again, the comparison among the three options clearly indicates the effectiveness of the proposed two add-on procedures in working with Marple's DHT algorithm.

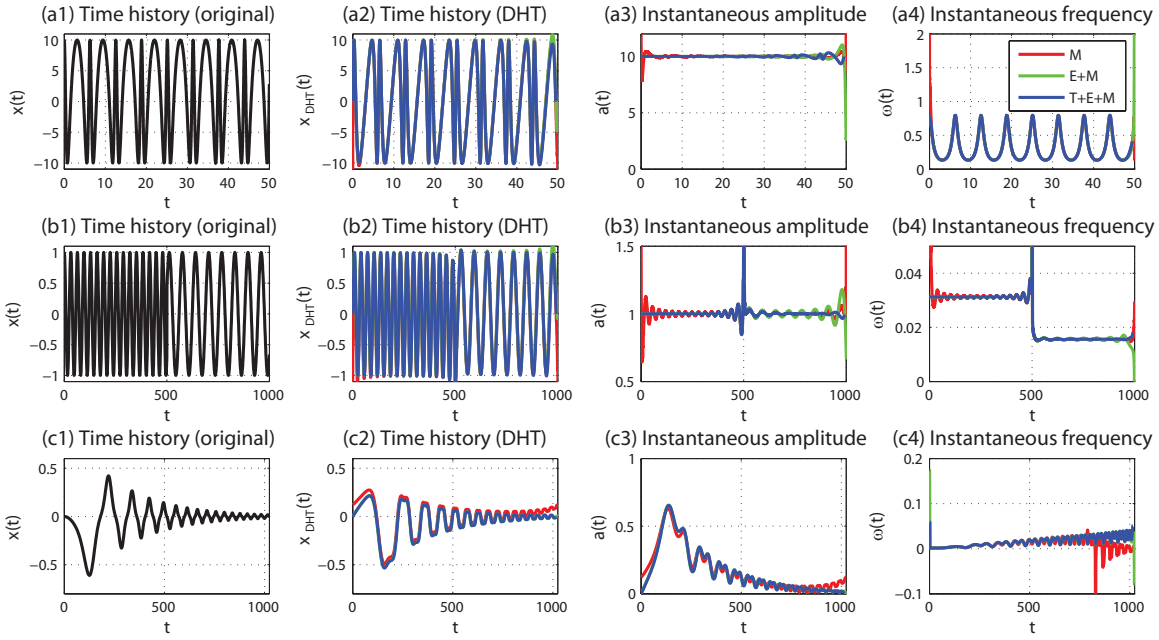

Figure 2.8: Comparisons for the second set of case studies by using the three different options in executing DHT, where "M", "E+M", and "T+E+M" stand for using the Marple's DHT algorithm only, using the Marple's DHT algorithm with the proposed even extension, and using the Marple's DHT algorithm with the proposed local extrema trimming and even extension, respectively. Case (a) is adopted from [66], where $x(t) = 10\cos\left(2t + 2\arctan\frac{\sin t}{2-\cos t} + 2\arctan\frac{\sin t}{3-\cos t}\right)$ with sampling frequency 100Hz. Case (b) is a frequency shift cosine wave adopted from Fig. 24 in reference [44]. Case (c) is damped Duffing wave with chirp frequency adopted from [45], where $x[n] = e^{-n/256}\cos(\pi/64\,(n^2/512+32) + 0.3\sin(\pi/32\,(n^2/512+32))$ with $n = 0, 1, \cdots, 1024$. Disclaimer: Panels (a3), (a4), (b2), (b3), (b4) and (c4) are zoomed-in views such that not all points are shown.

2.6 Conclusion

Motivated by applications of HT in vibration signal analysis, two delicate and critical numerical details that can make the Marple's DHT algorithm more robust for processing vibrations with multiple cycles of oscillations have been proposed, justified and validated in this chapter. The proposed two add-on numerical procedures (to be used in conjunction with the Marple's DHT algorithm) enable wider acceptance and more successful practice of DHT in similar engineering practice and more. Two major DHT algorithms have been thoroughly examined with mathematical equivalence established between them, which helps improve understanding and utilization of these powerful algorithms in the DSP community. An additional formula for the situation involving odd-numbered signal length has also been derived for one of these algorithms. In addition to validations using two sets of numerical case studies, quantities analysis of DHT has been carried out whenever possible.

Chapter 3

NOISY BACKBONE: ANALYSIS OF INTERACTION AND SEPARATION OF TWO MONO-COMPONENTS

3.1 Introduction

3.1.1 Background and motivations

The Hilbert transform (HT) has been an important signal processing tool for many years. Among a vast body of HT literature is a technique called "backbone", developed by Dr. Michael Feldman (e.g., [23, 24, 27, 28, 29, 30]), which is of interest to this research topic. Its major utility could be to classify different types of nonlinear behavior underlying a dynamical system's response via the backbone, which is a mapping between the instantaneous amplitude and instantaneous frequency. Both of these instantaneous quantities are obtained from the system's response signal via the HT; the backbone's profile is the key to system identification. For example, a linear

single-degree-of-freedom (SDOF) system possesses a straight vertical backbone, while a hardening or softening Duffing oscillator has a backbone bending to the right or left, respectively. This technique has the potential for being a classifier with efficiency in time and labor cost for an unknown dynamical system using outputs only.

[23] illustrates the capability of the backbone technique for identifying many types of nonlinearity of SDOF models including but not necessarily limited to nonlinear spring models (such as hardening, softening, backlash, pre-compressed strings, bilinear, or impact), and nonlinear damping models (frequency-dependent or frequency-independent). However, when this technique was applied in a naive manner, [46] encountered very "noisy" backbones. Indeed similar "noisy" backbones had appeared (unnoticed by us) much earlier in Figs. 2, 6 and 10 of [32]. Causes and remedies for such "noisy" backbones motivated this study (not signal decomposition methods). It was a long journey through classical HT literature, while exercising mathematical, physical and numerical reasoning, which shed light on this issue. By making this contribution, we hope to complement a part of Dr. Feldman's work.

3.1.2 Technical challenge, significance and structure of this chapter

We shall show that, at least, some of the noise is not entirely an accident or a mistake. Rather, it could be due to the inherent nature of signals or even the technique itself. In particular, two mono-components in a response can interact and lead to oscillatory behavior in the backbone of their sum signal, thus appearing to be noise. It will also be shown that this so-called "noise" is useful when decomposing such double-component signals. As part of this study, a key formula for computing the instantaneous frequency of a double-component signal is revised. In addition, a key integral formula in reference [27] is revised. These would be the major contributions of this study. We highlight here that signal decomposition is neither the motivation

nor the primary focus of this study. The main purpose is to exercise quantitative analysis to understand and resolve the "noisy" backbone issue, formulated here as a certain type of double-component signal.

A suite of commonly seen signals will be studied in this chapter. They include pure harmonics, frequency-modulated (FM) harmonics (called chirps), amplitude-modulated (AM) harmonics, and amplitude-modulated frequency-modulated (AM-FM) harmonics. To enable analysis, it is essential to obtain the instantaneous characteristics of these signals, hence Hilbert transform needs to be applied. Although Bedrosian's identity ([4]) is a powerful tool that greatly simplifies computations of the Hilbert transform of products, it has a strict condition on signals not covering most cases to be studied here. Therefore, to be consistent, discrete Hilbert transform, DHT, is employed for all case studies in this chapter. The subtlety and numerical treatment of DHT has be addressed in Chapter 2.

The structure of the rest of this chapter is as follows. In Chapter 3.2, key concepts are reviewed with a focus on the motivation for their definitions and subtleties involved. Feldman's backbone is formally introduced, where a definition is presented based on the author's understanding of his work. Two key formulas in Feldman's series of publications concerning interactions of two mono-component signals are given. In Chapter 3.3, results from several case studies are presented with a focus on how two relatively simple backbones, each of which is from a mono-component signal, can produce a backbone that is much more complicated after the two signals have been summed. Chapter 3.4 gives an in-depth treatment of several theoretical issues involved in the backbone of the sum of two mono-component signals. Chapter 3.4 also presents a signal decomposition procedure and some preliminary simulation results in Chapter 3.4.6. Given the focus of this chapter on noisy backbones, Chapter 3.4.6 only sketches the proposed signal decomposition technique which needs to be further developed and extensively validated. Finally, discussions and conclusions are

given in Chapters 3.5 and 3.6, respectively. E to H contain supporting proofs and/or explanations developed in this work.

3.2 Literature Review

3.2.1 Analytic signal and Hilbert transform

Concepts to be reviewed in this and next subsections are fairly well known; however, physical meaning and mathematical reasoning associated with these concepts are subtle and fraught with ambiguities as pointed out in reference [17] and discussed in reference [38] and [16].

A well-known concept is that starting from a real signal $x(t)$, we can construct a unique complex signal $z(t)$. Originally proposed in [35] and based on the Hilbert transform, it is nowadays called the *analytic signal* (AS) corresponding to $x(t)$:

$$z(t) \;=\; x(t) + j\tilde{x}(t), \text{ with } \tilde{x}(t) \;=\; \mathcal{H}[x(t)] \tag{3.1}$$

where $j = \sqrt{-1}$ is the imaginary unit. $\mathcal{H}[\cdot]$ denotes the Hilbert transform operator, and the alternative notation $\tilde{x}(t)$ is used here for convenience.

The Hilbert transform of $x(t)$ is the time convolution of $x(t)$ with $\frac{1}{\pi t}$ (e.g., Eq. (1.9) on pp. 4 in reference [37]):

$$\tilde{x}(t) \;=\; x(t) * \frac{1}{\pi t} \;=\; \frac{1}{\pi} P \int_{-\infty}^{\infty} \frac{x(\tau)}{t-\tau} d\tau \tag{3.2}$$

where $x(t)$ and $\tilde{x}(t)$ are the original and transformed signals, respectively. Due to the singularity of the integrand at $\tau = t$, the integral in Eq. (3.2) is defined as an improper integral in the sense of the Cauchy principal value, denoted by P (e.g., Eq. (1.8) on pp. 4 in reference [37]). Directly relevant to this study, an important property of the Hilbert transform operator $\mathcal{H}[\cdot]$ is that it is linear ([37]).

An analytic signal can also be expressed in unique polar form as follows (e.g., Eq. (15b) on pp. 522 in reference [5]):

$$z(t) \;=\; \mathfrak{a}(t)e^{j\phi(t)} \tag{3.3}$$

where $\mathfrak{a}(t)$ and $\phi(t)$ are called, respectively, the *instantaneous amplitude* and *instantaneous phase* of $z(t)$. Different definitions for instantaneous amplitude and phase exist as pointed out in reference [17]; not to cause any confusion to the readers, we stick to one of the well-accepted definitions where instantaneous amplitude is restricted to be non-negative. A pair of polar functions $[\mathfrak{a}(t),\ \phi(t)]$ corresponding to an analytic signal is referred to as a *canonical pair* (e.g., [65], [7]). After matching real and imaginary parts of $z(t)$ in Eqs. (3.1) and (3.3), we can form the following four real equations:

$$x(t) \;=\; \mathfrak{a}(t)\cos\phi(t) \tag{3.4}$$

$$\tilde{x}(t) \;=\; \mathfrak{a}(t)\sin\phi(t) \tag{3.5}$$

$$\mathfrak{a}(t) \;=\; \sqrt{x^2(t)+\tilde{x}^2(t)} \tag{3.6}$$

$$\phi(t) \;=\; \arctan\frac{\tilde{x}(t)}{x(t)} \;+n(t)\pi, \quad \text{unwrapped phase} \tag{3.7}$$

Therefore for a canonical pair, it is clear from Eqs. (3.4) and (3.5) that

$$\mathcal{H}[\mathfrak{a}(t)\cos\phi(t)] \;=\; \mathfrak{a}(t)\sin\phi(t) \tag{3.8}$$

What needs to be emphasized here is that Eq. (3.8) is *not* a direct outcome of Bedrosian's identity, i.e., $\mathcal{H}[\mathfrak{a}(t)\cos\phi(t)] \;=\; \mathfrak{a}(t)\mathcal{H}[\cos\phi(t)]$ when comparatively $\mathfrak{a}(t)$ is a lower-frequency signal while $\phi(t)$ is a higher-frequency signal whose spectra do not overlap; furthermore, $\mathcal{H}[\cos\phi(t)]$ is not necessarily $\sin\phi(t)$ as pointed out in [65]. It is worth mentioning that Bedrosian's identity only states a sufficient condition but not a necessary condition. For a signal $x(t)$ written in the form of Eq. (3.4), i.e., $x(t) =$

$f(t)\cos(g(t))$, there are actually infinitely many pairs of $f(t)$ and $g(t)$ corresponding to $x(t)$ [17]. Therefore, Eq. (3.8) does not hold in general, i.e., $\mathcal{H}[f(t)\cos(g(t))] \neq f(t)\sin(g(t))$ in general.

3.2.2 Instantaneous frequency and mono-component signal

A commonly accepted definition of *instantaneous frequency* is that it is the time derivative of the instantaneous phase $\phi(t)$, as shown below (e.g., Eq. (18) on pp. 522 in reference [5]):

$$\omega(t) \;=\; \frac{d\phi(t)}{dt} \tag{3.9}$$

This seemingly straightforward definition can lead to paradoxes. An example from [14] (Example 2.4 on pp. 40-41) vividly demonstrates this situation by presenting a signal that is the sum of two harmonics: $x(t) = \mathfrak{a}_1\cos(\omega_1 t) + \mathfrak{a}_2\cos(\omega_2 t)$, with $\mathfrak{a}_1$ and $\mathfrak{a}_2$ constants, and ω_1 and ω_2 constants and positive and $\omega_1 \neq \omega_2$. Although the original signal contains two constant positive frequencies ω_1 and ω_2, the result from Eq. (3.9) is time-dependent and can even be negative. Even with $\mathfrak{a}_1$ and $\mathfrak{a}_2$ both positive, there are still issues with the instantaneous frequency of $x(t)$; this will be verified in Chapter 3.3.2. In other words, instantaneous frequency for this seemingly simple two-tone signal lacks physical meaning at certain time points or intervals, even though it is mathematically well defined.

To avoid this troublesome issue, [5] argues that instantaneous frequency is physically meaningful only for *mono-component signals*. According to [5] (pp. 527) and [7] (pp. 19), a mono-component signal is characterized in the time-instantaneous frequency domain by a single "ridge", corresponding to an elongated region of energy concentration. Moreover, "the crest of the 'ridge"' being interpreted as "a graph of IF vs. time" needs to be a single-valued function. When expressed as an analytic signal, a mono-component signal takes the form in Eq. (3.3). Eq. (3.8) will be used

in this study as the starting point for proofs in E (the foundation for F and G), where mono-component signals are treated as infinite-length continuous-time signals to facilitate mathematical analysis.

As far as the author is concerned, there is no widely accepted rigorous mathematical definition for mono-component signals. In the process of selecting and/or designing these finite-length discretized signals, we adhere to the guiding principle in reference [5] mentioned above. Other viewpoints regarding mono-component signals, e.g., instantaneous amplitude $\mathfrak{a}(t)$ is real and positive, and instantaneous phase $\phi(t)$ is differentiable and often further required to be monotonically increasing to ensure that its time derivative – the instantaneous frequency – is physically meaningful (see e.g. [66]), have been considered as well.

To extract physically meaningful instantaneous quantities from a *multi-component signal*, i.e., a sum of two or more mono-components, it is needed to first decompose the multi-component signal into a series of mono-components, and study the instantaneous attributes of each component. Nonetheless, we can still try to extract meaningful information from a multi-component signal by looking into its instantaneous characteristics, although the outcome may be physically meaningless.

The simplest multi-component signal would be the case of a *double-component signal*. For some dynamical systems, a double-component signal could be an acceptable approximation to the system's free vibration response, as long as a third mono-component (and beyond) would be negligible. For example, the free response of a damped hardening Duffing oscillator might have only two clearly separated "ridges" in the short-time Fourier spectrum, as shown in Fig. 3.1. If the two "ridges" could be approximated by two mono-components, then this example indicates that a third mono-component would not contribute significantly to the response energy. Having said this, we will focus on the study of double-component signals in this chapter.

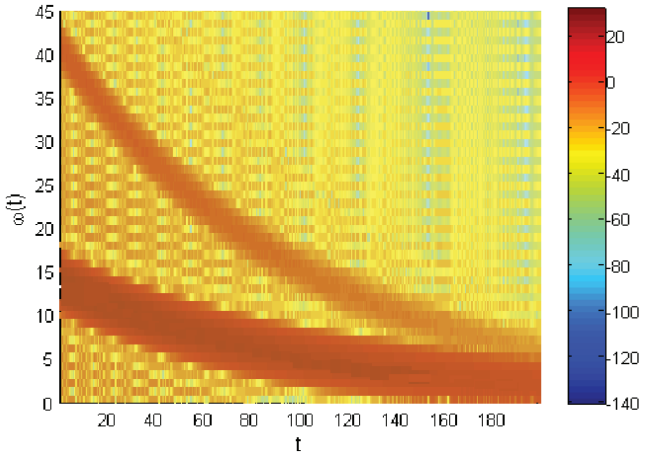

Figure 3.1: The time-frequency distribution (TFD) of the response of Duffing equation $\ddot{x}(t)+0.03\dot{x}(t)+x(t)+x(t)^3=0$ with initial condition $x(0)=100$ and $\dot{x}(0)=0$. TFD plot is obtained by using MATLAB [59] built-in function spectrogram, with parameter values chosen as follows: Hamming window length 256; number of overlapping samples 255; FFT length 512; Fs = 500. The free response is approximated by using MATLAB built-in function ode45.

3.2.3 Feldman's backbone

The backbones to be discussed hereafter are those in Feldman's work, e.g., [23, 29, 30]. A rigorous definition based on the understanding of Feldman's work is proposed: The backbone for a real signal $x(t)$ is the curve $\{(\omega(t),\ \mathfrak{a}(t)) \mid t \geq 0\}$ in the amplitude-frequency plane, where $\mathfrak{a}(t)$ is the instantaneous amplitude and $\omega(t)$ is the instantaneous frequency of the signal $x(t)$, respectively. Although the Hilbert transform is a linear operator on the signal $x(t)$ and thus the analytic signal is too, the backbone is not since it is defined via Eqs. (3.6) and (3.9). The mapping from instantaneous amplitude to instantaneous frequency (or vice versa) is not even necessarily one-to-one, even though a one-to-one mapping would be preferred for applications in vibration analysis. Alternatively, the backbone could be viewed as a projection of a three-dimensional curve $(t,\ \mathfrak{a}(t),\ \omega(t))$ onto the plane of $\mathfrak{a}$ and ω - with t playing an important role in understanding the backbone.

This chapter focuses on the backbone of double-component signals. We will exam-

ine how a backbone is affected when a signal is composed of two mono-components, knowing that the backbone of each component could be as simple as indicated in reference [23].

3.2.4 Original formulas for the Hilbert transform of double-component signal

Considering two mono-component signals with zero initial phases, $x_1(t)$ and $x_2(t)$, their sum, a double-component signal, $x(t) = x_1(t) + x_2(t)$, is given as follows:

$$x(t) = \underbrace{\mathfrak{a}_1(t)\cos\left(\int_0^t \omega_1(\tau)d\tau\right)}_{x_1(t)} + \underbrace{\mathfrak{a}_2(t)\cos\left(\int_0^t \omega_2(\tau)d\tau\right)}_{x_2(t)} \tag{3.10}$$

whose instantaneous amplitude and instantaneous frequency are given in reference [31] (Eqs. (3) and (4) on pp. 700), [25] (Eqs. (14) and (15) on pp. 479), [27] (Eq. (2) on pp. 520), [28] (pp. 957), [30] (Eq. (35) on pp. 772), and [29] (Eqs. (4.8) and (4.9) on pp. 51; Eq. (5.2) on pp. 62), with no proof, as follows:

$$\mathfrak{a}^2(t) = \mathfrak{a}_1^2(t) + \mathfrak{a}_2^2(t) + 2\mathfrak{a}_1(t)\mathfrak{a}_2(t)\cos\left(\int_0^t (\omega_2(\tau) - \omega_1(\tau))d\tau\right) \tag{3.11}$$

$$\omega(t) = \omega_1(t) + \frac{[\omega_2(t) - \omega_1(t)]\left[\mathfrak{a}_2^2(t) + \mathfrak{a}_1(t)\mathfrak{a}_2(t)\cos\left(\int_0^t(\omega_2(\tau) - \omega_1(\tau))d\tau\right)\right]}{\mathfrak{a}^2(t)} \tag{3.12}$$

Similar formulas with $\mathfrak{a}_1$ and $\mathfrak{a}_2$ constants are stated in [14] (Eqs. (2.80) and (2.81) on pp. 40), which are applied to two harmonics. E provides a derivation of Eqs. (3.11) and (3.12) based on canonical pairs, the latter of which results in a different formula that will be introduced and discussed in Chapter 3.4.3.

3.3 Case Studies

3.3.1 Overview of case studies

A collection of double-component signals will be investigated hereafter, most of which might mimic approximated solutions to SDOF dynamical systems. DHT is performed to obtain the Hilbert transform of a given signal in all six cases as shown in Table 3.1. All signals are qualified as mono-component signals in the sense of [5]; see Fig. 3.2 for typical concentrated instantaneous frequency "ridge" in every signal. However, the $f_i(t)$ and $g_i(t)$ as shown in Table 3.1 are only for simplicity of presentation; they do not form canonical pairs except for Case 1. Two requirements on the relationship between the instantaneous quantities of each case is that (e.g., Eq. (5.2) on pp. 62 in reference [29]):

$$\mathfrak{a}_1(t) \ > \mathfrak{a}_2(t), \ \forall t > 0 \tag{3.13}$$

$$\omega_1(t) \ < \omega_2(t), \ \forall t > 0 \tag{3.14}$$

Table 3.1: Overview of case studies. † $x(t)$ in Case 1 is an approximate solution of $\ddot{x}(t) + x(t) + x^3(t) = 0$ with $x(0) = 1, \dot{x}(0) = 0$.

ID	Mono-component $x(t) = \sum_{i=1}^{2} f_i(t) \cos(g_i(t))$			Parameter values adopted
		$f_i(t)$	$g_i(t)$	
1	pure sinusoid †	$\mathfrak{a}_i$	$\omega_i t$	$\begin{cases} a_1 = 0.9820,\ \omega_1 = 1.3180 \\ a_2 = 0.01796,\ \omega_2 = 3.9539 \end{cases}$
2	FM signal	$\bar{a}_i$	$\bar{\omega}_i t + \frac{\rho_i t^2}{2}$	$\begin{cases} \bar{a}_1 = 10,\ \bar{\omega}_1 = 1,\ \rho_1 = 0.05 \\ \bar{a}_2 = 2,\ \bar{\omega}_2 = 3,\ \rho_2 = 0.05 \end{cases}$
3	AM signal	$\bar{a}_i \cos\left(\bar{\omega}_i^f t\right) + \bar{a}_i^f$	$\bar{\omega}_i^g t$	$\begin{cases} \bar{a}_1 = 10,\ \bar{\omega}_1^f = 0.3,\ \bar{a}_1^f = 20,\ \bar{\omega}_1^g = 2 \\ \bar{a}_2 = 2,\ \bar{\omega}_2^f = 1,\ \bar{a}_2^f = 3,\ \bar{\omega}_2^g = 6 \end{cases}$
4	exponentially decaying sinusoid	$\bar{a}_i e^{-\alpha_i t}$	$\bar{\omega}_i t$	$\begin{cases} \bar{a}_1 = 10,\ \alpha_1 = 0.05,\ \bar{\omega}_1 = 1 \\ \bar{a}_2 = 2,\ \alpha_2 = 0.05,\ \bar{\omega}_2 = 3 \end{cases}$
5	AM-FM signal - 1	$\bar{a}_i e^{-\alpha_i t}$	$\bar{\omega}_i t + \frac{\rho_i t^2}{2}$	$\begin{cases} \bar{a}_1 = 10,\ \alpha_1 = 0.1,\ \bar{\omega}_1 = 1,\ \rho_1 = 0.05 \\ \bar{a}_2 = 2,\ \alpha_2 = 0.2,\ \bar{\omega}_2 = 3,\ \rho_2 = 0.05 \end{cases}$
6	AM-FM signal - 2	$\bar{a}_i e^{-\alpha_i t}$	$\bar{\omega}_i t + \gamma_i e^{\rho_i t}$	$\begin{cases} \bar{a}_1 = 10, \alpha_1 = 0.05, \bar{\omega}_1 = 1, \\ \quad \rho_1 = -0.3,\ \gamma_1 = -1.5 \\ \bar{a}_2 = 2,\ \alpha_2 = 0.1,\ \bar{\omega}_2 = 3, \\ \quad \rho_2 = -0.3,\ \gamma_2 = -5 \end{cases}$

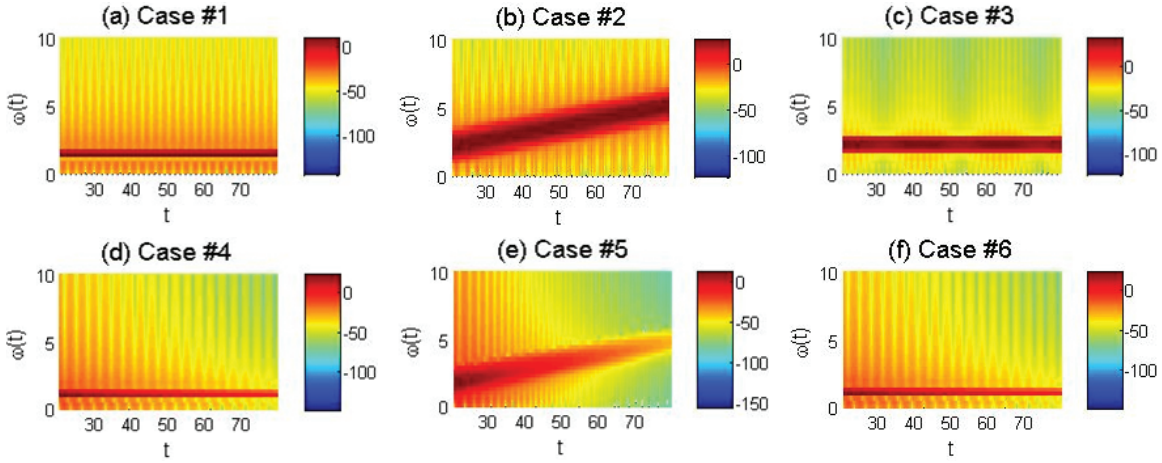

Figure 3.2: The time-frequency distribution (TFD) of the first mono-component, $x_1(t)$, of all six case studies, while that of the second mono-component, $x_2(t)$, of six case studies is similar. TFD plot is obtained by using MATLAB built-in function spectrogram, with parameter values chosen as follows: Hamming window length 2048; number of overlapping samples 2047; FFT length 1024; Fs = 50.

3.3.2 Case study #1: summation of two harmonics

To start simple, $\mathfrak{a}_1$, $\mathfrak{a}_2$, ω_1 and ω_2 are all constants for the first case study. Consequently, the backbone of either $x_1(t)$ or $x_2(t)$ is a single point. The backbone of

$x(t) = x_1(t) + x_2(t)$, however, is not as simple. Time histories of the first 25 seconds can be found in Fig. 3.3 (a) for all signals, i.e., $x(t)$, $x_1(t)$ and $x_2(t)$, (b) for their instantaneous amplitudes, and (c) for their instantaneous frequencies, while all backbones based on 50 seconds of a full length signal can be found in Fig. 3.3(d). Also in Panel (c) of Fig. 3.3 is a mathematical quantity $\hat{\omega}(t)$ defined as the difference between the instantaneous frequency of the sum signal and the first mono-component:

$$\hat{\omega}(t) \;=\; \omega(t) - \omega_1(t) \tag{3.15}$$

This introduced mathematical quantity is important to this study and will be analyzed in Chapter 3.4.7. The design of Fig. 3.3 will be repeated in Figs. 3.5 to 3.9 for Cases #2 to #6.

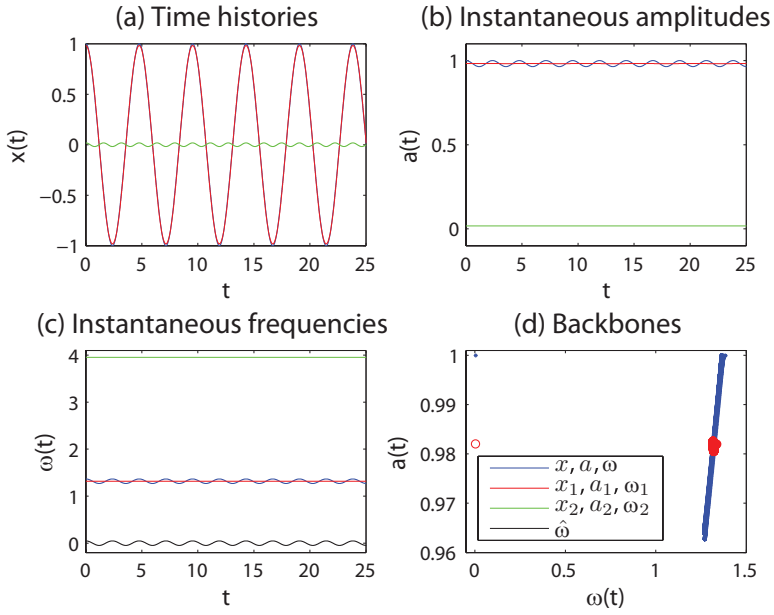

Figure 3.3: Case #1: Summation of two harmonics, where $x_1(t) = 0.9820\cos(1.3180t)$ and $x_2(t) = 0.01796\cos(3.9539t)$ as given in Table 3.1. This is an approximated response of an undamped Duffing equation $\ddot{x}(t) + x(t) + x^3(t) = 0$ with $x(0) = 1$ and $\dot{x}(0) = 0$. Legend follows the same manner in Figs. 3.6- 3.9 and is thus omitted hereafter.

Fig. 3.4 duplicates the results in Fig. 3.3 without using DHT based on the fact that

$f_i(t)$ and $g_i(t)$ (with $i = 1, 2$) form canonical pairs for this case. In other words, Fig. 3.4 depicts the ideal Fig. 3.3, which would result for the infinite-length continuous-time signal. To gain more insights into this case, the instantaneous frequency of the sum signal, by definition, is (as will be elaborated later in Chapter 3.4.3):

$$\omega(t) = \frac{\omega_1 + \omega_2}{2} - \frac{(\omega_2 - \omega_1)(\mathfrak{a}_1^2 - \mathfrak{a}_2^2)}{2} \frac{1}{\mathfrak{a}^2(t)} \tag{3.16}$$

Eq. (3.16) represents a mapping from $\mathfrak{a}(t)$ to $\omega(t)$ in a polynomial with a negative exponent. Deviations from ideal results are most obvious in the backbone of the double-component signal (enlarged in (d)). The errors in Fig. 3.3 are mainly attributable to the end effect (finite length of time) of the DHT. Fig. 3.4 clearly illustrates the transition of the backbones from two points to one curve - without the disruption caused by the end effect. Unfortunately, such errors exist to varying degrees for all six cases. The focus is mainly on the body of the backbones rather than the two ends when we are trying to understand how mixing two mono-components affects the backbone.

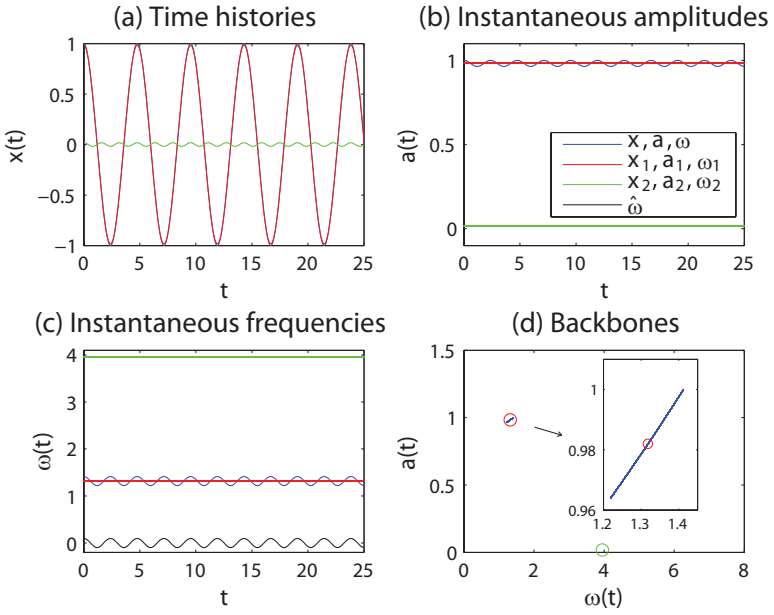

Figure 3.4: A duplicate of Fig. 3.3 without using DHT.

The transition from two points to one curve is interesting; either point does not seem easy to be recovered from the curve directly. However, this recovery can be done effectively when the proposed decomposition method is applied, which will be given in detail later.

Equation (3.16) can also be utilized to examine the sign of the instantaneous frequency of such a double-component signal. Suppose we would like to find the necessary and sufficient condition for $\omega(t)$ in Eq. (3.16) to be negative, meaning that the following inequality holds for at least one time instance t_s:

$$\frac{\omega_1+\omega_2}{2}-\frac{(\omega_2-\omega_1)(\mathfrak{a}_1^2-\mathfrak{a}_2^2)}{2}\frac{1}{\mathfrak{a}^2(t_s)} \;<\; 0 \tag{3.17}$$

which leads to

$$\omega_1\mathfrak{a}_1^2+\omega_2\mathfrak{a}_2^2 \;<\; (\omega_1+\omega_2)\mathfrak{a}_1\mathfrak{a}_2 \tag{3.18}$$

Without losing generality, we can assume $\mathfrak{a}_1 > \mathfrak{a}_2$ and eventually obtain a necessary and sufficient condition:

$$\omega_1\mathfrak{a}_1 \;<\; \omega_2\mathfrak{a}_2, \text{ (with } \mathfrak{a}_1 > \mathfrak{a}_2) \tag{3.19}$$

3.3.3 Case study #2: summation of two linear chirps

Figure 3.5 presents the behavior of two linear chirps and their sum. Observations are made as follows:

Panel (b): $\mathfrak{a}(t)$ centers around $\bar{a}_1$ and fluctuates within $[\bar{a}_1-\bar{a}_2, \bar{a}_1+\bar{a}_2]$.

Panel (c): Similarly, $\omega(t)$ oscillates around $\omega_1(t)$, i.e., $\omega(t)-\omega_1(t)$ in Eq. (3.15), seems to vary between some positive and negative values almost periodically. In fact, a signal decomposition method called Hilbert vibration decomposition ([27]), HVD, is a vivid application of this property. Nonetheless,

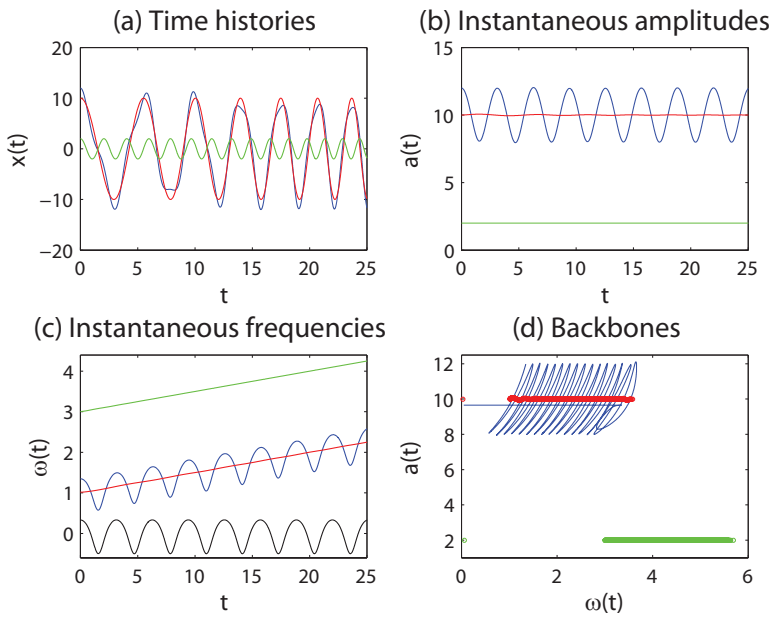

Figure 3.5: Case #2: Summation of two linear chirps, where $x_1(t) = 10\cos(1t + \frac{0.05t^2}{2})$ and $x_2(t) = 2\cos(3t + \frac{0.05t^2}{2})$ as given in Table 3.1.

observations are not rigorous proofs/analyses. The theoretical study will be carried out in Chapter 3.4.

Panel (d): The backbone of $x(t)$ fluctuates around the horizontal line segment corresponding to the backbone of $x_1(t)$, and could be considered noisy. Even though the backbone of the mono-component signals displays a trend of a horizontal line (as it would intuitively).

3.3.4 Case study #3: summation of two amplitude modulated (AM) signals

Figure 3.6 presents the behavior of two AM signals and their sum. Similar observations are made as before; however, the profile of the backbone of $x(t)$ does not seem regular. This case study sets a standard for the proposed theoretical study: this seemingly irregular case should be able to be comprehended.

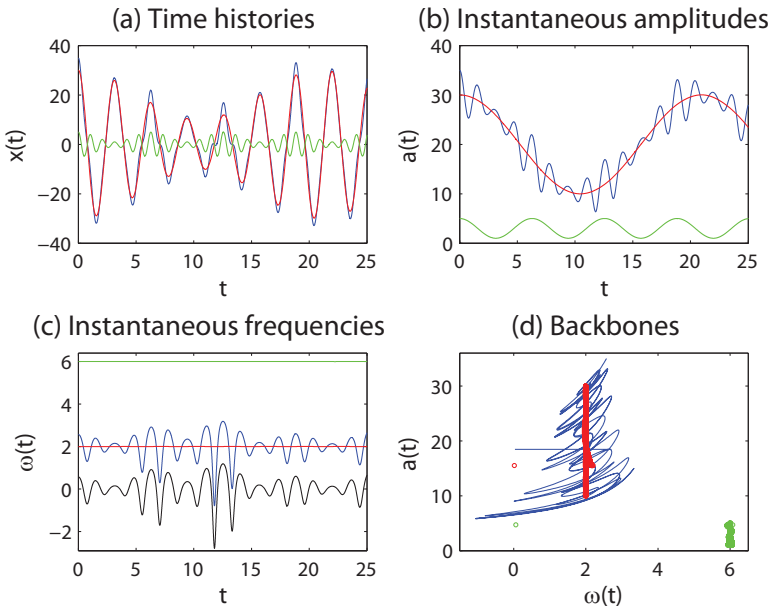

Figure 3.6: Case #3: Summation of two amplitude modulated sinusoids, where $x_1(t) = (20 + 10\cos(0.3t))\cos(2t)$, and $x_2(t) = (3 + 2\cos(1t))\cos(6t)$ as given in Table 3.1.

3.3.5 Case study #4: summation of two LTI SDOF responses

To mimic the free response of a simple beam being modeled as a lumped mass at mid-span, the beam's first and third modes would be dominant that can be represented by using a double-component signal, we may have $\mathfrak{a}_2(t) < \mathfrak{a}_1(t)$ and $\omega_2(t) > \omega_1(t)$ for all t to follow the conditions specified in Eqs. (3.13) and (3.14). Taking $x_1(t) = 10e^{-0.01t}\cos(1t)$ and $x_2(t) = 5e^{-0.015t}\cos(3t)$ as an example, the analysis is given in Fig. 3.7. Similar observations are made as for Cases #2 except that the individual backbones should be vertical here.

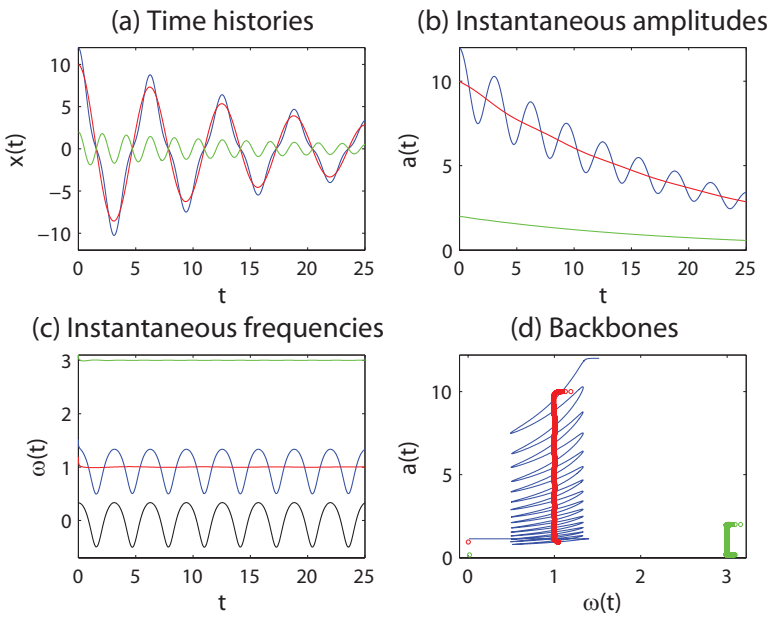

Figure 3.7: Case #4: Summation of two exponentially decaying sinusoids, where $x_1(t) = 10e^{-0.05t}\cos(1t)$ and $x_2(t) = 2e^{-0.05t}\cos(3t)$ as given in Table 3.1.

3.3.6 Case studies #5 and #6: summation of two amplitude modulated and frequency modulated (AM-FM) signals

Two different kinds of AM-FM signals are studied in Figs. 3.8 and 3.9, where the first is a summation of two exponentially decaying sweeping-up linear chirps while the second is a summation of two exponentially decaying sweeping-down exponential chirps. See Table 3.1 for their expressions. These two cases are designed to mimic different bending behaviors of backbones; however, these two cases do not replicate softening and hardening Duffing oscillators. Similar observations can be made as before, which further confirms a need for a theoretical study.

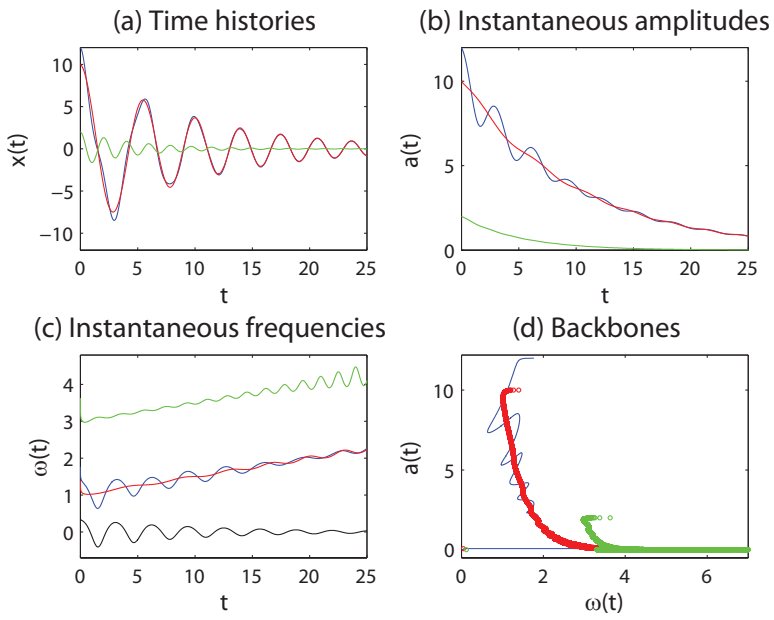

Figure 3.8: Case #5: Summation of two exponentially decaying sweeping-up linear chirps, where $x_1(t) = 10e^{-0.1t}\cos(1t + \frac{0.05t^2}{2})$, and $x_2(t) = 2e^{-0.2t}\cos(3t + \frac{0.05t^2}{2})$ as given in Table 3.1.

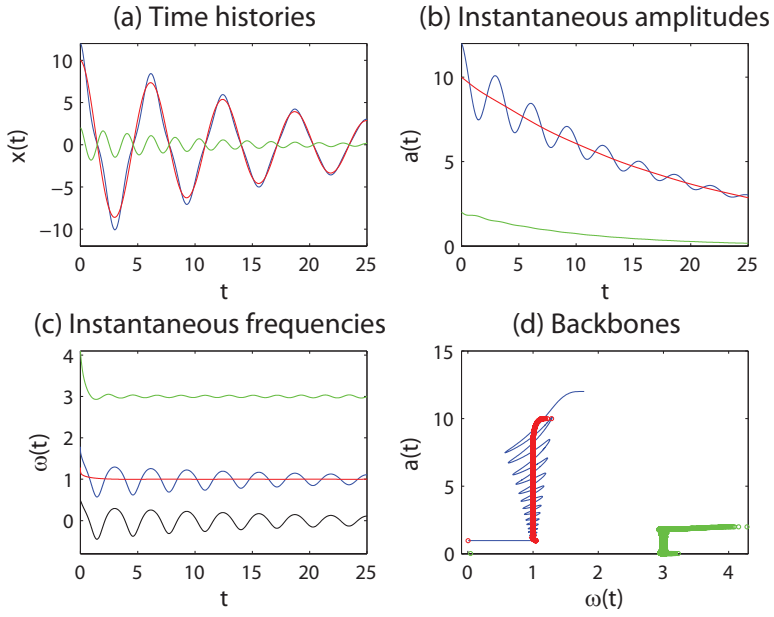

Figure 3.9: Case #6: Summation of two exponentially decaying sweeping-down exponential chirps, where $x_1(t) = 10e^{-0.05t}\cos(1t - 1.5e^{-0.3t})$, and $x_2(t) = 2e^{-0.1t}\cos(3t - 5e^{-0.3t})$ as given in Table 3.1.

3.4 Theoretical Issues

Theoretical issues related to double-component signals are discussed herein referring back to the case studies presented above. This is to confirm and generalize the observations in these case studies for more quantitative relations and eventually, for a new signal decomposition method. Attention will be paid first and foremost to the time histories of instantaneous parameters: instantaneous amplitude $\mathfrak{a}(t)$, instantaneous phase $\phi(t)$, and instantaneous frequency $\omega(t)$. This is because first, as mentioned previously, the backbone is a mapping from $\omega(t)$ to $a(t)$ or $a(t)$ to $\omega(t)$ after all. Given the definition in Eq. (3.9), we feel it necessary to examine $\phi(t)$ in order to understand $\omega(t)$, which turns out to be a beneficial strategy.

To start, two mono-component signals, $x_1(t)$, $x_2(t)$, and their sum (a double-component signal), $x(t)$, can be denoted as follows following Eq. (3.1):

$$\begin{aligned} z_1(t) &= x_1(t) + j\tilde{x}_1(t), \quad z_2(t) = x_2(t) + j\tilde{x}_2(t), \\ \underbrace{z_1(t) + z_2(t)}_{z(t)} &= \underbrace{x_1(t) + x_2(t)}_{x(t)} + j\underbrace{[\tilde{x}_1(t) + \tilde{x}_2(t)]}_{\tilde{x}(t)} \end{aligned} \tag{3.20}$$

where $z_1(t)$, $z_2(t)$ and $z(t)$ are the analytic signal of $x_1(t)$, $x_2(t)$ and $x(t)$, respectively, while $\tilde{x}_1(t)$, $\tilde{x}_2(t)$ and $\tilde{x}(t)$ are the corresponding Hilbert transforms.

3.4.1 Assumptions

In this study, the following assumptions are made:

Assumption #1 $\mathfrak{a}_1(t) > \mathfrak{a}_2(t)$ and $\omega_1(t) < \omega_2(t)$, $\forall t$, which are Eqs. (3.13) and (3.14). This assumption is adopted from [27, 30] and [29] (pp. 62) and applied throughout this chapter.

Assumption #2 $\mathfrak{a}_i(t)$ and $\omega_i(t)$'s are all slow varying for $i = 1, 2$, adopted from [30] (pp. 746). This assumption is applied whenever specified in this

section. This assumption is interpreted as $\mathfrak{a}_i(t)$ and $\omega_i(t)$'s first and second time derivatives being negligible.

3.4.2 Vector representation

In a Cartesian coordinate system for analytic signal, $z_1(t)$, $z_2(t)$ and $z(t)$ can be depicted in Fig. 3.10 by vectors $\overrightarrow{OA}$, $\overrightarrow{OB}$, and $\overrightarrow{OC}$, respectively. In this representation, the angle with respect to the real axis and the length of a vector are *wrapped phase* and instantaneous amplitude of an analytic signal, respectively. *Unwrapped phase* would be the corresponding wrapped phase plus a multiple of 2π's depending on how many full cycles the vector has rotated at time t as given in Eq. (3.7).

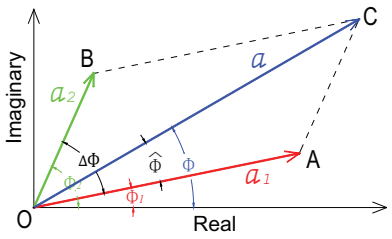

Figure 3.10: Analytic signals in complex coordinate plane for an arbitrary time instance t, where $\overrightarrow{OA}$, $\overrightarrow{OB}$ and $\overrightarrow{OC}$ depict the analytic signals $z_1(t)$, $z_2(t)$ and $z(t)$, respectively.

Applying the assumptions in Chapter 3.4.1, Fig. 3.11 illustrates a typical rotation cycle involving $z_1(t)$, $z_2(t)$ and $z(t)$ with an additional assumption that $z_1(t)$ and $z_2(t)$ start off with no difference in wrapped phase and they both happen to be on the real axis - as shown in Panel (a). Time instances corresponding to Panels (a), (c) and (e) are of particular interest, when $z_1(t)$ and $z_2(t)$ are in phase, antiphase, and in phase again. To capture these special moments, a mapping will be introduced shortly.

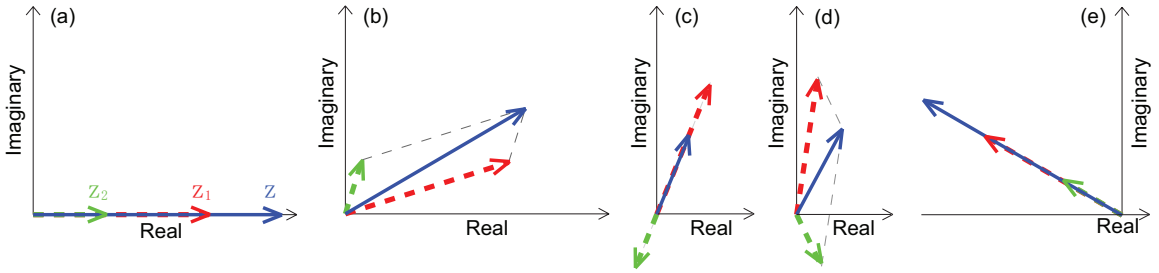

Figure 3.11: Evolution of $z_1(t)$, $z_2(t)$ and $z(t)$ with time. Time increases gradually from Panels (a) to (e). As will be shown in Chapter 3.4.4, (a) $t = t_0 = 0$, (c): $t = t_1$, and (e): $t = t_2$.

3.4.3 Revised formulas for the Hilbert transform of double-component signal

To continue, it is first necessary for us to get back to the two key formulas in Eq. (3.11) and (3.12). It is discovered in this study that Eq. (3.12) is not accurate in general. A more accurate formula is developed in E and presented below:

$$\omega(t) \ = \omega_1(t) + \hat{\omega}(t) \tag{3.21}$$

with

$$\hat{\omega}(t) \ = \ \frac{[\mathfrak{a}_2^2(t) + \mathfrak{a}_1(t)\mathfrak{a}_2(t)\cos\Delta\phi(t)]}{\mathfrak{a}^2(t)}\Delta\omega(t) + \frac{\mathfrak{a}_1(t)\dot{\mathfrak{a}}_2(t) - \dot{\mathfrak{a}}_1(t)\mathfrak{a}_2(t)}{\mathfrak{a}^2(t)}\sin\Delta\phi(t) \tag{3.22}$$

where

$$\Delta\phi(t) \ = \ \phi_2(t) - \phi_1(t), \ \text{with} \ \phi_i(t) \ = \ \int_0^t \omega_i(\tau)d\tau + \varphi_i, \ \text{for} \ i = 1, 2 \tag{3.23}$$

$$\Delta\omega(t) \ = \ \omega_2(t) - \omega_1(t) \tag{3.24}$$

Equations (3.21) and (3.22) simplify to Eq. (3.12) when the following condition is met:

$$\mathfrak{a}_1(t)\dot{\mathfrak{a}}_2(t) - \dot{\mathfrak{a}}_1(t)\mathfrak{a}_2(t) \;=\; 0 \tag{3.25}$$

which is not always satisfied. Therefore, Eq. (3.12) is only an approximation of Eqs. (3.21) and (3.22).

3.4.4 Time indices

A mapping

$$f : n \mapsto t_n, \text{ with } n \in \mathbb{N}^0 \tag{3.26}$$

is defined such that

$$\Delta\phi(t_{n+1}) - \Delta\phi(t_n) \;=\; \pi \tag{3.27}$$

where $\Delta\phi(t)$ is defined in Eq. (3.23). The mapping f is well-defined once the initial time instance t_0 is fixed, which will be done shortly after.

Time instance t_n has a clear physical interpretation: From t_n to t_{n+1}, $\Delta\phi(t)$, the phase difference between $\vec{z}_2(t)$ and $\vec{z}_1(t)$, is increased by π. In Fig. 3.11, t_n's with $n = 0$, 1, and 2 correspond to the time instances when the three vectors $\vec{z}_1(t_n)$, $\vec{z}_2(t_n)$ and $\vec{z}(t_n)$ line up, i.e., in Panels (a), (c) or (e) at $t = t_0$, $t = t_1$, and $t = t_2$, respectively. $\vec{z}_2(t)$ rotates π more than $\vec{z}_1(t)$ from t_n to t_{n+1}.

The innovation in this study depends heavily on the introduction of both t_n and $\Delta\phi(t_n)$, while a quantitative expression for $\Delta\phi(t_n)$ is not in place yet because Fig. 3.11 is only a special case contrasting with a more general situation when $\vec{z}_1(t_0)$ and $\vec{z}_2(t_0)$ do not line up. That is, $\phi_1(t_0) \neq \phi_2(t_0)$ when $t_0 = 0$. To address this challenge, the starting point t_0 needs a more careful definition. We choose not to define $t_0 = 0$ in general. Rather, t_0 is defined as the time instance when the two vectors $\vec{z}_1(t)$ and $\vec{z}_2(t)$ are rotated to an angle such that they both line up and point to the same direction

for *the first time*. In other words, t_0 should satisfy the following equation:

$$\Delta\phi(t_0) \;=\; \begin{cases} 0, & \text{if} \quad \varphi_1 \geq \varphi_2 \\ 2\pi, & \text{if} \quad \varphi_1 < \varphi_2 \end{cases} \tag{3.28}$$

where φ_1 and φ_2 are the initial phases of $z_1(t)$ and $z_2(t)$, respectively. When $\varphi_1 = \varphi_2 = 0$, $t_0 = 0$ is obtained as shown in Fig. 3.11(a).

Combining Eqs. (3.27) and (3.28) yields the following non-iterative formula:

$$\Delta\phi(t_n) = \begin{cases} n\pi \;+\; 0, & \text{if} \quad \varphi_1 \geq \varphi_2 \\ n\pi \;+\; 2\pi, & \text{if} \quad \varphi_1 < \varphi_2 \end{cases} \tag{3.29}$$

Figure 3.12(a) illustrates an important property, for $n \in \mathbb{N}^0$, $\vec{z}(t)$ and $\vec{z}_1(t)$ have the same phase value:

$$\phi(t_n) \;=\; \phi_1(t_n), \quad \forall n \in \mathbb{N}^0 \tag{3.30}$$

This can be justified by applying Assumption #1 and the idea of mathematical induction starting with $\phi(t_0) \;=\; \phi_1(t_0)$; more details are given in F. Since $\phi(t) \in \mathcal{C}$ and $\phi_1(t) \in \mathcal{C}$, $\hat{\phi}(t) \triangleq \phi(t) - \phi_1(t) \in \mathcal{C}$. Given the continuity of $\hat{\phi}(t)$, $\phi(t) - \phi_1(t)$ remains the same sign between t_n and t_{n+1}. Eq. (3.30) lays the foundation for the proposed signal decomposition method.

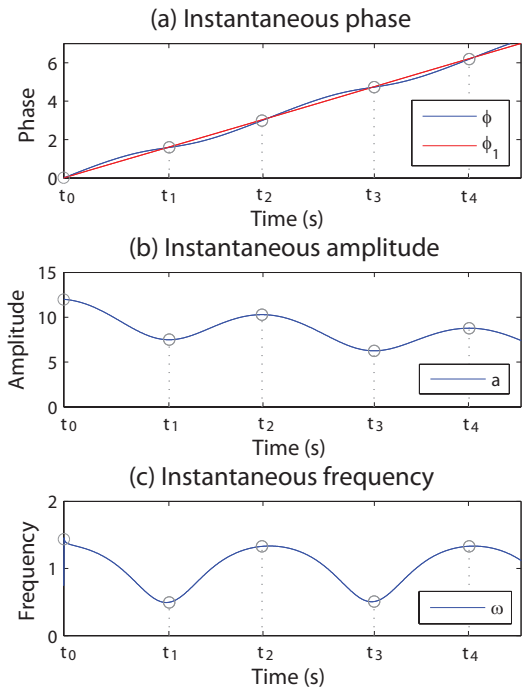

Figure 3.12: A zoom-in view of Case #4, where the two mono-component signals are both exponentially decaying sinusoids. Panel (a) illustrates the relationship between $\phi(t)$ and $\phi_1(t)$. Panels (b) and (c) indicate simultaneous local maxima and minima for $\mathfrak{a}(t)$ and $\omega(t)$ in an approximate sense.

Under Assumptions #1 and #2, G shows that $\mathfrak{a}(t_n)$ and $\omega(t_n)$ reach local extrema simultaneously. This property is illustrated in Fig. 3.12(b) and (c) using one of the case studies presented above, a closer look at which shows that the local extrema of $\mathfrak{a}(t)$ do not exactly line up with the local extrema of $\omega(t)$. This is as expected due to Assumption #2. This approximation also lays the foundation for the proposed signal decomposition method while introducing errors that call for further studies.

3.4.5 Local extrema and bounds

The non-negative integer set $\mathbb{N}^0$ can be divided into two subsets, i.e., the even set $\mathbb{E}$ and odd set $\mathbb{O}$, with $\mathbb{E} = \{0, 2, 4, \ldots\}$, and $\mathbb{O} = \{1, 3, 5, \ldots\}$. Also shown in G, under Assumptions #1 and #2, both $\mathfrak{a}(t)$ and $\omega(t)$ reach their local maxima and minima at t_n when $n \in \mathbb{E}$ and $n \in \mathbb{O}$, respectively. Thus, the two subsets, $\mathbb{E}$ and

$\mathbb{O}$, map to all local maxima and minima of a backbone, respectively. These are the two bounds of the backbone. Unfortunately, there are no closed-form expressions for these bounds. Nonetheless, this property does lead to closed-form expressions for the following instantaneous quantities:

$$\mathfrak{a}(t_n)_{\max} = \mathfrak{a}_1(t_n) + \mathfrak{a}_2(t_n), \quad \forall n \in \mathbb{E} \tag{3.31}$$

$$\mathfrak{a}(t_n)_{\min} = \mathfrak{a}_1(t_n) - \mathfrak{a}_2(t_n), \quad \forall n \in \mathbb{O} \tag{3.32}$$

$$\omega(t_n)_{\max} = \omega_1(t_n) + \frac{\mathfrak{a}_2(t_n)}{\mathfrak{a}_1(t_n) + \mathfrak{a}_2(t_n)} \left(\omega_2(t_n) - \omega_1(t_n)\right), \quad \forall n \in \mathbb{E} \tag{3.33}$$

$$\omega(t_n)_{\min} = \omega_1(t_n) + \frac{-\mathfrak{a}_1(t_n)}{\mathfrak{a}_1(t_n) - \mathfrak{a}_2(t_n)} \left(\omega_2(t_n) - \omega_1(t_n)\right), \quad \forall n \in \mathbb{O} \tag{3.34}$$

where subscripts max and min denote local maxima and minima, respectively. Eqs. (3.31) and (3.32) are obtained by applying Eqs. (G.3) to (E.3), while Eqs. (3.33) and (3.34) are obtained by applying Eqs. (G.3) to (3.21).

For the purpose of developing a signal decomposition method, the instantaneous amplitude of the first and second mono-components can be approximated by using Eqs. (3.31) and (3.32): The summation of these two equations would be $2\mathfrak{a}_1(t)$, while the difference of these two equations would yield $2\mathfrak{a}_2(t)$. This approximation, unfortunately, cannot be directly applied to Eqs. (3.33) and (3.34). It is important to stress that both Assumptions #1 and #2 are applied to this approximation.

3.4.6 Proposed decomposition method

The procedure of the proposed signal decomposition method is given as follows:

1. Perform DHT of a given double-component signal $x(t)$ that satisfies Assumptions #1 and #2 in Chapter 3.4.1 to obtain $\mathfrak{a}(t)$, $\phi(t)$, and $\omega(t)$.

2. Option A: Locate all local maxima and minima of $\mathfrak{a}(t)$; Option B: Locate all local maxima and minima of $\omega(t)$. With either option, all corresponding time

instances form the set of t_n with $n \in \mathbb{N}^0$.

3. Find all $\phi(t_n)$ values corresponding to all t_n. Given Eq. (3.30), these $\phi(t_n)$ will be considered as $\phi_1(t_n)$.

4. If Option A is adopted in Step #2: Curve fit all local maxima and minima of $\mathfrak{a}(t_n)$ for approximated Eqs. (3.31) and (3.32), respectively. If Option B is adopted in Step #2: Locate all local extrema of $\mathfrak{a}(t_n)$ by picking the individual values of $\mathfrak{a}(t_n)$ with t_n obtained in Step 3. Afterwards, curve fit all maxima and minima of $\mathfrak{a}(t_n)$, respectively. Average the two approximated curves for approximated $\mathfrak{a}_1(t)$.

5. Curve fit all $\phi_1(t)$ identified above to approximate $\phi_1(t)$. Note that the instantaneous frequency $\omega_1(t)$ can be obtained by numerically differentiating $\phi_1(t)$.

6. Construct $x_1(t)$ by $x_1(t) \ = \ \mathfrak{a}_1(t)\cos\phi_1(t)$.

7. Obtain $x_2(t)$ by using $x_2(t) \ = \ x(t) - x_1(t)$.

This signal decomposition method is named after "index method" as it relies first on identifying all time instances corresponding to t_n with $n \in \mathbb{N}^0$ through identifying peaks and valleys in $\mathfrak{a}(t)$ or $\omega(t)$. Unfortunately, Step #2 involves approximations thus introducing errors with both options according to Chapter 3.4.5. Another prominent feature of the index method is to rely on the property revealed in Eq. (3.30) to unlock the first component from the sum time history. Eq. (3.30) only involves Assumption #1; however, the execution of Eq. (3.30) under Step #3 receives errors from Step #2.

The index method is tested on all six case studies with results presented in Figs. 3.13 and 3.14 to contrast the exact and approximated $x_1(t)$ and $x_2(t)$, respectively, and in Figs. 3.15 and 3.16 to contrast the original and recovered backbones of each mono-component. The index method would not work well when $\mathfrak{a}(t)$ or $\omega(t)$

stops oscillating, which prevents identifying those t_n's via finding the local maxima and minima in $\mathfrak{a}(t)$ or $\omega(t)$. This limitation is expected and actually shows up in Cases #5 and #6, as shown in Panels (e) and (f) in Fig. 3.14. In Case #5, the extrema of instantaneous amplitude of the sum signal are not obvious approaching the tail as shown in Fig. 3.8(b) leading to not well approximated second mono-components there. In Case #6, this issue is more severe. The approximated first and second mono-components become erroneous starting from around 45 seconds. Fortunately, this issue can potentially be overcome by using $\omega(t)$ to locate the t_n's instead. Improved approximated results are presented in Fig. 3.17 when Option B is chosen in Step #2.

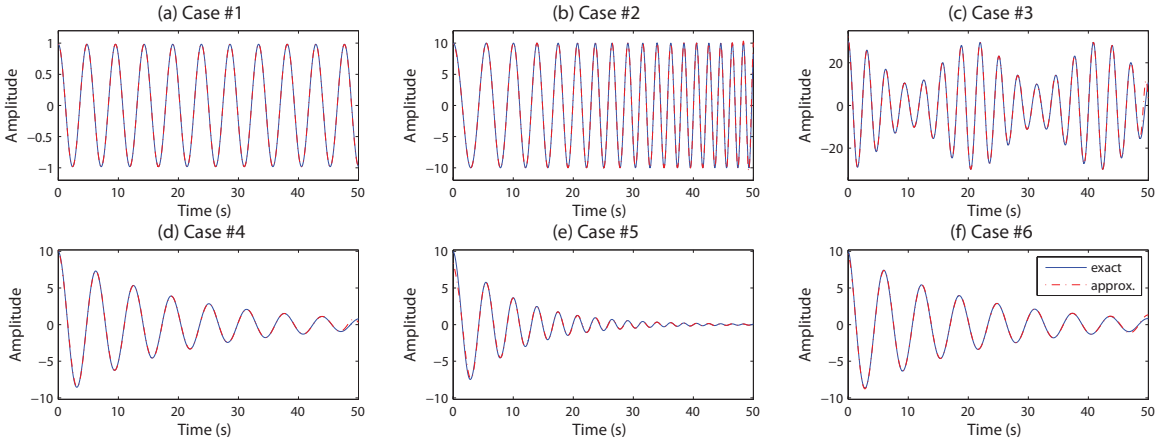

Figure 3.13: Validation of the proposed index method using approximated versus exact $x_1(t)$ in all case studies. Option A is utilized for all cases to locate time indices t_n in Step #2.

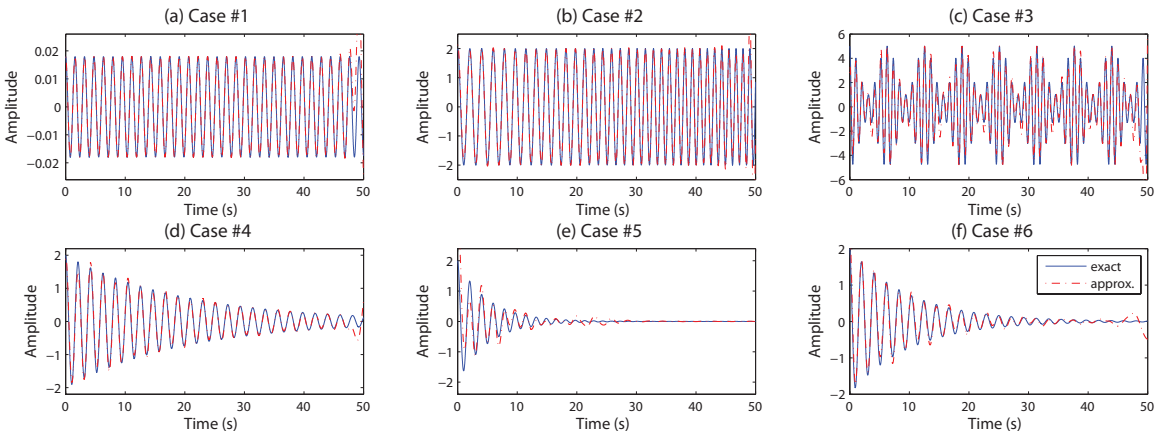

Figure 3.14: Validation of the proposed index method using approximated versus exact $x_2(t)$ in all case studies. Option A is utilized for all cases to locate time indices t_n in Step #2.

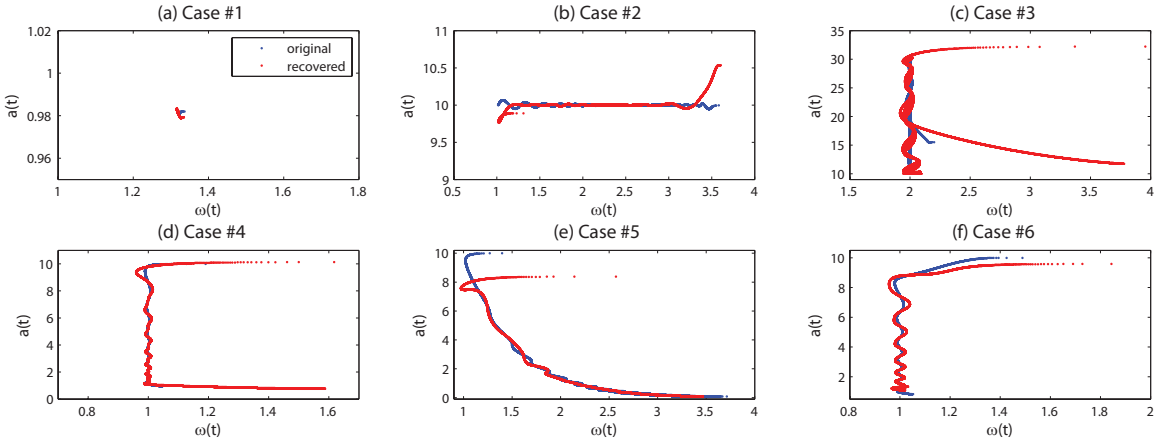

Figure 3.15: Validation of the proposed index method using recovered versus original backbones of the first mono-component in all case studies. Option A is utilized for all cases to locate time indices t_n in Step #2.

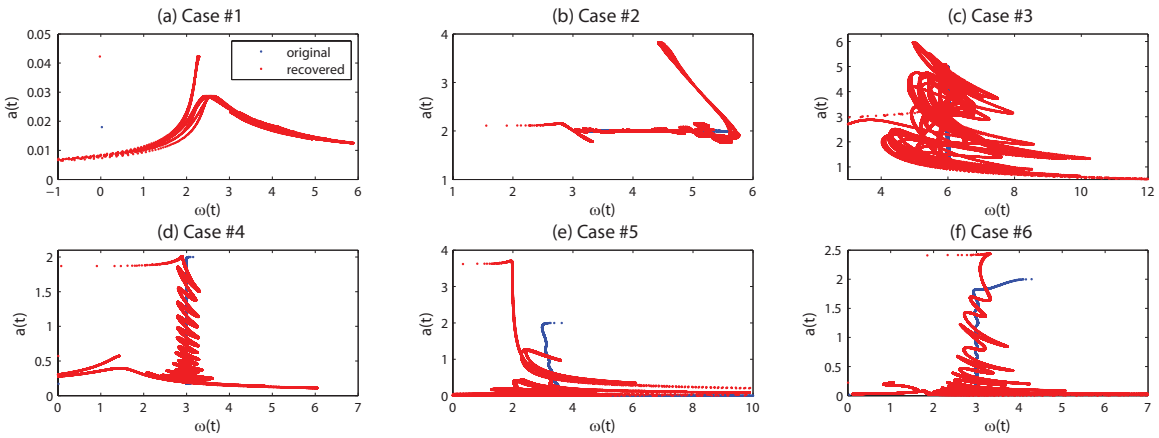

Figure 3.16: Validation of the proposed index method using recovered versus original backbones of the second mono-component in all case studies. Option A is utilized for all cases to locate time indices t_n in Step #2.

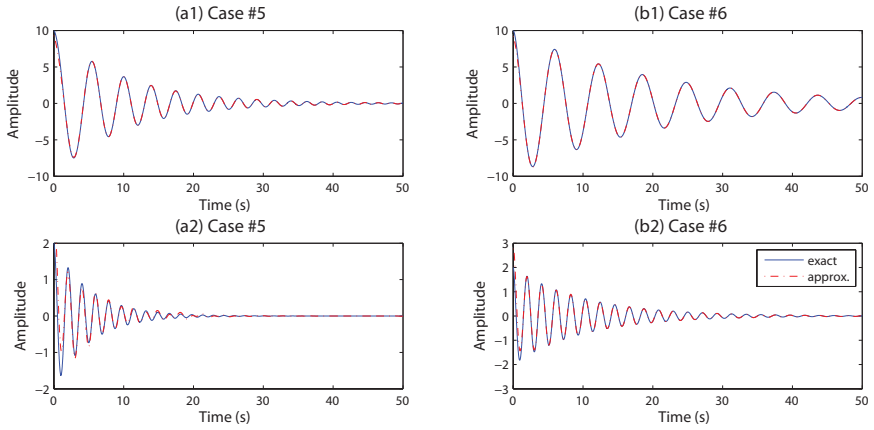

Figure 3.17: Validation of the proposed index method using approximated versus exact component signals of (1) $x_1(t)$ and (2) $x_2(t)$ in (a) Case #5, and (b) Case #6. Option B is utilized to locate time indices t_n in Step #2.

A different challenge is manifested in the extracted second mono-component in Case #3. As shown in Fig. 3.14(c), substantial errors in the approximated amplitude of the second mono-component exist throughout. This could be resulted from abrupt variations in the instantaneous frequency of the sum signal as shown in Fig. 3.6(c).

The index method is also tested on a Duffing oscillator described earlier in Fig. 3.1. The simulation result is shown in Fig. 3.18. From Fig. 3.18(b), it can be seen that the extracted first mono-component yields a much less oscillatory backbone curve

compared with that for the original response. It can be seen that in Fig. 3.18(c), the instantaneous frequency of the approximated first mono-component agrees well with the TFD plot. However, the approximated second mono-component is not as satisfactory as shown in Fig. 3.18(c).

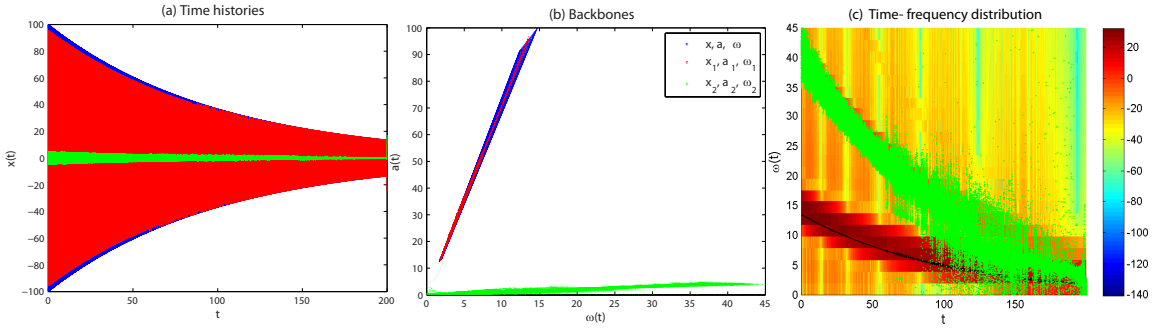

Figure 3.18: Validation of the proposed index method using Duffing equation $\ddot{x}(t) + 0.03\dot{x}(t) + x(t) + x^3(t) = 0$ with initial condition $x(0) = 100$ and $\dot{x}(0) = 0$. Option A is utilized to locate time indices t_n in Step #2. Panel (a), and (b) are the time histories, and backbones, respectively. Panel (c) overlays the instantaneous frequencies of the approximated first (in black) and second (in green) mono-components with the TFD plot.

While error analysis will be pursued in future work, other implementation details are under further refinement. So far, cubic spline is used for Steps #4 and #5 as in reference [44]. Possibly, envelopes' envelope as in reference [30] could be an option. Numerical differentiation involved in Step #6 should be carried out with caution to control high-frequency noise (e.g., [75]). Also, $\mathfrak{a}_2(t)$ obtained from Step #7 could be validated with using half of the difference of Eqs. (3.31) and (3.32).

3.4.7 The integral in reference [27]

Part of the theoretical work can be used to examine a special integral that is the cornerstone for the HVD method in reference [27].

Integrating both sides of Eq. (3.21) from t_n to t_{n+1} with $n \in \mathbb{N}^0$ leads to the

following equation:

$$\phi(t_{n+1}) - \phi(t_n) \;=\; \phi_1(t_{n+1}) - \phi_1(t_n) \;+\; \int_{t_n}^{t_{n+1}} \hat{\omega}(\tau) d\tau \tag{3.35}$$

From Eq. (3.30), $\phi(t_{n+1}) = \phi_1(t_{n+1})$ and $\phi(t_n) = \phi_1(t_n)$. Therefore, Eq. (3.35) becomes:

$$\int_{t_n}^{t_{n+1}} \hat{\omega}(\tau) d\tau \;=\; 0 \tag{3.36}$$

where $\hat{\omega}$ can be found in Eq. (3.22). This is an important integral concerning $\omega(t)$ and $\omega_1(t)$ given that $\hat{\omega}(t) \triangleq \omega(t) - \omega_1(\tau)$. Such an integral was previously studied in reference [27]. It is stated in reference [27] (Eq. (3) on pp. 521) that

$$\int_0^T \frac{(\omega_2(t) - \omega_1(t)) \left[\mathfrak{a}_2^2(t) + \mathfrak{a}_1(t)\mathfrak{a}_2(t) \cos\left(\int_0^t (\omega_2(\tau) - \omega_1(\tau)) d\tau\right)\right]}{\mathfrak{a}^2(t)} dt \;=\; 0 \tag{3.37}$$

with $T = 2\pi/(\omega_2 - \omega_1)$ where the use of T as period would be debatable since T is time-dependent due to the fact that both ω_1 and ω_2 are generally time-dependent. Furthermore, as explained earlier in Chapter 3.4.3, the two integrands in Eqs. (3.36) and (3.37) are not the same in general, Eq. (3.37) would thus be inaccurate even if T were properly defined. Fundamentally, differences between Eqs. (3.36) and (3.37) are caused by those between Eqs. (3.21) and (3.12) - controlled by the condition specified in Eq. (3.25). In summary, Eq. (3.36) may be considered a modification and generalization of Eq. (3.37).

Equation (3.36) is numerically verified successfully using all six cases as presented in Fig. 3.19, where Eq. (3.37) is also presented as a comparison. The results of Eqs. (3.36) and (3.37) would be the same theoretically in Case Study #1 because the condition specified in Eq. (3.25) is met. The difference at the tail is caused by the error (end effect) of DHT. In contrast, their differences are small but do exist when Eq. (3.25) is not met, as shown in other case studies. Again, the error caused by

DHT also exists.

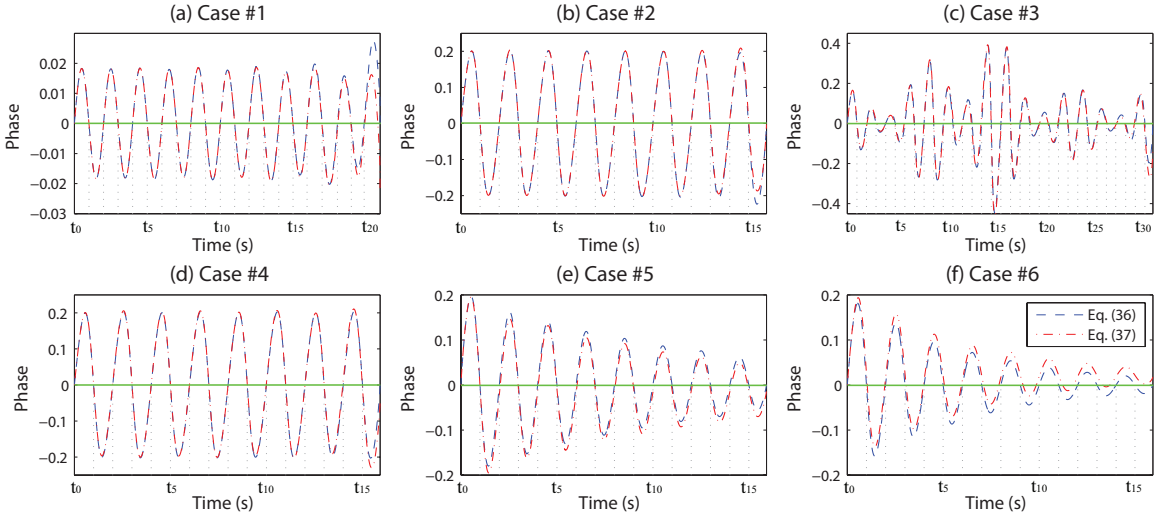

Figure 3.19: Time histories of the integrals in Eqs. (3.36) and (3.37) for Case Studies #1 to #6 in Chapter 3.3.

3.5 Discussions

The seemingly simple Case Study #1 in fact can help understand the backbone of an undamped Duffing oscillator under free vibration given in the following equation of motion:

$$\ddot{x}(t) + \omega_n^2 x(t) + \epsilon x^3(t) \;=\; 0, \tag{3.38}$$

where the response $x(t)$ can be approximated as a sum of two harmonics following [27, 62]:

$$x(t) \;=\; \mathfrak{a}_1 \cos(\omega_0 t) + \mathfrak{a}_3 \cos(3\omega_0 t) \tag{3.39}$$

where $\mathfrak{a}_1$, $\mathfrak{a}_3$ and ω_0 are all constants depending on system parameters. Using harmonic balance method, H derives a system of equations that can be solved numerically for $\mathfrak{a}_1$, $\mathfrak{a}_3$ and ω_0. An example of ten such backbones is given in Fig. 3.20 corresponding to a series of ten different initial displacements while initial velocities are always zero. Also in Fig. 3.20, ten other backbones are obtained by applying

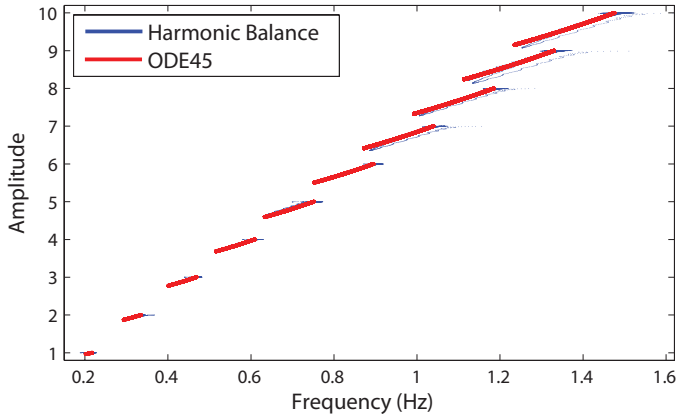

Figure 3.20: Two sets of backbones of different approximated solutions to an undamped Duffing equation $\ddot{x}(t) + x(t) + x^3(t) = 0$ using different initial displacements only.

DHT on the approximated solutions to Eq. (3.38) using Runge-Kutta 45 algorithm (implemented using MATLAB solver ode45). The backbones of the approximated double-component response approximate the simulated response quite well.

As this study is directly built on Feldman's work and aims at understanding and improving it, future work needs to verify the proposed changes including the new signal decomposition method. In particular, [27] states that Eq. (3.37) holds for a triple-component signal. While we would agree with this in principle, we feel that several much more stringent conditions may be required for the triple-component signal as follows:

1. For all time instances, the instantaneous amplitude of the first mono-component needs to be larger than that of the sum of the other two mono-components.

2. For all time instances, the instantaneous frequency of the first mono-component needs to be slower than that of the sum of the other two mono-components.

Under these two conditions, the sum of the second and third components may be considered a new component (which is not necessarily a mono-component). Having said this, the triple-component signal may be considered a sum of two signals: one

is mono-component, while the other may be not. The remaining analysis and result may be similar to those in this study, which is to be studied.

To be more specific about some of the work to be done with the proposed signal decomposition method, the Hilbert Vibration Decomposition method [27] was applied to the six case studies by employing the code available online [1]. Results are presented in Figs. 3.21 and 3.22 together with the results generated by the proposed signal decomposition method. In Fig. 3.21, all signals are noise free, like the rest of this chapter, while 5% Gaussian white noise was added in Fig. 3.22. The values of root-mean-square error in both Figs. 3.21 and 3.22 are presented in Table 3.2. It can be seen that the proposed signal decomposition results are superior to the HVD results for noise-free cases. However, it can also be seen that 5% noise alters the results of both methods, such that there is no apparent reason to prefer the proposed approach based on these six cases. This challenge could be understood by the fact that although the Hilbert transform of white noise is white noise [9], instantaneous quantities are obtained using nonlinear operators, thus backbone noise is not simply Gaussian white noise. In practical application of Feldman's backbone technique, we typically start with measured accelerations that include "noise". State estimation using proper Kalman filters (e.g. [74]) is one of the popular and effective means of obtaining cleaned displacement data, which would help ease the challenge discussed here and is to be explored in future studies.

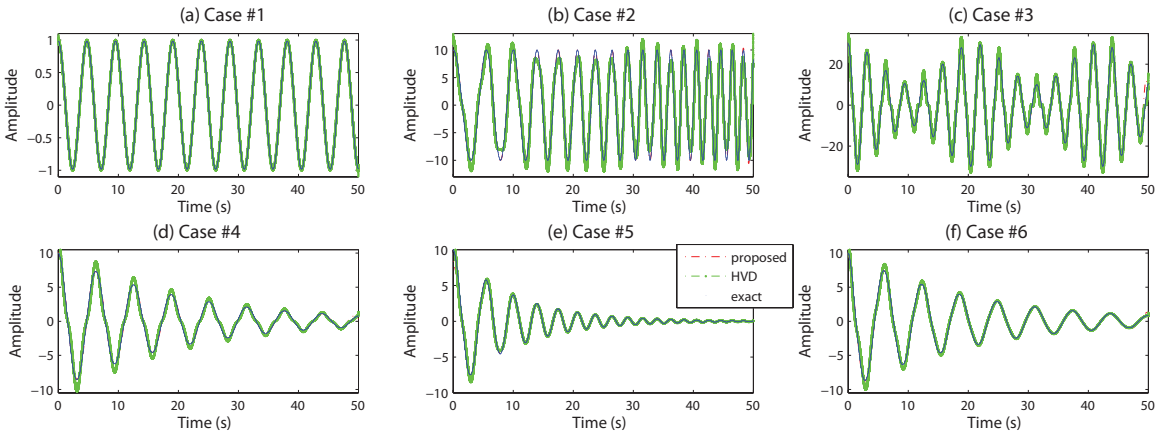

Figure 3.21: Comparison of the HVD decomposition method and the proposed signal decomposition method where the signals are the same as previous six cases without noise.

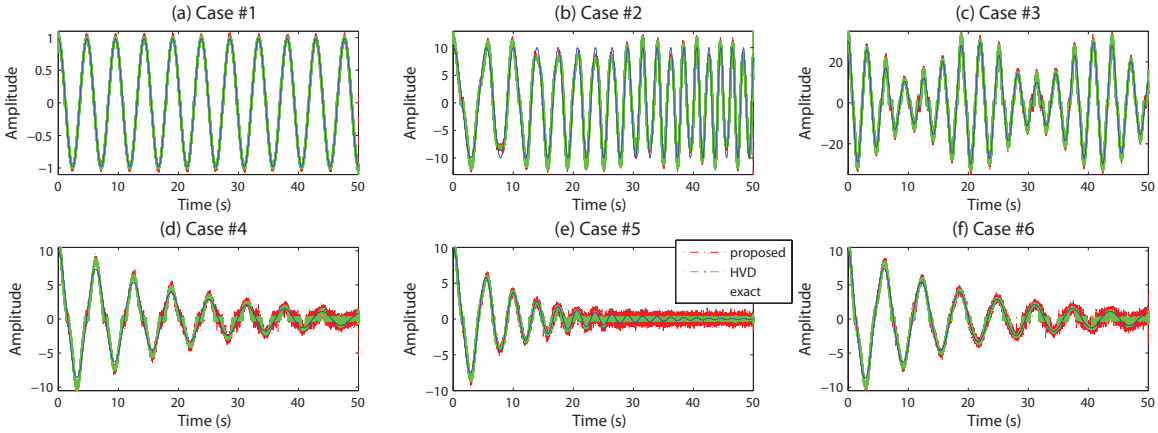

Figure 3.22: Comparison of the HVD decomposition method and the proposed signal decomposition method where 5% Gaussian white noise was added in all six cases.

Table 3.2: Root-mean-square error (RMSE) values in Figs. 3.21 and 3.22.

	Case #1	Case #2	Case #3	Case #4	Case #5	Case #6
without noise, proposed	0.00	0.24	1.22	0.10	0.26	0.10
without noise, HVD	0.00	1.42	2.36	0.64	0.33	0.46
with noise, proposed	0.00	1.47	2.57	0.76	0.54	0.60
with noise, HVD	0.00	1.43	2.59	0.81	0.46	0.60

Chapter 3.4 may be explained by using function composition. The challenge of the backbone of a double-component signal lies in the following fact: $\mathfrak{a}^{-1}(t)$ and $\omega^{-1}(t)$ may not exist making $\mathfrak{a}(t) \mapsto \omega(\mathfrak{a}(t))$ and $\omega(t) \mapsto \mathfrak{a}(\omega(t))$, the two possible mappings

for the backbone, not necessarily functions. Fig. 3.23 depicts this challenge, where noisy backbones are entirely caused by non-functional mapping rather than noise in data or from numerical operations. If the variable $\mathfrak{a}(t)$ could be replaced with $\mathfrak{a}_1(t)$, the backbone would become more manageable because $\mathfrak{a}_1^{-1}(t)$ generally exists.

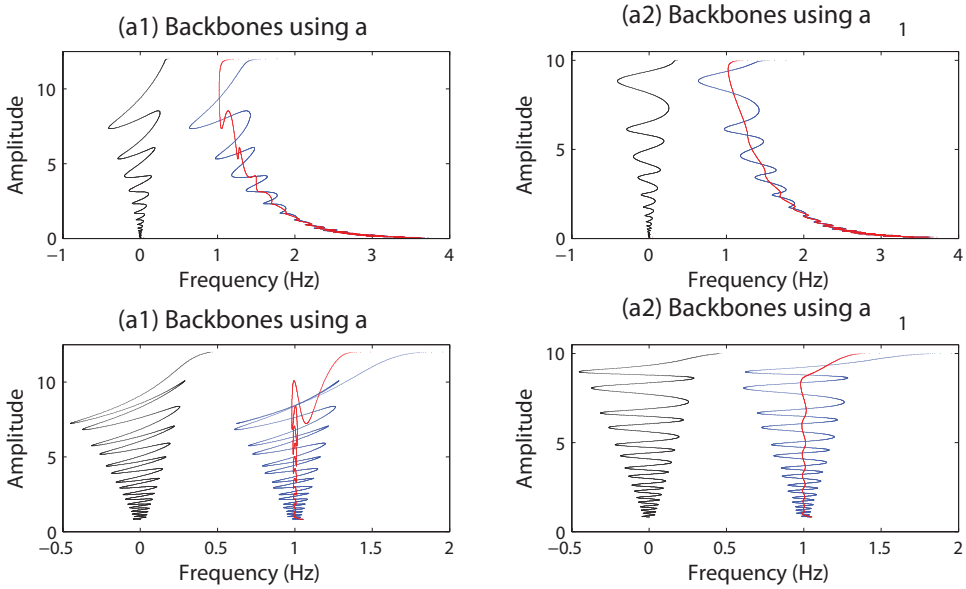

Figure 3.23: Exercises of function composition applied to Case Studies #5 and #6, where (a1) and (a2) $x_1(t) = 10e^{-0.1t}\cos(1t + \frac{0.05t^2}{2})$, $x_2(t) = 2e^{-0.2t}\cos(3t + \frac{0.05t^2}{2})$, and (b1) and (b2) $x_1(t) = 10e^{-0.05t}\cos(1t - 1.5e^{-0.3t})$, and $x_2(t) = 2e^{-0.1t}\cos(3t - 5e^{-0.3t})$.

Last but not least, the wild behavior of simulated backbones - even occurring for some mono-component signals - in the case studies is noted. The cause of this behavior can be manifold. Two of the possible causes are: First, it could come from the fact that the backbone is a highly nonlinear operator on a signal, which could potentially lead to distortions in the result; Second, the end effect of the DHT is hard to eradicate as explained in Chapter 2. This wild behavior deserves further investigations.

3.6 Conclusions

In this chapter, quantitative analysis has been carried out to understand possible causes and remedies of "noise" encountered when implementing Dr. Feldman's backbone technique. The problem was formulated here in terms of double-component signals with specified conditions. Double-component signals have been examined in relation to their mono-components using instantaneous quantities (amplitude, phase, and frequency) in terms of time histories and backbones. Six case studies have been presented, clearly revealing behaviors of double-component signals that are much more complicated than those of their constituent mono-components. Equally important, analytic forms of these double-component signals have been studied in depth. A theoretical investigation has been attempted to illuminate the observations from the case studies. First, an equation for instantaneous frequency of a double-component signal has been refined and generalized. Time indices have been defined to characterize special time instances that directly help decouple the two mono-components. Eventually, a signal decomposition method was implemented and tested on all six cases (and more), yielding promising simulation results while illustrating issues for further improvement. In addition, an important integral previously introduced in reference [27] has been examined and a more rigorous form of the integral has been provided.

Chapter 4

INSTANTANEOUS BANDWIDTH FOR BACKBONE TECHNIQUE DEMONSTRATED BY SINGLE-DEGREE-OF-FREEDOM DUFFING OSCILLATOR

4.1 Introduction

4.1.1 Motivations

Since the "backbone" technique was introduced a little over two decades ago and continuously being developed [23, 30, 29], its applications to real-world vibration signal analysis become increasingly important. Specifically for structural dynamics, one

may wonder if the backbone technique is suitable for a wide range of dynamical system parameter values that are practical. This constitutes the first practical question to be studied in this chapter, which focuses on investigating whether the backbone technique works and works robustly, and if not, how to make these happen. More specifically, the author has long been inspired by [23] to use the backbone as a pattern classifier for the types of underlying nonlinearity, see [46] as an example. For this purpose, we would need a backbone as non-oscillatory and simple as possible – rather than "noisy" backbones discussed in both [46] and Chapter 3.

Next, we consider a practical situation involving directly measured acceleration rather displacement time histories. Naturally, two options would be possible: (i) obtaining the backbone of the measured acceleration – called "acceleration backbone" hereafter, or (ii) approximating displacement based on acceleration before obtaining a backbone using the approximated displacement time history, i.e., "displacement backbone". In particular, we need to understand what an acceleration backbone entails for applying the backbone technique in structural dynamics and other experimental mechanics situations. This is because so far, backbone technique has been mainly used to produce displacement backbones.

Answering these two practical questions is the primary motivation.

Theoretically, Dr. Michael Feldman has applied numerous techniques from electrical engineering to his comprehensive backbone studies [30, 29] and HVD algorithm [27]. Among them, however, it does not seem that instantaneous bandwidth, another important concept concerning the instantaneous characteristic of a signal in Hilbert transform theory, has been applied. We thus wonder whether there is a role for this concept to play in the backbone technique, which is the secondary motivation. It turns out that instantaneous bandwidth is the theoretical foundation and/or practical measure/indicator to fulfill the first motivation specified above.

4.1.2 Technical solutions

Throughout this chapter, we choose Duffing oscillator to account for both hardening and softening nonlinearity in a single-degree-of-freedom (SDOF) dynamical system. Runge-Kutta 45 method is used to solve the governing equation of motion, which is a second-order nonlinear ordinary differential equation (ODE) – for the free vibration response subject to a positive initial displacement.

To answer the first practical question, we examine how the backbone technique performs with the system parameters – including natural frequency of the linear portion of the SDOF system, and damping ratio – varying within the ranges that are considered meaningful in structural engineering. We run into two specific challenges in the process: One is caused by large damping ratio, and the other is caused by mono-components of more than two in the signal given the nature of the solution to a Duffing oscillator. These challenges are quite typical for engineering practice. We provide algorithmic solutions with one concerning discrete Hilbert transform (DHT) and the other using digital filters; we validate these algorithmic solutions as a robust means to make the backbone technique applicable to these otherwise difficult situations.

For the other practical question, we utilize continuous Hilbert transform in a quantitative analysis; we obtain a necessary condition for acceleration and displacement backbones to be identical. Since this condition can hardly be satisfied by most free vibration signals, it indicates that acceleration and displacement backbones are often not identical. As expected, simulations using six mono-component signals and Duffing oscillator validate the derived necessary condition.

The concept of instantaneous bandwidth plays an essential role when we derive the aforementioned necessary condition to address the second practical question; instantaneous bandwidth also shed light in all algorithmic solutions to answer the first practical question. We further discover that, for a Duffing oscillator, the backbone proposed by Dr. Feldman may be considered a two-dimensional projection of a three-

dimensional backbone. This three-dimensional backbone may be constructed by using instantaneous amplitude, instantaneous frequency – as used by Dr. Feldman – and instantaneous bandwidth as proposed in this study. This three-dimensional backbone would be a more proper phase portrait for Duffing oscillator as we show in the analysis. To complete the discussion on instantaneous bandwidth, we show that a damping estimation method in Dr. Feldman's work is actually based on instantaneous bandwidth.

As a chapter in a series of investigations by the authors and their co-author on the backbone technique, the DHT algorithm in Chapter 2 will be utilized for numerically obtaining all backbones in this chapter. The signal decomposition technique proposed in Chapter 3 for double-mono-component signals will not only be utilized but also be refined to deal with multi-component signals – free response of Duffing oscillators and to obtain a backbone as smooth as possible for use as a pattern classifier.

4.1.3 Intended contributions

This study complements the existing work on the backbone technique in terms of both applications and theoretical development. With the proposed piecewise DHT algorithm and refined signal decomposition method, challenging free vibration responses due to large damping ratio and multi-component signals will be taken care of, respectively, leading to correct and smooth backbones. Instantaneous bandwidth, for the first time, is applied to the backbone technique. Not only does instantaneous bandwidth offer insights to displacement backbone versus acceleration backbone, but also instantaneous bandwidth should be used as an indicator for the validity of computed instantaneous frequency - following the concept in reference [15], which is established in Hilbert transform theory but has not benefited the backbone technique. The trio of instantaneous amplitude, frequency, and bandwidth is analyzed to be the governing state variable set for Duffing oscillator; Feldman's backbone is thus a two-dimensional

projection of this complete trio. This broader view justifies Feldman's backbone, and also implies its potential limitation – which can be addressed by examining the companion instantaneous bandwidth.

4.1.4 Structure of this chapter

The structure of this chapter follows a natural order when we settle the two research questions defined in Chapter 4.1 one after another in Chapters 4.3 and 4.4. Before addressing the research questions, the concept of instantaneous bandwidth is reviewed briefly in Chapter 4.2. After settling the two research questions, we reveal a so-called three-dimensional backbone in Chapter 4.4.3. Before concluding this study in Chapter 4.6, we make one more installment on the understanding and application of instantaneous bandwidth in Chapter 4.5 in terms of an illuminating example and damping estimation following Feldman's lead but explicitly using instantaneous bandwidth, respectively. I to L contain all derivations in this study.

4.2 Instantaneous Bandwidth

The concept of *instantaneous bandwidth* – denoted as $\mathfrak{b}$ in this study – is first closely related to instantaneous frequency. The formula for IB is formally introduced in reference [15] as shown below:

$$\mathfrak{b}(t) \;=\; \left|\frac{\dot{\mathfrak{a}}(t)}{\mathfrak{a}(t)}\right| \tag{4.1}$$

where $\mathfrak{a}(t)$ is the instantaneous amplitude and $\dot{\mathfrak{a}}(t)$ is its first time derivative. The relationship between the IB and IF is an the same as the relationship between bandwidth and frequency of a signal [15]. That is, the bandwidth of a signal is an indicator of the range of frequencies exist during the total duration of the signal, therefore, the IB of a signal is an indicator of the range of frequencies exist at every time instance. More concretely, the IB is a measure of the standard deviation of the IF. The for-

mula in Eq. (4.1) is derived step by step in reference [15] following the fundamentals of probability theory and is verified rigorously there. Later in Chapter 4.5, we will provide more comments and a provoking example to shed light on this definition.

Since instantaneous bandwidth captures the spread-out of instantaneous frequency, the magnitude of instantaneous bandwidth is a good indicator of the "accuracy" of instantaneous frequency estimation. The smaller instantaneous bandwidth is, the more accurate and meaningful the use of instantaneous frequency would be.

4.3 Applicable Range of Backbone to SDOF Structural Dynamics

4.3.1 Overview

As an important equation, the following mass-normalized equation of motion for a Duffing oscillator has been utilized by Dr. Feldman for a couple of times (e.g., [23, 27, 30, 29]). It will be served as a benchmark equation for this study, where linear viscous damping is assumed:

$$\ddot{x}(t)+2\zeta(2\pi f_n)\dot{x}(t)+(2\pi f_n)^2 x(t)+\alpha x^3(t) \;=\; 0, \;\; \text{with} \;\; x(0)>0, \;\; \text{and} \;\; \dot{x}(0)=0 \quad (4.2)$$

The parameters f_n, ζ, α, $x(0)$ and $\dot{x}(0)$ are the natural frequency, damping ratio, nonlinear stiffness, initial displacement and initial velocity, respectively. Without losing generality, we fix $\dot{x}(0) = 0$ throughout this study to simplify the parametric study on the initial condition (IC).

To consider meaningful values for f_n and ζ, references in structural engineering such as [12, 64] are consulted. Typical values for f_n range from 0.3 to 22 Hz, damping ratios are summarized in Table 4.1 following [64], while values as high as 25% are considered in other literature [52]:

Table 4.1: Maximum damping ratios of real-world structures adopted from Table A17.5 in reference [64]

Type	Steel (Welded)	Steel (Bolted)	Concrete (Reinforced)	Concrete (Prestressed)	Masonry (Reinforced)	Wood Trusses	Wood Frames
ζ (%)	2.0	4.0	5.0	3.0	6.0	9.0	7.0

It is learned from [23] that a backbone curve of Eq. (4.2) intersects the $\mathfrak{f}$-axis at the natural frequency of the linear portion of the SDOF system. This is because when $x \to 0$, the nonlinear term x^3 can be discarded, leading to a linear SDOF that has a constant frequency at f_n. With 6%, a mid-range ζ value, Figs. 4.1 and 4.2 indicate how the backbone curves are affected by varying f_n values – with two different ICs.

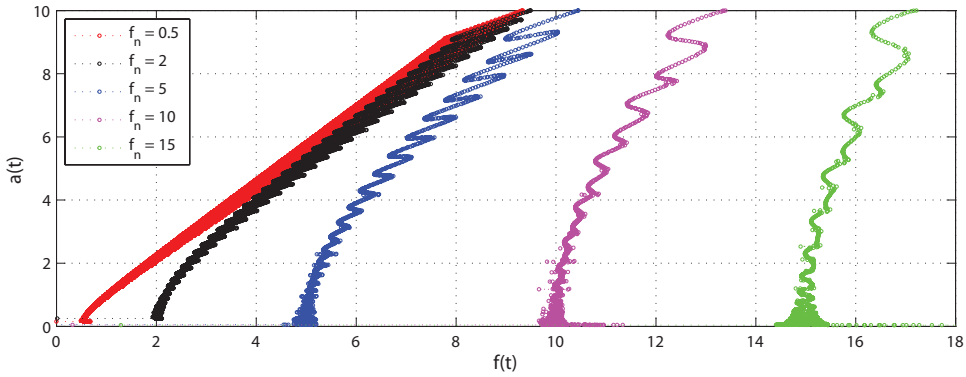

Figure 4.1: Backbones affected by natural frequency f_n in the Duffing oscillator of $\ddot{x}(t)+2\times 6\%\times(2\pi f_n)\dot{x}(t)+(2\pi f_n)^2 x(t)+40x^3(t)=0$ with initial condition $x(0)=10$ and $\dot{x}(0)=0$.

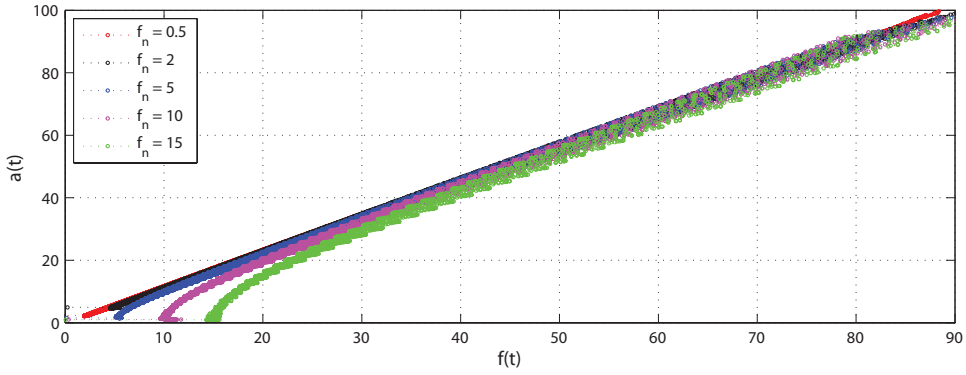

Figure 4.2: Backbones affected by natural frequency f_n in the Duffing oscillator of $\ddot{x}(t)+2\times 6\%\times(2\pi f_n)\dot{x}(t)+(2\pi f_n)^2 x(t)+40x^3(t)=0$ with initial condition $x(0)=100$ and $\dot{x}(0)=0$.

It can be seen that f_n shifts backbone horizontally. The backbone always crosses the $\mathfrak{f}$-axis at f_n, where the bending slope is affected by f_n. All backbones corresponding to different f_n tend to converge to the limiting case with $f_n = 0$ – if the initial displacement is large enough – as can be seen in Fig. 4.2. The limiting case may be obtained by simplifying Eq. (4.2) as $\ddot{x} + \alpha x^3 = \mathbf{0}$. It seems that $\mathfrak{a}(t)$ and $\mathfrak{f}(t)$ are approximately linearly correlated in this case.

A smaller ζ value is used to repeat Fig. 4.2 and saved as Fig. 4.3 – without causing any major alteration to the features of the backbone curves. Fig. 4.4 further confirms that ζ affects only the "density" of a backbone curve, but not its bending behavior at all. An intuitive explanation is that the damping ratio affects only the decaying speed of the response, resulting in a difference in the density of the backbone curve.

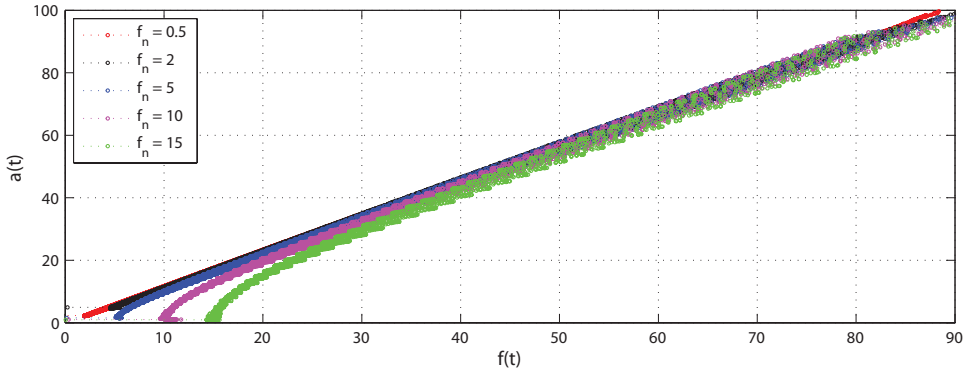

Figure 4.3: Backbones affected by natural frequency f_n in the Duffing oscillator of $\ddot{x}(t)+2\times 2\%\times(2\pi f_n)\dot{x}(t)+(2\pi f_n)^2 x(t)+40x^3(t) = 0$ with initial condition $x(0) = 100$ and $\dot{x}(0) = 0$.

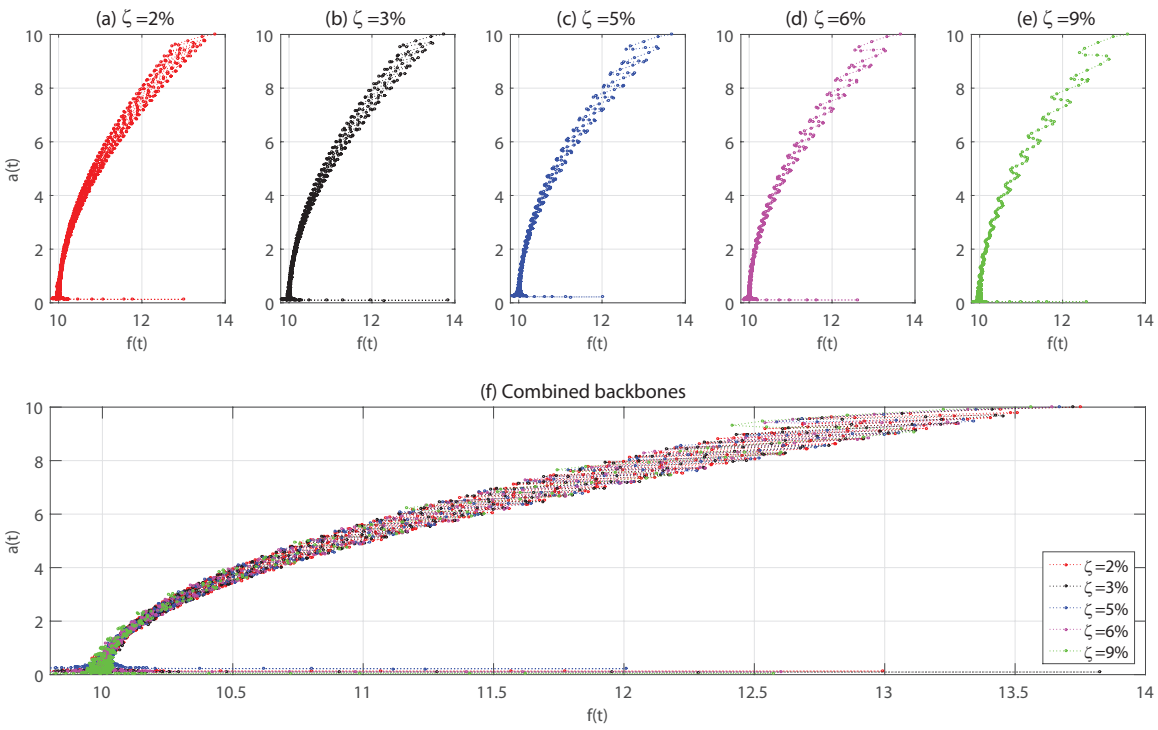

Figure 4.4: Backbones affected by damping ratio ζ in the Duffing oscillator of $\ddot{x}(t) + 2 \times \zeta \times (2\pi \times 10)\dot{x}(t) + (2\pi \times 10)^2 x(t) + 40x^3(t) = 0$ with initial condition $x(0) = 10$ and $\dot{x}(0) = 0$. The corresponding damping ratios are 2%, 3%, 5%, 6%, 9%.

As expected, α does significantly affect the bending behavior of the backbone as shown in Fig. 4.5. Zero, positive, negative values for α correspond to straight-up, right-bending and left-bending backbone, respectively. Moreover, the larger the α value is, the greater the backbone bends. These are all consistent with [23]: The nonlinear term is in the third power of the response, hence the larger α is, the more rapidly $\mathfrak{a}$ is affected.

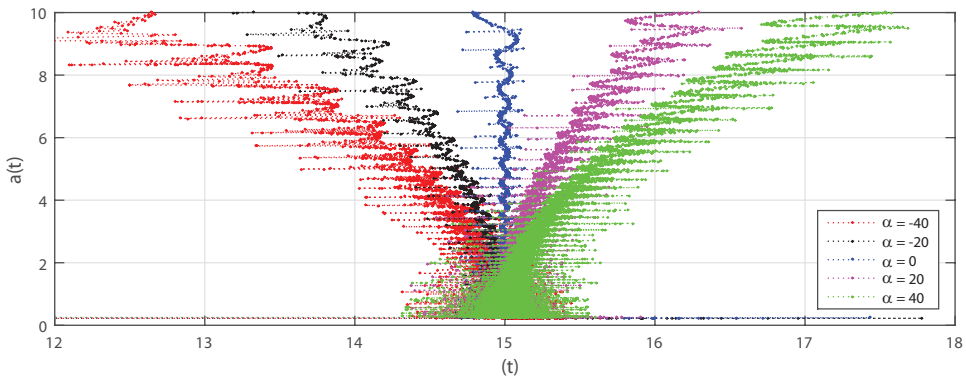

Figure 4.5: Backbones affected by cubic stiffness α in the Duffing oscillator of $\ddot{x}(t) + 2 \times 2\% \times (2\pi \times 15)\dot{x}(t) + (2\pi \times 15)^2 x(t) + \alpha x^3(t) = 0$ with initial condition $x(0) = 10$ and $\dot{x}(0) = 0$.

For a softening Duffing oscillator, its phase portrait contains one attraction point and two saddle points as depicted in Fig. 3.3(d) in reference [51]. This very fact is paid attention to when deciding the combinations of parameter values and ICs for softening case so that the free response dies out to the attraction point rather.

Based on the observations above, we would like now to connect the backbones of a damped Duffing oscillators with an undamped one. On one hand, damping ratio seems to have no affect on the bending behavior of the backbone. On the other hand, IC seems to affect only the "length" of the backbone, but neither the bending behavior nor the "density". Based on these two observations, it is reasonable to argue that the backbone of a damped Duffing oscillator could be represented by an undamped Duffing by sampling representative ICs consecutively as illustrated in Fig. 4.7.

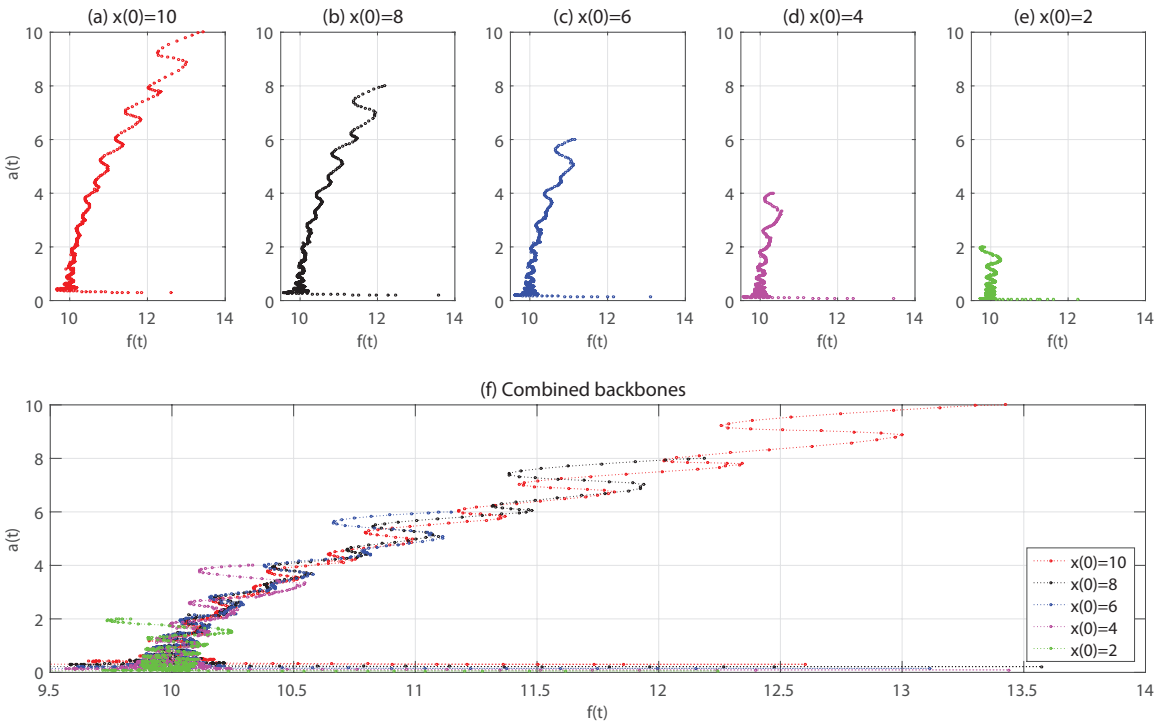

Figure 4.6: Backbones affected by initial displacement x_0 in the Duffing oscillator of $\ddot{x}(t) + 2 \times 6\% \times (2\pi \times 10)\dot{x}(t) + (2\pi \times 10)^2 x(t) + 40x^3(t) = 0$ with initial condition $x(0) = x_0$ and $\dot{x}(0) = 0$.

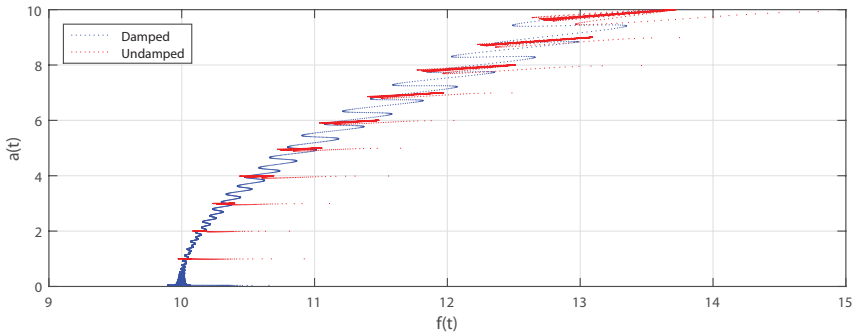

Figure 4.7: Backbones of damped (in blue) and undamped (in red) Duffing oscillator of the form $\ddot{x}(t) + 2\zeta \times (2\pi \times 15)\dot{x}(t) + (2\pi \times 15)^2 x(t) + 40x^3(t) = 0$, with $\zeta = 3\%$ and 0% for the damped and the undamped cases, respectively. For the damped case, $x(0) = 10$, $\dot{x}(0) = 0$. For the undamped cases, ten nonzero initial displacements vary from 1 to 10 while initial velocities are set to zero throughout.

4.3.2 Proposed piecewise discrete Hilbert transform

During the parameter study and specifically in the process of producing Figs. 4.1 and 4.7, a very "noisy" tail of a backbone was encountered routinely as typified in Fig. 4.8.

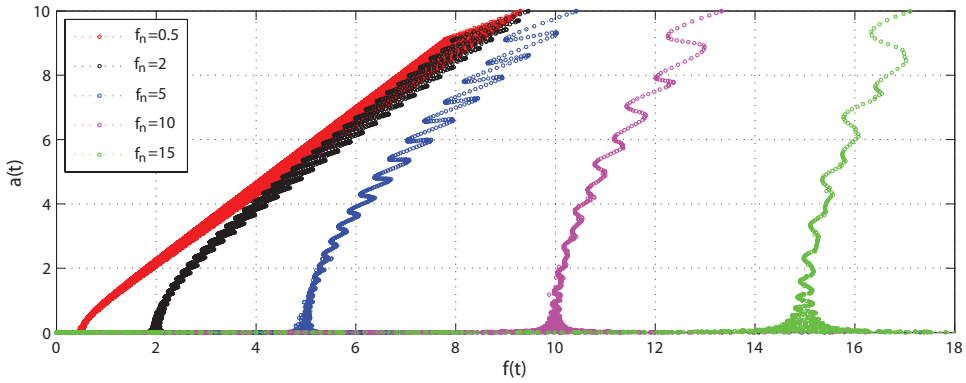

Figure 4.8: Backbones with noisy ends when using the same parameter values as in Fig. 4.1 but with longer durations.

Extensive troubleshooting took place until we noticed the incorrect DHT result towards the tail of these signals, i.e., the amplification of the transformed signal at towards the end. We believe that the roots of this end amplification problem is the large value of $\frac{x_{\max}^{\text{start}}}{x_{\max}^{\text{end}}}$, where $x_{\max}^{\text{start}}$ and $x_{\max}^{\text{end}}$ correspond to the magnitude at the beginning and at end of the signal, respectively. $x_{\max}^{\text{start}}$ ($x_{\max}^{\text{end}}$) are computed by subtracting the first (last) local maximum from the first (last) local minimum. To simplify the analysis, we name this factor the decaying factor and denote is as κ.

When the duration T of a time history is unnecessarily long as shown in Fig. 4.8, κ is as high as 10^6. All values of T and κ in Figs. 4.1 to 4.6 are given in Table 4.2.

Table 4.2: Values of T (second) and κ in Figs. 4.1 to 4.6. Note that the column of κ only indicates the magnitude level, rather than exact values.

Figure ID	Parameter type	Value	Duration (sec)	Decaying factor
Fig. 4.1	natural frequency (f_n)	0.5 Hz	30	$1e2$
		2 Hz	6	$1e2$
		5 Hz	3	$1e2$
		10 Hz	1.5	$1e2$
		15 Hz	1	$1e2$
Fig. 4.2	natural frequency (f_n)	0.5 Hz	30	$1e2$
		2 Hz	6	$1e2$
		5 Hz	3	$1e2$
		10 Hz	1.5	$1e2$
		15 Hz	1	$1e2$
Fig. 4.3	natural frequency (f_n)	0.5 Hz	90	$1e2$
		2 Hz	20	$1e2$
		5 Hz	10	$1e2$
		10 Hz	4	$1e2$
		15 Hz	3	$1e2$
Fig. 4.4	damping ratio (ζ)	2%	7	$1e2$
		3%	5	$1e2$
		5%	2.5	$1e2$
		6%	2.5	$1e2$
		9%	2	$1e2$
Fig. 4.5	nonlinear stiffness (α)	-40	2	$1e2$
		-20	2	$1e2$
		0	2	$1e2$
		20	2	$1e2$
		40	2	$1e2$
Fig. 4.6	initial displacement ($x(0)$)	10	1	$1e2$
		8	1	$1e2$
		6	1	$1e2$
		4	1	$1e2$
		2	1	$1e2$

This incorrect DHT performance can occur easily when ζ is large, even when time history is not that long. See Fig. 4.9(a) for an example when $\zeta = 30\%$ and when the time history includes a period of time when the amplitude of $x(t)$ is small. In particular, κ is as large as 1e5. An interesting detail worth mentioning is that the instantaneous amplitude goes through a abrupt change around 1.7 second and its value drops to almost zero and at the same time the instantaneous frequency drops to a unreasonably small value, as can be seen in Fig. 4.9(a2) and (c). The abrupt change causes IB to a sudden increase, which can be explained either way: the variation in IA is drastic, and the computed IF is meaningless at this time instance.

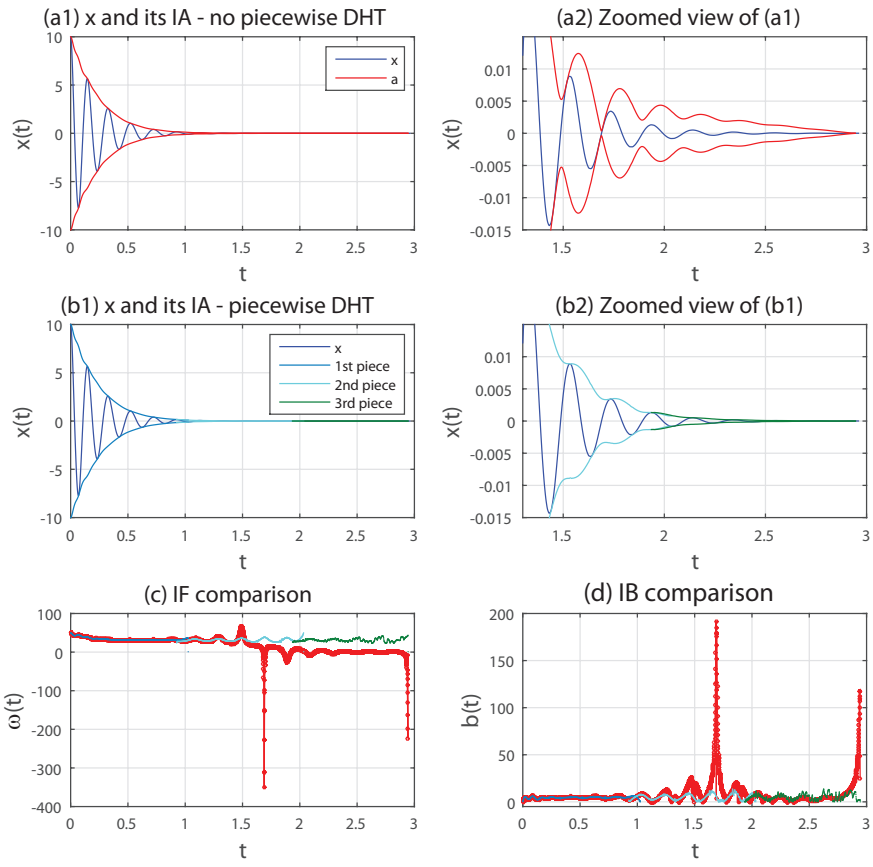

Figure 4.9: Monolithic piece DHT contrasted with piecewise DHT using $\ddot{x}(t) + 2 \times 30\% \times (2\pi \times 5)\dot{x}(t) + (2\pi \times 5)^2 x(t) + 20x^3(t) = 0$ with initial condition $x(0) = 10$ and $\dot{x}(0) = 0$. The first and second rows contrast the entire piece (as commonly done) and the proposed piecewise DHT, while the third row uses $\omega(t)$ and $\mathfrak{b}(t)$ to reveal the insights into the contrast.

This challenge with DHT motivates the authors to thoroughly understand the cause and provide a remedy. While we fabricate a toy problem in I to comprehend the cause using analysis based on DHT, a quick explanation would be that when the scale of the magnitude of $x(t)$ differs tremendously, the circular convolution of the DHT algorithm tends to incorrectly amplify the tail of $\tilde{x}(t)$ leading to an incorrectly amplified $\mathfrak{a}(t)$. Thus, when we carefully choose the duration T such that κ is not too large, correct DHT results were obtained, so that better backbones are possible, as shown in Figs. 4.1 to 4.6.

A meaningful question would be: "What can we do when we cannot manually

choose the duration and cannot truncate the portion with relatively smaller magnitude?" That is, what is the correct procedure to perform DHT when κ is ensured to be large? The remedy proposed in this study is to perform DHT in a piecewise manner. The improved DHT result under piecewise transformation is given in Fig. 4.9(b), where the improvement on the estimated $\mathfrak{a}$ is evident.

Nonetheless, another rational research question would be: "Practically, how would we know whether we need to perform piecewise DHT? Alternatively, how would we know enough pieces have been chosen?" To address the question, we can first observe the decaying factor, i.e., κ. If it is too large, say beyond 10^4, then it might be necessary to use piecewise DHT instead. We also believe computing $\omega(t)$ and $\mathfrak{b}(t)$ a good alternative. While $\mathfrak{b}(t)$ would be formally introduced shortly after, the main idea here is to use a concentrated $\omega(t)$ or a small-valued $\mathfrak{b}(t)$ to infer a reliable DHT result. A dispersed $\omega(t)$ or a large-valued $\mathfrak{b}$ are signs for an unreliable DHT result. Both scenarios are contrasted in Fig. 4.9(c) and 4.9(d) highlighting the effectiveness of using $\omega(t)$, and more importantly, $\mathfrak{b}(t)$, a concept still unknown to the backbone community.

4.3.3 Improved signal decomposition method

With applying piecewise DHT whenever necessary as described above, all backbones of Duffing oscillators studied here would still be oscillatory, i.e., not being simple enough as a pattern classifier. Directly applying the signal decomposition algorithm proposed in Chapter 3 still does not lead to a non-oscillatory backbone of the dominant mono-component. This is due to two reasons as we understand: First, the free response of a Duffing oscillator consists of numerous mono-components as the harmonic balance or multi-scale solution (e.g., in reference [62]) implies, which causes the instantaneous amplitude and moreover the instantaneous frequency to oscillate significantly. Next, the estimation of instantaneous frequency is an inherently chal-

lenging topic (e.g., in reference [6]). The instantaneous frequency estimated by the signal decomposition method proposed in Chapter 3 is observed to contain high frequencies. See Panel (b) in Figs. 4.10 to 4.13 – four typical cases representing those in Chapter 4.3.1 – for instantaneous frequencies, and Panel (h) of these figures for noisy backbone of the dominant mono-components.

$\mathfrak{b}(t)$ is shown in Panels (c) and (g) of Figs. 4.10 to 4.13 presented earlier. Smaller values of $\mathfrak{b}$ in Panel (g) compared with those in Panel (c) indicate an improvement in instantaneous frequency estimation after adopting the proposed modified signal decomposition procedure.

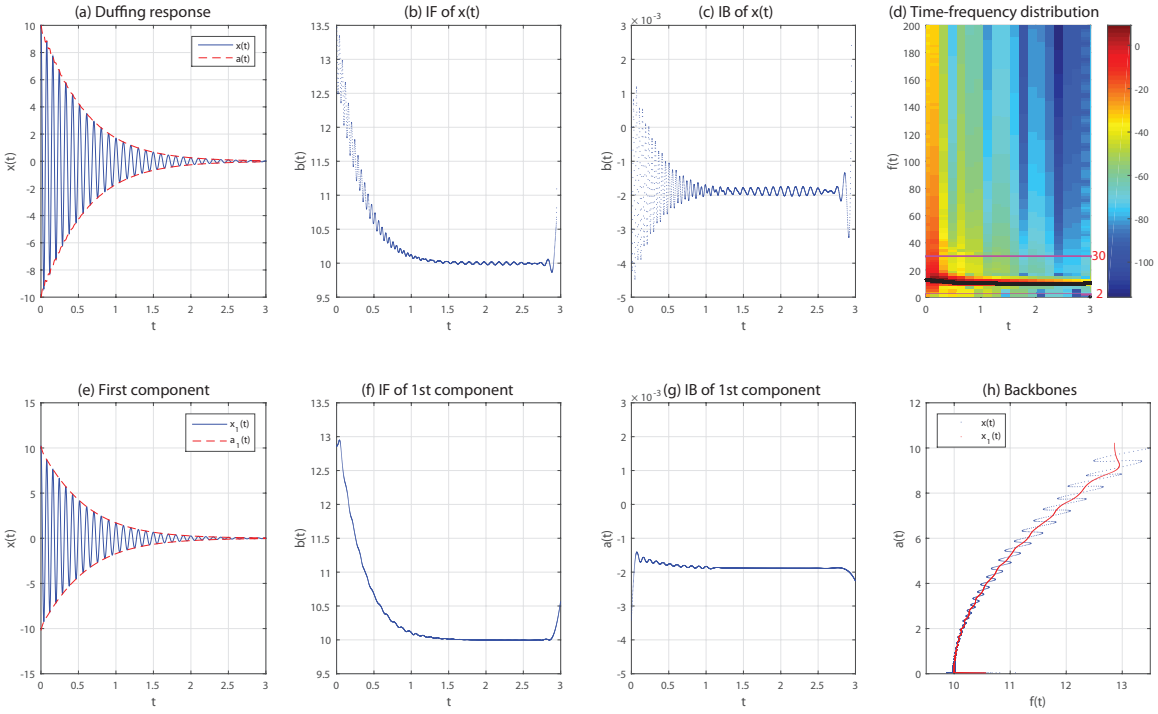

Figure 4.10: Demonstration of the effect of the modified signal decomposition procedure when $f_n = 10Hz$, $\zeta = 0.06$, $\alpha = 40$, $x(0) = 10$, $\dot{x}(0) = 0$. In panel (d), the black curve is the instantaneous frequency of the first decomposed component, and the two magenta lines are the two cutoff frequencies of the bandpass filter. The same design is used for Figs. 4.11 to 4.13.

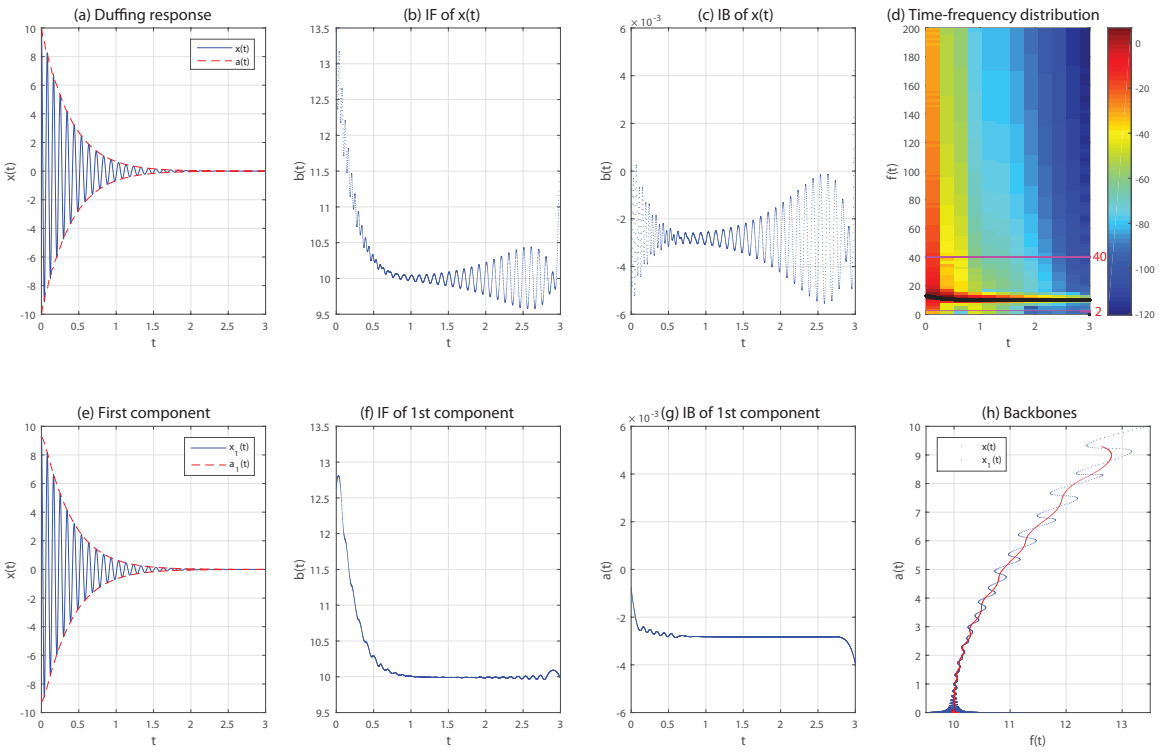

Figure 4.11: Demonstration of the effect of the modified signal decomposition procedure when $f_n = 10Hz,\ \zeta = 0.09,\ \alpha = 40,\ x(0) = 10,\ \dot{x}(0) = 0.$

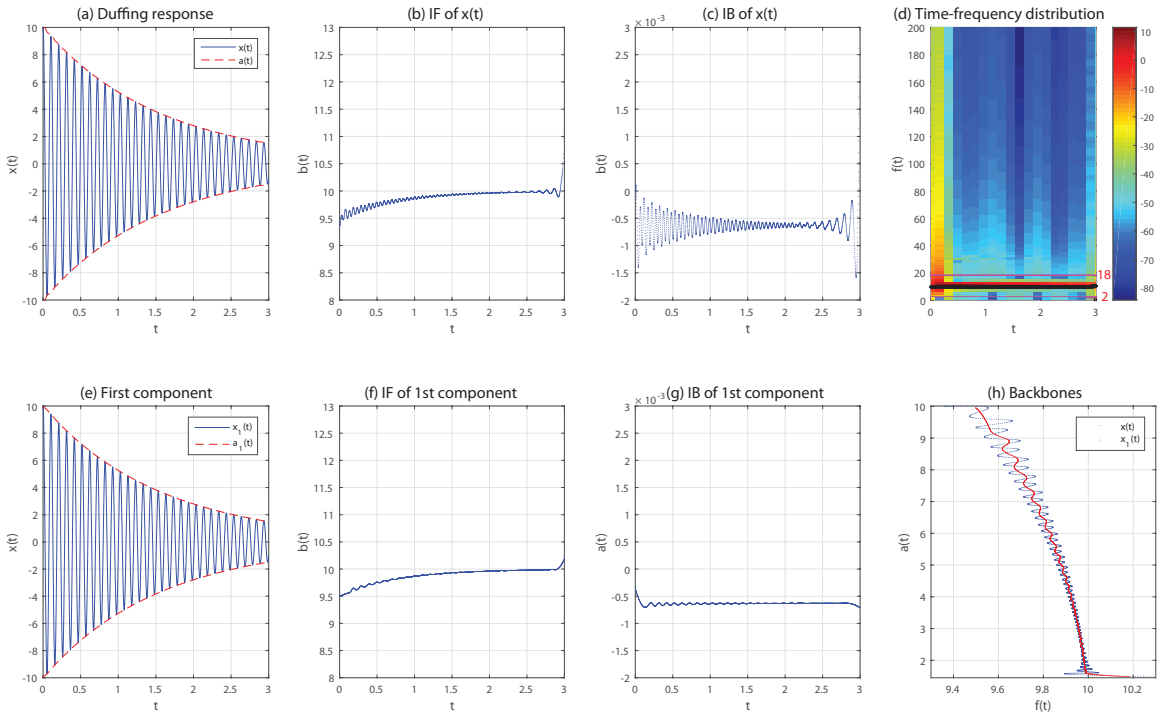

Figure 4.12: Demonstration of the effect of the modified signal decomposition procedure when $f_n = 10Hz,\ \zeta = 0.02,\ \alpha = -5,\ x(0) = 10,\ \dot{x}(0) = 0.$

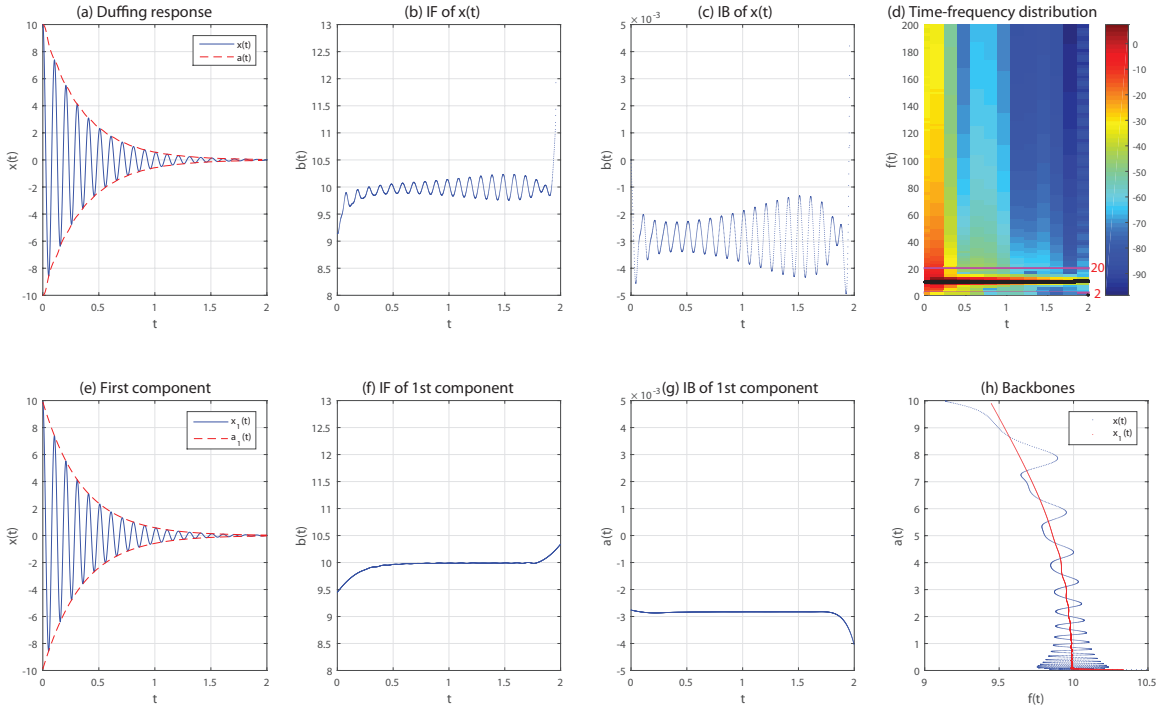

Figure 4.13: Demonstration of the effect of the modified signal decomposition procedure when $f_n = 10Hz,\ \zeta = 0.09,\ \alpha = -5,\ x(0) = 10,\ \dot{x}(0) = 0.$

With the goal of producing a less oscillatory backbone with a simple pattern, we improve the signal decomposition procedure as follows:

1. Perform DHT to $x(t)$ by following Chapter 3. Beyond Chapter 3, the decaying ratio and the DHT response are checked to make sure the end amplification issue does not exist, otherwise, piecewise DHT procedure is taken out.

2. Compute instantaneous amplitude, instantaneous phase, instantaneous frequency, and instantaneous bandwidth – with the last item to be explained later in Chapter 4.4. The backbone obtained is called an *unfiltered backbone* of $x(t)$ hereafter. In particular, the numerical differentiation is done by using central difference method; the MATLAB [59] code adopted is a slightly modified central_diff.m [10] to ensure forward and backward difference for the left and right ends, respectively.

3. Use a bandpass filter on instantaneous amplitude to locate their "local extrema" and corresponding time instances called time indices, t_n, a concept developed and explained in Chapter 3. Although both instantaneous amplitude and instantaneous frequency are possible choices in this step, we stick to instantaneous amplitude based on the assumption that instantaneous frequency generally contains very high level of noise.

   The reasons for using a bandpass filter – for the purpose of obtaining unbiased estimation of the time indices – is as follows: On one hand, misleading high frequency kinks in the instantaneous amplitude need to be filtered out with a low enough low cut-off frequency; see Fig. 4.14(b1) for an example. In numerical simulations, the high frequency kinks are severe especially when the damping ratio is low even when the Duffing response is not added with any noise. The reason for this could be the fact that Duffing response is a sum of infinite many harmonics and that the existence of numerical error in the Duffing response. For

practical consideration, high frequency kinks would be highly possible, therefore, filtering them out is a good choice in general. On the other hand, local extrema could possibly be overwhelmed by a rapidly decaying $\mathfrak{a}$ due to a large damping ratio. These local extrema, especially their corresponding time indices can be recovered with a high enough high cut-off frequency; see Fig. 4.14(c1) for an example. To clearly illustrate this practical decision, low- and high-cutoff frequencies used in producing smoothen backbones highlighted in red in Panel (h) of Figs. 4.10 to 4.13 are indicated as two constant lines in magnate in Panel (d) of these figures. The low cutoff frequency is chosen based on the assumption that the decaying profile being considered half a cycle. For the high cutoff frequency, an initial value is picked so that it is about twice the natural frequency of the Duffing oscillator. Further tuning is done based on the performance of the decomposed first mono-component.

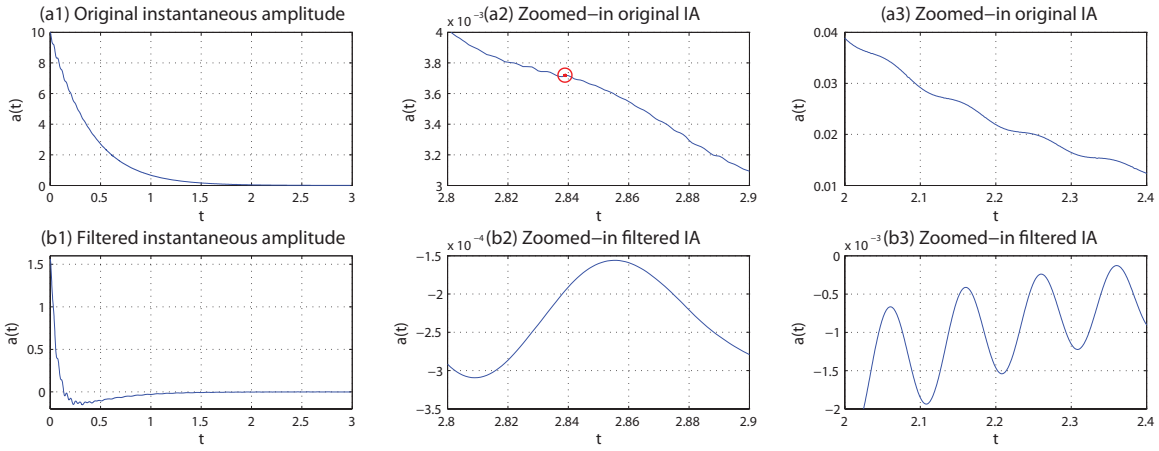

Figure 4.14: Instantaneous amplitude of the response of a Duffing oscillator with $\omega = 10$, $\zeta = 0.09$, $\alpha = 40$, $x(0) = 10$, $\dot{x}(0) = 0$. The first and second rows give unfiltered and filtered time histories, respectively. The first column gives an overview, while the second and third columns illustrate the need of using lowpass and highpass filter, respectively.

The rest of the procedure follows precisely that in Chapter 3:

4. Curve fit the local maxima and minima, respectively. In this study, cubic spline

interpolation is utilized throughout, however other methods could be explored in future studies.

5. Obtain the instantaneous amplitude of the first mono-component $\mathfrak{a}_1(t_n)$ by averaging the fitted local maxima and minima.

6. Obtain values of the instantaneous phase at t_n. Use cubic spline interpolation to interpolate the values to yield $\phi_1(t_n)$.

7. Compute $x_1(t) \;=\; \mathfrak{a}_1(t)\cos\phi_1(t)$.

8. Obtain the backbone of $x_1(t)$ by following Chapter 3, called a *filtered backbone* of $x_1(t)$, the dominant mono-component.

4.4 Backbones of Displacement, Velocity and Acceleration

4.4.1 Major finding

Start with $x(t)$ in its analytic signal form as follows:

$$x(t) \;=\; \mathfrak{a}(t)e^{j\phi(t)} \tag{4.3}$$

where $\mathfrak{a}(t)$ and $\phi(t)$ are the instantaneous amplitude and phase of $x(t)$. Now, we will express $\dot{x}(t)$ in analytic signal using $\mathfrak{a}(t)$ and $\phi(t)$ as follows:

$$\begin{aligned}
\dot{x}(t) \;&= \dot{\mathfrak{a}}(t)e^{j\phi(t)} + j\omega(t)\mathfrak{a}(t)e^{j\phi(t)} \\
&= \dot{\mathfrak{a}}(t)e^{j\phi(t)} + \omega(t)\mathfrak{a}(t)e^{j\left(\phi(t)+\frac{\pi}{2}\right)} \\
&= \sqrt{\dot{\mathfrak{a}}^2(t) + \left(\omega(t)\mathfrak{a}(t)\right)^2}\, e^{j\left(\phi(t)+\arctan\frac{\dot{\mathfrak{a}}(t)}{\omega(t)\mathfrak{a}(t)}\right)} \\
&= \mathfrak{a}(t)\sqrt{\mathfrak{b}^2(t) + \omega^2(t)}\, e^{j\left(\phi(t)+\arctan\frac{\mathfrak{b}(t)}{\omega(t)}\right)}
\end{aligned} \tag{4.4}$$

where $\mathfrak{b}(t)$ is given in Eq. (4.1) If we choose $\mathfrak{b}(t)$ to be nonnegative, based on the fact that $\mathfrak{b}$ is an indicator of the standard deviation of the estimated $\omega(t)$ (which will be introduced and explained shortly after), we will have

$$\mathfrak{b}(t) \;=\; \left|\frac{\dot{\mathfrak{a}}(t)}{\mathfrak{a}(t)}\right| \tag{4.5}$$

Continuing on, practically the instantaneous amplitude and frequency of $\dot{x}(t)$ are as follows:

$$\mathfrak{a}_{\dot{x}}(t) \;= \mathfrak{a}(t)\sqrt{\mathfrak{b}^2(t)+\omega^2(t)} \tag{4.6}$$

$$\omega_{\dot{x}}(t) \;= \frac{d\left(\phi(t)+\arctan\frac{\mathfrak{b}(t)}{\omega(t)}\right)}{dt} \;=\; \omega(t)+\frac{1}{1+\frac{\mathfrak{b}^2(t)}{\omega^2(t)}} \tag{4.7}$$

It can be seen that these instantaneous characteristics for $\dot{x}(t)$ are affected by both $\mathfrak{b}(t)$ and $\omega(t)$ of $x(t)$ in a nonlinear fashion. Only if $\mathfrak{b}(t) \equiv 0$ and $\omega(t) =$ constant, the backbone of $\dot{x}(t)$ is an undistorted version of that of $x(t)$.

A similar analysis can be applied to compare the backbones of $\dot{x}(t)$ and $\ddot{x}(t)$ with the same conclusion drawn. The difference between the backbones from $x(t)$ and $\ddot{x}(t)$, i.e., displacement backbone and acceleration backbone, would thus be even more complicated. Considering nonlinearities underlying general SDOF systems that we try to capture, we cannot anticipate displacement backbone being identical to acceleration backbone with the understanding that acceleration backbone would be far more complicated. Therefore, typical patterns of displacement backbone given in reference [23] cannot be conveniently generalized for acceleration backbone. With this said, it seems wise to use displacement backbone only in practice so that the correlations between backbone patterns and underlying system nonlinearities as established in reference [23] can be utilized for pattern classification.

4.4.2 Numerical results of displacement/velocity/acceleration backbones

Numerical examples are provided in Figs. 4.15 and 4.16 to verify the complexity of acceleration backbone over those of velocity and displacement backbone – except for cases where both ω and $\mathfrak{b}$ are constants with respect to time. For a simple swept sine signal in Column (b) in Fig. 4.15, acceleration backbone completely destroys the dominant feature that is shown clearly in displacement backbone. In Fig. 4.16 that uses Duffing oscillator and unfiltered backbone, acceleration backbones are far more spread out that their displacement backbone counterparts. Given the results in Fig. 4.15 using mono-components in each case, we anticipate the filtered backbones in Fig. 4.16 differ drastically between displacement backbone and acceleration backbone.

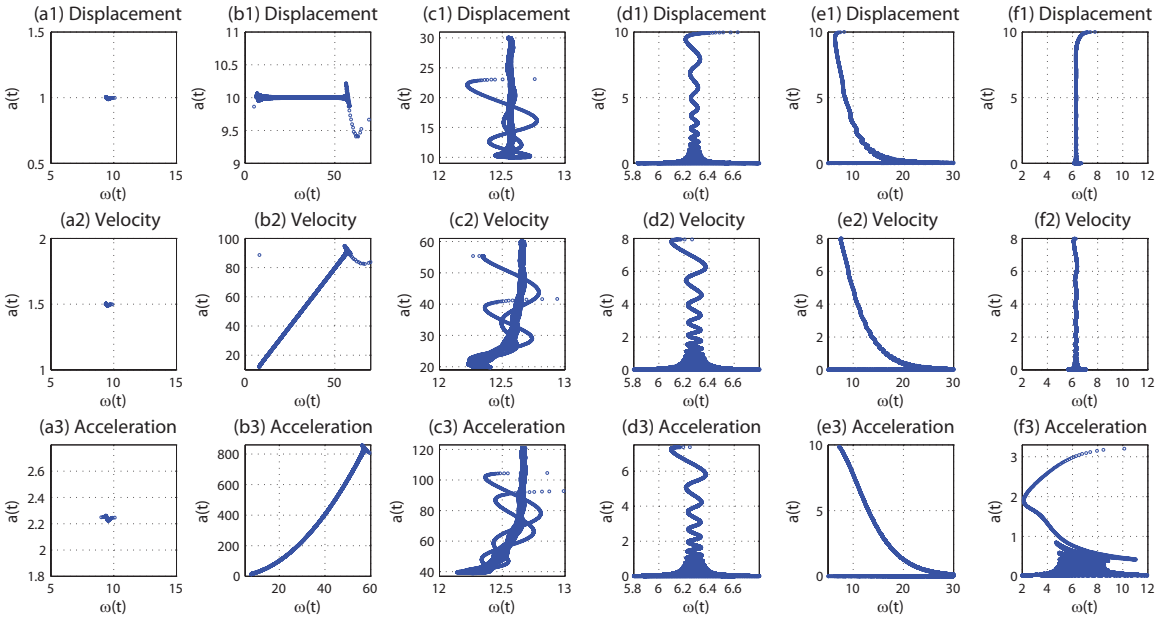

Figure 4.15: Displacement, velocity and acceleration backbones of Cases 1 to 6 in Chapter 3.

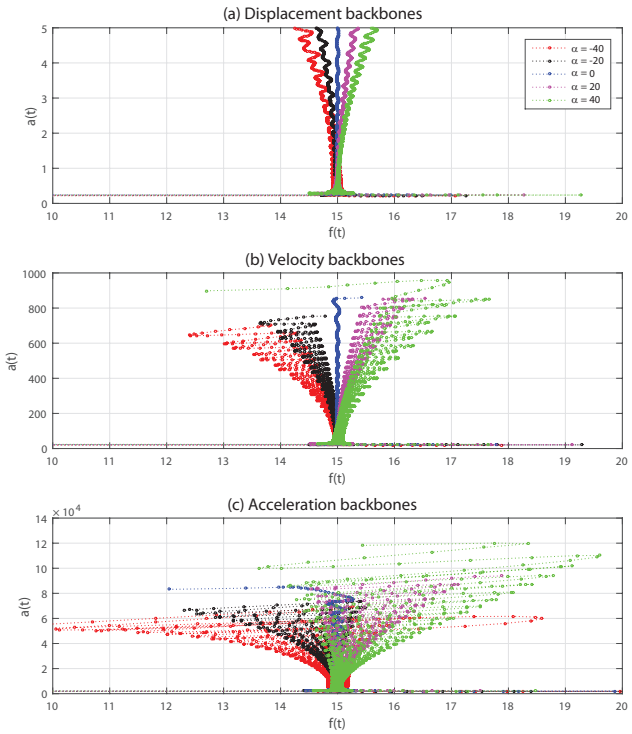

Figure 4.16: Displacement, velocity and acceleration backbones affected by natural frequency f_n in the Duffing oscillator of $\ddot{x}(t) + 2 \times 2\% \times (2\pi f_n)\dot{x}(t) + (2\pi f_n)^2 x(t) + 40x^3(t) = 0$ with initial condition $x(0) = 1$ and $\dot{x}(0) = 0$.

4.4.3 Three-dimensional backbone

The state variables for a SDOF Duffing oscillator is well-known to be x and $\dot{x}$, which are in a Cartesian coordinate system. With the view of analytic signal, the state variable and equation may be given as follows for an unforced Duffing oscillator following both the assumption and details given in J:

$$\mathbf{u} = \begin{pmatrix} u_1 \\ u_2 \\ u_3 \end{pmatrix} = \begin{pmatrix} \mathfrak{a} \\ \mathfrak{b} \\ \omega \end{pmatrix} \tag{4.8}$$

$$\dot{\mathbf{u}} = \begin{pmatrix} u_1 u_2 \\ -\frac{3}{4}\alpha u_1^2 - u_2^2 - c u_2 + u_3^2 - k \\ -2u_2 u_3 - c u_3 \end{pmatrix} \tag{4.9}$$

It seems that the free Duffing model can be characterized by $\mathfrak{a}(t)$, $\omega(t)$, and $\mathfrak{b}(t)$. Note that the $\mathfrak{b}(t)$ here is slight different from the original definition in Eq. (4.5) in the sense that the absolute sign is removed. This is only the location in this chapter where IB is defined differently. How could this affect the understanding of backbone? This indicates that the backbone defined by $\mathfrak{a}(t)$ and $\omega(t)$ only examines two out of the three state variables – not all. A backbone with all these three state variables examined would be a more complete view of the underlying dynamics. Fig. 4.17 gives a sample of this new kind of three-dimensional backbone, which we think better capture the underlying dynamics but does not help with pattern classification and data compression.

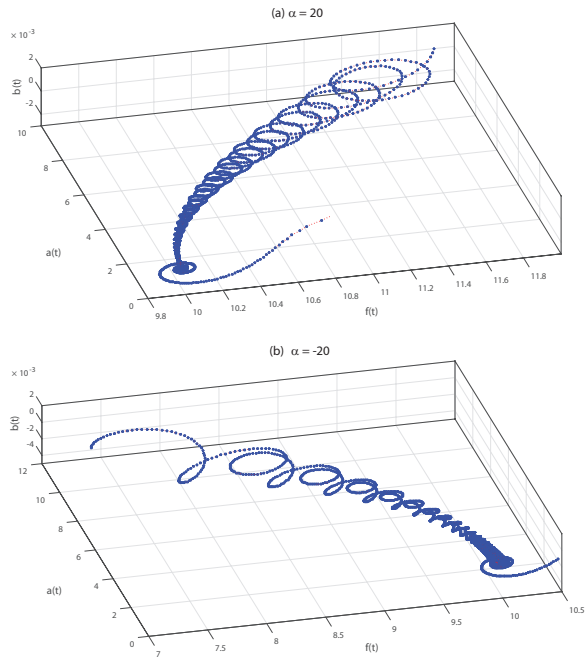

Figure 4.17: Backbone in 3D for two Duffing oscillators of the form $\ddot{x}(t) + 2 \times 2\% \times (2\pi \times 10)\dot{x}(t) + (2\pi \times 10)^2 x(t) + \alpha x^3(t) = 0$ subject to $x(0) = 10$ and $\dot{x}(0) = 0$. (a) $\alpha = 20$; (b) $\alpha = -20$.

4.5 Discussions

4.5.1 More on instantaneous bandwidth

As stated previously, backbone technique is based on the instantaneous quantities of a vibration signal. This may cause confusion or even lead us to a wrong understanding if not being careful enough. We believe that instantaneous bandwidth helps make it easier in this regard. First, we supplement another physical interruption of instantaneous bandwidth with details given in K:

$$|\mathfrak{b}(t)||x(t)| \;=\; |\dot{x}(t)+\omega(t)\tilde{x}(t)|, \text{ or equivalently, } |\mathfrak{b}(t)| \;=\; \left|\frac{\dot{x}(t)}{x(t)}+\omega(t)\frac{\tilde{x}(t)}{x(t)}\right| \quad (4.10)$$

Following [15] where a probabilistic viewpoint is employed, for a given signal $x(t)$, there are infinitely many ways of representing $x(t)$ in amplitude-phase format, where the amplitude would be $\mathfrak{a}(t)$, while the phase is the time integral of $\omega(t)$. $\mathfrak{a}(t)$ and $\omega(t)$ are thus inherently correlated. The way we choose to represent $x(t)$ would affect $\omega(t)$. Fortunately, we can utilize $\mathfrak{b}(t)$ to guard us against making mistakes. This justifies whey we promote the use of $\mathfrak{b}(t)$ with the backbone technique.

To make us clearer, Fig. 4.18 presents instantaneous characteristics of two seemingly simple signals, both of which is a sum of two sinusoidal waves, i.e., a double-component signal Chapter 3. With only a slight difference in the amplitude of one component, the instantaneous characteristics may change drastically. By looking at $\mathfrak{a}(t)$ and $\omega(t)$ of $x_r(t)$, we would very likely to draw the conclusion that the signal is a mono-component signal with a constant frequency. However, its $\mathfrak{b}(t)$ indicates that this conclusion is not correct. Large $\mathfrak{b}(t)$ hints that $\omega(t)$ is not accurate in this case. Looking more closely, the instantaneous phase, $\phi(t)$, in this case does not satisfy the continuity property as pointed out in reference [72] to make the estimation of $\mathfrak{a}(t)$ and $\omega(t)$ valid.

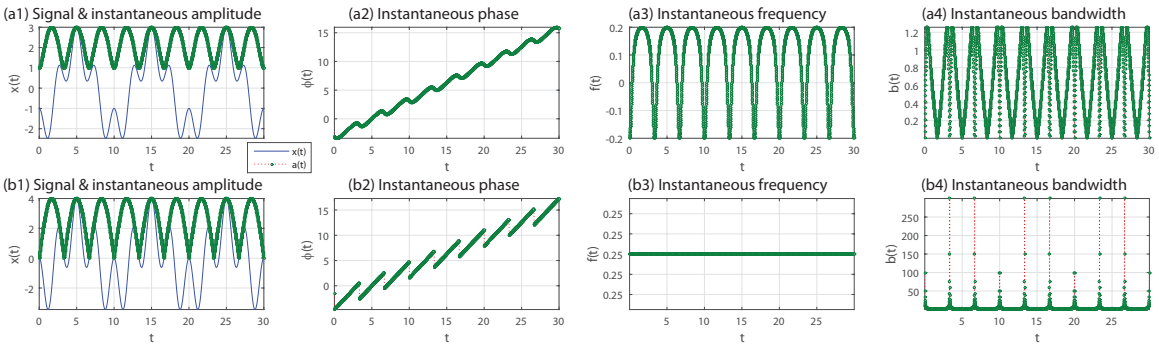

Figure 4.18: The instantaneous frequency for the signal $x_a(t) = -2\cos(2\pi 0.1t) + \cos(2\pi 0.4t)$ (upper 5 panels) and $x_b(t) = -2\cos(2\pi 0.1t) + 2\cos(2\pi 0.4t)$ (lower 5 panels). Following Chapter 3, for $x_a(t)$, $\mathfrak{a} = (5 - 4\cos(2\pi 0.3t))^{1/2}$, $\omega = 2\pi 0.25 + 2\pi 0.15\frac{-3}{5-4\cos(2\pi 0.3t)}$; For $x_b(t)$, $\mathfrak{a} = (8 - 8\cos(2\pi 0.3t))^{1/2}$, $\omega = 2\pi 0.25$, i.e., 0.25Hz. For $x_a(t)$, negative $\omega(t)$ occurs when instantaneous bandwidth blows up as shown in (a4). This implies instantaneous bandwidth being a potential indicator of the correctness of the instantaneous frequency estimation. For x_b, $\omega(t)$ is constant but without physical meaning. Instantaneous bandwidth in (b4) behaves even worse than in (a4), indicating a worse instantaneous frequency estimation.

4.5.2 Damping estimation

The importance of the concept instantaneous bandwidth cannot be emphasized more. For example, the assumed viscous damping in Eq. (4.2) is closely related to instantaneous bandwidth following [30], even though the concept of instantaneous bandwidth is not used in that reference. Review notes on damping estimation are presented in L. It is clear that Eq. (L.6) for damping estimation is heavily dependent on instantaneous quantities. Moreover, [30] omits the second term on the RHS in Eq. (L.6), which we don't see the reasoning yet. As a counter example, Fig. 4.19 presents a comparison of the estimated damping coefficients with and without the second term, where the one with the second term yields a slightly better result.

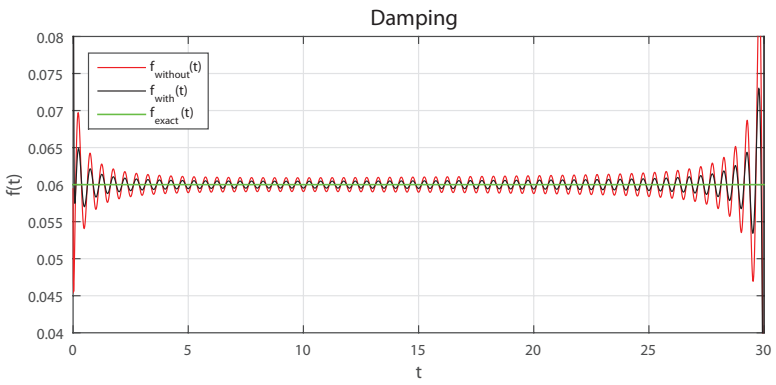

Figure 4.19: Damping estimation of an exponentially decaying signal $x(t) = e^{-\zeta\omega t}\cos(2\pi\omega t)$ with $\zeta = 6\%$ and $\omega = 2$ Hz. f_{with}, f_{without} and f_{exact} correspond to the estimated damping with the second term on RHS of Eq. (L.6), estimated damping without the second term and exact damping, respectively.

4.6 Conclusions

A couple of important aspects related to the applicable range of the backbone technique have been thoroughly studied in this chapter, all of which is closely related to the concept of instantaneous bandwidth that has not been applied to the backbone technique.

First of all, a parametric study has been carried out to examine the performance of the backbone technique – with contributions in Chapter 3 – applied to unforced SDOF Dufffing oscillator with parameter values that can represent meaningful structural dynamics. The goal is to obtain a non-oscillatory and simple pattern from the backbone of the dominant mono-component – in order to build on the promising correlations between the patterns and underlying types of nonlinearities given in reference [23] for system identification and damage detection.

Overall, this seemingly simple task is not straightforward involving many nontrivial details. First, severe errors have been observed for DHT result towards the tail of the response. Causes have been revealed; a practical guidance has been provided to avoid the errors in the first place. A piecewise DHT solution has been further

proposed to overcome the errors with the efficacy of the solution demonstrated in the simulation. Next, we have refined the signal decomposition procedure given in Chapter 3 in order to produce a filtered version of the backbone of the dominant mono-component that would otherwise not be suitable for pattern classification, the intended application of the backbone. Design parameters of the proposed bandpass filter have been discussed to facilitate applications to real-world data.

We have also quantified the relationship between displacement, velocity and acceleration backbones. We have shown that the velocity/acceleration backbone will be distorted in a nonlinear fashion compared with the displacement/velocity backbone for general signals. Necessary condition for an undistorted backbone has been given in this study, which is not normally satisfied in practice. Acceleration backbone and displacement backbone would thus be of different patterns, based on which we recommend obtaining displacement from acceleration measurement as the first step in applying the backbone technique so that those displacement backbone patterns presented in reference [23] will remain useful.

Theoretically, we have introduced the concept of instantaneous bandwidth to the backbone technique. We have computed instantaneous bandwidth in numerical exercises to demonstrate a unique, critical, and easily-obtained insight it brings in seeking a correct backbone and its filtered version. The necessary condition mentioned above for backbones of velocity and acceleration being undistorted from those of displacement is another example for the usefulness of instantaneous bandwidth. To complement the seminal work in reference [15], we have supplemented another physical interpretation of instantaneous bandwidth. For unforced Duffing oscillator studied here, we have shown that instantaneous amplitude, instantaneous frequency, and instantaneous bandwidth could be the governing state variables, and they form a three-dimensional backbone. In other words, a backbone made up of instantaneous amplitude and instantaneous frequency can be a projection of this three-dimensional

backbone. This viewpoint helps understand and generalize the concept of backbone, even though it may not directly help with pattern classification and data compression. We have also pointed out an important application in damping estimation, when instantaneous bandwidth was used in Dr. Feldman's work but without the name.

Chapter 5

APPLICATIONS OF IMPROVED BACKBONE TECHNIQUE TO REAL-WORLD ACCELERATION MEASUREMENTS

5.1 Introduction

We demonstrate and validate the improved backbone technique developed in previous three chapters by using a couple of typical real-world data sets. To achieve this goal, several critical technical details are addressed in the process of developing this work:

First, we propose to use the concepts of effective bandwidth and effective duration to check the information richness of a given data set. Next, we exercise one particular design of Kalman filter published in reference [69] to estimate displacement time history based on acceleration measurement. We contrast acceleration backbone and displacement displacement backbone. These are in addition to applying the algorithms and numerical procedures presented in the previous chapters.

An overview of the selected data sets is given in Table 5.1. They form a total of four cases and nine different data sets:

Table 5.1: An overview of all acceleration measurements to be studied. †The only data set not collected by this research team and not tested under free vibration; this data set was provide by Dr. Steven D. Glaser to Dr. Jin-Song Pei.

Case ID	Brief Description	Ref.	Significance	Accelerometer for Data Acquisition & Sampling Rate
1 †	a timber wall	[61]	for validating the use of effective bandwidth and effective duration only	built-in accelerometer to "mote". f_s = 64 Hz
2	a SDOF metal building model	OU CEES 5683	as the presumed best candidate for a SDOF system being linear and elastic	Silicon Designs 2210-002. f_s = 10 kHz
3a	a full-scale prestressed concrete girder taken from a real-world bridge, tested under simply supported condition, and measured at mid-span	[33]	for modeling a continuous system as a SDOF system at the beam's mid-span and for modeling a prestressed concrete girder after more than four decades in service	Silicon Designs 2210-002. f_s = 10 kHz
3b	same s3a except for reinforcement detail of the cross-section, span and with an overhang on one side	[33]	similar to 3a	Silicon Designs 2210-002. f_s = 1000 Hz
3c	same as 3b except for being tested after the mid-span soffit was cracked	[33]	similar to 3b but for a damaged specimen	Silicon Designs 2210-002. f_s = 10 kHz
4a-c	a prototype timber beam-column joint model designed to behave as a SDOF model	[57]	for demonstrating nonlinear response according to the existing literature	Analog Devices ADXL 105EM-3. f_s = 500 Hz
4d	a prototype timber beam-column frame model designed to behave as a SDOF model	[57]	same as 4a-c	Analog Devices ADXL 105EM-3. f_s = 500 Hz

Case #1 is different from the rest: The quality of the data is significantly less satisfactory than that in other cases. This is caused by adopting an early wireless sensor product called "mote" and using a slow sampling rate. This data set is thus

visually of poor quality; it is merely used for demonstrating the proposed effective bandwidth and duration concepts to quantify the information richness of a given data set. How this data set was collected may be out of date, however the research need in quantifying information richness of collected data is not. For example, when one wishes to utilize the free vibration caused by an earthquake excitation for applying the backbone technique, one may need to question first if the information carried in the data is sufficiently rich when the magnitude of the earthquake is low. Using the product of effectiveness bandwidth and effective duration, also known as bandwidth duration product, as a quantitative measure is adopted from electrical engineering; this proposed add-on pre-processing procedure to the backbone technique leads to a more robust implementation.

Cases #2 to 4 contain meaningful data sets collected from structural systems that could be modelled as SDOF systems. While the significance of each case is listed in Table 5.1, three major challenges exist - especially for Cases #3 and 4. These challenges are from the accuracy of SDOF system modeling, the complexity of the adopted construction material, and the unknown damage status. These challenges would be elaborated later in Section 5.4.1; the key message is that these data sets are far more complicated than simulated results of Duffing oscillator (studied earlier by us). This entails the need for additional signal processing effort.

The structure of this chapter is as follows: In Section 5.2, effective bandwidth and effective duration, the two key concepts are reviewed, after which the product of these two quantities is estimated for the data set under Case #1 as a measurement for the data information richness. Section 5.3 reviews and implements a Kalman filter that estimates displacement out of acceleration time history. Simulated data is used to validate the implemented Kalman filter. Section 5.4 contains all investigations on Cases #2 to 4. First, domain knowledge is given in Section 5.4.1 for anticipated result of these cases – when they are available. Time-frequency analysis

and frequency-domain analysis are then carried out in Section 5.4.2 before acceleration backbone for each case is presented in Section 5.4.3. Finally, an attempt is made to estimate displacement time histories, from which displacement backbones are generated. Preliminary – including unsatisfactory – results are given in Section 5.4.4. This, together with other challenges are discussed in Section 5.5 before conclusions are drawn in Section 5.6.

5.2 Effective Bandwidth and Effective Duration

5.2.1 Concepts

The definition of effective bandwidth and effective duration is a somewhat controversial issue as different definitions exist [7, 56]. To follow, two typical definitions are provided hereafter with one for continuous case given in reference [35, 5, 7] and the other for discrete case given in reference [71].

According to [7], effective bandwidth B_e and effective duration T_e for a continuous signal are as follows:

$$B_e^2 = \frac{\int_{-\infty}^{\infty} \omega^2 |X(\omega)|^2 d\omega}{\int_{-\infty}^{\infty} |X(\omega)|^2 d\omega} \tag{5.1}$$

$$T_e^2 = \frac{\int_{-\infty}^{\infty} t^2 |x(t)|^2 dt}{\int_{-\infty}^{\infty} |x(t)|^2 dt} \tag{5.2}$$

The $B_e T_e$ product is considered a measure for the richness of the signal [5, 7, 56]; a product of greater than 10 is considered acceptable [5, 7]. Therefore, we propose to run a "BT test" first to check if a specified signal is meaningful to process.

Since we are dealing with real-world signals, discrete formulas for B_e and T_e would

thus be desirable. A discrete form of B_e and T_e is given as follows in [71]:

$$B_e^2 = 2\frac{\sum_{k=0}^{N/2-1}(kN/F_s)^2 X[k]N/F_s}{\sum_{k=0}^{N/2-1} X[k]N/F_s} \tag{5.3}$$

$$T_e^2 = 2\frac{\sum_{m=0}^{N-1}(m/F_s)^2 x[m]/F_s}{\sum_{m=0}^{N-1} x[m]/F_s} \tag{5.4}$$

These discrete formulas, however, are quite inconsistent with the formulas for the continuous case. The denominator in Eq. (5.4) is simply the mean of the discrete signal scaled by a constant of N/F_s, which could be zero even when the numerator is not zero. In the author's understanding, the discrete formulas may be given in the following to mimic the continuous case – with the corrected terms presented in red:

$$B_e^2 = 2\frac{\sum_{k=0}^{N/2-1}(kN/F_s)^2 |X[k]|^2 N/F_s}{\sum_{k=0}^{N/2-1} |X[k]|^2 N/F_s} \tag{5.5}$$

$$T_e^2 = 2\frac{\sum_{m=0}^{N-1}(m/F_s)^2 |x[m]|^2/F_s}{\sum_{m=0}^{N-1} |x[m]|^2/F_s} \tag{5.6}$$

5.2.2 BT test of the "mote" data

To quantify B_e and T_e by using Case #1 data set, we encountered a great deal of challenge. The discrete formulas are only the author's own interpretation but without any supporting references. We thus tried to validate such choices in computing B_eT_e product using a couple of signals with known property. Fig. 5.1 shows the BT tests on 12 test signals. It can be seen that these B_eT_e results may not be quite helpful for indicating the richness of information. The reason for this could be that the BT

formulas for continuous signals may not be directly applicable to discrete signals.

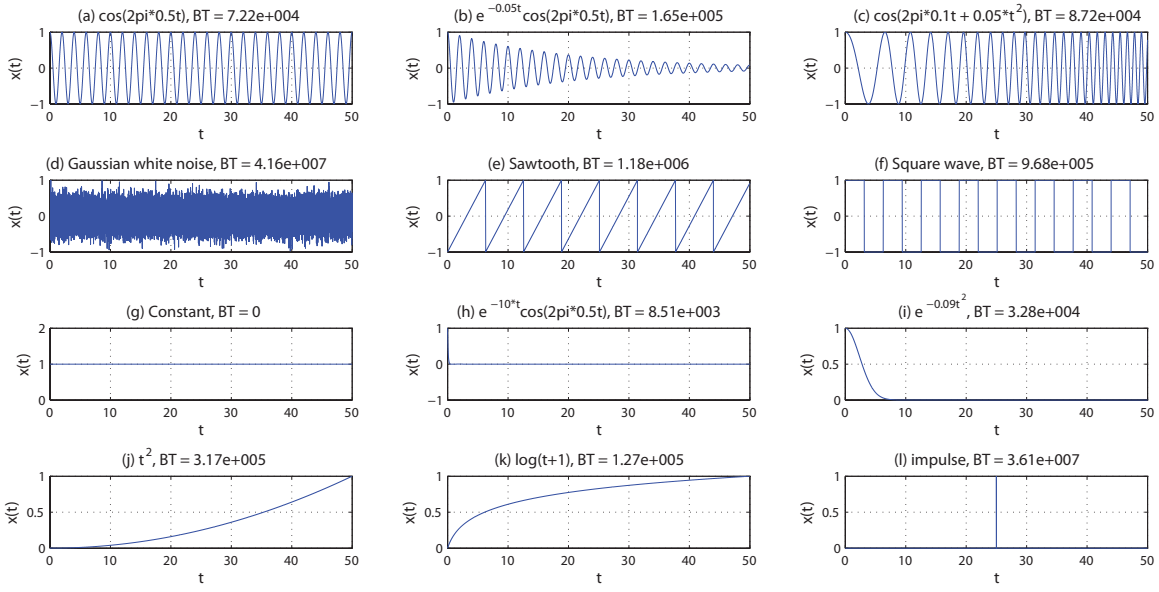

Figure 5.1: 12 carefully designed test signals with their BT products.

A typical data set from Case #1 is presented in Fig. 5.2. Despite the challenge given above, we still computed the BT product of the signal in Case #1; see Fig. 5.2. It is worth mentioning that the BT product in Cases #2 to #4 are about 10 times larger than that of Case #1, the fact of which is consistent with better quality of the data in these cases than that in Case #1. Nonetheless, we feel that we have not yet obtained a reliable means of computing meaningful BT, which we are still trying to achieve.

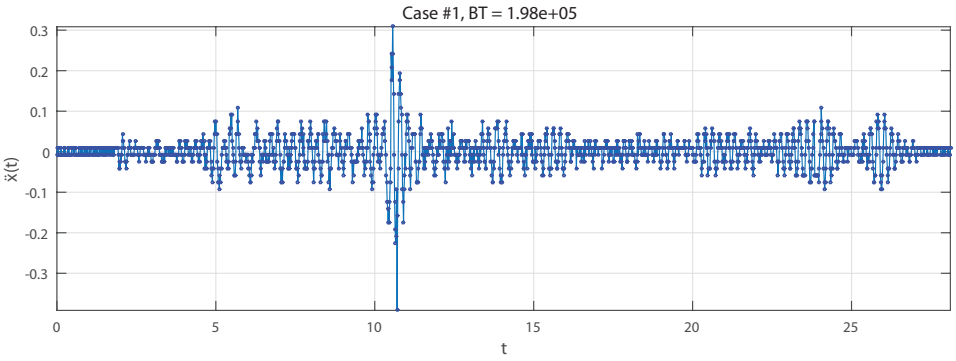

Figure 5.2: Reconstructed time history of Case #1. The original measurements contain a total of 16 missing data points out of the truncated 1800 data points. Next neighborhood interpolation was used to reconstruct the missing data points. The B_eT_e product of the reconstructed time history is 1.95e5.

5.3 Estimating Displacement from Measured Acceleration

In the community of system identification, displacement estimation from acceleration has long been an important and active research topic. According to [39, 40], basically, there are two categories of methods: time domain method and frequency domain method. [69] introduced a Kalman filter based technique by using absement, time integral of displacement. Here, we will present a quick review of [69] and validate it with three numerical examples.

5.3.1 Literature review

In this study, the technique of using Kalman filter for velocity and displacement estimation is directly adopted from [69]. The fundamental assumption of the technique is that there is no significant permanent displacement of the structure under test – which is satisfied in the case studies – and the signal is linear. The last assumption is not necessarily satisfied by the data sets. Nonetheless, we will still test out this technique in conjunction with some filtering procedure as will be explained later on.

The technique starts with forming a state-space equation. The state vector $\mathbf{x}$ is defined as follows:

$$\mathbf{x}[k] \;=\; \begin{pmatrix} v[k] \\ d[k] \\ z[k] \end{pmatrix} \tag{5.7}$$

where $v[k],\ d[k],\ z[k]$ are the velocity, displacement and absement at time index k, respectively. The state space equation is then formulated as

$$\mathbf{x}[k] \;= \mathbf{A}\mathbf{x}[k-1] \;+\; \mathbf{B}\left(\mathbf{u}[k] + \mathbf{w}[k]\right) \tag{5.8}$$

$$\mathbf{y}[k] \;= \mathbf{C}\mathbf{x}[x] \;+\; \mathbf{v}[k] \tag{5.9}$$

where $\mathbf{A},\ \mathbf{B},\ \mathbf{C}$ are as usually defined, $\mathbf{u}$ is the input, i.e., the acceleration, $\mathbf{w}$ and $\mathbf{v}$ are the equipment and measurement noise that have normal probability distributions with zero mean and covariances of $\mathbf{Q}$ and $\mathbf{R}$, respectively. We have

$$\mathbf{A} \;=\; \begin{pmatrix} 1 & 0 & 0 \\ T_s & 1 & 0 \\ T_s^2/2 & T_s & 1 \end{pmatrix},\ \mathbf{B} \;=\; \begin{pmatrix} T_s \\ T_s^2/2 \\ T_s^3/6 \end{pmatrix},\ \mathbf{C} \;=\; \begin{bmatrix} 0 & 0 & 1 \end{bmatrix}$$

where T_s is the sampling interval, i.e., the reciprocal of sampling frequency F_s.

Following Kalman filter design, the prediction equations are:

$$\hat{\mathbf{x}}[k|k-1] \;= \mathbf{A}\hat{\mathbf{x}}[k-1] \;+\; \mathbf{B}\mathbf{u}[k] \tag{5.10}$$

$$\mathbf{P}[k|k-1] \;= \mathbf{A}\mathbf{P}[k-1]\mathbf{A}^T \;+\; \mathbf{B}\mathbf{Q}\mathbf{B}^T \tag{5.11}$$

and the correction (update) equations are:

$$\mathbf{K}[k] \;= \mathbf{P}[k|k-1]\mathbf{C}^T \left(\mathbf{C}\mathbf{P}[k|k-1]\mathbf{C}^T + \mathbf{R}\right)^{-1} \tag{5.12}$$

$$\hat{\mathbf{x}}[k] \;= \hat{\mathbf{x}}[k|k-1] \;+\; \mathbf{K}[k]\left(y[k] - \mathbf{C}\hat{\mathbf{x}}[k|k-1]\right) \tag{5.13}$$

$$\mathbf{P}[k] \;=\; \left(\mathbf{I} - \mathbf{K}[k]\mathbf{C}\right)\mathbf{P}[k|k-1] \tag{5.14}$$

The estimated state $\hat{\mathbf{x}}$ can thus be computed leading to approximated displacement and velocity.

5.3.2 Validation using simulated data

The adopted Kalman filter technique is tested on three simulated data sets. The three data sets are a sinusoidal wave, an exponentially decaying sinusoidal wave, and a free response of a damped Duffing oscillator, all of which are polluted with simulated Gaussian white noise to mimic real-world signals. All three signals are carefully designed with known exact acceleration, velocity and displacement, except for the Duffing case where the exact means the numerical results obtained by using RK45. It can be seen in Fig. 5.3, for each signal, the displacement is recovered reasonably well, indicating the promise of this technique.

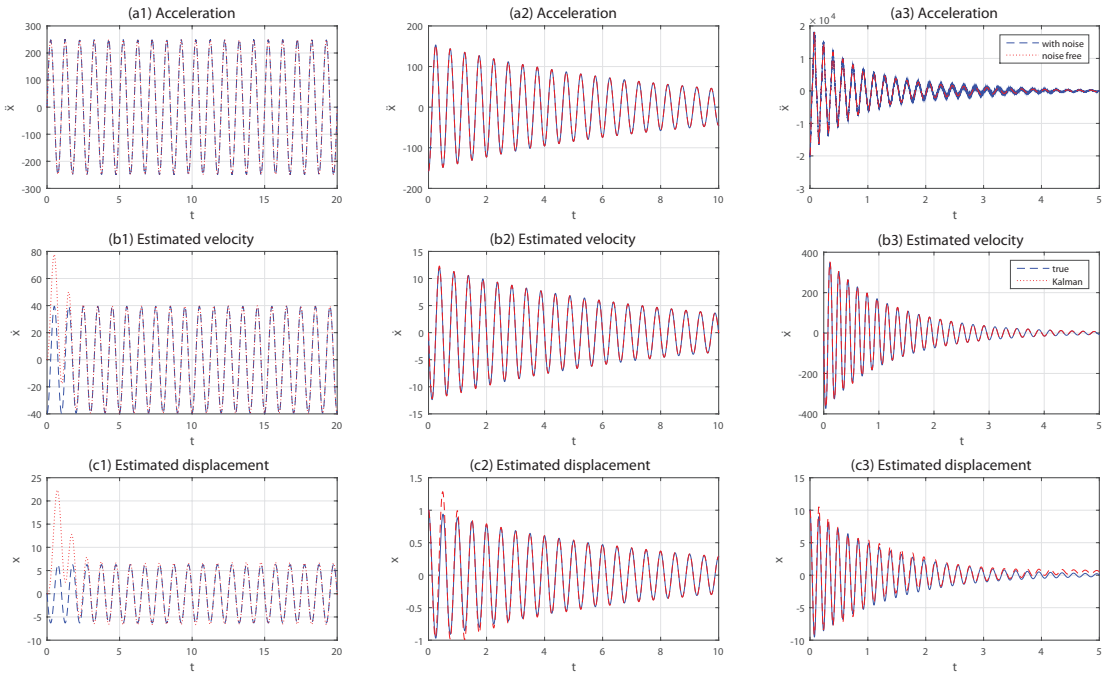

Figure 5.3: Validating Kalman filter-based displacement estimation method: (a1) pure sinusoidal wave; (a2) exponentially decaying sinusoidal wave, and (a3) free damped Duffing response. All acceleration time histories are added with Gaussian white noise. Each signal is tested ten times independently; the converging time and averaged root mean square error (RMSE) of the converged parts are recorded as follows: (a) 5 seconds and RMSE is 0.27; (b) 1.5 seconds and RMSE is 0.034, and (c) nearly 0 second and RMSE is 1.51.

5.3.3 Drift problem

It needs to emphasize that for the Duffing case, the displacement estimation seems to be very sensitive to the noise. Drastically different estimates are observed during ten tests, some of which have very obvious drift as in Fig. 5.4(a1) and (a2). To resolve this issue, we use a highpass filter on the displacement estimation to filter out the drift as shown in Fig. 5.4 (b1) and (b2). Nonetheless, the filtered displacement can still have obvious drift at the two ends (not shown in Fig. 5.4). In that case, the two ends are discarded.

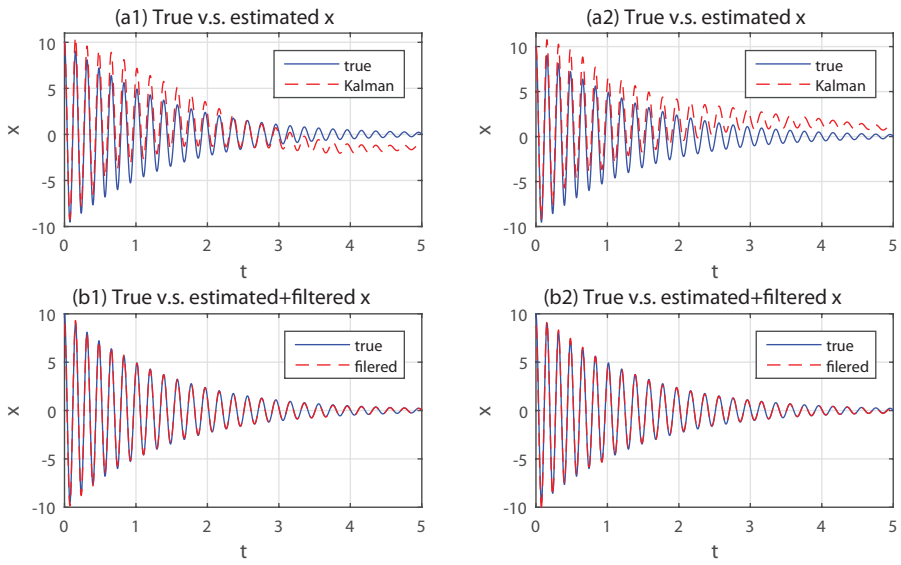

Figure 5.4: Two realizations of displacement estimation of the Duffing response that shows obvious drift is corrected with a highpass filter. (a1) and (a2) are the two Kalman estimation with obvious drift, and (b1) and (b2) are the corresponding filtered displacement estimates. The root mean square error (RMSE) in (b1) and (b2) are 0.1361 and 0.1591, respectively.

5.4 Case Studies

5.4.1 Domain knowledge

Photos taken to show the setup of Case #2 are presented in Figure 5.5. The superstructure is intended to be used as a SDOF model for teaching demonstration, while the substructure is meant to be fixed. Two accelerometers are mounted to the top and bottom mass of the superstructure, respectively, while the difference in their reading is what is interested in data analysis. A modal hammer was used to excite the superstructure; on other occasions, the top mass of the superstructure was pulled along the SDOF direction before being released suddenly to create a non-zero initial displacement.

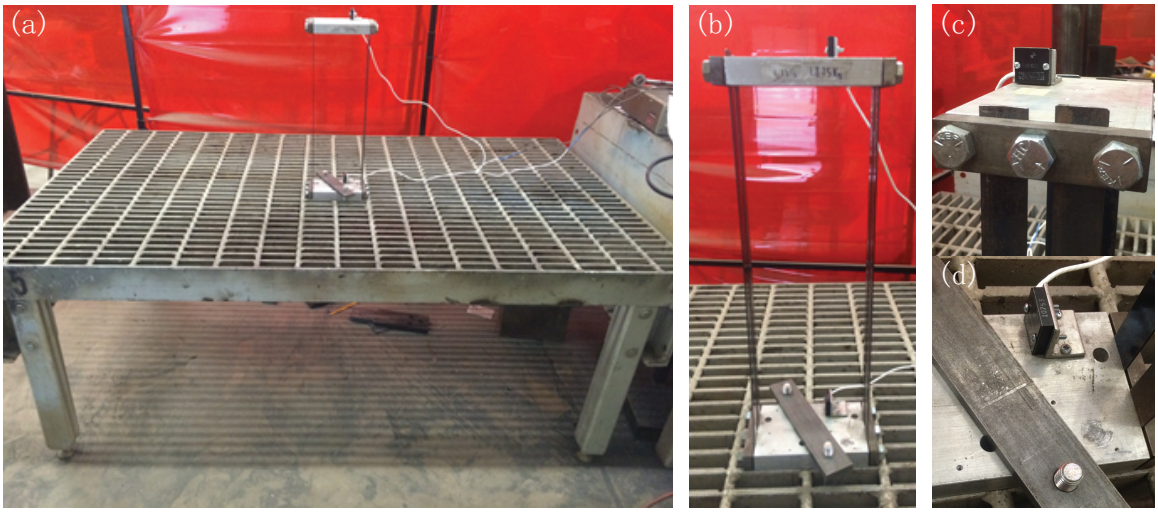

Figure 5.5: Test setup of Case #2. (a) is an overview; (b) is the superstructure; (c) is the accelerometer mounted on the top mass, and (d) is the accelerometer mounted on the bottom mass.

The following details belong to the estimation of the natural frequency of this model building:

$$f_n = \frac{1}{2\pi}\sqrt{\frac{k}{m}}$$

where $mg = 4.1276$ lbf, and k is estimated as follows:

$$k = 4\bar{k}, \quad \bar{k} = \frac{12EI}{h^3}$$

with $E = 22.324 \times 10^6$ psi, and

$$I = \frac{1}{12}bd^3, \quad \text{with} \quad b = 1.0 \text{ in} \quad \text{and} \quad d = 0.0625 \text{ in}$$

Finally, the clearance is 18 in, while the thickness of each plate is 1 in. Thus, $h = 19$ in. This leads to the estimated $f_n = 2.74$ Hz.

For Cases #3, Fig. 5.6 shows a simple beam model:

Figure 5.6: A model of a simply-supported beam.

An existing formula to calculate the simple beam's in-plane vertical vibration modal frequencies is employed:

$$\omega_n \;=\; \left(\frac{n\pi}{L}\right)^2 \sqrt{\frac{EIg}{\rho A}}, \tag{5.15}$$

where L is the span, E is Young's modulus, I is the moment of inertia of the beam cross-section, g is standard gravity, and ρ is linear weight of the material.

E was estimated using the empirical formula recommended by the American Concrete Institute [2] as follows:

$$E \;=\; 57000\sqrt{f_c}$$

where f_c is the cylindrical compressive strength of the concrete in the unit of psi.

ρ in the unit of lbf/in is calculated as follows:

$$\rho \;=\; \frac{150}{12^3} \times A$$

where A denote the cross-sectional area of the girder and is in the unit of in^2.

Plugging in all values to Eq. (5.15), we have the following results. See Table 5.2 for a summary:

Table 5.2: Estimated modal frequencies using a simple beam model for Case #3. †The adopted design value.

Case ID	L (ft)	$f'c$ (psi)	A (in^2)	I (in^4)	f_1 (Hz)
3a	29	7205	471	99249	27.62
3b & 3c	23	5000 †	369	50979	32.45

As to Case #4, Fig. 2 in reference [57] presents a scaled drawing of the timber

beam-column joint designed to demonstrate the correlation between the connection design detailing, and the type of nonlinearity underlying the data - following the lead in reference [34]. This detail is applied to Case #4a to c. Two identical beam-column joints are used in one frame model, which is applied to Case #4d. Each joint and frame model was tested in two different fashions: forced vibration from an APS shake table with an ordered swept sine excitation, and unforced vibration using a modal hammer. See Fig. 1 in reference [57] for the test setup. While the forced vibration data was analyzed using a traditional frequency response function (FRF)-based backbone, the result of which is presented in Figs. 5 and 6 in reference [57] for the joint and frame models, respectively, processing the result of the unforced tests using the backbone technique was not successfully carried out till this study.

According to Table 1 in reference [57], the timber used was kiln dried SPF, type two pine. The four selected models for Case #4a to d are denoted as LN-L721, LN-N723, LN-LN726, and LN-N711, respectively, where LN stands for using "L-Plate" (Simpson Strong-Tie A21Z) and "Nails" (specifically, Grip Rite 12d 2-1/4", bright common) as the connectors for the top joint in all models, while "L-Plate" alone, "Nail" alone, "L-Plate" and "Nails", and "L-Plate" alone are used as the connectors for the bottom joint of Case #4a to d, respectively.

Following Section 5.1, Table 5.1 summarizes technical challenges in modeling, which would be directly reflected in the data and requires further signal conditioning.

Table 5.3: More detailed overview of Cases #2 to 4. †Results in Table 2 in reference [57] for Case #4.

Case ID	Accuracy of SDOF Model	Level of Material Complexity	Probability for Existing Damage	Anticipated Result †
2	good except for base fixity	low	unlikely	$f_n = 2.74$ Hz
3a	continuous system but modelled as SDOF	high due to concrete's time-dependent behavior, e.g., creep, as well as possible corrosion of prestressing strand	likely due to real-world service	$f_1 = 27.62$ Hz for the first mode, which is vertical motion
3b	same as 3a	same as 3a	very likely due to real-world service and repetitive lab tests under both static and dynamic load	same as 3a except for $f_1 = 32.45$ Hz
3c	same as 3b	same as 3b	same as 3b plus cracks caused by lab testing	f_1 would be lower than that in 3b
4a	out-of-plane motions measured as well	high due to inherent nonlinear behavior and organic nature of timber	likely due to repetitive lab dynamic tests taken place before	softening in 2006 but inconclusive in 2007
4b	same as 4a	same as 4a	same as 4a	same as 4a
4c	same as 4a	same as 4a	same as 4a	linear in 2006 but hardening in 2007
4d	same as 4a	same as 4a	same as 4a	hardening in 2007

First, adopting SDOF models is an approximation that could challenge the analysis and may demand additional signal processing effort. For example, Case #2 would be considered the closest to a linear time-invariant SDOF system, however, the fixity of the base is in question making the data demonstrate a double-component behavior. Case #3 is about continuous systems, however they are modelled - in an approximate sense - as SDOF systems following common practice in structural dynamics. Case #4 concerns prototype models developed to demonstrate SDOF nonlinear dynamics, however they do display motions beyond the specified direction as indicated by the acceleration measurements.

Next, the complexity of construction materials involved deserves a close attention. While Case #2 concerns metal in room temperature thus being straightforward, Case #3 deals with prestressed concrete. Even though the design philosophy for prestressed concrete is to make an "elastic material" [53], for the concrete alone, it is known to have been subject to long-term loading and unloading fatigue in addition to creep behavior. In general, steel strands in these girders suspectable for corrosion in the ends due to an inconsiderate design detail back forty years ago, which introduces another source in complexity. Case #4 uses timber and typical connectors for timber joints or frames. Timber is an inherently nonlinear construction material. Timber also contains natural defects from being an organic material. The adopted connectors would lead to different types of nonlinearities [34] - the very motivation for the design of these timber joint or frame models [57].

Last, each specimen in Cases #3 and 4 was not in a pristine condition as detailed in Table 5.3, i.e., they likely had existing damages before undergoing the free vibration tests.

5.4.2 Time-frequency analysis and frequency-domain analysis

As a first step, eight test data sets under Cases #2 to 4 are analyzed in frequency domain by using short time Fourier transform (STFT) and power spectral density (PSD) estimation. In all figures to be presented hereafter, all PSD plots are rotated 90 degrees so that they can be compared with their corresponding STFT plots more conveniently. For every case study, the STFT and PSD of the entire time history are given first. After that, the portions with interest are extracted and the corresponding STFT and PSD are given. For Case #4, multiple portions are extracted in each case, depending on how many independent tests there are in each data set.

Case #2

The time history together with its STFT and PSD is shown in Figs. 5.13 and 5.8. Fig. 5.8 indicates that the response may be approximated as a sum of two mono-components.

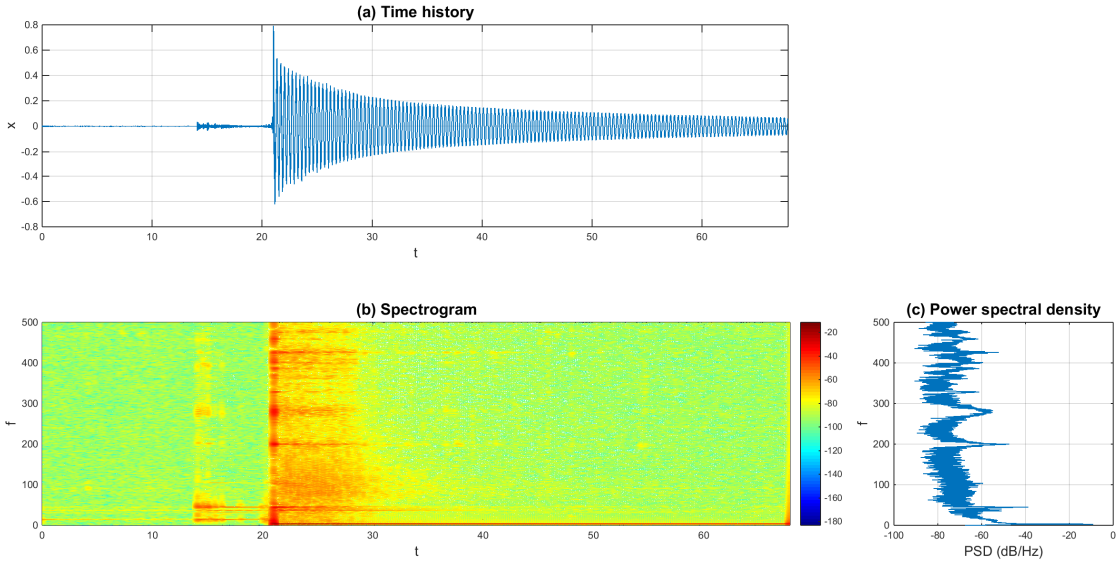

Figure 5.7: Case #2: time history, STFT and PSD. The acceleration measurement is down-sampled to 1000 Hz.

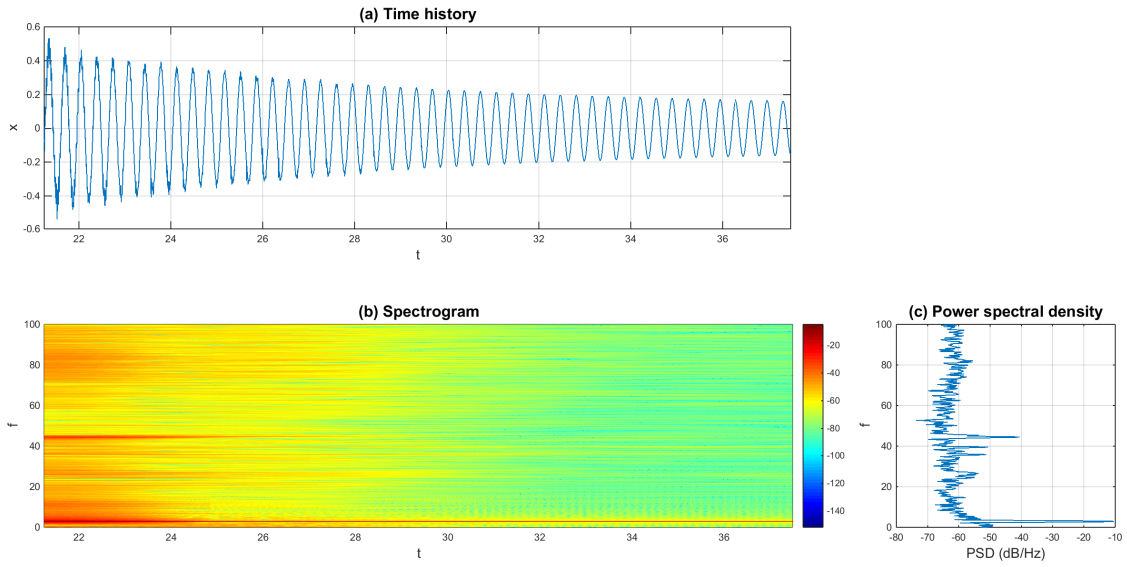

Figure 5.8: Case #2 selected portion: time history, STFT and PSD. The acceleration measurement is down-sampled to 200 Hz.

Case #3a

The entire time history together with its STFT and PSD is shown in Fig. 5.13. The first observation is that right at the impulse force around 13 seconds, the STFT shows a large range of frequency band that is excited. A couple of frequency components are outstanding, possibly corresponding to different structural modes. In the PSD plots, the frequency value of the first peak is consistent with the modal analysis; this mode is also visible in STFT that lasts for at least three seconds. Another obvious peak around 250Hz is quite interesting as it seems to contain higher energy level than the fundamental frequency component as shown in the PSD plot. One reason for this is that this is the PSD of the acceleration time history rather than displacement. Therefore, the amplitude of higher frequency components tends to be amplified in acceleration compared with displacement following the relationship between their Fourier transforms, i.e.,

$$\mathcal{F}\{\ddot{x}(t)\} \;=\; -\omega^2 \mathcal{F}\{x(t)\} \tag{5.16}$$

Fig. 5.10 presents the time history together with its STFT and PSD plots of the portion we are interested in and will be further processed later on. It can be seen that in the PSD plot, the 250Hz mode does not dominate anymore. This is consistent with the fact that higher mode dies out more rapidly in the free vibration of a concrete girder.

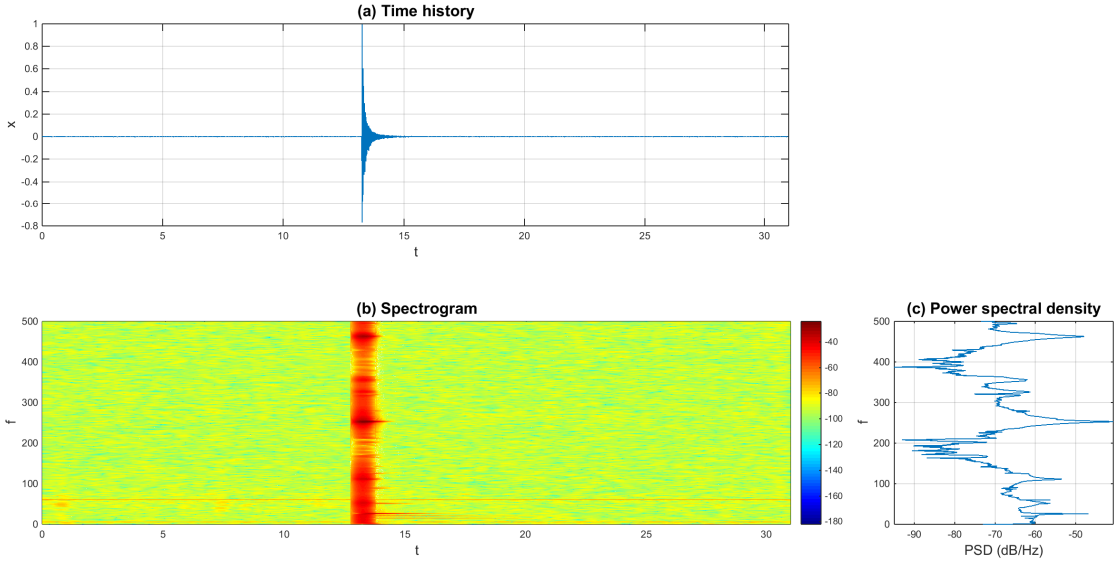

Figure 5.9: Case #3a: time history, short time Fourier transform (STFT) and power spectral density (PSD). The acceleration measurements is down-sampled to 1000Hz.

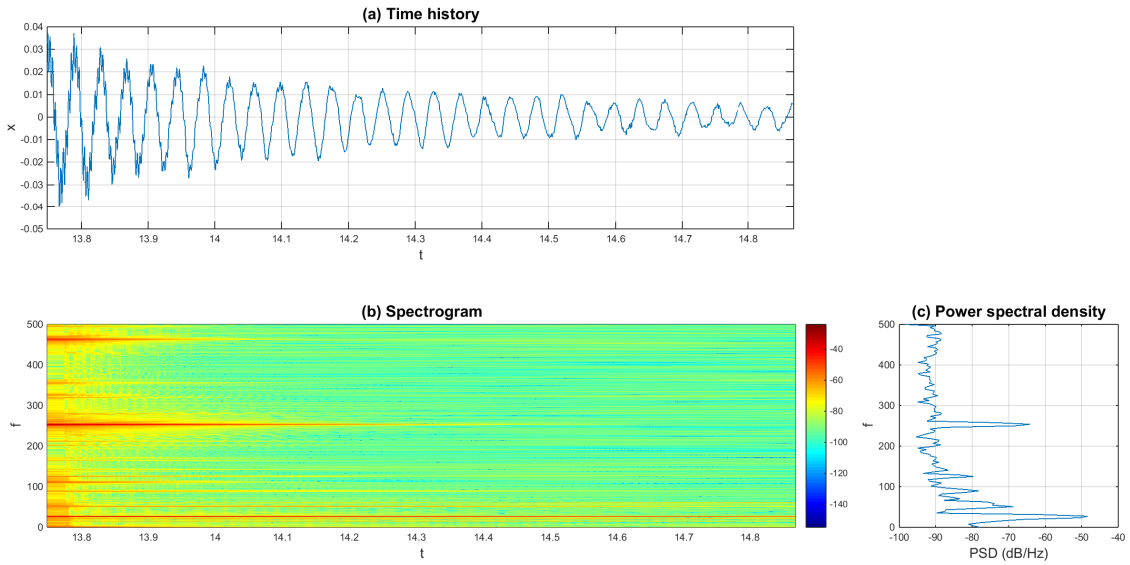

Figure 5.10: Case #3a selected portion: time history, short time Fourier transform (STFT) and power spectral density (PSD). The acceleration measurements is down-sampled to 1000Hz.

Case #3b

The time history together with its STFT and PSD is shown in Figs. 5.11 and 5.14.

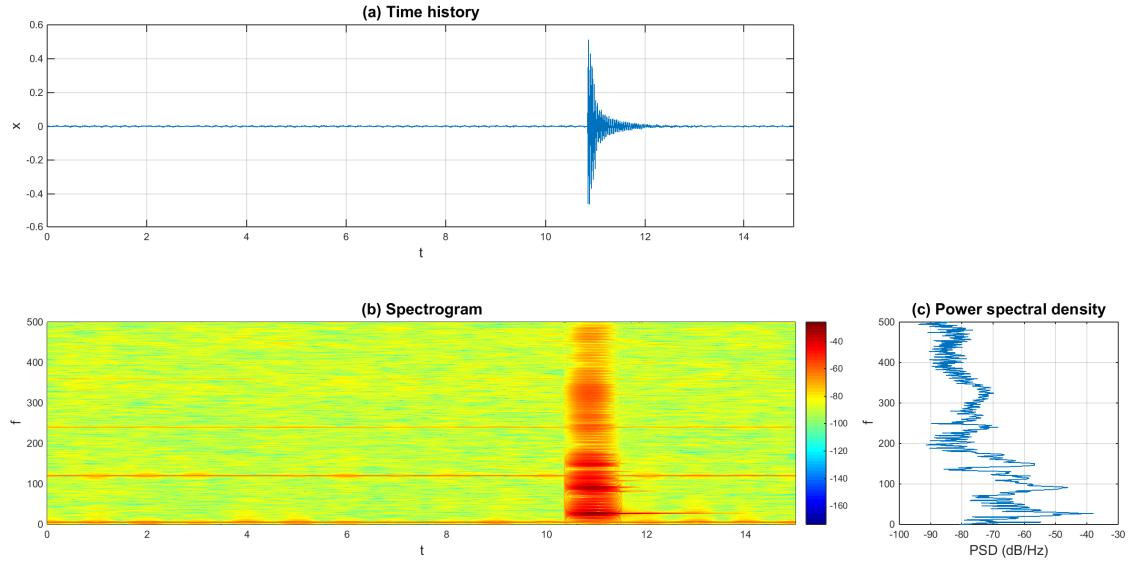

Figure 5.11: Case #3b: time history, STFT and PSD.

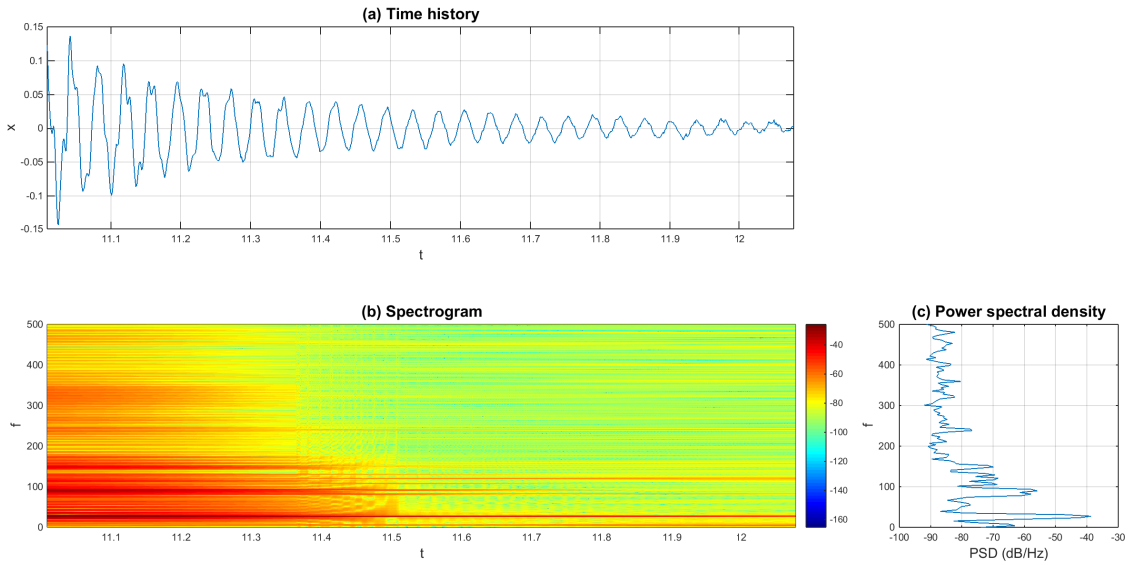

Figure 5.12: Case #3b selected portion: time history, STFT and PSD.

Case #3c

As mentioned before, this is the same girder as in Case #3b but after being cracked. It can be seen that the frequency response displays many more low frequency components than in Case #3b as expected. The time history does not have an obvious periodic behavior as in Case #3b due to the existence of a large range of low frequency components. This would very likely increase the difficulty of applying the decomposition method as the signal does not satisfy the condition that the first component is absolutely dominant.

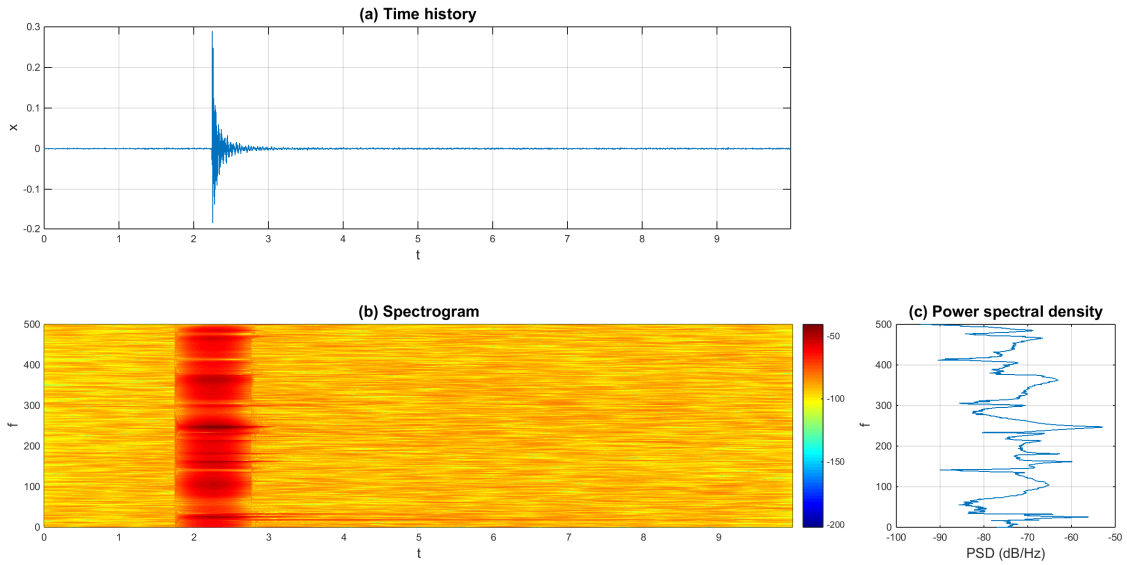

Figure 5.13: Case #3c: time history, STFT and PSD. The acceleration measurements is down-sampled to 1000Hz.

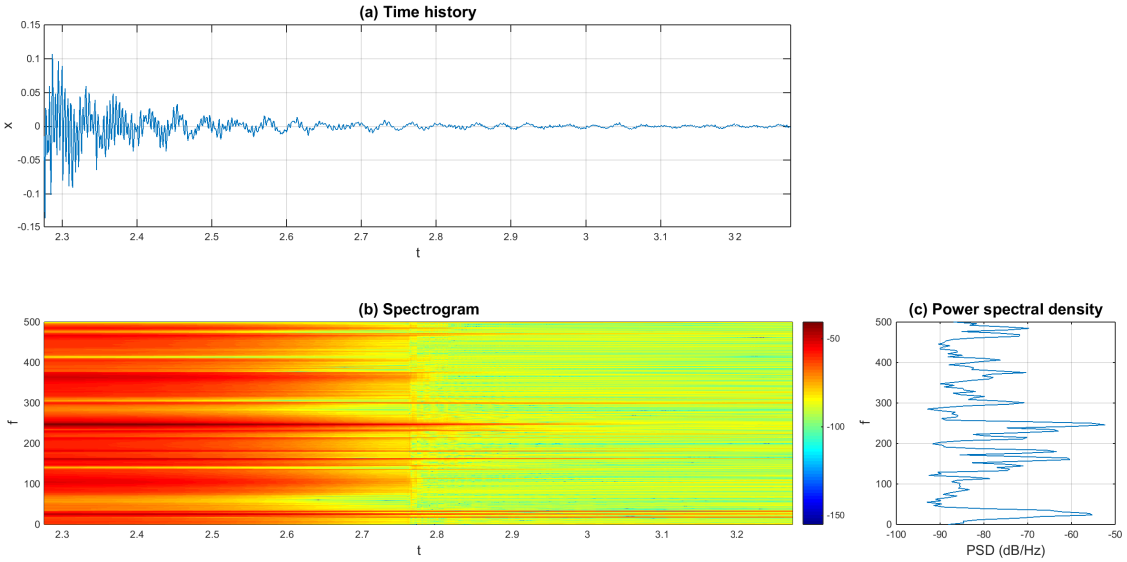

Figure 5.14: Case #3c selected portion: time history, STFT and PSD. The acceleration measurements is down-sampled to 1000Hz.

Case #4a

The time history together with its STFT and PSD is shown in Figs. 5.15 and 5.18.

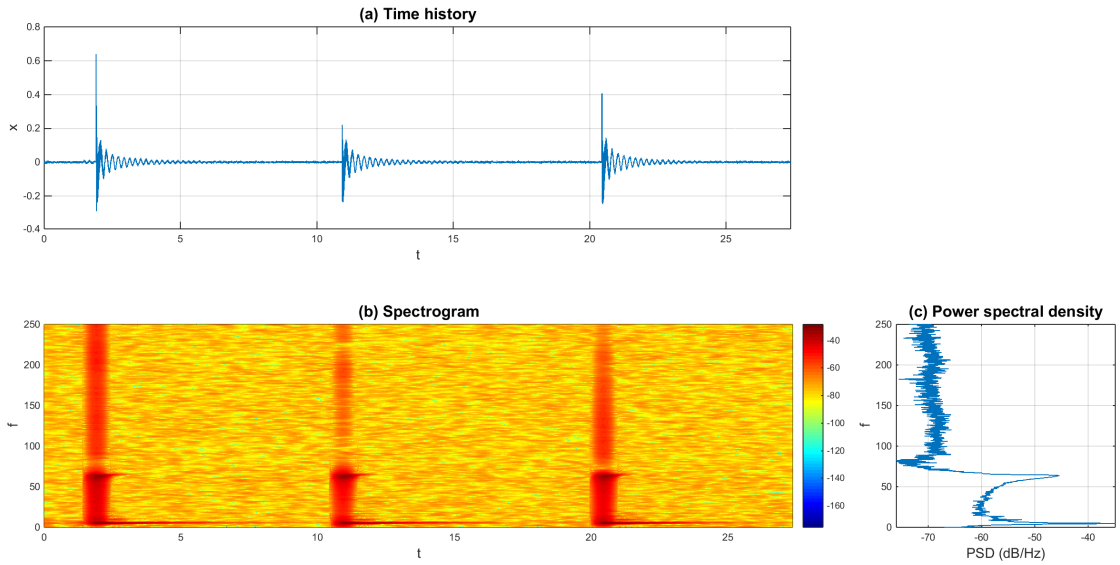

Figure 5.15: Case #4a: time history, STFT and PSD.

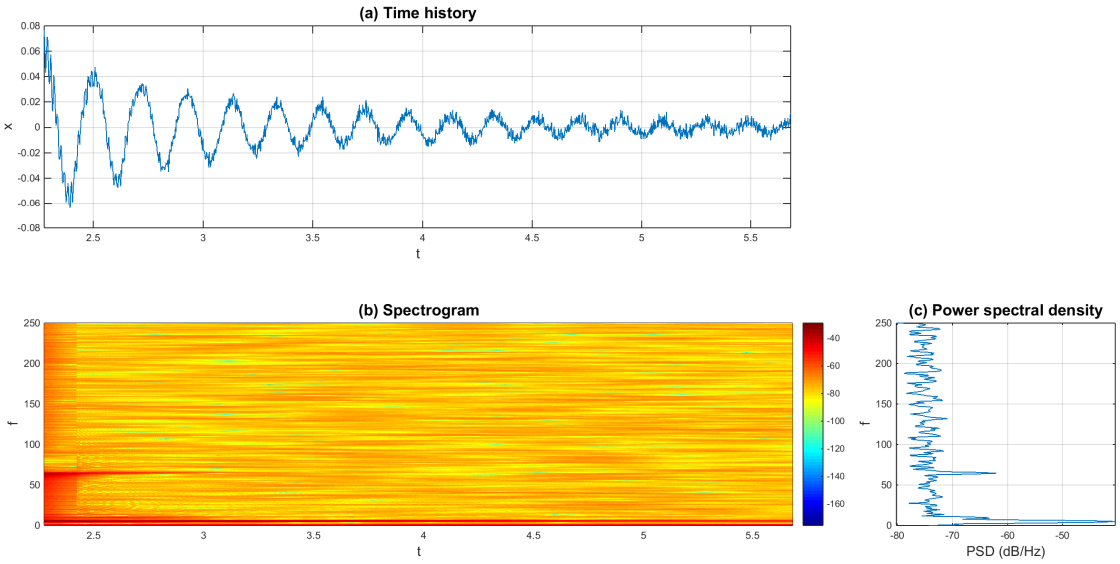

Figure 5.16: Case #4a selected portion 1: time history, STFT and PSD.

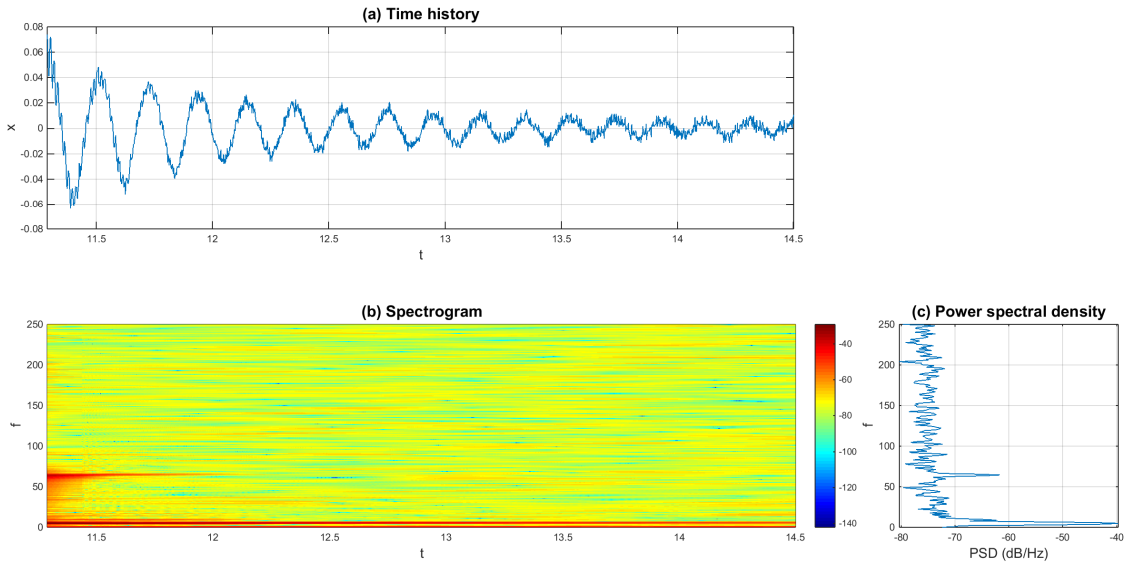

Figure 5.17: Case #4a selected portion 2: time history, STFT and PSD.

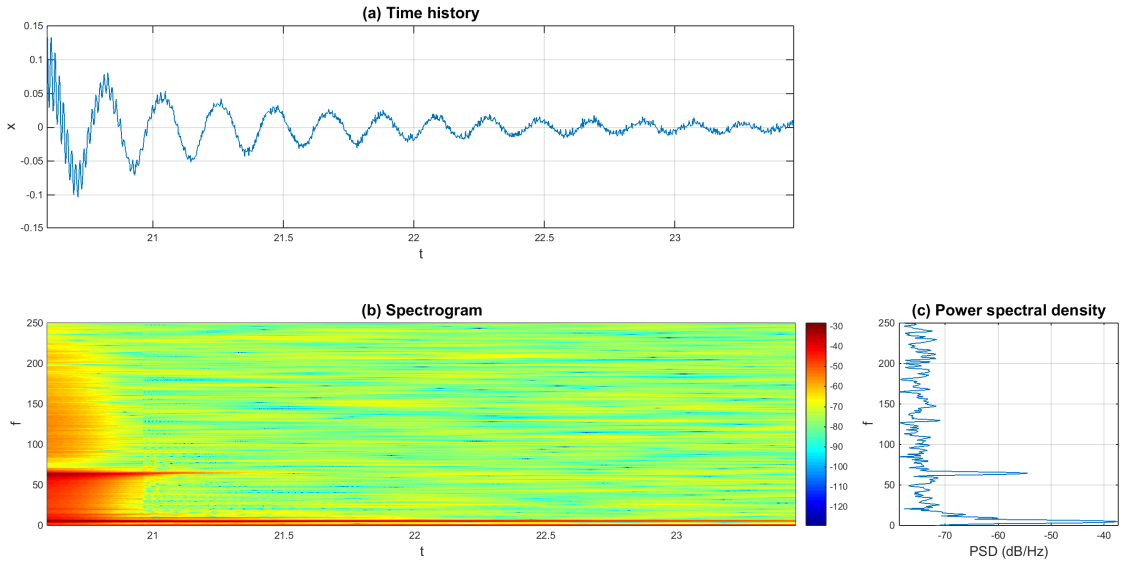

Figure 5.18: Case #4a selected portion 3: time history, STFT and PSD.

Case #4b

The time history together with its STFT and PSD is shown in Figs. 5.19 and 5.22.

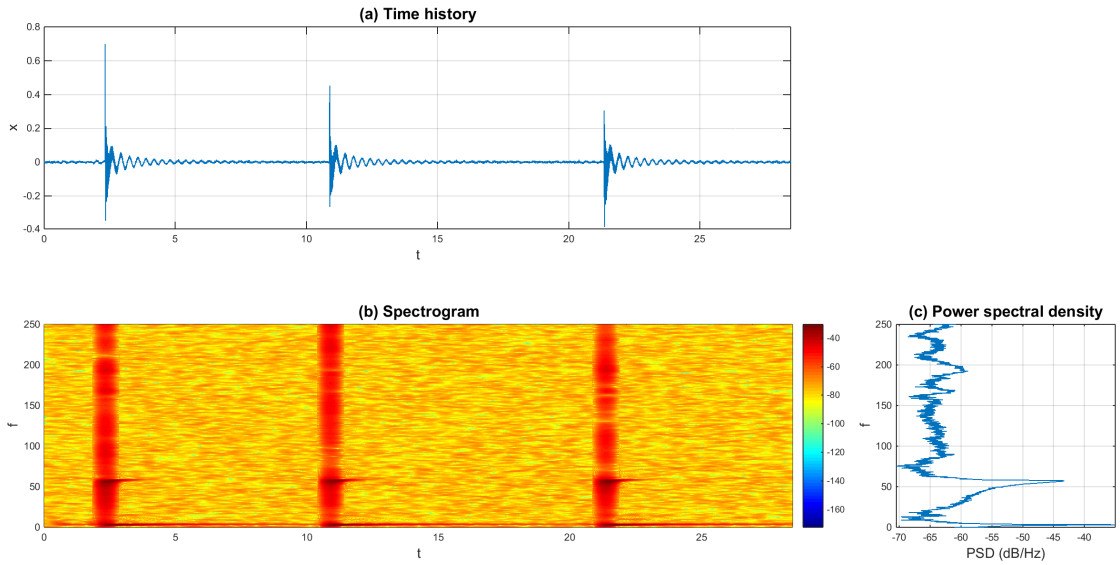

Figure 5.19: Case #4b: time history, STFT and PSD.

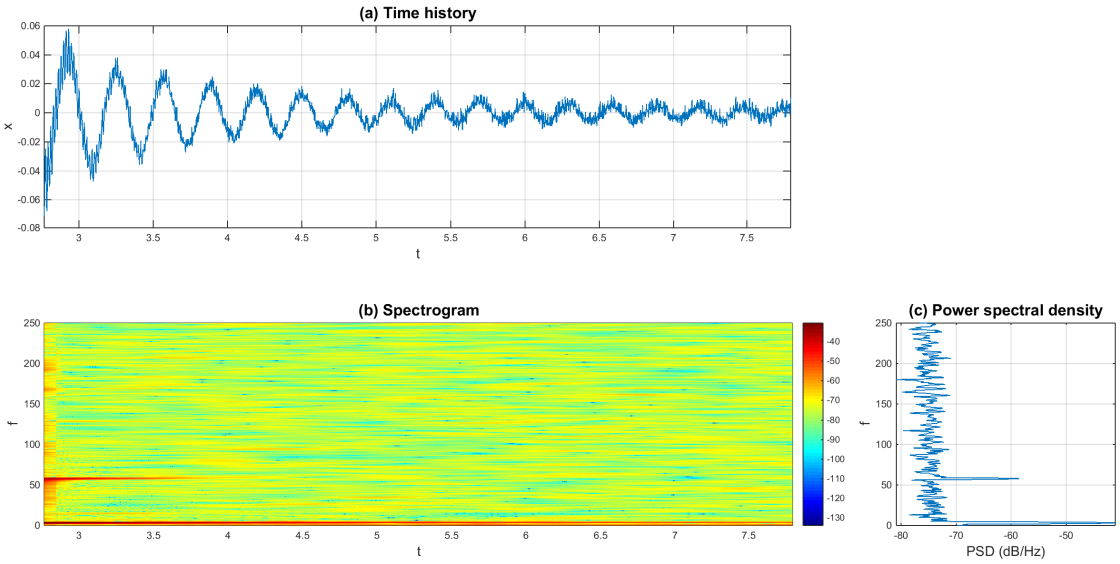

Figure 5.20: Case #4b selected portion 1: time history, STFT and PSD.

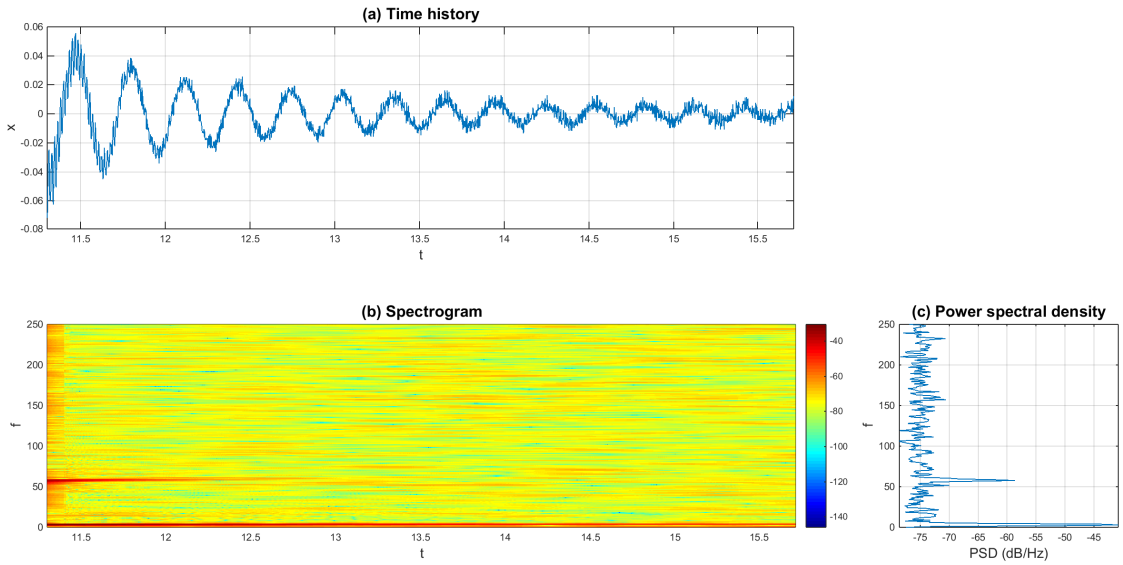

Figure 5.21: Case #4b selected portion 2: time history, STFT and PSD.

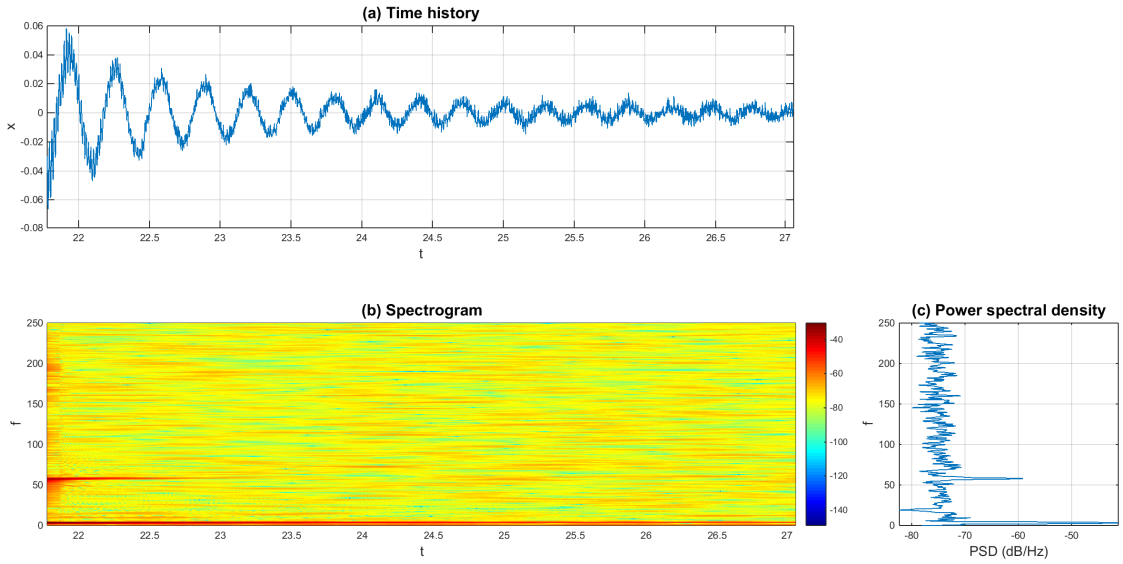

Figure 5.22: Case #4b selected portion 3: time history, STFT and PSD.

Case #4c

The time history together with its STFT and PSD is shown in Figs. 5.23 and 5.26.

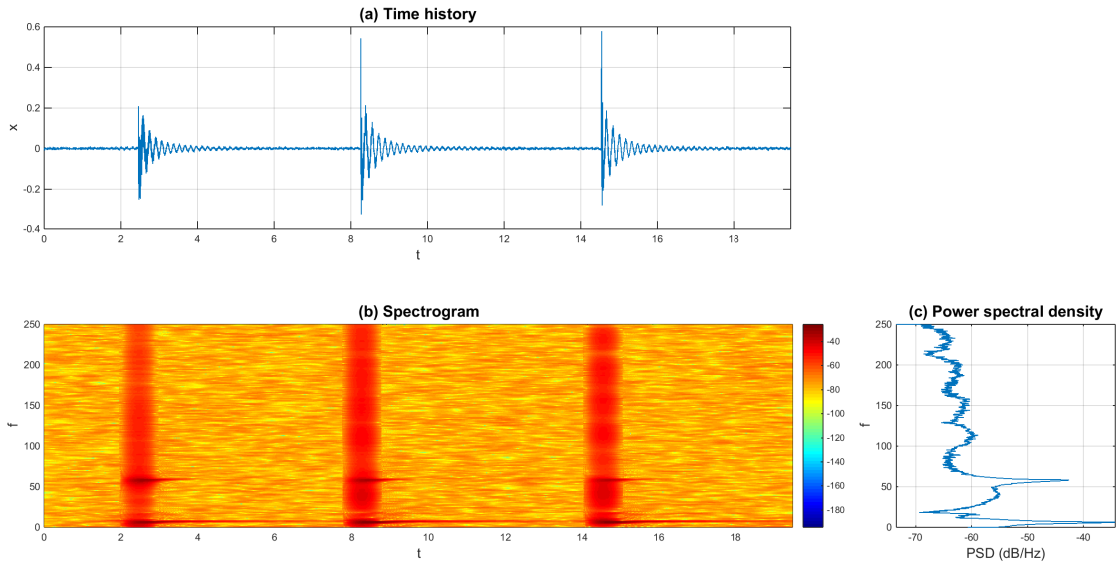

Figure 5.23: Case #4c: time history, STFT and PSD.

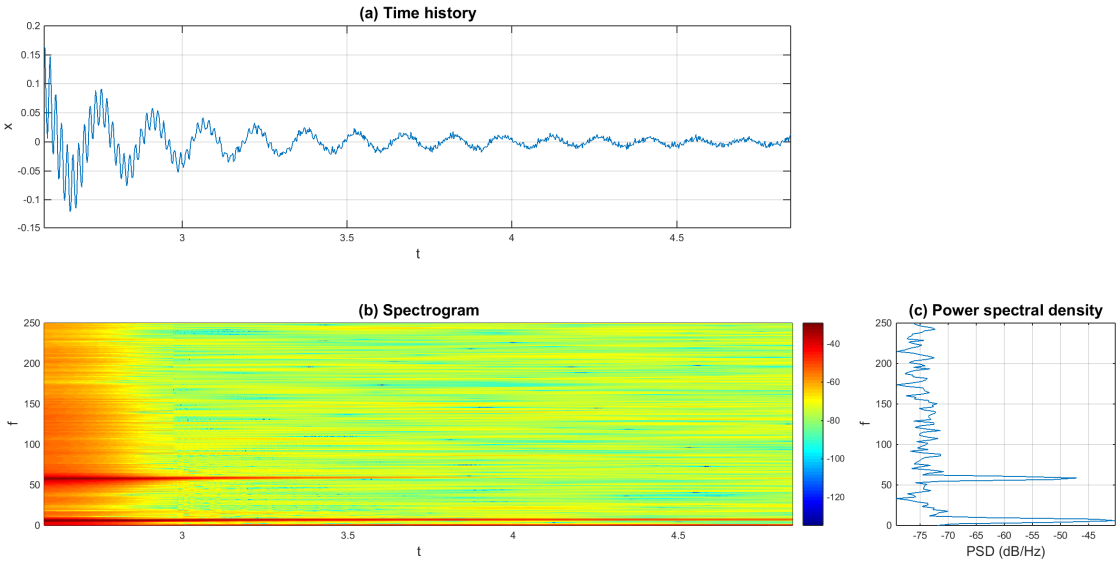

Figure 5.24: Case #4c selected portion 1: time history, STFT and PSD.

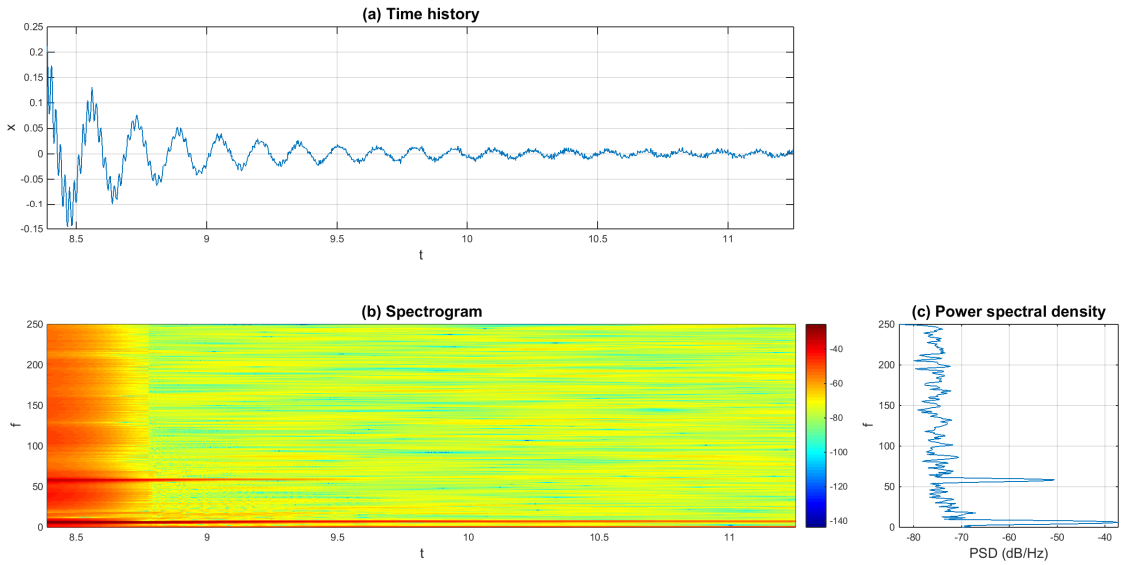

Figure 5.25: Case #4c selected portion 2: time history, STFT and PSD.

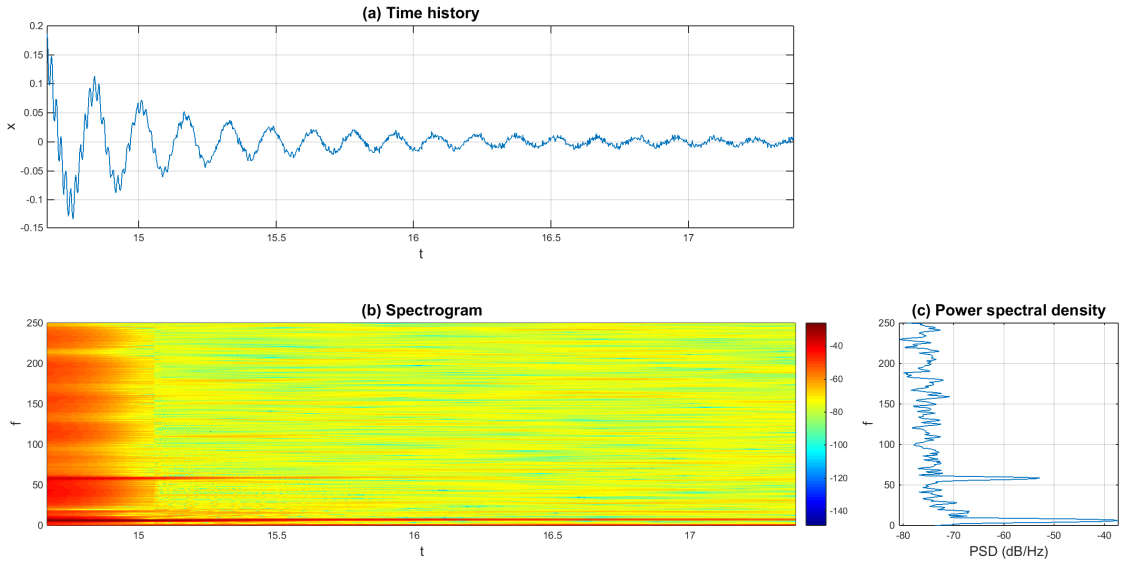

Figure 5.26: Case #4c selected portion 3: time history, STFT and PSD.

Case #4d

The time history together with its STFT and PSD is shown in Figs. 5.27 and 5.31.

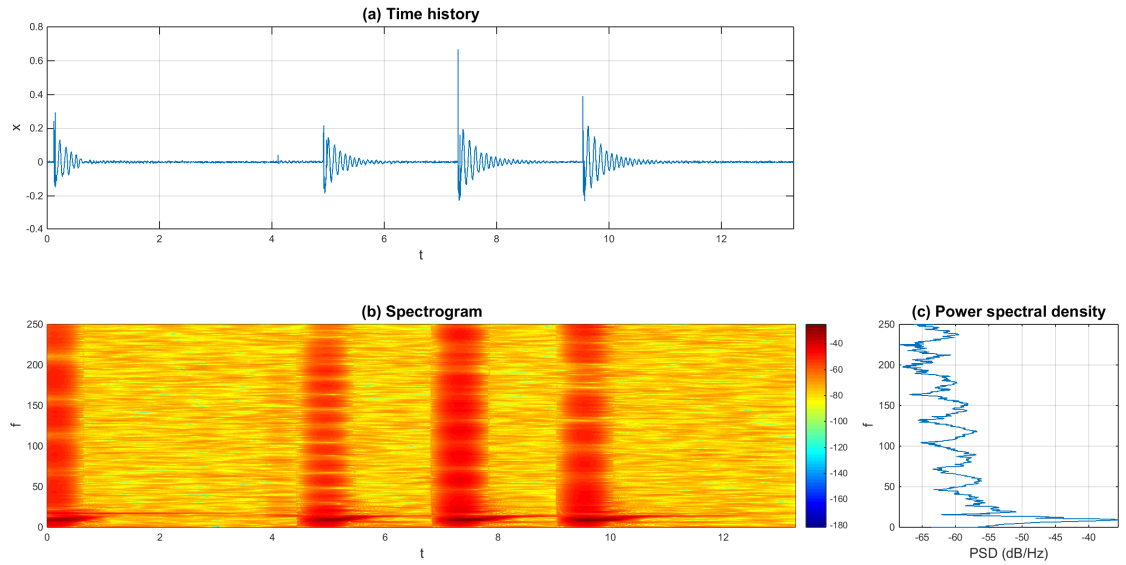

Figure 5.27: Case #4d: time history, STFT and PSD.

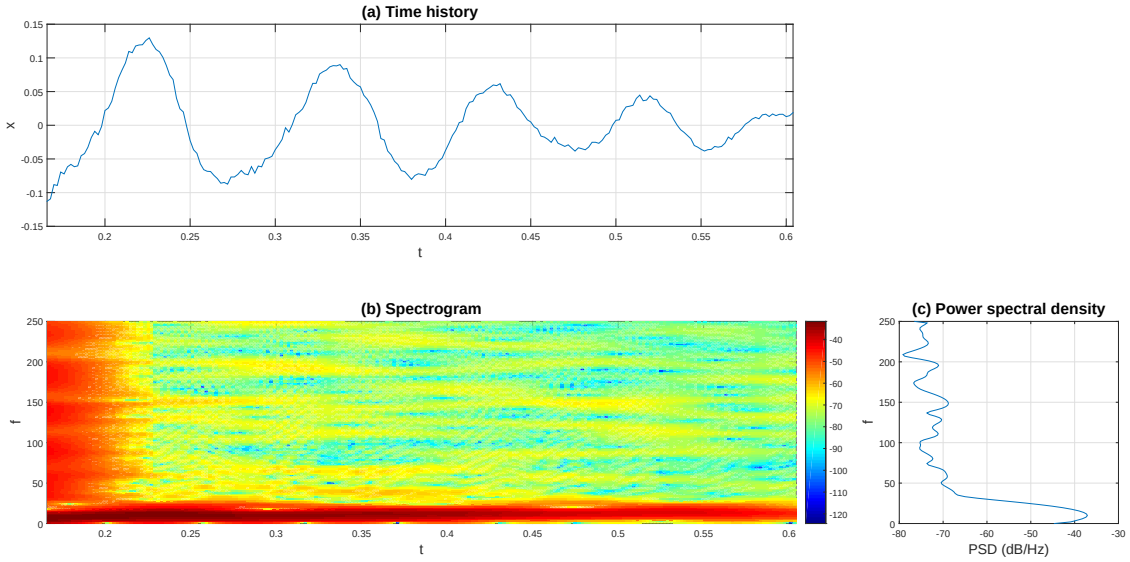

Figure 5.28: Case #4d selected portion 1: time history, STFT and PSD.

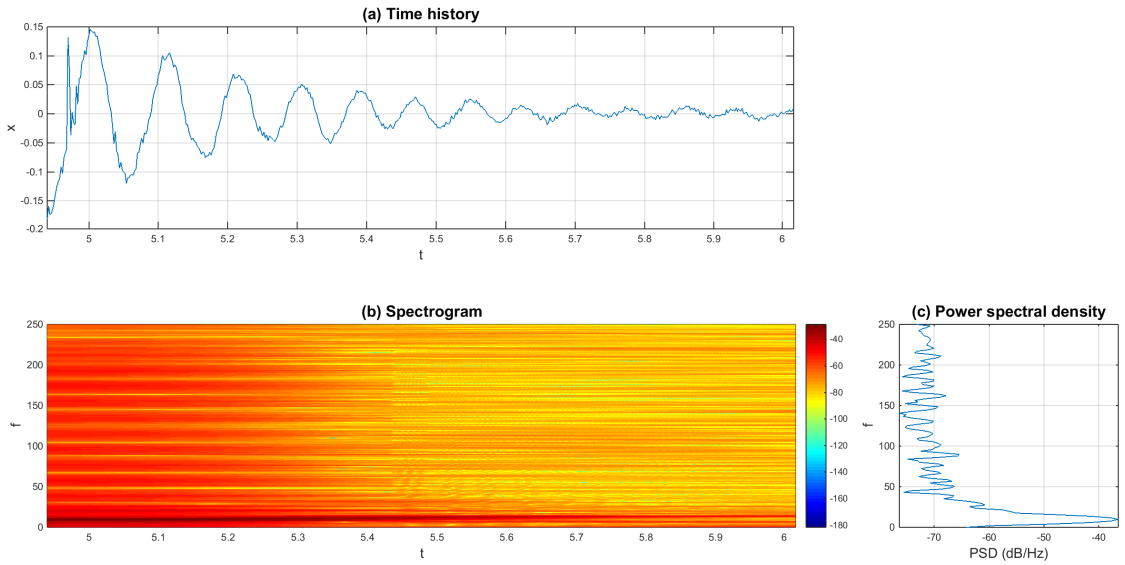

Figure 5.29: Case #4d selected portion 2: time history, STFT and PSD.

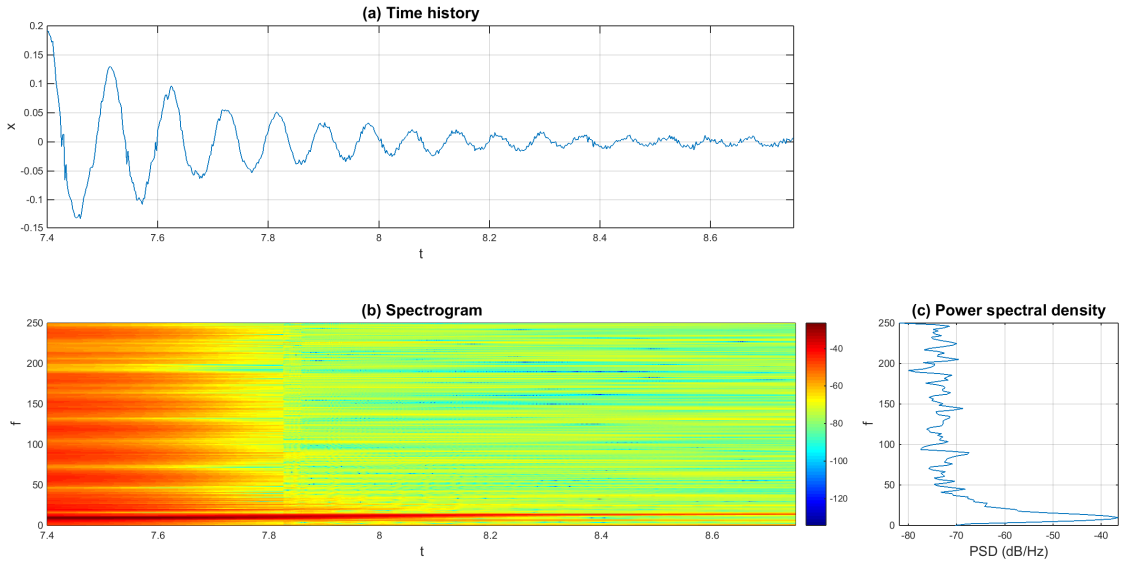

Figure 5.30: Case #4d selected portion 3: time history, STFT and PSD.

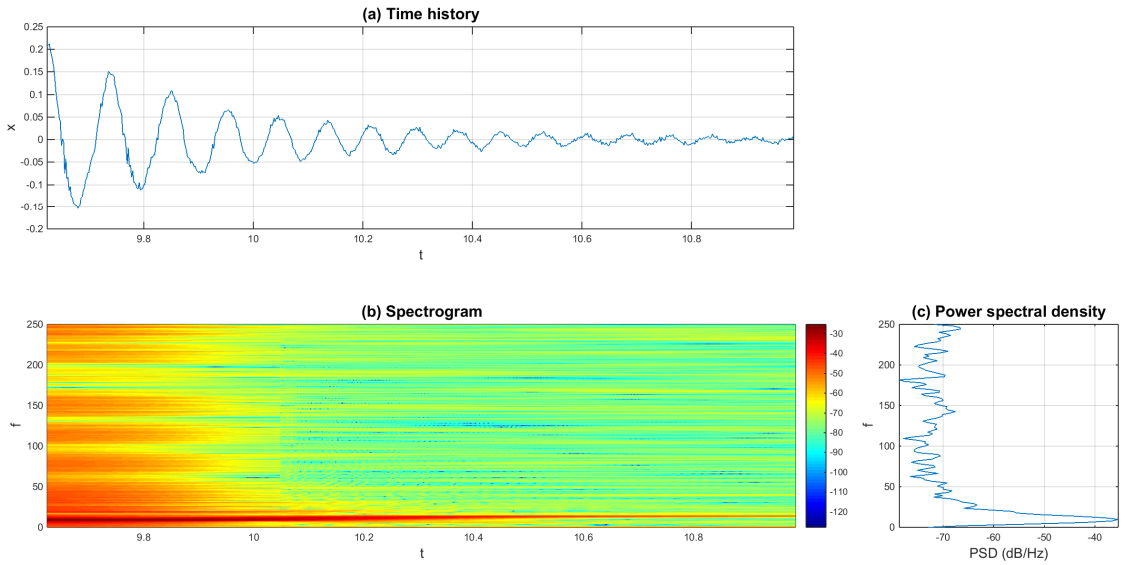

Figure 5.31: Case #4d selected portion 4: time history, STFT and PSD.

5.4.3 Acceleration backbone

Even though we recommend using displacement backbones over acceleration backbones, it would still be meaningful to take a look at the acceleration backbones first. For contrasting purpose, it would be interesting to examine some "raw" acceleration backbones, i.e., the backbones obtained by processing the measured acceleration data without filtering or decomposition. Fig. 5.32 shows two accelerations backbones of Case #3a. It can be seen that the backbone is rather noisy. In fact, the instantaneous frequency value spreads out in a unreasonable range, indicating that the instantaneous frequency is not trustworthy.

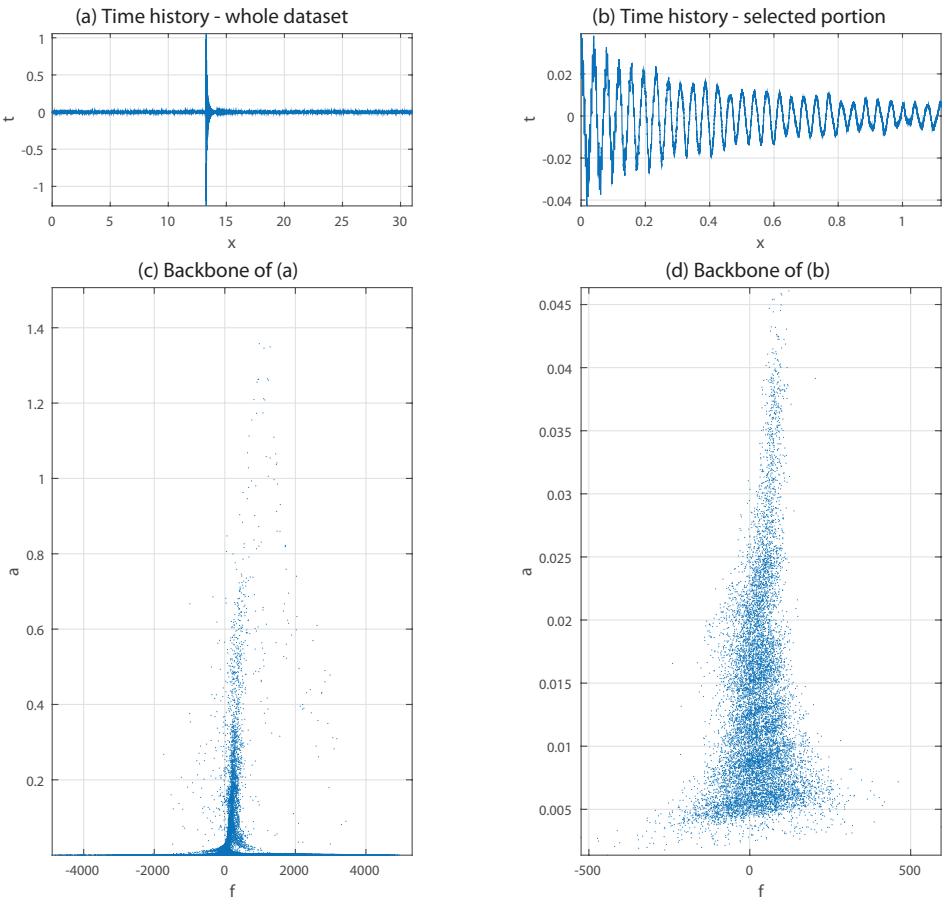

Figure 5.32: Case #3a: backbones of acceleration measurements without filtering or decomposition.

Since the original acceleration time histories are rather noisy, we use a lowpass filter first. The cutoff frequency is chosen with great care so that only high frequency noisy is filtered out but not the modes at high frequencies. The filtered acceleration time histories are then decomposed by using the proposed decomposition procedure given in Chapter 3. The backbones of both the filtered acceleration and its first component are finally obtained. This procedure is applied to all cases. All results are presented in Figs. 5.33 to 5.40.

None of these backbones is simple. We may agree that the backbones of the first decomposed components indicate a linear behavior in Cases #2 and #3a, which agrees with the expectation given the setup of these tests. Case #3b may be deemed linear,

which does not necessarily agree with our expectation. For Case #3c, however, we are not able to decompose the original signal successfully. The main reason, we believe, is that the original signal does not satisfy the assumption that the first component dominates.

Last but not least, a clear left bending behavior associated with softening nonlinearity can be seen in all four tests in Case #4d as shown in Fig. 5.40, which complements the previous work done by our previous team members in reference [57]. This is consistent with the design of the timber joint. A left bending behavior is also observed in Cases #4a - #4c but is not as obvious. These observations partially agree with those in the work done by our previous team [57] and will be discussed later.

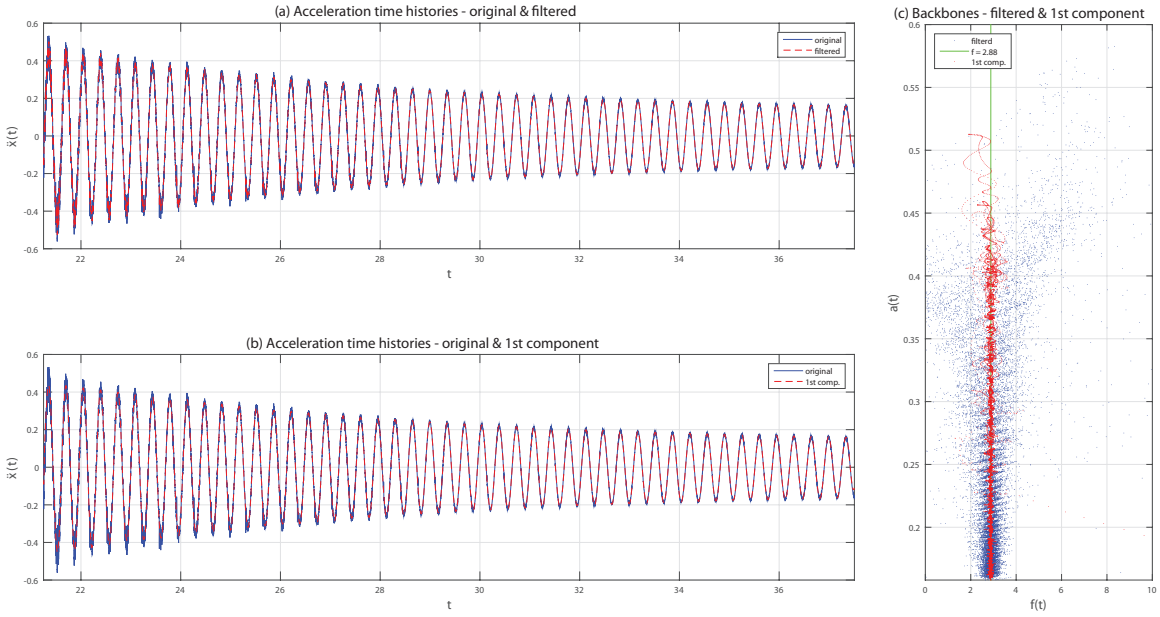

Figure 5.33: Processed results for Case #2. (a) is the original and filtered acceleration time histories of the processed data; (b) is the original and decomposed first component acceleration time histories of the processed data, and (c) is the backbones of the filtered acceleration time history and the decomposed first component. The green vertical line in (c) is the mean value of the instantaneous frequency of the first component.

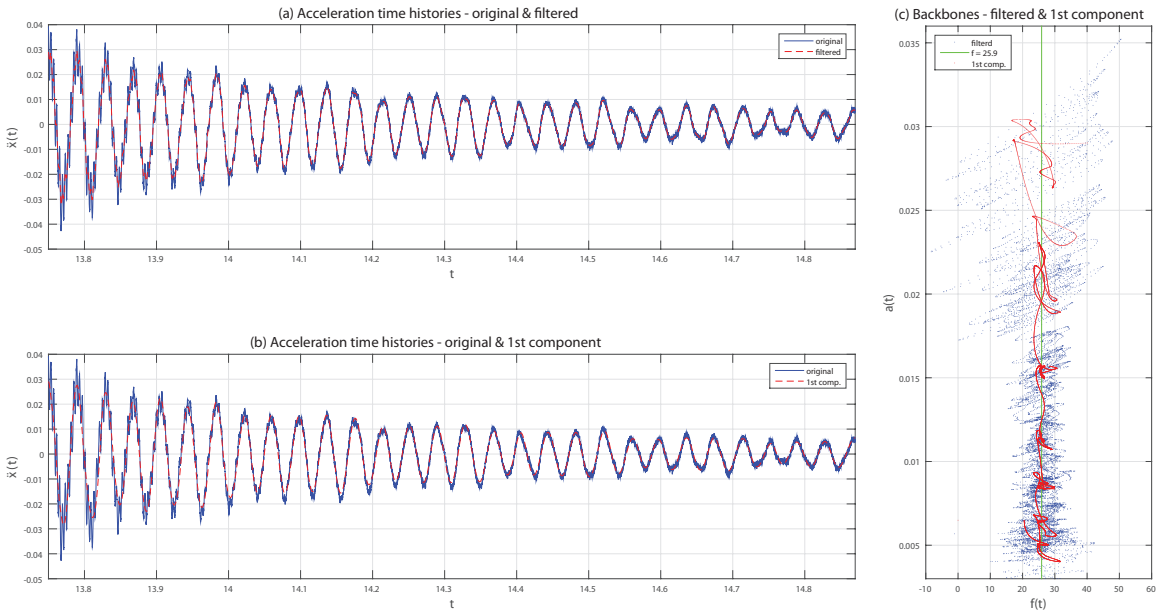

Figure 5.34: Processed results for Case #3a; the design of this figure follows that of Fig. 5.33.

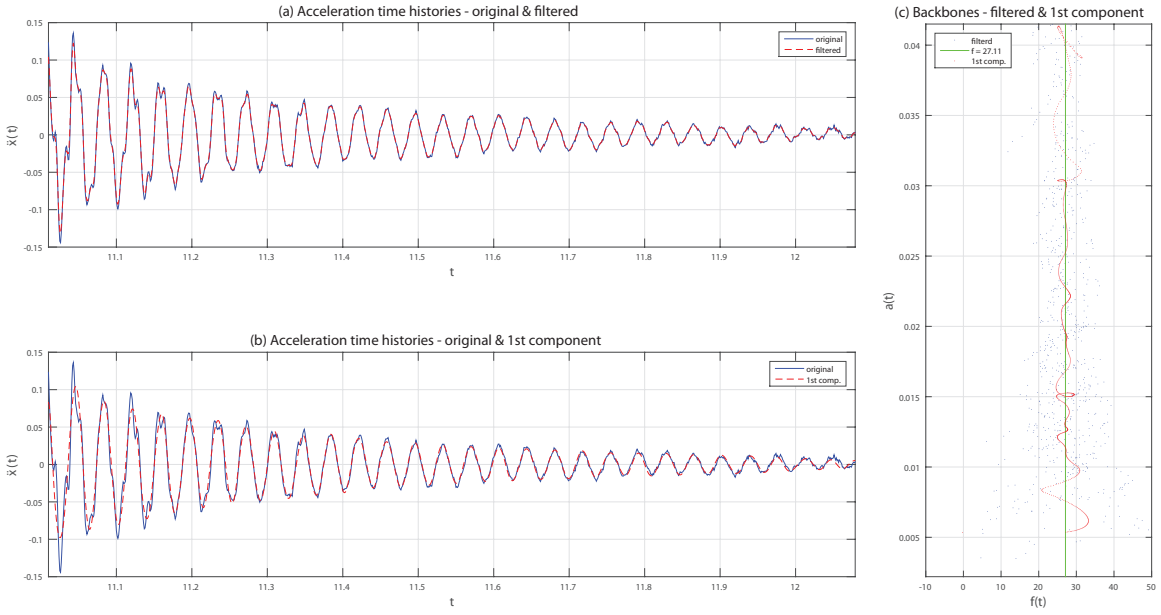

Figure 5.35: Processed results for Case #3b; the design of this figure follows that of Fig. 5.33.

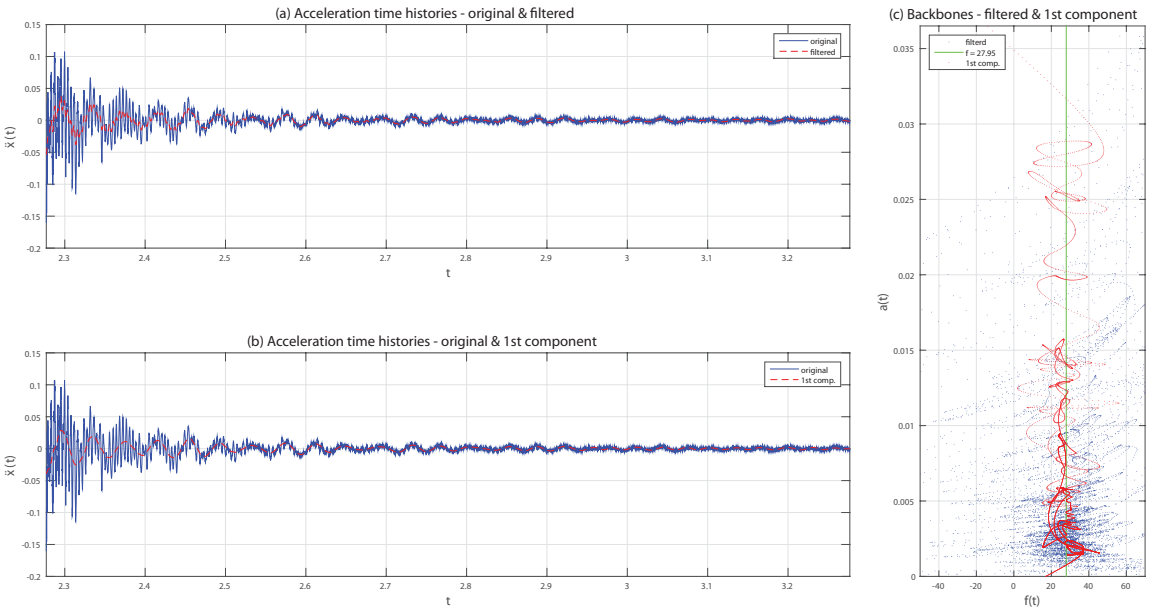

Figure 5.36: Processed results for Case #3c; the design of this figure follows that of Fig. 5.33.

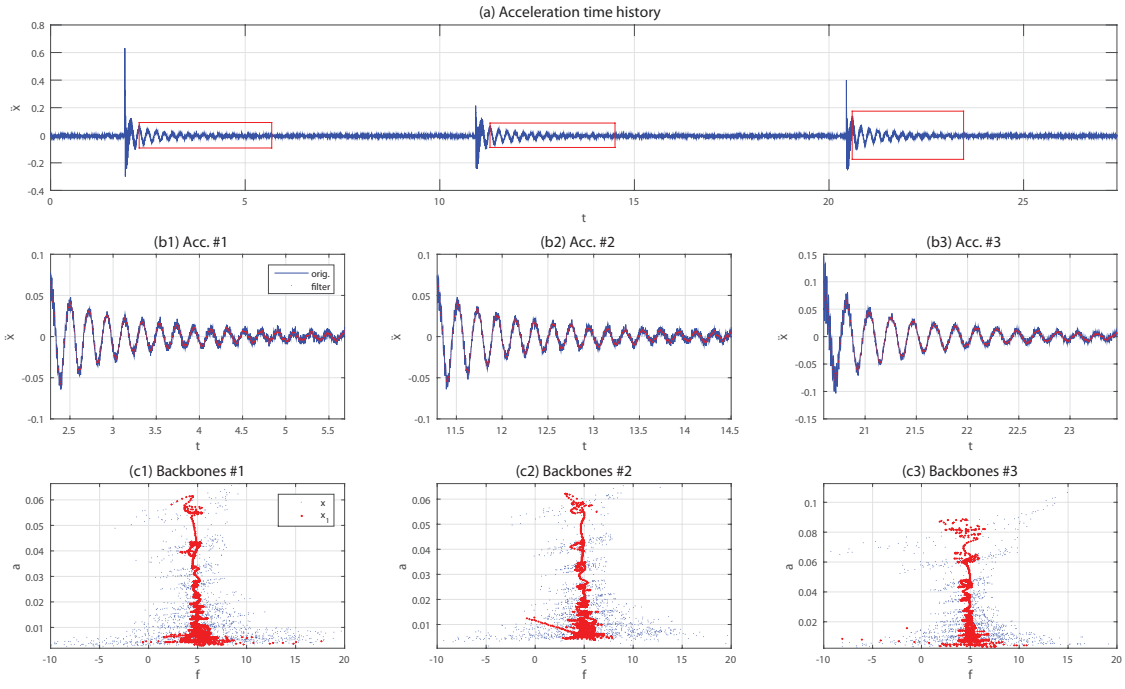

Figure 5.37: Processed results for Case #4a. (a) is the full relative acceleration time history of the timber joint; (b1)-(b3) are the original and filtered acceleration time histories of three selected portions in (a), and (c1)-(c3) are the corresponding backbones of (b1)-(b3).

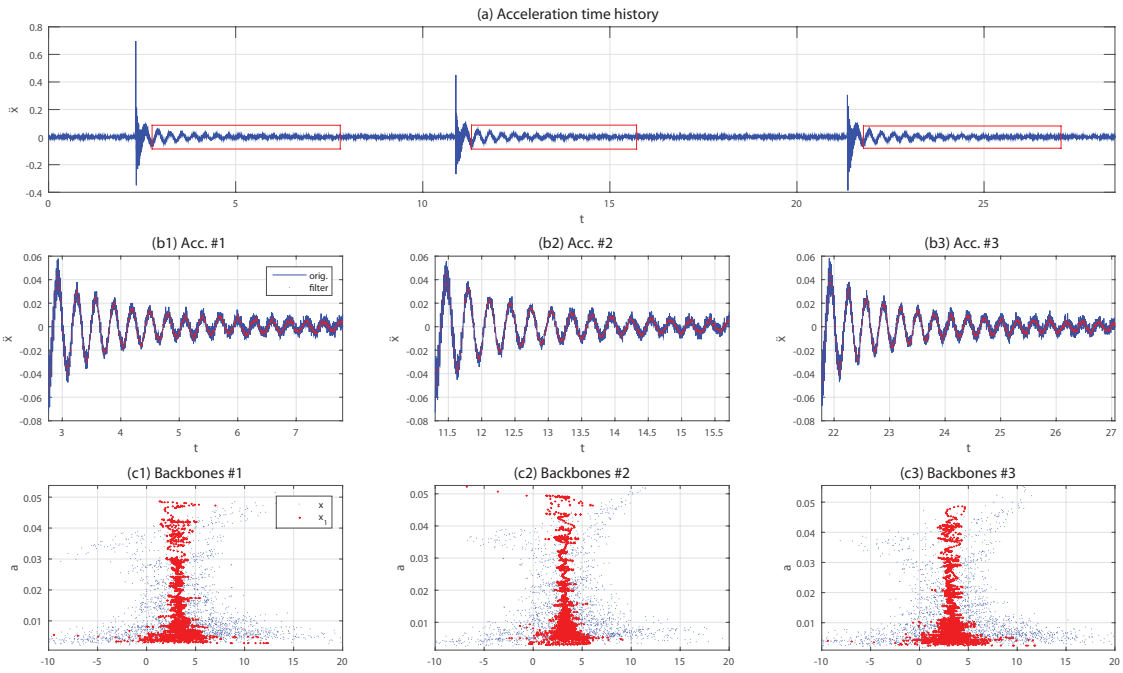

Figure 5.38: Processed results for Case #4b. The design follows the same pattern as in Fig. 5.37.

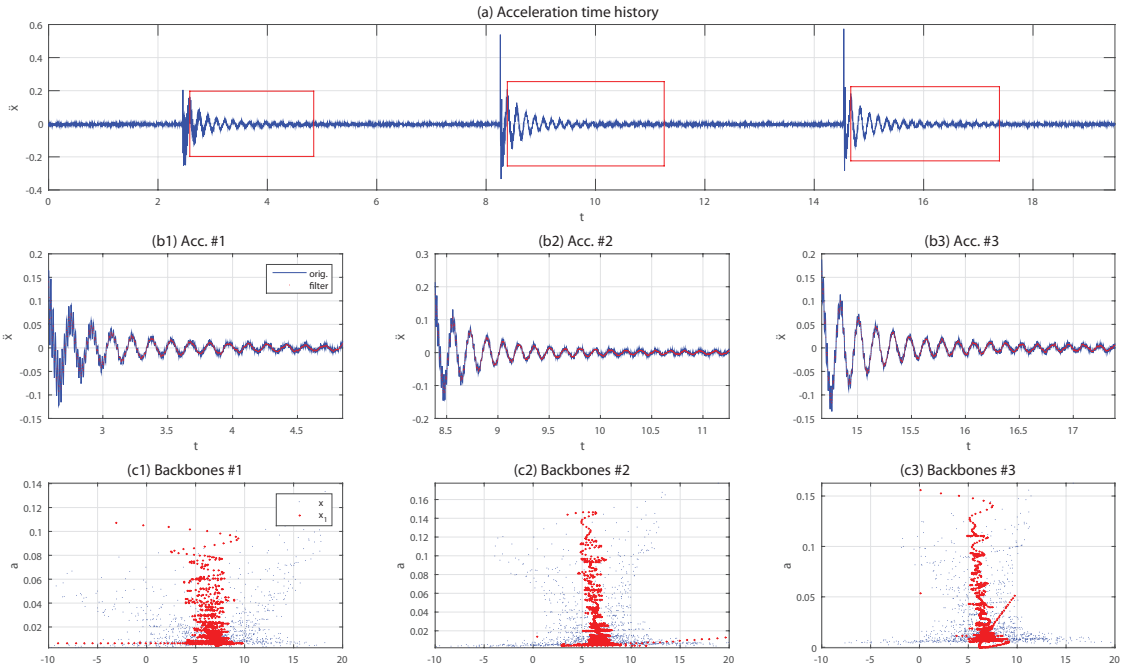

Figure 5.39: Processed results for Case #4c. The design follows the same pattern as in Fig. 5.37.

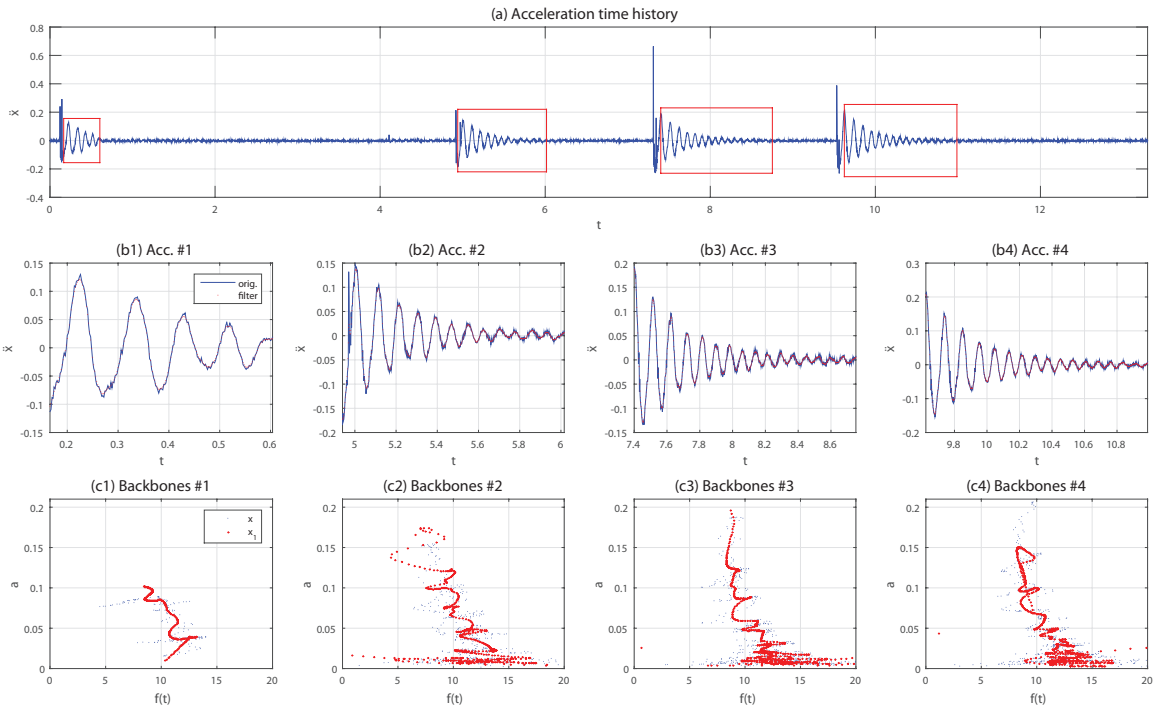

Figure 5.40: Processed results for Case #4d. The design follows the same pattern as in Fig. 5.37. The only difference is that we have four selected portions in this case.

5.4.4 Estimated displacement and displacement backbone

Cases #2, #3a, #3b, and #4 data sets are further processed; displacements are estimated in these tests by using the Kalman filter reviewed and validated earlier. Afterwards, each estimated displacement time history is decomposed before obtaining its first mono-component. Backbones are then obtained from both the displacement and its first mono-component.

Unfortunately, the displacement estimation in these tests are not very good. Similar to the Duffing signal tested previously in Fig. 5.4(a1) and (a2), obvious drift is observed making the estimated displacement questionable. To overcome this problem, we again filter the displacement estimation with a highpass filter, just like what we did in Fig. 5.4(b1) and (b2).

The processed results of Cases #2, #3 and #4 are presented in Figs. 5.41 to 5.48, respectively. The backbones in Panel (e) indicate a linear behavior in both Cases #2

and #3a, even though they are still noisy. The backbones in Case #3b, however, is a little confusing. In particular, the tip of the first decomposed component seems to bend slightly to the left, indicating a softening behavior. However, this nonlinearity indication may not be entirely trustworthy, especially at the two ends of the backbone, due to the use of highpass filtering. The mean frequencies are practically the same as those in the acceleration backbones for all three cases, a good indicator for the displacement estimates.

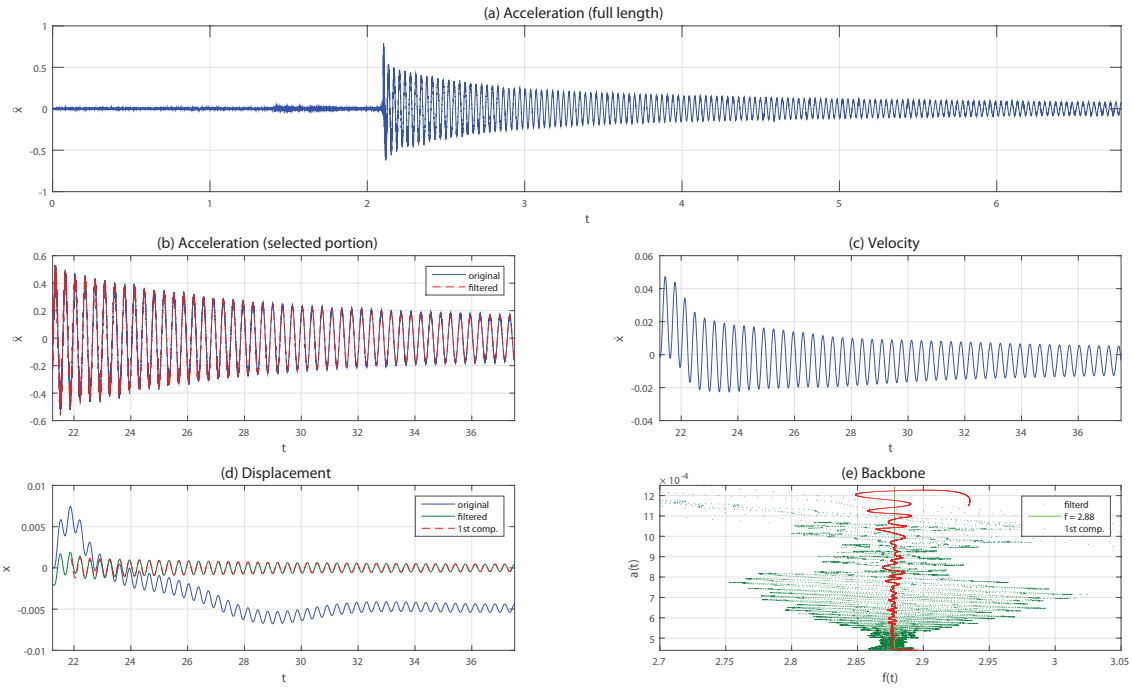

Figure 5.41: Processed results for Case #2. (a) is the entire acceleration time history; (b) is the processed acceleration time history; (c) is the velocity estimation; (d) is a combined plot of the displacement estimation (blue), filtered displacement (green), and decomposed first component of the filtered displacement (red), and (e) is a combined plot of the backbones of the filtered displacement (blue) and the first component (red). The green vertical line in (e) is the mean value of the instantaneous frequency of the first component.

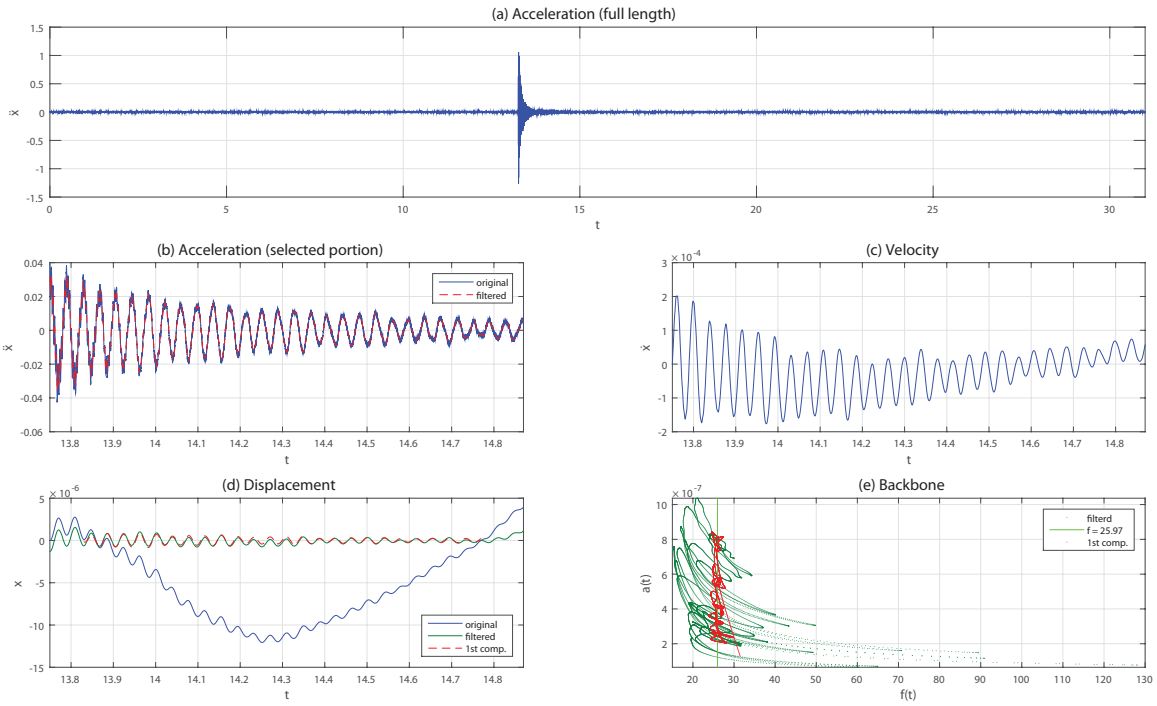

Figure 5.42: Processed results for Case #3a; the design of this figure follows that of Fig. 5.33.

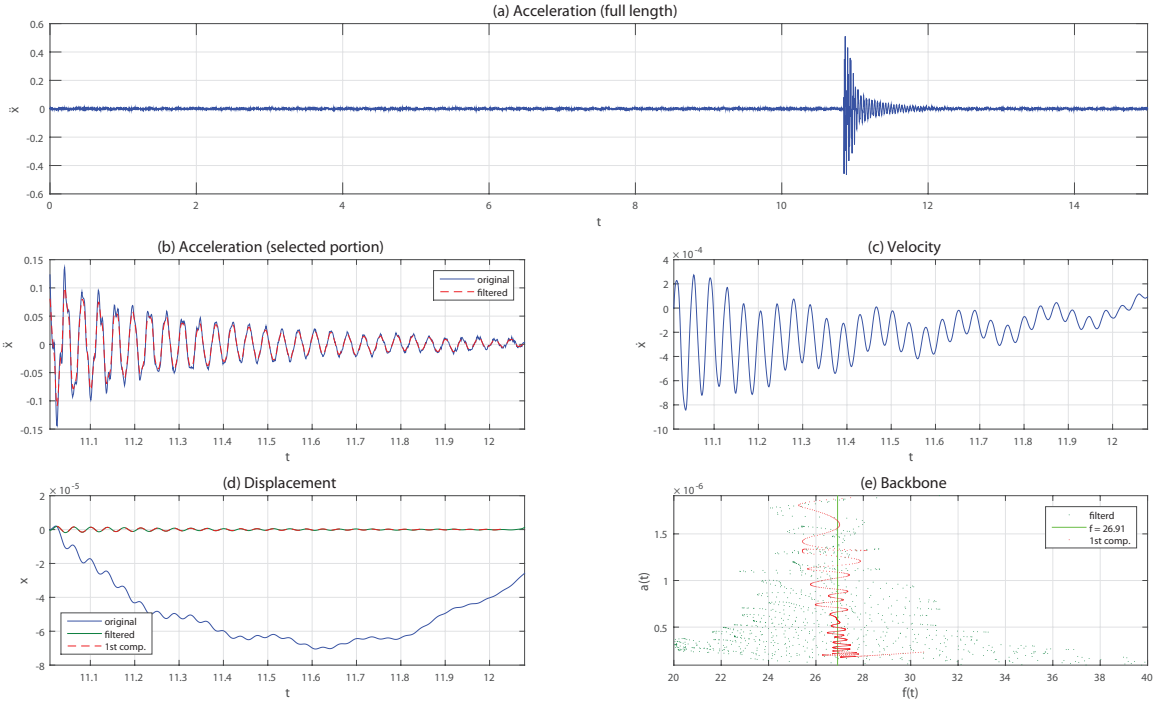

Figure 5.43: Processed results for Case #3b; the design of this figure follows that of Fig. 5.33.

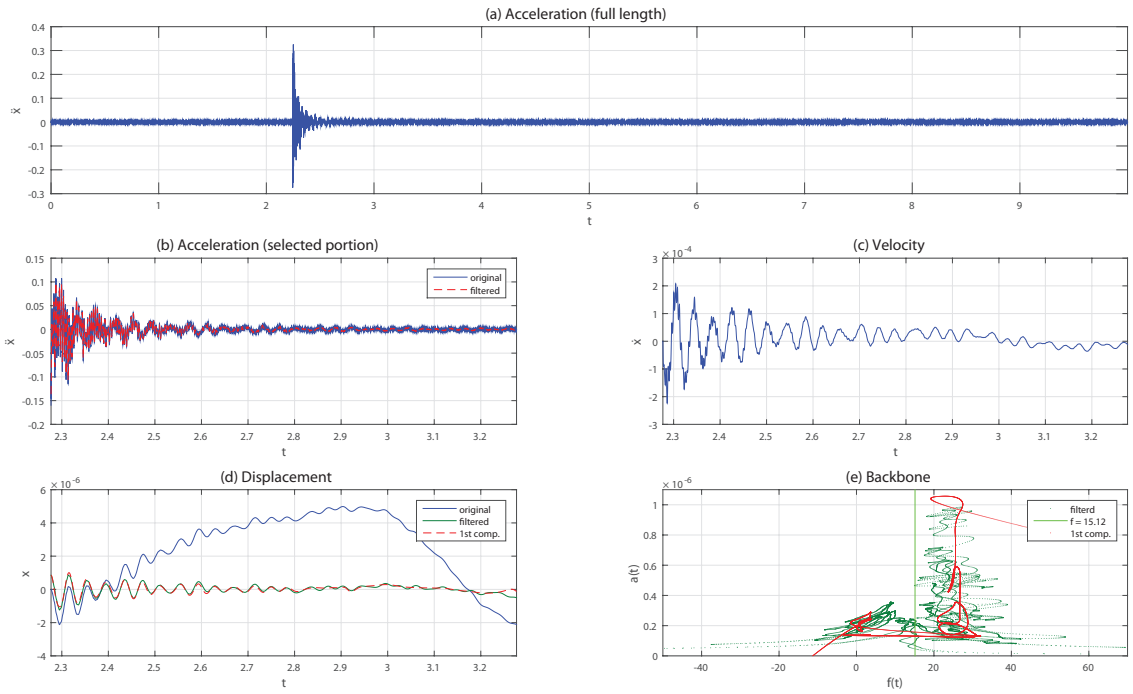

Figure 5.44: Processed results for Case #3c; the design of this figure follows that of Fig. 5.33.

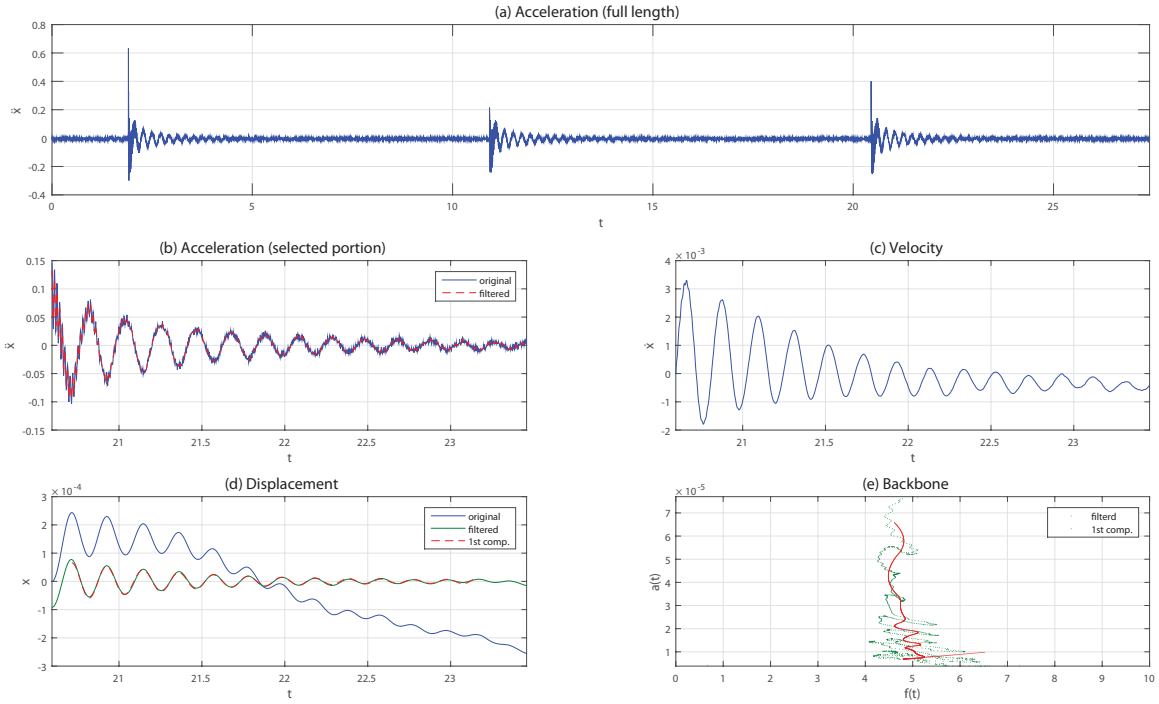

Figure 5.45: Processed results for Case #4a; the design of this figure follows that of Fig. 5.33.

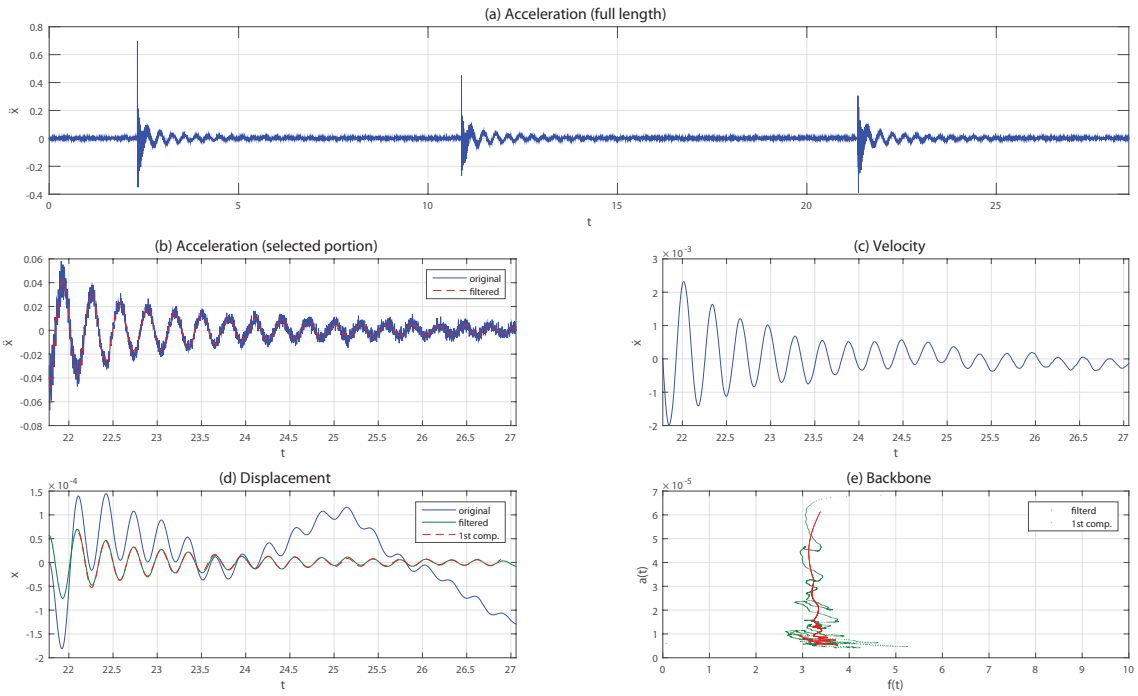

Figure 5.46: Processed results for Case #4b; the design of this figure follows that of Fig. 5.33.

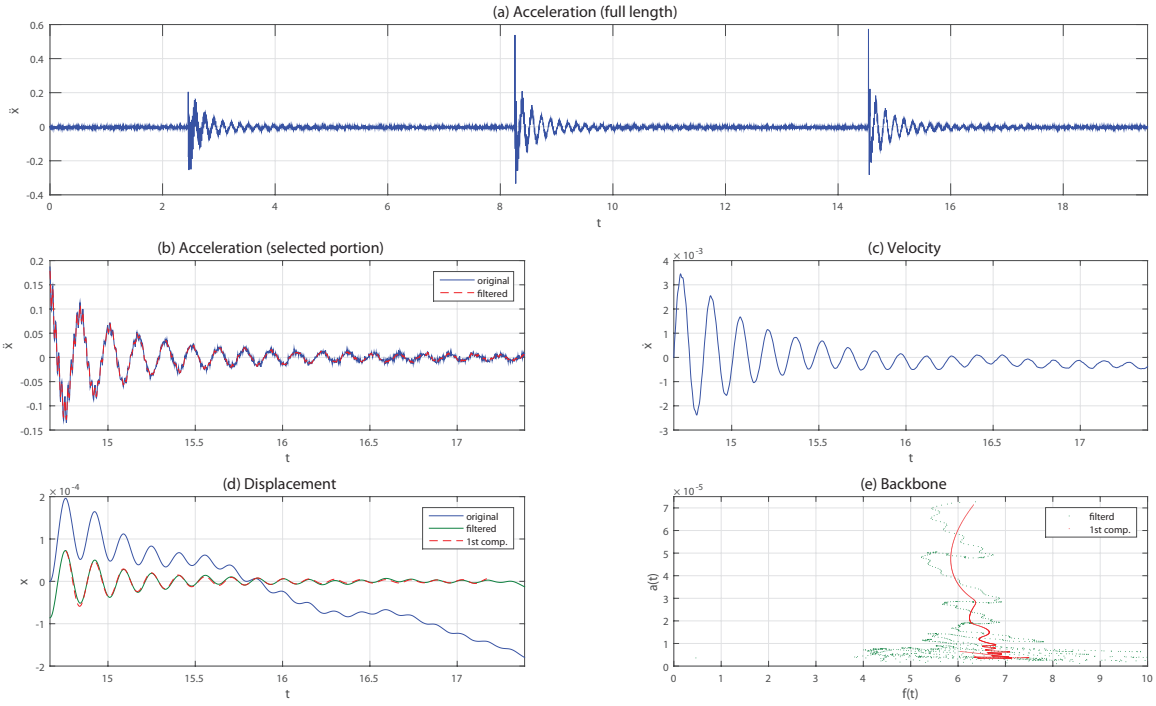

Figure 5.47: Processed results for Case #4c; the design of this figure follows that of Fig. 5.33.

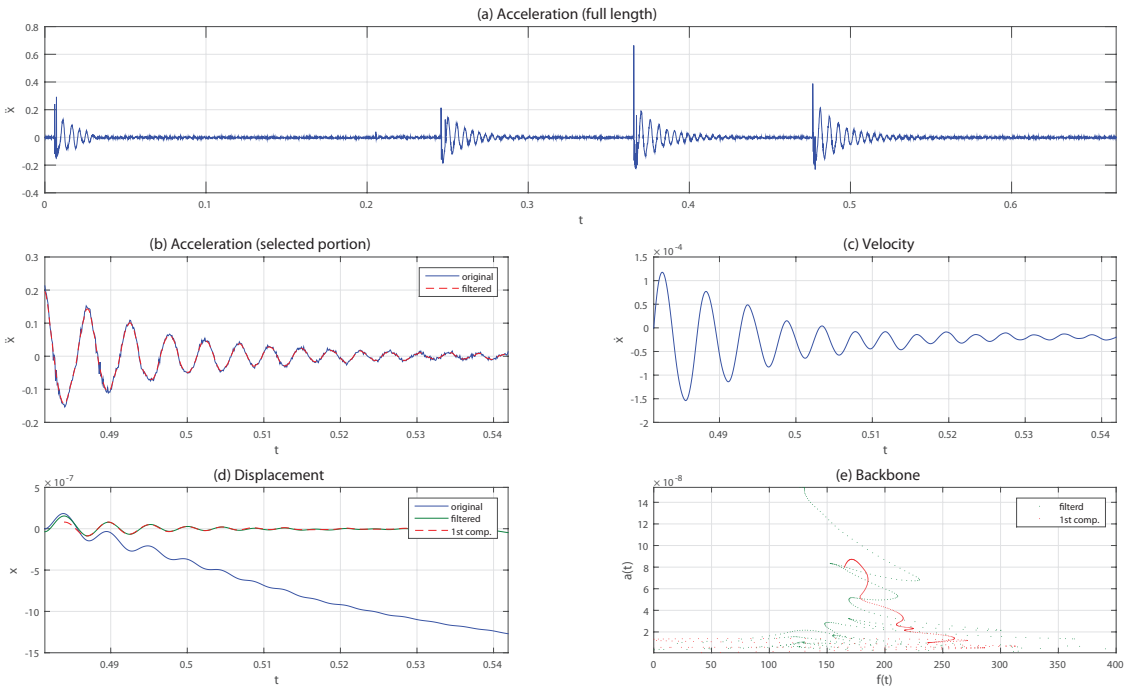

Figure 5.48: Processed results for Case #4d; the design of this figure follows that of Fig. 5.33.

Unfortunately, the displacement backbones are not meaningful for Cases #3c and #4d as shown in Figs. 5.44 and 5.48, respectively. For Case #3c, the reason is very likely that the acceleration measurement contains high nonlinearity which fails the displacement estimation. For Case #4d, the backbone is spread out in a very large frequency band, in addition to a wrong frequency range compared with the acceleration backbone and the PSD result. The reason might be that the displacement estimation is not accurate, which causes the decomposed first component erroneous ending up with incorrect backbones.

5.5 Discussions

The Kalman filter approach for displacement recovery deserves further investigations. In concrete, this method would fail in quite some cases when the acceleration is too limited in length or has nonlinearity. The reason might be that the algorithm in

reference [69] enforces a very strict condition on the output, i.e., the noisy absement is always zero. Other displacement estimation methods may be worth studying, such as frequency domain methods [39, 40].

Even with a trustworthy recovered displacement, the obtained backbone can still be highly oscillatory. Such an issue can occur even when the backbone is obtained from the first decomposed displacement. Other techniques such as envelope's envelope might be a good alternative to smooth the ultimate backbone [30].

It is worthwhile to mention that there is another kind of backbone among structural and mechanical engineers, i.e., an frequency response function (FRF) based backbone. The FRF backbone is the mapping between the driving frequency and peak amplitude of a model with different damping ratios. Taking a free Duffing oscillator as an example, Feldman's backbone also has two versions: (a) is based on Hilbert transform of numerical solution to the Duffing equation, while (b) is based on an approximate solution to the Duffing equation leading to the backbone in the form of $\omega^2 = (1 + \frac{3}{4}\mathfrak{a}^2)$ (see Reference [30]). This is illustrated in Fig. 5.49.

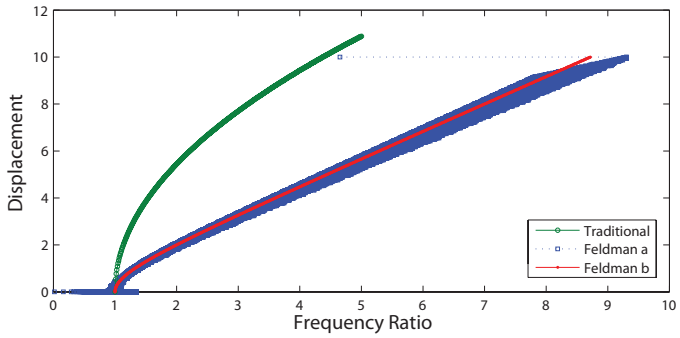

Figure 5.49: Different backbones of a Duffing oscillator. The equation of motion is $\ddot{x} + \zeta\dot{x} + x + x^3 = F$. For Feldman's backbone No. 1, ζ is taken as 0.05. Note that the frequency in Feldman's No. 1 backbone is actually normalized, i.e., the frequency shown is actually the true instantaneous frequency divided by the natural frequency.

5.6 Conclusion

In this chapter, the improved backbone technique has been tested on a couple of case studies, where all data sets are collected acceleration measurements from real world. We have attempted to apply the effective bandwidth and effective duration to quantify information richness in data, however, we are not successful yet. An existing Kalman filter approach for displacement recovery from acceleration seems to have mixed performances. The improved backbone technique has some successes yet with some issues to overcome.

Chapter 6

CONCLUSIONS

The author has studied a couple of aspects related to the backbone technique for processing and analyzing the free responses of nonlinear single-degree-of-freedom (SDOF) systems. While specific conclusions for Chapters 2 to 5 are given therein, the conclusion for this entire dissertation is given as follows:

First of all, the "bottom-up" research strategy used to carry out this research seems to be fruitful in demystifying some critical yet detail-lacking contents in the original backbone technique.

The Hilbert transform (HT) and discrete Hilbert transform (DHT) arena seems to be colorful; different viewpoints do exist. One needs to make a rational choice based on his/her application purpose. More importantly, one needs to bear in mind the approximate nature of instantaneous frequency and the conditions for all instantaneous quantities to be physically meaningful. Technically, DHT needs to be implemented with a great deal of care. The governing convolution formula for DHT is an efficient means for mathematical manipulation. Within the scope of this study, mathematical reasoning has been provided to justify two add-on procedures to fix the end effect. In addition, piecewise DHT has been put forth and stressed for needed situations. The analysis performed to the interaction of double-component signals and the sig-

nal decomposition method directly help improve the original backbone technique and beyond. The introduction of instantaneous bandwidth to the package of backbone technique is an added contribution.

In terms of handling real-world free vibration acceleration measurements, the author has experienced a set of challenging cases. Additional filtering becomes necessary due to increased complexity of the systems involved. Some future research topics are effectively identified in this process.

Chapter 7

FUTURE WORK

While specific future work recommendations for Chapters 2 to 5 are given therein, the future work for this entire dissertation is given as follows:

The concept of mono-component deserves further discussions. As explained in the introduction, researchers may have misunderstanding in this concept. A better definition may be even worth a consideration.

Rigorous analysis of more general multi-component signals (with more than two components) may be fruitful for even more fundamentally improving the backbone technique and more. The goal is to obtain a smooth backbone out of the first decomposed component. This goal, unfortunately, is only partially fulfilled regardless of the improvement achieved. This proposed analysis would be one of the means to achieve this goal.

The proposed piecewise discrete Hilbert transform (DHT) procedure can be further streamlined. First, the criteria for selecting the cutting off point is currently manually chosen. A better approach would be to define a threshold for the decaying ratio such that the piecewise procedure can be automated. Next, the current extrema detection method is based on the a very fundamental peak-picking method but suffers heavily from noise. It can be potentially improved with other suitable methods.

Following introducing instantaneous bandwidth to the backbone technique, group delay may deserve some serious investment so that the backbone technique is even more firmly grounded in classical Hilbert transform (HT) and DHT theories.

Forced response and multi-degree-of-freedom (MDOF) systems can be investigated in the future, even though Dr. Feldman has explored these two topics to some extent.

The signal decomposition procedure proposed in this work needs to be further improved in both algorithm and programming. In particular, the following aspects deserve further investigation: First, we currently choose instantaneous frequency over instantaneous amplitude in the process of obtaining the time indices due to the reason that instantaneous frequency generally contains high frequency noise. It would be interesting to investigate whether this potential issue can be resolved by using a bandpass filter on instantaneous frequency – just like what we performed on instantaneous amplitude – with some carefully chosen passband. Second, for the passband, especially the highpass cutoff frequency, is currently chosen manually. It would be more beneficial to make it much more robust in future work. Together, this would be another means to achieve the goal for making the backbone technique a pattern classifier.

Directly measured displacement would be more desired for the backbone technique. In addition, other methods to derive robust displacement estimation from acceleration and denoising techniques should be investigated for better handling real-world free vibration data.

Bibliography

[1] Hilbert transform applications in mechanical vibration, matlab ©simulink scripts and examples: Vibration signals, dynamic systems, signal procedures. `http://ht.technion.ac.il/`. Accessed: 2015-07-23.

[2] ACI Committee 318. *Building Code Requirements for Structural Concrete and Commentary*. American Concrete Institute, 2011.

[3] George B Arfken. *Mathematical methods for physicists*. Academic press, 2013.

[4] Edward Bedrosian. A product theorem for Hilbert transforms. *Proceedings of the IEEE*, 51(5):868–869, 1963.

[5] Boualem Boashash. Estimating and interpreting the instantaneous frequency of a signal. I. fundamentals. *Proceedings of the IEEE*, 80(4):520–538, 1992.

[6] Boualem Boashash. Estimating and interpreting the instantaneous frequency of a signal. II. algorithms and applications. *Proceedings of the IEEE*, 80(4):540–568, 1992.

[7] Boualem Boashash. *Time frequency analysis*. Elsevier Science, 2003.

[8] S Braun and M Feldman. Time-frequency characteristics of non-linear systems. *Mechanical systems and signal processing*, 11(4):611–620, 1997.

[9] S. Caddemi and G. Muscolino. *IUTAM Symposium on Advances in Nonlinear Stochastic Mechanics*, chapter Extension of The Stochastic Differential Calculus To Complex Processes, pages 89–98. Springer Netherlands, 1996.

[10] R. Canfield. central_diff.m. `http://www.mathworks.com/matlabcentral/fileexchange/12-central-diff-m/content/central_diff.m`, 2001.

[11] P. C. Chang, A. Flatau, and S. C. Liu. Review paper: Health monitoring of civil infrastructure. *Structural Health Monitoring (SHM)*, 2(3):257–267, 2003.

[12] A.K. Chopra. *Dynamics of Structures: Theory and Applications to Earthquake Engineering*. Prentice-Hall, Inc., second edition edition, 2001.

[13] Vaclav Cizek. Discrete Hilbert transform. *IEEE Transactions on Audio and Electroacoustics*, 18(4):340–343, 1970.

[14] Leon Cohen. *Time-frequency analysis*. Prentice Hall PTR New Jersey, 1995.

[15] Leon Cohen and Chongmoon Lee. Instantaneous bandwidth for signals and spectrogram. In *Acoustics, Speech, and Signal Processing, 1990. ICASSP-90., 1990 International Conference on*, pages 2451–2454. IEEE, 1990.

[16] Leon Cohen and Patrick Loughlin. Authors' reply. *Signal Process.*, 83(8):1821–1822, August 2003.

[17] Leon Cohen, Patrick Loughlin, and David Vakman. On an ambiguity in the definition of the amplitude and phase of a signal. *Signal Processing*, 79(3):301–307, 1999.

[18] Scott W Doebling, Charles R Farrar, Michael B Prime, and Daniel W Shevitz. Damage identification and health monitoring of structural and mechanical systems from changes in their vibration characteristics: a literature review. Technical report, Los Alamos National Lab., NM (United States), 1996.

[19] John R Dormand and Peter J Prince. A family of embedded runge-kutta formulae. *Journal of computational and applied mathematics*, 6(1):19–26, 1980.

[20] Mohamed Elfataoui and Gagan Mirchandani. A frequency-domain method for generation of discrete-time analytic signals. *Signal Processing, IEEE Transactions on*, 54(9):3343–3352, 2006.

[21] Charles R Farrar and Keith Worden. An introduction to structural health monitoring. *Philosophical Transactions of the Royal Society of London A: Mathematical, Physical and Engineering Sciences*, 365(1851):303–315, 2007.

[22] Charles R Farrar, Keith Worden, Michael D Todd, Gyuhae Park, Jonathon Nichols, Douglas E Adams, Matthew T Bement, and Kevin Farinholt. Nonlinear system identification for damage detection. Technical Report LA-14353, Los Alamos National Laboratory, 2007.

[23] Michael Feldman. Non-linear system vibration analysis using Hilbert transform - I. free vibration analysis method "FREEVIB". *Mechanical Systems and Signal Processing*, 8(2):119–127, 1994.

[24] Michael Feldman. Non-linear system vibration analysis using Hilbert transform - II. forced vibration analysis method "FORCEVIB". *Mechanical Systems and Signal Processing*, 8(3):309–318, 1994.

[25] Michael Feldman. Non-linear free vibration identification via the Hilbert transform. *Journal of Sound and Vibration*, 208(3):475–489, 1997.

[26] Michael Feldman. Time-varying and non-linear dynamical system identification using the hilbert transform. In *ASME 2005 International Design Engineering Technical Conferences and Computers and Information in Engineering Conference*, pages 1309–1317. American Society of Mechanical Engineers, 2005.

[27] Michael Feldman. Time-varying vibration decomposition and analysis based on the Hilbert transform. *Journal of Sound and Vibration*, 295(3):518–530, 2006.

[28] Michael Feldman. Considering high harmonics for identification of non-linear systems by Hilbert transform. *Mechanical Systems and Signal Processing*, 21(2):943–958, 2007.

[29] Michael Feldman. *Hilbert Transform Applications in Mechanical Vibration*. John Wiley & Sons, 2011.

[30] Michael Feldman. Hilbert transform in vibration analysis. *Mechanical Systems and Signal Processing*, 25:735–802, 2011.

[31] Michael Feldman and S Braun. Decomposition of double-component vibration signals. *Proc. of the 25th Israel conf. on Mechanical Engineering*, pages 700–702, 1994.

[32] Michael Feldman and Simon Braun. Identification of non-linear system parameters via the instantaneous frequency: application of the hilbert transform and wigner-ville techniques. In *Proc. of the XIII Int. Modal Analysis Conf.*, pages 637–642, Nashville, TN, 1995.

[33] R. W. Floyd, J.-S. Pei, C. D. Murray, P. F. Tang, and B. Cranor. Understanding the behavior of prestressed girders after years of service. Technical report, University of Oklahoma, 2015. Annual Project Status Report FFY 2015 for ODOT SP&R Item Number 2256.

[34] G. C. Foliente. Hysteresis modeling of wood joints and structural systems. *ASCE Journal of Structural Engineering*, 121(6):1013–1022, 1995.

[35] D Gabor. Theory of communication. *Journal of the Institute of Electrical Engineers Part III*, 93:429–457, 1946.

[36] D Goyal and BS Pabla. The vibration monitoring methods and signal processing techniques for structural health monitoring: A review. *Archives of Computational Methods in Engineering*, pages 1–10, 2015.

[37] Stefan L Hahn. *Hilbert transforms in signal processing*, volume 2. Artech House Boston, 1996.

[38] Stefan L Hahn. On the uniqueness of the definition of the amplitude and phase of the analytic signal. *Signal processing*, 83(8):1815–1820, 2003.

[39] Sangbo Han. Retrieving the time history of displacement from measured acceleration signal. *KSME international journal*, 17(2):197–206, 2003.

[40] Sangbo Han. Measuring displacement signal with an accelerometer. *Journal of Mechanical Science and Technology*, 24(6):1329–1335, 2010.

[41] Fredric J Harris. On the use of windows for harmonic analysis with the discrete Fourier transform. *Proceedings of the IEEE*, 66(1):51–83, 1978.

[42] G. W. Housner, L. A. Bergman, T. K. Caughey, A. G. Chassiakos, R. O. Claus, S. F. Masri, R. E. Skelton, T. T. Soong, B. F. Spencer, and J. T. P. Yao. Structural control: Past, present, and future. *ASCE Journal of Engineering Mechanics, special issue*, 123(9):897–971, 1997.

[43] Daji Huang, Jinping Zhao, and Jilan Su. Practical implementation of the Hilbert-Huang transform algorithm. *Acta Oceanologica Sinica*, 22(1):1–14, 2003.

[44] N. E. Huang, S. Zheng, S. R. Long, M. C. Wu, H. H. Shih, Q. Zheng, N-C Yen, C. C. Tung, and M. H. Liu. The empirical mode decomposition and the Hilbert spectrum for nonlinear and non-stationary time series analysis. *Proc. R. Soc. Lond.*, 454(1971):903–995, Mar 1998.

[45] Norden E Huang, Zhaohua Wu, Steven R Long, Kenneth C Arnold, Xianyao Chen, and Karin Blank. On instantaneous frequency. *Advances in Adaptive Data Analysis*, 1(02):177–229, 2009.

[46] J. D. Jones and J. S. Pei. Embedded algorithms within an FPGA to classify nonlinear single-degree-of-freedom systems. *IEEE Sensors Journal*, 9(11):1486–1493, November 2009. Special Issue on Sensor Systems for Structural Health Monitoring.

[47] SC Kak. The discrete finite Hilbert transform. *Indian Journal Pure and Applied Mathematics*, 8:1385–1390, 1977.

[48] G. Kerschen, K. Worden, A. F. Vakakis, and J. C. Golinval. Past, present and future of nonlinear system identification in structural dynamics. *Mechanical Systems and Signal Processing*, 20(3):505–592, 2006.

[49] Frederick W King. *Hilbert transforms, Volume 1*. Encyclopedia of Mathematics and its Applications, 2009.

[50] Frederick W King. *Hilbert transforms, Volume 2*. Encyclopedia of Mathematics and its Applications, 2009.

[51] I. Kovacic and M. J. Brennan. *The Duffing Equation*. Wiley, 2011.

[52] Z. Liang, G. C. Lee, G. F. Dargush, and J. Song. *Structural Damping: Applications in Seismic Response Modification*. CRC Press, 2012.

[53] T. Y. Lin and N. H. Burns. *Design of Prestressed Concrete Structures*. Wiley, 3 edition, 1981.

[54] P.J. Loughlin. Time varying frequencies of a signal. In *Proc. of SPIE*, pages 109–122, 1997.

[55] J. P. Lynch and K. J. Loh. A summary review of wireless sensors and sensor networks for structural health monitoring. *The Shock and Vibration Digest*, 38(2):91–128, March 2006.

[56] Bassem R Mahafza. *Radar signal analysis and processing using MATLAB*. CRC Press, 2008.

[57] E. C. Mai, Y. P. Sugeng, J. S. Pei, S. M. Zimmermann, C. V. Borchard, Y. Li, and K. Piyawat. Development of small wood models to demonstrate nonlinear dynamics. In *Proceedings of IMAC-XXVI: A Conference & Exposition on Structural Dynamics*, Orlando, FL, February 2008.

[58] S Lawrence Marple Jr. Computing the discrete-time "analytic" signal via FFT. *IEEE Transactions on Signal Processing*, 47(9):2600–2603, 1999.

[59] MATLAB. *R2014a*. The MathWorks Inc., Natick, Massachusetts, 2014.

[60] S. K. Mitra. *Digital Signal Processing: A Computer-Based Approach*. McGraw-Hill Companies, 3rd edition, 2006.

[61] K. M. Mosalam, C. Machado, K.-U. Gliniorz, C. Naito, E. Kunkel, and S. A. Mahin. Seismic evaluation of an asymmetric three-story woodframe building. Technical Report CUREE Publication No. W-19, University of California, Berkeley, 2002.

[62] A. H. Nayfeh and D. T. Mook. *Nonlinear Oscillations*. Wiley-VCH, Weinhein, 2004.

[63] Alan V. Oppenheim and Ronald W. Schafer. *Discrete-time Signal Processing*. Prentice-Hall, Inc., Upper Saddle River, NJ, USA, 1989.

[64] M. Paz. *International Handbook of Earthquake Engineering: Codes, Programs, and Examples*. Civil engineering. Springer US, 1994.

[65] Bernard Picinbono. On instantaneous amplitude and phase of signals. *IEEE Transactions on Signal Processing*, 45(3):552–560, 1997.

[66] Tao Qian. Mono-components for decomposition of signals. *Mathematical methods in the applied sciences*, 29(10):1187–1198, 2006.

[67] Tao Qian and Qiuhui Chen. Characterization of analytic phase signals. *Computers & Mathematics with Applications*, 51(9):1471–1482, 2006.

[68] Andrew Reilly, Gordon Frazer, and Boualem Boashash. Analytic signal generation-tips and traps. *Signal Processing, IEEE Transactions on*, 42(11):3241–3245, 1994.

[69] SM Sharkh, M Hendijanizadeh, M Moshrefi-Torbati, and Abusara Mohammad. A novel kalman filter based technique for calculating the time history of vertical displacement of a boat from measured acceleration. *Marine Engineering Frontiers (MEF)*, 2:24–30, 2014.

[70] Hoon Sohn, Charles R Farrar, Francois M Hemez, and Jerry J Czarnecki. A review of structural health review of structural health monitoring literature 1996-2001. Technical report, Los Alamos National Laboratory, 2002.

[71] Nathan Stevenson, Edward Palmer, James Smeathers, and Boualem Boashash. The bt product as a signal dependent sample size estimate in hypothesis testing: An application to linear/nonlinear discrimination in bandwidth limited systems. In *Signal Processing and Its Applications, 2003. Proceedings. Seventh International Symposium on*, volume 2, pages 551–554. IEEE, 2003.

[72] D. E. Vakman. Do we know what are the instantaneous frequency and instantaneous amplitude of a signal. *Radiotekhnika i Elektronika*, 21:1275–1282, June 1976.

[73] David Vakman. On the analytic signal, the teager-kaiser energy algorithm, and other methods for defining amplitude and frequency. *IEEE Transactions on Signal Processing*, 44(4):791–797, 1996.

[74] E.A. Wan and R. van der Merwe. The unscented kalman filter for nonlinear estimation. In *Adaptive Systems for Signal Processing, Communications, and Control Symposium 2000. AS-SPCC. The IEEE 2000*, pages 153–158, 200.

[75] K Worden. Data processing and experiment design for the restoring force surface method, part I: integration and differentiation of measured time data. *Mechanical Systems and Signal Processing*, 4(4):295–319, 1990.

[76] Keith Worden, Charles R Farrar, Jonathan Haywood, and Michael Todd. A review of nonlinear dynamics applications to structural health monitoring. *Structural Control and Health Monitoring*, 15(4):540–567, 2008.

[77] Zhaohua Wu and Norden E Huang. Ensemble empirical mode decomposition: a noise-assisted data analysis method. *Advances in Adaptive Data Analysis*, 1(01):1–41, 2009.

Appendix A

Quantitative Analysis of Toy Problem

We will use the frequency domain technique in reference [13] to obtain the Hilbert transform of the given signal $x[n]$ in this toy problem: $x[n] = \cos(2\pi\omega n/Fs)$ with $n = 0, 1, \cdots, N-1$. To comprehend quantitatively the issues illustrated in Fig. 2.1, consider the following scenarios, i.e.,

$$x_1[n] = \cos(2\pi\omega n/Fs),\ n = 0, 1, \cdots, N_1 - 1 \tag{A.1}$$

$$x_2[n] = \cos(2\pi\omega n/Fs),\ n = 0, 1, \cdots, N_2 - 1 \tag{A.2}$$

where $N_2 = N_1 + 1$ and $Fs = \omega N_1$ such that $x_1[n]$ is exactly one full period as in Fig. 2.1(a1), while $x_2[n]$ is one full period plus an extra point as in Fig. 2.1(b1).

For $x_1[n]$, we obtain its DFT by definition as follows:

$$\begin{aligned} X_1[n] &= \sum_{k=0}^{N_1-1} x_1[k] e^{-j2\pi kn/N_1} \\ &= \sum_{k=0}^{N_1-1} \frac{e^{j2\pi\omega k/Fs} + e^{-j2\pi\omega k/Fs}}{2} e^{-j2\pi kn/N_1} \\ &= \frac{1}{2} \sum_{k=0}^{N_1-1} \left(e^{j2\pi\omega k(1-n)/Fs} + e^{-j2\pi\omega k(1+n)/Fs} \right) \end{aligned} \tag{A.3}$$

It is obvious that $X_1[1] = X_1[N_1 - 1] = N_1/2$. For other n's, $X_1[n]$ can be calculated using the sum of geometric series as follows:

$$X_1[n] = \frac{1}{2} \frac{\left(e^{j2\pi\omega(1-n)/Fs}\right)^{N_1} - 1}{e^{j2\pi\omega(1-n)/Fs} - 1} + \frac{1}{2} \frac{\left(e^{-j2\pi\omega(1+n)/Fs}\right)^{N_1} - 1}{e^{-j2\pi\omega(1+n)/Fs} - 1} \tag{A.4}$$

Since

$$\left(e^{j2\pi\omega(1-n)/Fs}\right)^{N_1} - 1 = e^{j2\pi(1-n)} - 1 = 0 \tag{A.5}$$

$$\left(e^{-j2\pi\omega(1+n)/Fs}\right)^{N_1} - 1 = e^{-j2\pi(1+n)} - 1 = 0 \tag{A.6}$$

We have

$$X_1[n] = \begin{cases} N_1/2 & n = 1, N_1 - 1 \\ 0 & \text{otherwise} \end{cases} \tag{A.7}$$

Its DHT would be as follows:

$$\tilde{X}_1[n] = X_1[n] H_c[n] = \begin{cases} -jN_1/2 & n = 1 \\ jN_1/2 & n = N_1 - 1 \\ 0 & \text{otherwise} \end{cases} \tag{A.8}$$

The inverse DFT of $\tilde{X}_1[n]$ can be conveniently derived as follows:

$$\tilde{x}_1[n] \;=\; \sin(2\pi\omega n/Fs) \tag{A.9}$$

This corresponds to Fig. 2.3(a).

For $x_2[n]$, the derivation is similar, except that the two special points, i.e., $n = 1$ and $n = N_1 - 1$ is not that special anymore. Following the sum of geometric series, we will obtain the DFT of $x_2[n]$ as follows:

$$X_2[n] \;=\frac{1}{2}\frac{e^{j2\pi\omega/Fs}-1}{e^{j2\pi(Fs+\omega-nFs)/Fs(Fs+\omega)}-1}+\frac{1}{2}\frac{e^{-j2\pi\omega/Fs}-1}{e^{-j2\pi(Fs+\omega+nFs)/Fs(Fs+\omega)}-1} \tag{A.10}$$

The DHT in this case would be

$$\begin{aligned}
&\tilde{X}_2[n]\\
=&X_2[n]H_c[n]\\
=&\begin{cases}
\frac{-j}{2}\frac{e^{j2\pi\omega/Fs}-1}{e^{j2\pi(Fs+\omega-nFs)/Fs(Fs+\omega)}-1}+\frac{-j}{2}\frac{e^{-j2\pi\omega/Fs}-1}{e^{-j2\pi(Fs+\omega+nFs)/Fs(Fs+\omega)}-1} & n=1,\cdots,\frac{N_2-1}{2}\\
0 & n=0\\
\frac{j}{2}\frac{e^{j2\pi\omega/Fs}-1}{e^{j2\pi(Fs+\omega-nFs)/Fs(Fs+\omega)}-1}+\frac{j}{2}\frac{e^{-j2\pi\omega/Fs}-1}{e^{-j2\pi(Fs+\omega+nFs)/Fs(Fs+\omega)}-1} & n=\frac{N_2+1}{2},\cdots,N_2-1
\end{cases}\\
=&\begin{cases}
\frac{-j}{2}\frac{\alpha^{\omega}-1}{\alpha e^{-j2\pi n/(Fs+\omega)}-1}+\frac{-j}{2}\frac{\alpha^{-\omega}-1}{\alpha^{-1}e^{-j2\pi n/(Fs+\omega)}-1} & n=1,\cdots,\frac{N_2-1}{2}\\
0 & n=0\\
\frac{j}{2}\frac{\alpha^{\omega}-1}{\alpha e^{-j2\pi n/(Fs+\omega)}-1}+\frac{-j}{2}\frac{\alpha^{-\omega}-1}{\alpha^{-1}e^{-j2\pi n/(Fs+\omega)}-1} & n=\frac{N_2+1}{2},\cdots,N_2-1
\end{cases}
\end{aligned} \tag{A.11}$$

where

$$\alpha \;=\; e^{j2\pi/Fs} \tag{A.12}$$

is a constant. Hence, we have the following steps:

$$
\begin{aligned}
&\tilde{x}_2[n] \\
=&\frac{1}{N_2}\sum_{k=0}^{N_2-1} X_2[k]e^{j2\pi kn/N_2} \\
=&\frac{1}{N_2}\sum_{k=0}^{N_2-1} X_2[k]e^{j2\pi\omega kn/(Fs+\omega)} \\
=&\frac{1}{N_2}\sum_{k=1}^{(N_2-1)/2}\left(\frac{-j}{2}\frac{\alpha^{\omega}-1}{\alpha e^{-j2\pi k/(Fs+\omega)}-1}+\frac{-j}{2}\frac{\alpha^{-\omega}-1}{\alpha^{-1}e^{-j2\pi k/(Fs+\omega)}-1}\right)e^{j2\pi\omega kn/(Fs+\omega)}+ \\
&\frac{1}{N_2}\sum_{k=(N_2+1)/2}^{N_2-1}\left(\frac{j}{2}\frac{\alpha^{\omega}-1}{\alpha e^{-j2\pi k/(Fs+\omega)}-1}+\frac{j}{2}\frac{\alpha^{-\omega}-1}{\alpha^{-1}e^{-j2\pi k/(Fs+\omega)}-1}\right)e^{j2\pi\omega kn/(Fs+\omega)}
\end{aligned}
\tag{A.13}
$$

Plugging this formula with $\omega = 1$ and $F_s = 20$, we can easily recover Fig. 2.1 (b2).

Fig. 2.1 (c2) can follow a similar manner as for Fig. 2.1 (b2), thus the derivation is omitted here.

Appendix B

Justification of the Two Properties of Marple's DHT Algorithm

Since $N \in \mathbb{O}$ is quite similar to $N \in \mathbb{E}$ in terms of derivation of the two properties, we only deal with the case of $N \in \mathbb{E}$ herein.

For the first property, it is automatically verified by using Eq. (2.3) as $\tilde{x}[n]$ is real.

For the second one, we have

$$
\begin{aligned}
&\sum_{n=0}^{N-1} \Re\{z[n]\}\Im\{z[n]\} \\
&= \sum_{n=0}^{N-1} x[n]\frac{1}{N}\sum_{k=0}^{N-1}\left[1-(-1)^{n-k}\right]x[k]\sum_{l=1}^{\frac{N}{2}-1}\sin\frac{2\pi l(n-k)}{N} \\
&= \frac{1}{N}\sum_{n=0}^{N-1}\sum_{k=0}^{N-1} x[n]x[k]\left(\sum_{l=1}^{\frac{N}{2}-1}\left[1-(-1)^{n-k}\right]\sin\frac{2\pi l(n-k)}{N}\right) \\
&= \frac{1}{N}\sum_{n=0}^{N-1}\sum_{k=0}^{N-1} x[n]x[k]h[n-k] \\
&= \frac{1}{N}\sum_{n=0}^{N-1}\sum_{i=1}^{(N-1)-n} x[n]x[n-i]h[i] + \frac{1}{N}\sum_{n=0}^{N-1}\sum_{i=1}^{(N-1)-n} x[n-i]x[n]h[-i] \\
&\quad + \frac{1}{N}\sum_{n=0}^{N-1} x[n]x[n]h[0] \\
&= \frac{1}{N}\sum_{n=0}^{N-1}\sum_{i=1}^{(N-1)-n} x[n]x[n-i]h[i] - \frac{1}{N}\sum_{n=0}^{N-1}\sum_{i=1}^{(N-1)-n} x[n]x[n-i]h[i] \\
&= 0
\end{aligned}
\tag{B.1}
$$

The oddness of function $h[n-k]$ is utilized during the manipulation, i.e., $h[n-k]+h[k-n]$.

We have now verified that Marple's DHT algorithm indeed satisfies the two properties.

Appendix C

Obtaining DHT of Signal after Even Extension

The impulse response in this case is

$$h_y[n] \;=\; \begin{cases} 0 & n \in \mathbb{E} \\ \frac{2}{2N-2} \cot \frac{n\pi}{2N-2} & n \in \mathbb{O} \end{cases} \tag{C.1}$$

Therefore,

$$
\begin{aligned}
\tilde{y}[n] &= \sum_{k=0}^{2N-3} y[k]h_y[n-k] \\
&= \sum_{k=0}^{N-1} x[k]h_y[n-k] + \sum_{k=N}^{2N-3} x[2N-2-k]h_y[n-k] \\
&= \sum_{k=0}^{N-1} x[k]h_y[n-k] + \sum_{l=N-2}^{1} x[l]h_y[n+l-(2N-2)] \\
&= \sum_{k=0}^{N-1} x[k]h_y[n-k] + \sum_{l=N-2}^{1} x[l]h_y[n+l] \\
&= \sum_{k=0}^{N-1} x[k]h_y[n-k] + \sum_{k=1}^{N-2} x[k]h_y[n+k] \\
&= \sum_{k=0}^{N-1} x[k]\left(h_y[n-k] + h_y[n+k]\right) - \left(x[0]h_y[n] + x[N-1]h_y[n+N-1]\right) \quad \text{(C.2)}
\end{aligned}
$$

the last equation of which is Eq. (2.15).

Appendix D

Zero Ending Caused by Even Extension

To dive into the derivation, let us first write down the value of $h_y[n]$ for several key n values by following Eq. (2.16):

$$h_y[0] = h_y[2N-2] = 0 \tag{D.1}$$

$$h_y[N-1] = 0 \tag{D.2}$$

$$h_y[N-1-k] + h_y[N-1+k] = 0, \quad \forall\, k \in \mathbb{Z} \tag{D.3}$$

Eqs. (D.1) is obvious; Eq. (D.2) is also easy to verify based on Eq. (2.16). For Eq. (D.3), the reasoning is straightforward as well: when $N-1-k$ is even, $h_y[N-$

$1-k] = h_y[N-1+k] = 0$ as $N-1+k$ is also even. When $N-1-k$ is odd, we have

$$\begin{aligned}
& h_y[N-1-k] + h_y[N-1+k] \\
&= \frac{1}{N-1}\cot\frac{(N-1-k)\pi}{2N-2} + \frac{1}{N-1}\cot\frac{(N-1+k)\pi}{2N-2} \\
&= \frac{1}{N-1}\cot\left(\frac{\pi}{2} - \frac{k\pi}{2N-2}\right) + \frac{1}{N-1}\cot\left(\frac{\pi}{2} + \frac{k\pi}{2N-2}\right) \\
&= \frac{1}{N-1}\tan\frac{k\pi}{2N-2} - \frac{1}{N-1}\tan\frac{k\pi}{2N-2} \\
&= 0
\end{aligned} \tag{D.4}$$

With Eqs. (D.1) to (D.3), Eq. (2.15) can be evaluated at $n = 0$ and $n = N-1$ conveniently as follows:

$$\tilde{y}[0] = \sum_{k=0}^{N-1} x[k]\left(h_y[-k] + h_y[k]\right) - \left(x[0]h_y[0] + x[N-1]h_y[N-1]\right) = 0 \tag{D.5}$$

$$\begin{aligned}
\tilde{y}[N-1] =& \sum_{k=0}^{N-1} x[k]\left(h_y[N-1-k] + h_y[N-1+k]\right) \\
& - \left(x[0]h_y[N-1] + x[N-1]h_y[2N-2]\right) = 0
\end{aligned} \tag{D.6}$$

Thus we have verified that the DHT is zero at the two ends.

Appendix E

Instantaneous Amplitude and Instantaneous Frequency of Double-Component Signal

The discussion herein follows Eq. (3.8) as elaborated in Chapter 3.2.2. A double-component signal of the following format is studied herein:

$$x(t) \;=\; \mathfrak{a}_1(t)\cos\phi_1(t) + \mathfrak{a}_2(t)\cos\phi_2(t) \tag{E.1}$$

where $\phi_i(t) = \int_0^t \omega_i(\tau)d\tau + \varphi_i$ for $i = 1, 2$, and $\mathfrak{a}_i(t)$, $\phi_i(t)$, $\omega_i(t)$ and φ_i are the instantaneous amplitude, instantaneous phase, instantaneous frequency and initial phase of the ith mono-component, respectively. Note that non-zero initial phases are considered in this study differing from Eq. (3.10). Here, $[\mathfrak{a}_i(t), \phi_i(t)]$ form a canonical pair for both $i = 1, 2$ as discussed in Chapter 3.2.2. Following the property of a canonical pair and the linearity property of Hilbert transform, we have

$$\tilde{x}(t) \;=\; \mathfrak{a}_1(t)\sin\phi_1(t) + \mathfrak{a}_2(t)\sin\phi_2(t) \tag{E.2}$$

The instantaneous envelope of $x(t)$ can be obtained by using Eq. (3.6):

$$\begin{aligned}
\mathfrak{a}^2(t) &= x^2(t) + \tilde{x}^2(t) \\
&= [x_1(t) + x_2(t)]^2 + [\tilde{x}_1(t) + \tilde{x}_2(t)]^2 \\
&= [\mathfrak{a}_1(t)\cos\phi_1(t) + \mathfrak{a}_2(t)\cos\phi_2(t)]^2 + [\mathfrak{a}_1(t)\sin\phi_1(t) + \mathfrak{a}_2(t)\sin\phi_2(t)]^2 \\
&= \mathfrak{a}_1^2(t) + \mathfrak{a}_2^2(t) + 2\mathfrak{a}_1(t)\mathfrak{a}_2(t)\cos\Delta\phi(t) \qquad \text{(E.3)}
\end{aligned}$$

where $\Delta\phi(t) = \phi_2(t) - \phi_1(t)$ and $\tilde{x}_i$ is the Hilbert Transform of x_i, for $i = 1, 2$.

For the instantaneous frequency of $x(t)$, on one hand, notice that

$$\omega(t) \triangleq \dot{\phi}(t) = \frac{d}{dt}\left[\arctan\left(\frac{\tilde{x}(t)}{x(t)}\right)\right] = \frac{x(t)\dot{\tilde{x}}(t) - \dot{x}(t)\tilde{x}(t)}{x^2(t) + \tilde{x}^2(t)} \qquad \text{(E.4)}$$

On the other hand, the following two equations are utilized

$$\dot{x}(t) = \dot{\mathfrak{a}}_1(t)\cos\phi_1(t) + \dot{\mathfrak{a}}_2(t)\cos\phi_2(t) - \omega_1(t)\mathfrak{a}_1(t)\sin\phi_1(t) - \omega_2(t)\mathfrak{a}_2(t)\sin\phi_2(t) \qquad \text{(E.5)}$$

$$\dot{\tilde{x}}(t) = \dot{\mathfrak{a}}_1(t)\sin\phi_1(t) + \dot{\mathfrak{a}}_2(t)\sin\phi_2(t) + \omega_1(t)\mathfrak{a}_1(t)\cos\phi_1(t) + \omega_2(t)\mathfrak{a}_2(t)\cos\phi_2(t) \qquad \text{(E.6)}$$

Thus, the following is obtained:

$$
\begin{aligned}
& x(t)\dot{\tilde{x}}(t) - \dot{x}(t)\tilde{x}(t) \\
&= \omega_1(t)\mathfrak{a}_1^2(t) + \omega_2(t)\mathfrak{a}_2^2(t) + (\omega_1(t) + \omega_2(t))\mathfrak{a}_1\mathfrak{a}_2 \cos\Delta\phi(t) \\
&\quad + \ (\mathfrak{a}_1(t)\dot{\mathfrak{a}}_2(t) - \dot{\mathfrak{a}}_1(t)\mathfrak{a}_2(t)) \sin\Delta\phi(t) \\
&= \omega_1(t)\mathfrak{a}^2(t) - (\mathfrak{a}_2(t) + 2\mathfrak{a}_1(t)\mathfrak{a}_2(t)\cos\Delta\phi(t)) + \omega_2(t)\mathfrak{a}_2^2(t) \\
&\quad + (\omega_1(t) + \omega_2(t))\mathfrak{a}_1\mathfrak{a}_2\cos\Delta\phi(t) + (\mathfrak{a}_1(t)\dot{\mathfrak{a}}_2(t) - \dot{\mathfrak{a}}_1(t)\mathfrak{a}_2(t))\sin\Delta\phi(t) \\
&= \omega_1(t)\mathfrak{a}^2(t) + \Delta\omega(t)\left(\mathfrak{a}_2^2(t) + \mathfrak{a}_1(t)\mathfrak{a}_2(t)\cos\Delta\phi(t)\right) + (\mathfrak{a}_1(t)\dot{\mathfrak{a}}_2(t) - \dot{\mathfrak{a}}_1(t)\mathfrak{a}_2(t))\sin\Delta\phi(t)
\end{aligned}
\tag{E.7}
$$

where $\Delta\omega(t) = \Delta\dot{\phi}(t) = \omega_2(t) - \omega_1(t)$. Plugging Eq. (E.7) into Eq. (E.4) yields

$$
\omega(t) \ = \ \omega_1(t) + \underbrace{\frac{\mathfrak{a}_2^2(t) + \mathfrak{a}_1(t)\mathfrak{a}_2(t)\cos\Delta\phi(t)}{\mathfrak{a}^2(t)}\Delta\omega(t) + \frac{\mathfrak{a}_1(t)\dot{\mathfrak{a}}_2(t) - \dot{\mathfrak{a}}_1(t)\mathfrak{a}_2(t)}{\mathfrak{a}^2(t)}\sin\Delta\phi(t)}_{\hat{\omega} \text{ in Eqs. (3.22) and (3.36)}}
\tag{E.8}
$$

Appendix F

Characteristics of Instantaneous Phase at Indexed Time Instances

The discussion here follows that in E. An important property regarding the relationship between instantaneous phase of the sum signal $x(t)$ and its first mono-component $x_1(t)$ is studied. Explanations can be given as follows by using Fig. 3.11:

From t_0 to t_1 in Figs. 3.11(a) to 3.11(c): The sum vector $\vec{z}$ leads the first component $\vec{z}_1$ resulting in $\phi(t) > \phi_1(t)$ as shown in Fig. 3.11(b). The inequality holds till $t = t_1$ when the three vectors line up, with $\vec{z}_2$ directing to an opposite direction as $\vec{z}_1$ and $\vec{z}$, as shown in Fig. 3.11(c). Note that $\vec{z}$ has the same direction as $\vec{z}_1$ as mentioned above. Keeping in mind $\phi(t) \in \mathcal{C}$ and $\phi_1(t) \in \mathcal{C}$, we have $\phi(t_1) = \phi_1(t_1)$.

From t_1 to t_2 in Figs. 3.11(c) to 3.11(e): Right after $t = t_1$, the first component surpasses the sum vector corresponding to $\phi(t) < \phi_1(t)$ as shown in Fig. 3.11(d). The inequality holds till $t = t_2$ where the three vectors line up and point to the same direction again for the first time as shown in Fig. 3.11(e). Again given $\phi(t) \in \mathcal{C}$ and $\phi_1(t) \in \mathcal{C}$, we have $\phi(t_2) = \phi_1(t_2)$.

With the idea of mathematical induction, it can be seen that $\phi(t_n) = \phi_1(t_n) \; \forall \; n \in \mathbb{N}^0$.

Appendix G

Characteristics of Instantaneous Amplitude and Instantaneous Frequency at Indexed Time Instances

The discussion here follows that in E and F. Taking the first time derivative on both sides of Eq. (E.3) leads to the following equation:

$$\begin{aligned} 2\mathfrak{a}(t)\dot{\mathfrak{a}}(t) &= 2\mathfrak{a}_1(t)\dot{\mathfrak{a}}_1(t) + 2\mathfrak{a}_2(t)\dot{\mathfrak{a}}_2(t) + 2\dot{\mathfrak{a}}_1(t)\mathfrak{a}_2(t)\cos\Delta\phi(t) \\ &\quad + 2\mathfrak{a}_1(t)\dot{\mathfrak{a}}_2(t)\cos\Delta\phi(t) - 2\mathfrak{a}_1(t)\mathfrak{a}_2(t)\Delta\omega(t)\sin\left(\Delta\phi(t)\right) \end{aligned} \tag{G.1}$$

Assumption #2 in Chapter 3.4.1 simplifies Eq. (G.1) into the following:

$$2\mathfrak{a}(t)\dot{\mathfrak{a}}(t) \approx -2\mathfrak{a}_1(t)\mathfrak{a}_2(t)\Delta\omega(t)\sin\Delta\phi(t) \tag{G.2}$$

A local extreme demands $\dot{\mathfrak{a}}(t) = 0$, i.e.,

$$\sin \Delta\phi(t) = 0 \quad \Leftrightarrow \quad \cos \Delta\phi(t) = \pm 1 \tag{G.3}$$

This corresponds to the time instances t_n such that $\Delta\phi(t_n) = n\pi$ with $n \in \mathbb{N}^0$ according to Eq. (3.29).

Taking a further time derivative on both sides of Eq. (G.1), discarding all terms containing $\dot{\mathfrak{a}}_1(t)$, $\dot{\mathfrak{a}}_2(t)$, $\dot{\omega}_1(t)$, and $\dot{\omega}_2(t)$ based on Assumption #2 again, and evaluating the equation at t_n lead to the following equation:

$$2\mathfrak{a}(t_n)\ddot{\mathfrak{a}}(t_n) \;\approx\; -2\mathfrak{a}_1(t_n)\mathfrak{a}_2(t_n)\Delta\omega^2(t_n)\cos\left(\Delta\phi(t_n)\right) \tag{G.4}$$

In this sense, Assumption #2 is a sufficient condition for Eqs. (G.2) and (G.4) to hold. These equations can be interpreted as follows:

When $\Delta\phi(t_n) = n\pi$ with $n \in \mathbb{E}$: $\dot{\mathfrak{a}}(t_n) = 0$, and $\ddot{\mathfrak{a}}(t_n) < 0$, which corresponds to a local maximum.

When $\Delta\phi(t_n) = n\pi$ with $n \in \mathbb{O}$: $\dot{\mathfrak{a}}(t_n) = 0$, and $\ddot{\mathfrak{a}}(t_n) > 0$, which corresponds to a local minimum.

Similar to obtaining Eqs. (G.2) and (G.4), we have:

$$\dot{\omega}(t) \;\approx\; \frac{2\left(\mathfrak{a}_1^2(t) - \mathfrak{a}_2^2(t)\right)}{\mathfrak{a}^3(t)}\Delta\omega(t)\dot{\mathfrak{a}}(t) \tag{G.5}$$

$$\ddot{\omega}(t_n) \;\approx\; 2\Delta\omega(t_n)\mathfrak{a}^{-3}(t_n)\left(\mathfrak{a}_1^2(t_n) - \mathfrak{a}_2^2(t_n)\right)\ddot{\mathfrak{a}}(t_n) \tag{G.6}$$

from Eq. (3.21) and by applying Assumption #2 in Chapter 3.4.1. Again, Assumption #2 serves as a sufficient condition for these equations. Further applying Assumption #1 in Chapter 3.4.1 to Eq. (G.6) leads to $\ddot{\omega}(t_n)$ bearing the same sign as $\ddot{\mathfrak{a}}(t_n)$.

In summary, Eqs. (G.5) and (G.6) indicate that $\mathfrak{a}(t)$ and $\omega(t)$ reach every local

maximum or minimum simultaneously under the assumptions applied. Together with Eqs. (G.2) and (G.4), it is concluded that local maxima and minima of both $\mathfrak{a}(t)$ and $\omega(t)$ occur when $\Delta\phi(t_n) = n\pi$ with $n \in \mathbb{E}$ and $n \in \mathbb{O}$, respectively.

Appendix H

Backbone of an Undamped Duffing Oscillator under Free Vibration

Following the idea of harmonic balance method (e.g., in reference [62]), the solution of Eq. (3.38) is assumed to be of the following form:

$$x(t) \;=\; \sum_{k=0}^{l} a_k \cos\left(k\psi(t)\right), \quad \text{where} \quad \psi(t) \;=\; \omega_0 t + \beta_0 \tag{H.1}$$

where a_k, ω_0 and β_0 are constants to be determined, with $a_3 \ll a_2 \ll a_1$.

Let us explore the solution up to $l = 3$, i.e.,

$$x(t) \;=\; a_0 + a_1 \cos\left(\psi(t)\right) + a_2 \cos\left(2\psi(t)\right) + a_3 \cos\left(3\psi(t)\right) \tag{H.2}$$

In this case, the first and second time derivatives of the solution are obtained as follows:

$$\dot{x}(t) = -\omega_0 a_1 \sin\left(\psi(t)\right) - 2\omega_0 a_2 \sin\left(2\psi(t)\right) - 3\omega_0 a_3 \sin\left(3\psi(t)\right) \tag{H.3}$$

$$\ddot{x}(t) = -\omega_0^2 a_1 \cos\left(\psi(t)\right) - 4\omega_0^2 a_2 \cos\left(2\psi(t)\right) - 9\omega_0^2 a_3 \cos\left(3\psi(t)\right) \tag{H.4}$$

Following harmonic balance method, a total of four homogeneous equations are obtained as follows:

$$\omega_n^2 a_0 + \epsilon a_0^3 + \frac{3}{2}\epsilon a_0 a_1^2 + \frac{3}{4}\epsilon a_1^2 a_2 + \frac{3}{2}\epsilon a_0 a_2^2 + \frac{3}{2}\epsilon a_0 a_3^2 + \frac{3}{2}\epsilon a_1 a_2 a_3 = 0 \tag{H.5}$$

$$\omega_n^2 a_1 - \omega_0^2 a_1 + 3\epsilon a_0^2 a_1 + \frac{3}{4}\epsilon a_1^3 + 3\epsilon a_0 a_1 a_2 + \frac{3}{4}\epsilon a_1^2 a_3 + 3\epsilon a_0 a_2 a_3 + \frac{3}{2}\epsilon a_1 a_2^2 + \frac{3}{2}\epsilon a_1 a_3^2 + \frac{3}{4}\epsilon a_2^2 a_3 = 0 \tag{H.6}$$

$$\omega_n^2 a_2 - 4\omega_0^2 a_2 + \frac{3}{2}\epsilon a_0 a_1^2 + 3\epsilon a_0^2 a_2 + 3\epsilon a_0 a_1 a_3 + \frac{3}{2}\epsilon a_1^2 a_2 + \frac{3}{2}\epsilon a_1 a_2 a_3 + \frac{3}{4}\epsilon a_2^3 + \frac{3}{2}\epsilon a_2 a_3^2 = 0 \tag{H.7}$$

$$\omega_n^2 a_3 - 9\omega_0^2 a_3 + \frac{1}{4}\epsilon a_1^3 + 3\epsilon a_0^2 a_3 + 3\epsilon a_0 a_1 a_2 + \frac{3}{2}\epsilon a_1^2 a_3 + \frac{3}{4}\epsilon a_1 a_2^2 + \frac{3}{2}\epsilon a_2^2 a_3 + \frac{3}{4}\epsilon a_3^3 = 0 \tag{H.8}$$

With initial conditions $x(0)$ and $\dot{x}(0)$, a total of six equations are available. Thus, there should be an analytical solution for the six unknowns $a_0, a_1, a_2, a_3, \omega_0$ and β_0.

The following discussion is only for $x(0) \neq 0$ and $\dot{x}(0) = 0$. $a_0 = 0$ is expected given that there is no permanent deformation of the response. In this case, Eq. (H.5) becomes

$$\frac{3}{4}\epsilon a_1^2 a_2 + \frac{3}{2}\epsilon a_1 a_2 a_3 = 0 \tag{H.9}$$

Since a_1 is the amplitude of the first term in $x(t)$, which cannot be zero, thus we have

$$a_1 a_2 + 2 a_2 a_3 = 0 \tag{H.10}$$

If $a_2 \neq 0$, then $a_3 = -\frac{1}{2}a_1$, which conflicts with the assumption of $a_3 \ll a_2 \ll a_1$. Thus, we claim $a_2 = 0$. Accordingly, Eq. (H.7) does not contain any information.

Meanwhile, Eqs. (H.6) and (H.8) simplify to:

$$\omega_n^2 a_1 - \omega_0^2 a_1 + \frac{3}{4}\epsilon a_1^3 + \frac{3}{4}\epsilon a_1^2 a_3 + \frac{3}{2}\epsilon a_1 a_3^2 \ = 0 \tag{H.11}$$

$$\omega_n^2 a_3 - 9\omega_0^2 a_3 + \frac{1}{4}\epsilon a_1^3 + \frac{3}{2}\epsilon a_1^2 a_3 + \frac{3}{4}\epsilon a_3^3 = 0 \tag{H.12}$$

Combining these two equations with the initial condition

$$a_1 + a_3 \ = \ x(0) \ \neq 0 \tag{H.13}$$

the three unknowns a_1, a_3 and ω_0 can be solved numerically following Eqs. (H.11) to (H.13) in lieu of solving an ODE numerically. Other initial conditions can be converted to the algebraic equations given above thus can be subsequently solved.

Appendix I

DHT of Signal with Large Decaying Ratio

In this section, we will look into a signal that challenges DHT and figure out why the envelope of the tail is amplified. To show this, we will compare the DHT of two signals, where the first signal $x[n]$ is defined for $n = 0, 1, \cdots, N-1$ with $N \in \mathbb{E}$ and the second signal $x_2[n_2]$ is defined for $n_2 = 0, 1, \cdots, N/2-1$. $x_2[n_2]$ is chosen as the second half of $x[n]$, i.e.,

$$x_2[n] \;=\; x[n + N/2 - 1],\ \forall\ n \in [0, N/2 - 1] \tag{I.1}$$

The goal here is to show that the envelope of the second half of $x[n]$ is an amplified version of $x_2[n_2]$, even though they are the same sequence.

To simplify the analysis, we make the following assumptions on the signal $x[n]$ considered here:

Assumption #1 The signal length N is a multiple of 4.

Assumption #2 Every point in the second half is $1/M$ of the point $N/2$ proceeding

it with $M \gg 1$. In other words, the following is true

$$x[n_2] \;=\; Mx_2[n_2],\ \forall\ n_2 \in [0, N/2-1],\ \text{where } M \gg 1 \tag{I.2}$$

Admittedly, Assumption #2 is quite stringent; the idea is to make sure $x[n]$ being fast decaying and simplify the derivation.

By definition, the DHT of $x[n]$ is as follows [13]:

$$\tilde{x}[n] \;=\; \sum_{k=0}^{N-1} x[k]h[n-k] \tag{I.3}$$

where h[n] is the impulse response given as follows

$$h[n] \;=\; \begin{cases} 0 & n \in \mathbb{E} \\ \frac{2}{N}\cot\frac{\pi n}{N} & n \in \mathbb{O} \end{cases} \tag{I.4}$$

By splitting the RHS into two parts, we have

$$\begin{aligned}
\tilde{x}[n] \;&=\; \sum_{k=0}^{N/2-1} x[k]h[n-k] + \sum_{k=N/2}^{N-1} x[k]h[n-k] \\
&=\; \sum_{k=0}^{N/2-1} Mx[k+N/2]h[n-k] + \sum_{k=N/2}^{N-1} x[k]h[n-k] \\
&=\; \sum_{l=N/2}^{N-1} Mx[l]h[n-l+N/2] + \sum_{k=N/2}^{N-1} x[k]h[n-k] \\
&=\; \sum_{k=N/2}^{N-1} x[k]\left(Mh[n-k+N/2] + h[n-k]\right) \\
&=\; \sum_{k=0}^{N/2-1} x_2[k]\left(Mh[n-k] + h[n-k-N/2]\right)
\end{aligned} \tag{I.5}$$

The second half of $\tilde{x}[n]$ can be rewritten as

$$\tilde{x}[n_2] \;=\; \sum_{k=0}^{N/2-1} x_2[k]\left(Mh[n_2-k+N/2]+h[n_2-k]\right),\ \forall\ n_2\in[0,N/2-1] \tag{I.6}$$

Note that

$$\tilde{x}_2[n_2] = \sum_{k=0}^{N/2-1} x_2[k]h_2[n_2-k] \tag{I.7}$$

where

$$h_2[n] \;=\; \begin{cases} 0 & n\in\mathbb{E} \\ \frac{2}{N/2}\cot\frac{\pi n}{N/2} & n\in\mathbb{O} \end{cases} \tag{I.8}$$

To show that the envelope of the second half is amplified, we only need to show that there exists an integer K whose absolute value is greater than 1 such that $\tilde{x}[n_2] = K\tilde{x}_2[n_2]$. By looking at Eqs. (I.6) and (I.7), it is sufficient to show the following is true for some $|K|>1$.

$$\underbrace{Mh[n_2-k+N/2]+h[n_2-k]}_{\bar{h}_1[n_2-k]} \;=\; K\underbrace{h_2[n_2-k]}_{\bar{h}_2[n_2-k]},\ \forall\ n_2-k\in[-N-1,N-1] \tag{I.9}$$

Although a mathematical proof is not given, Fig. I.1 presents the $\bar{h}_1[n_2-k]$ and $\bar{h}_2[n_2-k]$ for three typical N values when $M=100$. It can be seen that $\bar{h}_2[n]>\bar{h}_1[n]$ almost for any n. Given that the signal considered has a continuously decaying feature, it is reasonable for us to claim that Eq. (I.9) should be satisfied. Therefore, it is expected that the tail would be amplified when $M >> 1$ for a continuously decaying signal.

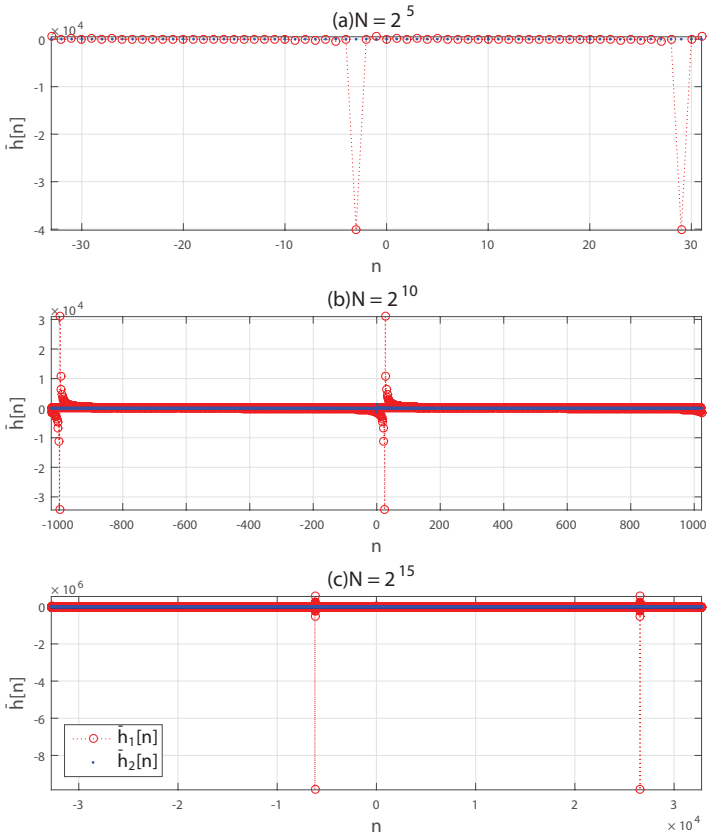

Figure I.1: $\bar{h}_1[n]$ and $\bar{h}_2[n]$ under different signal length N. Decaying ratio M is set to 100.

Appendix J

State-Space Representation of Analytic Signal Using Duffing Oscillator

The goal of working on this state-space view of unforce Duffing oscillator is to further understand Dr. Feldman' backbone concept, and to check if there is any similarity with the classic state-space representation since both methods represent the system with two signals in a cartesian coordinate.

In Cartesian coordinate, the state space of a Duffing oscillator $\ddot{x}+c\dot{x}+kx+\alpha x^3 = 0$ is as follows:

$$\dot{\mathbf{x}} = \begin{pmatrix} \dot{x} \\ \ddot{x} \end{pmatrix} = \begin{pmatrix} x_1 \\ -cx_2 - kx_1 - \alpha x_1^3 \end{pmatrix} \tag{J.1}$$

where

$$\mathbf{x} = \begin{pmatrix} x_1 \\ x_2 \end{pmatrix} = \begin{pmatrix} x \\ \dot{x} \end{pmatrix} \tag{J.2}$$

Following this idea, we will try to obtain a state-space representation of the Duffing model in polar coordinate with states $\phi(t)$ and $\mathfrak{a}(t)$ where $x(t) = \mathfrak{a}(t)\cos\phi(t)$

and $\mathfrak{a}(t)$ and $\phi(t)$ are the instantaneous amplitude and instantaneous phase of $x(t)$, respectively. First of all, it is important to emphasize only these two states are not enough, because they are both related to the current state of the system only and have nothing to do with evolution. Therefore, it would be necessary to add their first time derivatives in the states, which end up with the following state vector:

$$\mathbf{u} = \begin{pmatrix} u_1 \\ u_2 \\ u_3 \\ u_4 \end{pmatrix} = \begin{pmatrix} \mathfrak{a} \\ \phi \\ \dot{\mathfrak{a}} \\ \dot{\phi} \end{pmatrix} \tag{J.3}$$

The corresponding state equation is as follows:

$$\dot{\mathbf{u}} = \begin{pmatrix} \dot{\mathfrak{a}} \\ \dot{\phi} \\ \ddot{\mathfrak{a}} \\ \ddot{\phi} \end{pmatrix} = \begin{pmatrix} u_3 \\ u_4 \\ f_1(\mathbf{u}) \\ f_2(\mathbf{u}) \end{pmatrix} \tag{J.4}$$

To determine the f_1 and f_2, the formulas of x, $\dot{x}$, and $\ddot{x}$ could be plugged back into the equation of motion. First of all, we have

$$x = \mathfrak{a}(t)\cos\phi(t) \tag{J.5}$$

$$\dot{x} = \dot{\mathfrak{a}}(t)\cos\phi(t) - \dot{\phi}(t)\mathfrak{a}(t)\sin\phi(t) \tag{J.6}$$

$$\ddot{x} = \ddot{\mathfrak{a}}\cos\phi(t) - 2\dot{\mathfrak{a}}\dot{\phi}(t)\sin\phi - \mathfrak{a}(t)\ddot{\phi}(t)\sin\phi(t) - \mathfrak{a}\dot{\phi}^2(t)\cos\phi(t) \tag{J.7}$$

Substituting Eqs. (J.5)- (J.7) into the equation of motion yields the following:

$$\ddot{\mathfrak{a}}\cos\phi - 2\dot{\mathfrak{a}}\dot{\phi}\sin\phi - \mathfrak{a}\ddot{\phi}\sin\phi - \mathfrak{a}\dot{\phi}^2\cos\phi + c\dot{\mathfrak{a}}\cos\phi - c\dot{\phi}\mathfrak{a}\sin\phi + k\mathfrak{a}\cos\phi + \alpha\mathfrak{a}^3\cos^3\phi = 0 \tag{J.8}$$

Note that $\cos^3\phi = \frac{3}{4}\cos\phi + \frac{1}{4}\cos 3\phi$, Eq. (J.8) becomes the following

$$\begin{aligned}
&\ddot{\mathfrak{a}}\cos\phi - 2\dot{\mathfrak{a}}\dot{\phi}\sin\phi - \mathfrak{a}\ddot{\phi}\sin\phi - \mathfrak{a}\dot{\phi}^2\cos\phi + c\dot{\mathfrak{a}}\cos\phi - c\dot{\phi}\mathfrak{a}\sin\phi + k\mathfrak{a}\cos\phi \\
&+ \frac{3}{4}\alpha\mathfrak{a}^3\cos\phi + \frac{1}{4}\alpha\mathfrak{a}^3\cos 3\phi \\
&= 0
\end{aligned} \tag{J.9}$$

We need to extract two equations out of this single equation, one for $\ddot{\mathfrak{a}}$ and one for $\ddot{\phi}$. One way of doing so is to follow the idea of harmonic balance method, i.e., discarding the high frequency term in Eq. (J.9), and making the cos and sin terms to be zero, respectively, from which we have

$$\left(\ddot{\mathfrak{a}} - \mathfrak{a}\dot{\phi}^2 + c\dot{\mathfrak{a}} + k\mathfrak{a} + \frac{3}{4}\alpha\mathfrak{a}^3\right)\cos\phi = 0 \tag{J.10}$$

$$\left(-2\dot{\mathfrak{a}}\dot{\phi} - \mathfrak{a}\ddot{\phi} - c\dot{\phi}\mathfrak{a}\right)\sin\phi = 0 \tag{J.11}$$

Based on these equations, we have

$$\ddot{\mathfrak{a}} = \mathfrak{a}\dot{\phi}^2 - 2c\dot{\mathfrak{a}} - \omega_n^2\mathfrak{a} - \frac{3}{4}\alpha\mathfrak{a}^3 \tag{J.12}$$

$$\ddot{\phi} = -2c\dot{\phi} - 2\dot{\phi}\frac{\dot{\mathfrak{a}}}{\mathfrak{a}} \tag{J.13}$$

Therefore, the approximated state space equation of the Duffing oscillator is as follows:

$$\dot{\mathbf{u}} = \begin{pmatrix} u_3 \\ u_4 \\ u_1u_4^2 - cu_3 - ku_1 - \frac{3}{4}\alpha u_1^3 \\ -cu_4 - 2u_4\frac{u_3}{u_1} \end{pmatrix} \tag{J.14}$$

An interesting observation is that u_2 is not involved in the state equation, meaning

it is a redundant state. Therefore, the simplified state equation is given as follows:

$$\dot{\mathbf{u}} = \begin{pmatrix} u_3 \\ u_1 u_4^2 - c u_3 - k u_1 - \frac{3}{4}\alpha u_1^3 \\ -c u_4 - 2 u_4 \frac{u_3}{u_1} \end{pmatrix} \tag{J.15}$$

where

$$\mathbf{u} = \begin{pmatrix} u_1 \\ u_3 \\ u_4 \end{pmatrix} = \begin{pmatrix} \mathfrak{a} \\ \dot{\mathfrak{a}} \\ \dot{\phi} \end{pmatrix} = \begin{pmatrix} \mathfrak{a} \\ \dot{\mathfrak{a}} \\ \omega \end{pmatrix} \tag{J.16}$$

One step further is to replace the second states with $\mathfrak{b}$, i.e., $\frac{\dot{\mathfrak{a}}}{\mathfrak{a}}$. Notice that for the sake of manipulation, the $\mathfrak{b}$ here is the original definition but without the absolute sign. The substitution can be done similarly following the above manipulation, which ends up with the following state equation:

$$\dot{\mathbf{u}} = \begin{pmatrix} \dot{\mathfrak{a}} \\ \dot{\mathfrak{b}} \\ \ddot{\phi} \end{pmatrix} = \begin{pmatrix} u_1 u_2 \\ -\frac{3}{4}\alpha u_1^2 - u_2^2 - c u_2 + u_3^2 - k \\ -2 u_2 u_3 - c u_3 \end{pmatrix} \tag{J.17}$$

where the new state vector is

$$\mathbf{u} = \begin{pmatrix} \mathfrak{a} \\ \mathfrak{b} \\ \phi \end{pmatrix} \tag{J.18}$$

The derivation for the new state equation is as follows:

$$
\begin{aligned}
\dot{\mathbf{u}} &= \begin{pmatrix} \dot{\mathfrak{a}} \\ \dot{\mathfrak{b}} \\ \ddot{\phi} \end{pmatrix} \\
&= \begin{pmatrix} \dot{\mathfrak{a}} \\ -\left(\frac{\dot{\mathfrak{a}}}{\mathfrak{a}}\right)^2 + \frac{\ddot{\mathfrak{a}}}{\mathfrak{a}} \\ -c\dot{\phi} - 2\dot{\phi}\frac{\dot{\mathfrak{a}}}{\mathfrak{a}} \end{pmatrix} \\
&= \begin{pmatrix} \dot{\mathfrak{a}} \\ -\left(\frac{\dot{\mathfrak{a}}}{\mathfrak{a}}\right)^2 + \frac{\mathfrak{a}\dot{\phi}^2 - 2c\dot{\mathfrak{a}} - k\mathfrak{a} - \frac{3}{4}\alpha\mathfrak{a}^3}{\mathfrak{a}} \\ -c\dot{\phi} - 2\dot{\phi}\frac{\dot{\mathfrak{a}}}{\mathfrak{a}} \end{pmatrix} \\
&= \begin{pmatrix} \dot{\mathfrak{a}} \\ -\left(\frac{\dot{\mathfrak{a}}}{\mathfrak{a}}\right)^2 + \dot{\phi}^2 - c\frac{\dot{\mathfrak{a}}}{\mathfrak{a}} - k - \frac{3}{4}\alpha\mathfrak{a}^2 \\ -c\dot{\phi} - 2\dot{\phi}\frac{\dot{\mathfrak{a}}}{\mathfrak{a}} \end{pmatrix} \\
&= \begin{pmatrix} u_1 u_2 \\ -\frac{3}{4}\alpha u_1^2 - u_2^2 - cu_2 + u_3^2 - k \\ -2u_2 u_3 - cu_3 \end{pmatrix}
\end{aligned}
\tag{J.19}
$$

The following formula is used in the above manipulation:

$$
\frac{d\left(\frac{\dot{\mathfrak{a}}}{\mathfrak{a}}\right)}{dt} = \frac{\mathfrak{a}\ddot{\mathfrak{a}} - \dot{\mathfrak{a}}^2}{\mathfrak{a}^2} \tag{J.20}
$$

Appendix K

Physical Meaning of Instantaneous Bandwidth by Using Velocity

Although the definition of instantaneous bandwidth is readily given in Eq. (4.5), it would be helpful if we could come up with a physical interpretation that is NOT from a probabilistic viewpoint. The right-hand side is the absolute value of the ratio of the time derivative of $\mathfrak{a}(t)$ over $\mathfrak{a}(t)$, from where it is not easy to tell that it is a parameter that represents the spread of $\omega(t)$. As also stated above, [15] gives a detailed derivation of this equation, but still, it is more mathematically meaningful than physically. Having said this, here we try to make physical sense of this definition, a different and new point of view from that in reference [15].

Consider a signal $x(t)$ in the following amplitude-phase form:

$$x(t) \;=\; \mathfrak{a}(t)\cos(\phi(t)) \tag{K.1}$$

where $\mathfrak{a}(t)$ and $\phi(t)$ correspond to the instantaneous amplitude and instantaneous phase, respectively. Therefore, the Hilbert transform of $x(t)$ is

$$\tilde{x}(t) \;=\; \mathfrak{a}(t)\sin(\phi(t)) \tag{K.2}$$

First time derivative of $x(t)$ is

$$\dot{x}(t) \;=\; \dot{\mathfrak{a}}(t)\cos(\phi(t)) - \dot{\phi}(t)\mathfrak{a}(t)\sin(\phi(t)) \;=\; \dot{\mathfrak{a}}(t)\cos(\phi(t)) - \omega(t)\tilde{x}(t) \tag{K.3}$$

Notice that $\cos(\phi(t)) = x(t)/\mathfrak{a}(t)$, we have

$$\dot{x}(t) \;=\; \dot{\mathfrak{a}}(t)\frac{x(t)}{\mathfrak{a}(t)} - \omega(t)\tilde{x}(t) \tag{K.4}$$

Rearranging the terms yields

$$\frac{\dot{\mathfrak{a}}(t)}{\mathfrak{a}(t)}x(t) \;=\; \dot{x}(t) + \omega(t)\tilde{x}(t) \tag{K.5}$$

If we take the absolute value of both sides, we will end with

$$\left|\frac{\dot{\mathfrak{a}}(t)}{\mathfrak{a}(t)}\right| |x(t)| \;=\; |\dot{x}(t) + \omega\tilde{x}(t)| \tag{K.6}$$

Notice that $|\dot{\mathfrak{a}}(t)/\mathfrak{a}(t)|$ is what we define as $\mathfrak{b}(t)$, therefore, we have

$$|\mathfrak{b}(t)||x(t)| \;=\; |\dot{x}(t) + \omega(t)\tilde{x}(t)|, \text{ or equivalently, } |\mathfrak{b}(t)| \;=\; \left|\frac{\dot{x}(t)}{x(t)} + \omega(t)\frac{\tilde{x}(t)}{x(t)}\right| \tag{K.7}$$

Although the exact physical meaning of the above equation remain undiscovered, the two terms containing instantaneous bandwidth and instantaneous frequency, i.e., $\left|\frac{\dot{\mathfrak{a}}(t)}{\mathfrak{a}(t)}\right| |x(t)|$ on the LHS and $\omega(t)\tilde{x}(t)$ on the RHS are readily comparable, as $x(t)$ and $\tilde{x}(t)$ are merely two different representation of one given signal. Hence, we successfully connected instantaneous bandwidth and instantaneous frequency with a seemingly unusual equation. Eq. (K.7) indicates that instantaneous bandwidth can be interpreted as a weighted sum of its first time derivative and its Hilbert transform each normalized with respect to the original real signal.

It would be interesting to take a deeper look at the two terms on the RHS. Consider

a special case where $x(t) = cos(\omega t)$, i.e., a pure sinusoid. In this case, $\mathfrak{a}(t)$ is constant 1, and thus $\dot{\mathfrak{a}}(t)$ is zero. Thus, we have:

$$\dot{x}(t) \;=\; -\omega(t)\tilde{x}(t) \tag{K.8}$$

which makes $|\mathfrak{b}||x| = 0$, meaning $\mathfrak{b} = 0$. Although this is a trivial case, we can take a further look at the case when $\mathfrak{a}$ is really slowly varying, i.e., $\dot{\mathfrak{a}}(t)$ can be neglected. In this case,

$$\dot{x}(t) \;\approx\; -\omega(t)\tilde{x}(t) \tag{K.9}$$

and thus $\mathfrak{b} \approx 0$. The implication of this result is that for lightly damped system, the signal magnitude is slowly varying, hence the instantaneous amplitude.

Appendix L

Review Notes: Damping Estimation with Instantaneous Bandwidth

Damping estimation using instantaneous characteristics is proposed in reference [23, 30]. The following steps summarize these studies by Dr. Feldman. Consider a model with viscous damping and amplitude-dependent natural frequency as follows:

$$\ddot{x}(t) + h(t)\dot{x}(t) + \omega_x^2(t)x(t) \;=\; 0 \tag{L.1}$$

Replacing $x(t)$ with its corresponding analytic signal yields

$$\ddot{X}(t) + h(t)\dot{X}(t) + \omega_x^2(t)X(t) \;=\; 0 \tag{L.2}$$

where $X(t) = x(t) + j\tilde{x}(t)$. Since

$$\dot{X}(t) = X(t)\left(\frac{\dot{\mathfrak{a}}(t)}{\mathfrak{a}(t)} + j\omega(t)\right) \tag{L.3}$$

$$\ddot{X}(t) = X(t)\left(\frac{\ddot{\mathfrak{a}}(t)}{\mathfrak{a}(t)} - \omega^2(t) + j2\omega(t)\frac{\dot{\mathfrak{a}}(t)}{\mathfrak{a}(t)} + j\dot{\omega}(t)\right) \tag{L.4}$$

we have

$$X(t)\left(\frac{\ddot{\mathfrak{a}}(t)}{\mathfrak{a}(t)}\omega^2(t) + \omega_x^2 + 2h(t)\frac{\dot{\mathfrak{a}}(t)}{\mathfrak{a}(t)}j\left(2\frac{\dot{\mathfrak{a}}(t)}{\mathfrak{a}(t)} + \dot{\omega}(t) + 2h(t)\omega(t)\right)\right) = 0 \tag{L.5}$$

Hence

$$h(t) = -\frac{\dot{\mathfrak{a}}(t)}{\mathfrak{a}(t)} - \frac{\dot{\omega}(t)}{2\omega(t)} \tag{L.6}$$

$$\omega_x(t) = \omega^2(t) - \frac{\ddot{\mathfrak{a}}(t)}{\mathfrak{a}(t)} + 2\frac{\dot{\mathfrak{a}}^2(t)}{\mathfrak{a}^2(t)} + \frac{\dot{\mathfrak{a}}(t)\dot{\omega}(t)}{\mathfrak{a}(t)\omega(t)} \tag{L.7}$$

Appendix M

Selected MATLAB Codes Developed in this Work

M.1 Computing Discrete Hilbert Transform with Trimming and Even Extension

```
function [x_trim, x_tilde, loc_min, loc_max] = hilbert_TEM(x)
% hilbert_TEM compute Hilbert transform of a discrete signal with proposed two
% preprocessing steps.
%   x       - input signal (one dimension)
%   x_trim  - trimmed signal
%   x_tilde - Hilbert transform of x
%   loc_min - original start index of x_trim
%   loc_max - original end index of x_trim
%
% Example:
%   [x_trim, x_tilde, loc_min, loc_max] = hilbert_TEM(x);
%
x=x(:);
[~, loc1] = findpeaks(x);
[~, loc2] = findpeaks(-x);
if(max(loc1)>=max(loc2))
    loc = loc1;
else
    loc = loc2;
end
if(x(1)==max(x(1:min(loc))) && x(1)>0)
    loc_min = 1;
else
```

```
    loc_min = min(loc);
end
loc_max = max(loc)-1;
x_trim = x(loc_min:loc_max);
x_ref = flipud(x_trim(2:end-1));
x_new = [x_ref; x_trim];
x_HT = hilbert(x_new);
x_tilde = imag(x_HT(length(x_trim)-1:end));
```

M.2 Computing Instantaneous Amplitude, Instantaneous Phase and Instantaneous Frequency

```
function [A, F, P, loc_min, loc_max]=inst_TEM(x, Fs)
% inst_TEM compute IA, IP, IF of a discrete signal.
%   x   - input signal (one dimension)
%   Fs  - sampling frequency (Hz)
%   A   - instantaneous amplitude
%   F   - instantaneous frequency (Hz)
%   P
% Example:
%   [A, F, P, loc_min, loc_max]=inst_TEM(x, Fs);
%
x=x(:);
[x_trim, x_tilde, loc_min, loc_max] = hilbert_TEM(x);
A2 = x_tilde.^2 + x_trim.^2;
A = sqrt(A2);
phi = atan2(x_tilde, x_trim);
P = unwrap(phi);
F = Fs * diff_new(P,[1:length(P)]');
% diff_new is based on central_diff given in
% http://www.mathworks.com/matlabcentral/fileexchange/12-central-diff-m
```

M.3 Computing B_eT_e Product

```
function [BeTe] = BT(x, Fs)
% BT compute BT product of a discrete signal.
%   x   - input signal (one dimension)
%   Fs  - sampling frequency (Hz)
%   BeTe- BT product of x
%
% Example:
%   [BeTe] = BT(x, Fs);
```

```
%
x = x(:);
N = length(x);
t = 0:N-1/Fs;
X = fft(x);
m = [0:N-1]';
K = N;
k = [0:K/2-1]';
deltaT = 1/Fs;
deltaF = K/Fs;
sm = abs(x);
Sk = abs(X(1:K/2));
Be_num = sum((k.*deltaF).^2 .* Sk.^2 * deltaF);
Be_den = sum(Sk.^2 * deltaF);
Te_num = sum((m * deltaT).^2 .* sm.^2 * deltaT);
Te_den = sum(sm.^2 * deltaT);
Be = Be_num/Be_den;
Te = Te_num/Te_den;
BeTe = 2*sqrt(Be*Te);
```